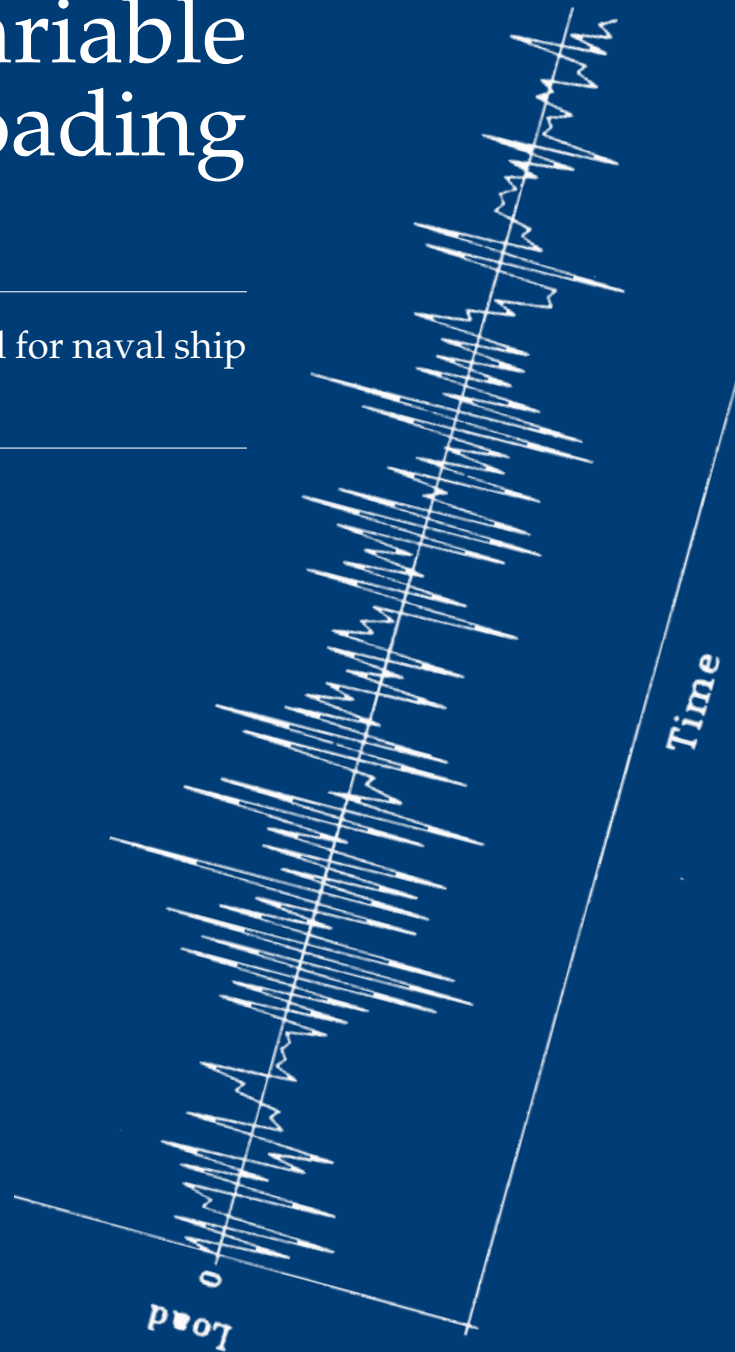


Fatigue damage accumulation in steel welded joints, subject to (random) variable amplitude loading conditions

An improved fatigue-life model for naval ship structural design

M. L. Deul



Fatigue damage accumulation in steel welded joints, subject to (random) variable amplitude loading conditions

An improved fatigue-life model for naval ship structural design

by

M. L. Deul

to obtain the degree of Master of Science in Marine Technology
at the Delft University of Technology,
to be defended publicly on Wednesday July 28, 2021 at 10:30 AM.

July 15, 2021

Student number: 4430816
Project duration: November 9, 2020 – July 28, 2021
Specialisation: Ship and Offshore Structures

Thesis committee:	Dr. ir. J. H. den Besten, <i>Assistant Professor Ship and Offshore Structures (3mE)</i>	TU Delft, chair
	Dr. C. L. Walters, <i>Associate Professor Ship and Offshore Structures (3mE)</i>	TU Delft
	Ir. G. Bufalari, <i>Lecturer, Researcher and PhD candidate Ship and Offshore Structures (3mE)</i>	TU Delft
	Prof. dr. M. Veljkovic, <i>Professor of Steel and Composite Structures (CiTG)</i>	TU Delft
	J. W. van Bergen, <i>Policy advisor Structures</i>	DMO

An electronic version of this thesis is available at <http://repository.tudelft.nl/>.

The figure on the front page is a random time signal of 150 peaks, as generated by Agerskov et al. [3] from the modified Pierson-Moskovich spectrum (PMMOD64). This is a typical spectrum load for maritime structures in waves. This time trace has a mean stress of zero MPa.

Preface

Dear reader,

The document before you is my master thesis on "Fatigue damage accumulation of welded joints in (random) variable amplitude loading conditions." This thesis is written as a conclusion of the master Marine Technology at the Delft University of Technology. The work was performed with the guidance and supervision of Henk den Besten (TU Delft), Weihong He and Jan van Bergen (both from the office Ship Vulnerability, of the Dutch Ministry of Defence).

My interest in ship structures has its origin several years back. After the BSc studies I spent a year in the industry, working at the R&D department of Royal IHC. Here I had the luck to be mentored by one of the designers with a lot of passion for steel structures who helped me to develop my interest in structural optimisation and metal fatigue by showing me their projects, ships and calculations. By that time fatigue was still a novel topic to me. Luckily this changed during the course "Fatigue Strength of Marine Structures", as taught by Henk den Besten. The link between the micro defects and macro failure grasped my attention.

The gratitude is expressed first and foremost to my supervisors: Henk den Besten, Weihong He and Jan van Bergen. Henk, thanks for guiding me with your excellent eye for detail and for training me in a critical scientific attitude. Your feedback is always thorough, which triggered me to keep improving my work and aim for more and more substantiation, understanding and insights. I have really enjoyed to aim for the goal that we set under your guidance!

Weihong, thanks for being my ally in the process. You opened my eye to the processes that go beyond the research, to show what is required to enable implementation of the results in a shipyard's practise and in class guidelines. Your valuable support with regards to the research process and, most importantly, with regards to storytelling has improved both the quality and readability of this work.

Jan, I would like to thank you for your contagious enthusiasm for the topic of fatigue, for initiating this graduation project and for connecting me throughout the sector. Which brings me to my next point: I would like to thank Paula van Lieshout, Noud Werter, Ingo Drummen, Bas Aberkrom, Gabriele Bufalari and the people of the Ship Vulnerability office for being my sparring partners. You all managed to expand my view on the fatigue matter and asked me tough questions when I needed it.

To all the friends and family that endured my brain-waves, brightened up the day during phone-calls, lunch-walks and coffee-runs, learned about fatigue with me and kept me sane in this odd period to be graduating: your contribution to this thesis is invaluable. *Mijn dank is groot!*

M. L. (Marije Louisa) Deul
Delft, July 2021

Postscriptum

During this project DNV has changed its name from DNV-GL to DNV [81] (as per March 1st, 2021). As the cited documents are published under the old name, the organisation is referenced as DNV-GL.

Summary

The current fatigue assessment methods for naval ships are intentionally conservative. This is due to fatigue assessment uncertainties related to both the demand (i.e. loading) and capacity (i.e. fatigue resistance), as to provide a safe platform for the crew. For the new generation of M-frigates the objective is to reduce the structural weight whilst maintaining the fatigue strength. To this extent novel approaches to the fatigue assessment are researched with the objective to reduce the conservatism and uncertainty. This fatigue assessment is characterised by five main sources of uncertainty: 1) Fatigue loading and response conditions, 2) FE model uncertainty (including mesh and choice of elements), 3) Fatigue resistance (including SSS versus FSS), 4) Fatigue damage criterion and 5) Fatigue damage accumulation. In this research improvements are proposed with respect to the fourth and fifth source. This is done to propose a feasible research, whilst acknowledging each of the five sources as a part of the fatigue puzzle.

A survey of scientific literature provides the statement that the currently applied fatigue damage accumulation model, the **Linear Damage Accumulation Model (LDAM)** by **Palmgren** and **Miner** is not sufficiently accurate to assess random variable amplitude loading histories. The safe-life engineering solution to this, is to employ a safety factor. This typically reduces the critical damage from 1.0 to 0.5, or even 0.2. The main flaw of the **LDAM** is that it does not properly account for the effects of previous loading cycles on the damage rate due to the current cycles. Its common application is due to the charming simplicity, and good track record (under the large safety factors). The literature study provides an overview of proposed damage accumulation theorems, to overcome the shortcomings of the **LDAM**, in three categories based on the classification of fatigue capacity in each of the dimensions: continuum mechanics, fracture mechanics and damage mechanics. Of all considered theorems the work by **Leonetti et al.** is selected because it complies the best, and to a sufficient extent, to a list of demands: the model should be non-linear, in the spectral domain, and be validated for random **VA** loading. **Leonetti et al.** provides a fracture mechanics domain approach by combining the damage limit concept from **Hirt and Kunz** with the **6 Parameter Random Fatigue Limit Model (6PRFLM)** from earlier work by **Leonetti et al.**. The model by **Leonetti et al.** is based on statistical inference of variable amplitude data. Improvement potential is identified when combining the model by **Leonetti et al.** with the **Effective Notch Stress Concept (ENSC)**, a criterion that includes the local information of the welded detail as well as the distribution of welding-induced residual stresses. The criterion allows to use one S-N curve for all welded details and typically has a smaller scatterband than the **NSC** based assessment. A smaller scatterband means better inference, and in line with the hypothesis: a more accurate fatigue life prediction. Frigates are now typically assessed with the **Hot Spot Structural Stress Concept (HSSSC)**, a method that is complexity- and effort-wise a compromise between the **NSC** and **ENSC**.

A database of random variable amplitude fatigue data is constructed to analyse the quality of each model variation. This database provides a variation in hot spot types, spectrum types, mean stress levels and geometries. The result of this report is a comparison of the scatter-index (90% percentile divided over the 10% percentile) of the ratio between the \log_{10} of the experimental over the predicted fatigue life, of the **VA** database specimens. This index is {1:1.28, 1:1.16, 1:1.13} for {the **HSSSC** combined with the Palmgren-Miner rule (i. e. the base-case), the **ENSC** with the Palmgren-Miner rule, the **ENSC** with the accumulation model by **Leonetti et al.**}. A scatter reduction poses a reduction of conservatism for the 97.7% probability of survival bound, as typically is used for structural design. A second comparison is of the **AIC**, being {-44.5, -62.6, -86.3} for the three model combinations, proving for the second time the benefits of the **NLDAM** over the **LDAM**.

The minimum (phenomenological) amount of scatter in fatigue test data originates from variations in weld quality, definition of experimental failures and process-induced residual stress variations. Using the **NLDAM** reduces the scatter due to spectrum shape variations, but does not fully remove it. It is observed that the optimum configuration of the parameters of the **NLDAM** is different for {low, mid-to-high} stress range dominated spectra. Considering the **NLDAM** as a fracture mechanics based model, this is attributed to the limited validity for crack initiation dominated specimens, subject to low stress range dominated spectra. A recommendation is to work on the combination of the **Total Stress Concept (TSC)** with the **NLDAM** to arrive at a total life criterion.

Samenvatting

De huidige modellen om de vermoeiingslevensduur van marineschepen te voorspellen zijn met opzet conservatief. Dit is gedaan met het zicht op de significante onzekerheden, zowel aan de kant van de vraag (i.e. belasting) als de capaciteit (i.e. weerstand tegen vermoeiing). Deze onzekerheden worden vertaald naar conservatisme om in een veilig platform voor de bemanning te voorzien. Voor de nieuwe generatie M-fregatten staat **DMO** voor de uitdaging om het staalgewicht te reduceren, zonder de voorspelde vermoeiingsweerstand te reduceren. Om dit te realiseren worden nieuwe vermoeiingsschade modellen onderzocht. Dit onderzoek beoogt het impliciete conservatisme in de voorspelling te reduceren. De onzekerheid in de berekening van de vermoeiingslevensduur wordt toegekend aan vijf hoofd-factoren: onzekerheid in 1) belasting en responsie condities, 2) het **FE** model (mesh en keuze van elementen), 3) de vermoeiings-weerstand (geldigheid van S-N curves van klasse), 4) het vermoeiings-schade criterium en 5) het schade-accumulatie model. Dit onderzoek spitst zich toe op de combinatie van bron 4 en 5. Deze combinatie is, in de context van de totale vermoeiings-analyse, gekozen om een haalbaar onderzoek te garanderen.

Het literatuuronderzoek wijst uit dat het huidige schade-accumulatie model, de lineaire schaderegel (LSR) van **Palmgren** en **Miner**, als niet voldoende accuraat wordt beschouwd om de vermoeiingslevensduur onder variabele belastingspatronen te voorspellen. Voor een *safe-life* analyse wordt een veiligheidsfactor geïntroduceerd. In de praktijk reduceert dit de kritische waarde van de schade van 1.0 tot 0.5, of zelfs 0.2, afhankelijk van de regelgeving. Het voornaamste gebrek van de lineaire schaderegel is het feit dat het geen rekening houdt met het effect van de belastingshistorie op de huidige schade-accumulatie. De regel wordt veelvuldig toegepast door de relatieve eenvoud van de methode en de vele geclassificeerde schepen die de levensduur halen. Dit laatste wordt echter bereikt met inachtneming van de grote veiligheidsfactoren, en kan zodoende ook wijzen op onnodig conservatisme. Het literatuuronderzoek geeft een overzicht van de belangrijkste voorgestelde accumulatieregels als alternatief voor de LSR. Dit is gedaan in drie categorieën: modellen gebaseerd op {continuüm-, breuk- en continuüm schade} mechanica. Van alle besproken modellen is het model zoals voorgesteld door **Leonetti et al.** het meest veelbelovend. Deze voldoet het beste aan de gestelde criteria; een non-lineaire accumulatie, geschikt voor spectrale berekeningen en gevalideerd voor willekeurige **VA** belastingen. Het model van **Leonetti et al.** is gebaseerd op breukmechanica en combineert het voorstel van **Hirt and Kunz** met de **Generalised Random Fatigue Limit (GRFL)**, ook van **Leonetti et al.**. Het accumulatiemodel gebruikt statistische inferentie om op basis van meetdata drie parameters te fitten. De toevoeging van dit onderzoek is de combinatie van de non-lineaire accumulatie van **Leonetti et al.** met de **Effective Notch Stress Concept (ENSC)**: een criterium waarin de geometrische informatie wordt verwerkt. De **ENSC** omvat een S-N curve voor alle geometrieën, en bevat minder spreiding dan de **NSC** (zoals toegepast bij **Leonetti et al.**). Minder spreiding geeft een betere statistische inferentie, en in het verlengde van de hypothese: een accuratere voorspelling van de vermoeiingslevensduur. Fregatten worden nu doorgerekend met de **Hot Spot Structural Stress Concept (HSSSC)**, een methode die qua complexiteit en accuraatheid een compromis is tussen de **NSC** en **ENSC**. Om de kwaliteit per schademodel te onderzoeken is een database met **VA** vermoeiingstesten opgesteld. Deze database bevat variaties in hot spot types, spectrum types, spanningsratio's en geometrieën. De kwaliteit wordt gekwantificeerd met levensduur-spreidings-indices (90% percentiel over het 10% percentiel) van de \log_{10} van de experimentele over de voorspelde levensduren. Dit is {1:1.28, 1:1.16, 1:1.13} voor {de **HSSSC** in combinatie met de LSR (i.e. de referentie casus), de **ENSC** in combinatie met de LSR, de **ENSC** met het model van **Leonetti et al.**}. Een reductie in de spreiding geeft een reductie van het conservatisme op de 97.7% overlevingskans, zoals in de praktijk wordt gebruikt voor het ontwerp van maritieme constructies. Een tweede vergelijking is gemaakt op basis van het **Akaike Information Criterion (AIC)**, zijnde {-44.5, -62.6, -86.3} voor de drie model-combinaties. Beide vergelijkingen tonen een significante verbetering van zowel de spreiding als de likelihood van de schatting van de vermoeiingslevensduur middels de non-lineaire schade accumulatie.

De minimale (fenomenologische) hoeveelheid spreiding in de vermoeiingsdata, die dus met geïdealiseerde lasgeometrieën niet te reduceren is, wordt toegewezen aan variaties in de laskwaliteit, de definitie van "falen" om een experiment te beëindigen en aan de variaties in de residuele spanningen. Het gebruik van de non-

lineaire schadeaccumulatie reduceert de verschillen in kwaliteit van de voorspelde levensduur. Echter, de verschillen zijn niet verdwenen. De voorgestelde methode is dus niet volledig generiek. Wel voorziet het in een relatieve verbetering ten opzichte van de LSR. De onderzoeksresultaten laten zien dat de optimale configuratie van de **NLDAM** verschillend is voor spectra die gedomineerd worden door {lage, midden-tot-hoge} belastings-cycli. Dit wordt toegewezen aan de breukmechanische-aard van het accumulatie model. De breukmechanica beschrijft de scheurgroei, maar niet de initiatie. Echter, bij lage spanningsniveaus wordt een deel van de levensduur, ook van gelaste verbindingen, doorgebracht in de initiatiefase. Om een generiek schademodel te ontwikkelen is de aanbeveling om het *Total Stress Concept (TSC)* te combineren met de **NLDAM** om de totale levensduur te modelleren.

Table of Contents

Summary	v
Samenvatting	viii
Table of Contents	ix
List of Figures	xii
List of Tables	xvi
Abbreviations	xix
1 Introduction	1
1.1 Motivation	1
1.2 Report outline	2
2 Problem definition	3
2.1 Uncertainty in fatigue assessment	3
2.2 Fatigue assessment of frigates	4
2.3 Problem statement	5
2.4 Research question	6
2.5 Research scope	6
2.6 Research goal	7
2.7 Research implications	7
I Literature review	9
3 Fatigue assessment concepts	11
3.1 Nominal Stress Concept	12
3.2 Hot Spot Structural Stress Concept	13
3.3 (Averaged) Effective Notch Stress Concept	15
3.4 Total Stress Concept	15
3.5 Fatigue resistance curves (CA)	16
3.6 Codes, guidelines and recommended practises	19
3.7 Concluding remarks	20
4 Fatigue damage accumulation models	21
4.1 Variable amplitude loading and response	21
4.2 The LDAM by Palmgren-Miner	26
4.3 State-of-the-Art fatigue damage accumulation models	32
4.4 Variable amplitude fatigue damage database	36
4.5 Concluding remarks	38

5 Method	41
5.1 Knowledge gap	41
5.2 Hypotheses	41
5.3 Methods to assess damage accumulation models	42
5.4 Research roadmap	43
II Modelling	45
6 Constant Amplitude analysis	47
6.1 Hot Spot Structural Stress Concept	47
6.2 Effective Notch Stress Concept	48
6.3 CA analysis of the DMO specimens	49
6.4 Generalised Random Fatigue Limit	59
6.5 CA analysis of the VA database specimens	62
6.6 Concluding remarks	65
7 Variable Amplitude analysis	67
7.1 LDAM by Palmgren and Miner	67
7.2 NLDAM by Hirt and Kunz, modified by Leonetti et al.	68
7.3 SCF- and spectrum analysis of the VA database	69
7.4 Results	81
7.5 Model interpretation	103
7.6 Concluding remarks	106
III Judgement and future work	107
8 Evaluation	109
8.1 Conclusions	111
8.2 Discussion	112
8.3 Recommendations	113
9 Implementation	115
9.1 Short term: continuing with the LDAM	115
9.2 Long term: implementing the NLDAM	116
Bibliography	119
A Damage accumulation models	129
A.1 Continuum mechanics based models after 1950	129
A.2 Fracture mechanics based models	143
A.3 (Continuum) Damage mechanics based models	147
B Cited derivations	153
B.1 Miner's physical derivation of the LDAM	153
B.2 Palmgren-Miner consistency with Fracture Mechanics	153
B.3 Leipholz derivation	154
B.4 Leonetti derivation	155
C Author's derivations	157
C.1 Equivalent stress formulations	157
C.2 Ln or log ₁₀	160
D DNV-GL HSSC analysis	161
D.1 DMO CA sample	161
D.2 VA database samples	165
E Through-thickness weld notch stress distributions	173

E.1	DMO CA sample	173
E.2	VA database samples	176
F	FE models for the ENSC	179
G	Results of optimisation per dataset	185
G.1	Comparison of predicted and experimental N	185
G.2	Comparison of CA and VA scatterbands	188

List of Figures

1.1	Fatigue tests of deck samples of the HMS Tromp after approx. 20 years of service [78]. The tests are performed on samples without initial cracks, and indicate significant conservatism w.r.t. the NEN 2063 norm for a K-40 detail. The test are conducted on the detail at Constant Amplitude (CA) and $R = 0 = F_{\min}/F_{\max}$. The assumed reason for the longer fatigue life of the test samples is the redistribution of the residual stresses due to the frigates operations. Secondly, it is speculated that the small plate thicknesses (ca. 9 mm) of the samples provide a longer fatigue life compared to the norm. The weld quality is concluded to be poor after a visual inspection: this is thus not further considered as a reason.	2
2.1	Mapping the uncertainty in fatigue assessment. The numbers in the red boxes indicate the separate sources of uncertainty.	3
2.2	The double sided cruciform joint that assessed in [78], which is a K 40 detail according to the NEN2063 tables [99].	4
2.3	Corrected comparison of the tested samples from the HMS Tromp to the K-40 detail from NEN2063. The lines show the mean stress curve and lower confidence bound of the K-40 criterion.	4
3.1	Fatigue assessment concepts overview [19], placing each concept on a global-local scale, considering intact or cracked geometries, in the stress/strain/energy domain. The bottom figures indicate the required S-N curve. The concepts that are discussed in this thesis are highlighted in blue.	11
3.2	HS Type sketch from DNVGL-CG-0129 [27]	12
3.3	A double sided T-joint with fillet welds, indicating the nominal stress and structural hot spot stress, figure from [19].	12
3.4	Nominal stress based fatigue resistance and influence factors, figure from [111]	13
3.5	Hot spot structural stress-based fatigue resistance and influence factors, figure from [111]	14
3.6	Averaged effective notch stress-based fatigue resistance and influence factors, figure from [111]	16
3.7	Total stress-based fatigue resistance and influence factors, figure from [111]	17
3.8	S-N curves resulting from for the Basquin-, ORFL- (i.e. based on Strohmeyer), BRFL-, and GRFL (or 6PRFLM, here the proposed relation) relations having the same parameters. For the GRFL model the effect of the parameter p ($\rho_{S\infty}$) on the curvature is shown. The figure is from [74].	18
4.1	Definition stress cycle	22
4.2	Load time history, figure is taken from [69]	23
4.3	Rain flow counting procedure example. Explanation based on [22, 69]	23
4.4	The Gassner eight-step block loading sequence [43] translated to a cumulative frequency distribution, figure from [127]	24
4.5	DNV-GL Class Guideline calculation of the longevity per shape factor ξ for a K-40 detail.	25
4.6	Gassner curve dependency on spectrum type as presented by Sonsino [127]	26
4.7	Explanation of the Palmgren-Miner model, from Eurocode 3 [100]	26
4.8	Explanatory figures LI and LS effects, from [121].	28
4.9	LS effects as subset of LI effects.	28
4.10	Research results of the Nordic offshore programme, from Gurney	29
4.11	Lognormal distribution of the D_{crit} , in red the DMO limit of 0.75 is indicated	30
4.12	Research results from Kahl et al., concluding the D_{crit} range of 0.5 to 1.0	31
4.13	Influence of the ζ parameter on the damage accumulation	35

4.14	Research results from Leonetti et al., showing the improved fit of the numerically predicted amount of cycles with the experimental data, compared to the Eurocode 3.	36
5.1	Research roadmap. The blue boxes indicate the means that are used to formulate the answer to the respective questions.	44
6.1	Sketch of the relevant parameters in the semi-analytical ENSC assessment of welded joints in a T- and cruciform joint respectively [112].	49
6.2	Layout of the test setup and the accessory.	50
6.3	Idealised actual weld geometries. Left: FP half-V joint (top attachment) - called the "normal configuration", right: FP half-V joint with counter weld at the root (top attachment) - called the "double configuration"	51
6.4	Free body diagram of the cruciform joint sample as tested by order of DMO. For illustration purposes this figure displays the roller boundary condition at the specimen-accessory interface.	52
6.5	FAT class from DNV-GL-CG-0129	52
6.6	Through-thickness weld notch stress distributions based on the structural stress over the total material thickness at the notch location. Example for the roller case. The numbers at the vertical axes indicate from -1 to 1 the base plate, and below -1 the amount of weld-material in line with the cross-section.	53
6.7	Through-thickness weld notch stress distributions based on the structural stress over the base plate thickness at the notch location. Example for the case with the roller boundary condition.	54
6.8	MLE regression results per fatigue damage criteria on only the regular (non-preloaded) samples and the complete DMO CA dataset, respectively.	57
6.9	MLE regression results per fatigue damage criteria on only the regular (non-preloaded) samples. The experimental data is compared to both the DNV-GL D curve [27] and the FAT100 [54].	57
6.10	Data is the courtesy of Yanxin Qin, it was presented in his paper [112].	58
6.11	ENSC CA fatigue data from [112] -expressing the stress range-, with the GRFL (6PRFLM) from [75] fitted and plotted as a dashed line.	61
6.12	HSSSC CA assessment of the VA database specimens: comparing the CA scatterband from the DNV-GL D curve to the CA fatigue tests.	63
6.13	HSSSC CA assessment of the VA database specimens: comparing the CA scatterband from the DNV-GL D curve to the CA fatigue tests, including the mean stress correction.	64
6.14	ENSC CA assessment of the VA database references: comparing the CA scatterband from [112] to the CA fatigue tests from the references that provide the VA datasets.	65
7.1	Optimisation routine for the GRFL combined with the damage accumulation by [52], as proposed by Leonetti et al.	70
7.2	PP DS Cruciform as tested by Klippstein and Schilling [63].	71
7.3	The histogram is compiled over 100 000 points. The frequency at which the time signal is plotted is 1 Hz.	72
7.4	FP DS Cruciform joint as tested by Agerskov et al. [3].	72
7.5	Frequency and time domain plot of the modified Pierson-Moskowitz spectrum as used in the experiments from [3].	72
7.6	Frequency and time domain plot of the white-noise based spectrum as used in the experiments from [3].	73
7.7	Rainflow histogram of 20000 peaks of the PMMOD64 distribution.	73
7.8	Rainflow histogram of 20000 peaks of the BROAD64 distribution.	73
7.9	PP DS Longitudinal attachment as tested by Agerskov et al. [3].	74
7.10	FP DS Butt joint as tested by Ota et al. [103].	75
7.11	Spectra as applied to the butt jointed joints [103], cycling down from the yield stress. The presented $r_{I,r}$ values represent the weighted mean over all cycles. This is not the value that is used in the calculations.	76
7.12	Spectra as applied to the butt jointed joints [103], cycling up from $\sigma_n = 0$	77
7.13	PP DS Longitudinal plate attachment as tested by Zhang and Maddox [147]	78
7.14	Example for the first three bins of the stress range histogram and corresponding time traces for the three variations as tested by [147].	78
7.15	PP DS Longitudinal edge attachment as tested by Zhang and Maddox [147]	79

7.16 FP DS Butt joint as tested by Zhang and Maddox [148]	79
7.17 Stress range histograms and corresponding time traces for the six spectra as tested by [148]. VT6 is actually the spectrum between VT4 and VT5.	80
7.18 Comparison of the experimental and predicted fatigue life from the LDAM in combination with the HSSSC (base-case). The critical damage is fixed on a value of $D_{crit} = 1$, in line with the original formulation [95, 104].	82
7.19 Comparison of the experimental and predicted fatigue life from the LDAM in combination with the HSSSC (base-case). The critical damage is fixed on a value of $D_{crit} = 1$, in line with the original formulation [95, 104]. For each of the tested specimens the equivalent stress is calculated and plotted on the ordinate.	83
7.20 Scatter histogram of the log10 of the experimental fatigue life over the calculated fatigue life for the LDAM in combination with the HSSSC (base-case).	83
7.21 Comparison of the experimental and predicted fatigue life from the LDAM in combination with the HSSSC (base-case). The critical damage is fixed on a value of $D_{crit} = 1$, in line with the original formulation [95, 104].	85
7.22 Comparison of the experimental and predicted fatigue life from the LDAM in combination with the HSSSC (base-case). The critical damage is fixed on a value of $D_{crit} = 1$, in line with the original formulation [95, 104]. For each of the tested specimens the equivalent stress is calculated and plotted on the ordinate.	85
7.23 Scatter histogram of the log10 of the experimental fatigue life over the calculated fatigue life for the LDAM in combination with the HSSSC (base-case).	86
7.24 Comparison of the experimental and predicted fatigue life from the LDAM in combination with the ENSC. The critical damage is fixed on a value of $D_{crit} = 1$, in line with the original formulation [95, 104].	87
7.25 Comparison of the experimental and predicted fatigue life from the LDAM in combination with the ENSC. The critical damage is fixed on a value of $D_{crit} = 1$, in line with the original formulation [95, 104]. For each of the tested specimens the equivalent stress is calculated and plotted on the ordinate.	88
7.26 Scatter histogram of the log10 of the experimental fatigue life over the calculated fatigue life for the LDAM in combination with the ENSC.	88
7.27 Convergence study on the length of the time trace.	91
7.28 Comparison of the experimental and predicted fatigue life from the NLDAM in combination with the ENSC.	93
7.29 Comparison of the experimental and predicted fatigue life from the NLDAM in combination with the ENSC. For each of the tested specimens the equivalent stress is calculated and plotted on the ordinate.	93
7.30 Scatter histogram of the log10 of the experimental fatigue life over the calculated fatigue life for the NLDAM in combination with the ENSC.	94
7.31 Indication of the results that fall outside of the expected scatterband or trend	95
7.32 Assessing the variations in the predicted and experimental fatigue lives of the HS type A specimens as tested by Zhang and Maddox.	97
7.33 Comparison of CA and VA scatterband of the PP DS Longitudinal attachments, subject to the BROAD64 spectrum from Agerskov et al. (set 2)	100
7.34 Comparison of CA and VA scatterband of the FP DS Butt joints, subject to the Rayleigh up load from Ota et al. (set 6)	100
7.35 Comparison of predicted and experimental fatigue lives of the PP DS Longitudinal attachments, subject to the BROAD64 spectrum from Agerskov et al. (set 2)	101
7.36 Comparison of predicted and experimental fatigue lives of the FP DS Butt joints, subject to the Rayleigh up load from Ota et al. (set 6)	101
7.37 The datapoints that are labeled with an "s" are subject to a peak stress of 441 MPa every 50 blocks (= 5e5 cycles) as is indicated for the 01 sequence in the top-right corner of the figure. The bottom-left corner of the figure contains respectively the 01 and 02 sequence blocks.	102
7.38 Bargraph containing the mean and error-bars of the optimal three θ_{VA} parameters, separated by the dominant stress range level of the spectra. The labels 'Mid-High' and 'Low' indicate the interpretation of the stress range level of the majority of the cycles in the spectrum.	102

7.39	The ENSC is multiplied with $(1/1.39)$ ($= 1/(K_s \cdot K_e)$) to represent the NSC level. The horizontal lines indicate the three equivalent stress levels at which the specimens are tested, according to the inference on the 38 CA specimens. The figure shows the conservative nature of the estimate with the generalised ENSC curve for these specimens.	105
A.1	Comparison of the DDCA with DLDT and DCA [88]	131
A.2	Sketch of the S-N curves of the damage models closely related to the Palmgren-Miner model	132
A.3	Modified S-N curve by Leipholz [70]	133
A.4	Research results from Ben-Amoz	135
A.5	Research results from Gao et al., comparing the traditional Corten-Dolan model [15], the existing model by Zhu et al. [151] and the proposed model by Gao et al. for two steel types.	138
A.6	Comparison of predicted fatigue life with experimental data for two-step cyclic loading of P355NL1 steel, from [115]	140
A.7	S-N Fatigue damage envelope by Pavlou, illustration of the concept.	141
A.8	Comparisons between tested lives and predicted lives of P355NL1 under spectrum loadings, from [152].	141
A.9	Research results from Liu et al., comparing three different models [42, 77, 141] for two steel types.	142
A.10	Representation of the Representative Volume Element, figure from [72]	149
D.1	DS Cruciform by Klippstein and Schilling	165
D.2	DS Attachment by Agerskov et al.	166
D.3	DS Half-V cruciform by Agerskov et al.	166
D.4	DS Butt welds by Ota et al.	167
D.5	DS Longitudinal attachment HS Type A by Zhang and Maddox	167
D.6	DS Longitudinal attachment HS Type B by Zhang and Maddox	168
D.7	SS Butt joint by Zhang and Maddox	168
D.8	DS Longitudinal attachment by Rörup and Petershagen	169
E.1	Through-thickness weld notch stress distributions based on the structural stress over the base plate thickness at the notch location. Boundary condition: Roller.	173
E.2	Through-thickness weld notch stress distributions based on the structural stress over the base plate thickness at the notch location. Boundary condition: Hinge.	174
E.3	Through-thickness weld notch stress distributions based on the structural stress over the base plate thickness at the notch location. Boundary condition: 5% of total force.	175
F.1	DS Cruciform by Klippstein and Schilling	179
F.2	DS Attachment by Agerskov et al.	180
F.3	DS Half-V cruciform by Agerskov et al.	180
F.4	DS Butt welds by Ota et al.	181
F.5	DS Longitudinal attachment HS Type A by Zhang and Maddox	181
F.6	DS Longitudinal attachment HS Type B by Zhang and Maddox	182
F.7	SS Butt joint by Zhang and Maddox	182
F.8	DS Longitudinal attachment by Rörup and Petershagen	183
G.1	PP DS Cruciform Rayleigh by Klippstein and Schilling	186
G.2	PP DS Longitudinal attachment type A BROAD64 by Agerskov et al.	186
G.3	PP DS Cruciform BROAD64 by Agerskov et al.	186
G.4	PP DS Cruciform PMMOD64 by Agerskov et al.	186
G.5	FP DS Butt joint Rayleigh down by Ota et al.	187
G.6	FP DS Butt joint Rayleigh up by Ota et al.	187
G.7	PP DS Longitudinal attachment type A Linear by Zhang and Maddox	187
G.8	PP DS Longitudinal attachment type B Linear by Zhang and Maddox	187
G.9	FP SS Butt joint Log-Linear by Zhang and Maddox	187
G.10	FP DS Cruciform Rayleigh mod. by DMO	187
G.11	PP DS Cruciform Rayleigh by Klippstein and Schilling	188
G.12	PP DS Longitudinal attachment type A BROAD64 by Agerskov et al.	188
G.13	PP DS Cruciform BROAD64 by Agerskov et al.	188

G.14 PP DS Cruciform PMMOD64 by Agerskov et al.	188
G.15 FP DS Butt joint Rayleigh down by Ota et al.	188
G.16 FP DS Butt joint Rayleigh up by Ota et al.	188
G.17 PP DS Longitudinal attachment type A Linear by Zhang and Maddox	189
G.18 PP DS Longitudinal attachment type B Linear by Zhang and Maddox	189
G.19 FP SS Butt joint Log-Linear by Zhang and Maddox	189
G.20 FP DS Cruciform Rayleigh mod. by DMO	189

List of Tables

3.1 Summary of class codes and recommended practises. DS = Double sided, SS = Single sided confidence interval	20
4.1 Counted reversals	23
4.2 Counted cycles	23
4.3 Histogram that results from the rain flow counting procedure applied to the load history from figure 4.2a	23
4.4 Database summary of random VA spectrum loading of steel welded joints	37
4.5 Table to summarise the comparison of the presented fatigue damage accumulation models. Green boxes indicate full compliance (three times a "yes") and yellow boxes indicate models that are not strictly non-linear, but comply with the demands for spectral calculations and validity for stochastic VA loads.	39
5.1 Knowledge gap visualisation. The references show the known research and class efforts. The grey marked cells indicate the combinations of fatigue damage criteria and damage accumulation models that are not yet made in literature. The last column contains the hypotheses of proportionality between the complexity and scatter reduction. The three roman numbers indicate the cases that are compared in this paper.	41
5.2 Visualisation of the four hypotheses and their relation. The letters in [brackets] are used to refer to each combination, whereas the H# indicates the hypotheses.	42
6.1 r_s values for the counter welds, for the structural stress as calculated over only the base plate or the total thickness (including the counterweld contribution). See figure 6.3 for the drawing of the double and normal weld configurations.	54
6.2 Stress in N/mm^2 at 10 kN load applied to the specimen, per fatigue damage criterion, using a roller connection. "Double" refers to the sample with a counter weld at the root, see figure 6.3.	55
6.3 Stress in N/mm (per unit sample width) at 10kN load applied to the specimen, per fatigue damage criterion, using a hinged connection. "Double" refers to the sample with a counter weld at the root, see figure 6.3.	55
6.4 Stress in N/mm (per unit sample width) at 10kN load applied to the specimen, per fatigue damage criterion., using a 5% force connection. "Double" refers to the sample with a counter weld at the root, see figure 6.3.	56
6.5 Based on amplitudes - not ranges, for comparison with the results from [112]	60
6.6 Optimum six parameters of the GRFL based on stress ranges	61
6.7 Database summary of CA fatigue tests of steel welded joints, equal to the specimens that form the VA database	62
6.8 Stresses corresponding to 100kN load in total (50kN on both sides), rounded to MPa.	62
7.1 Results for the cruciform samples from [63] for verification of the constructed model with the results from [75]	69

7.2	Specimens and characteristics: plate width w_p , base plate thickness t_b , attachment/ cross-plate thickness (i.e. height) t_c , weld leg length l_w and height h_w , whether it is symmetrical (δ) and the bending stress ratio r_s . All dimensions are in mm. For non symmetrical cruciforms two weld dimensions and r_s values are given: l_w , h_w and r_s half-V side / l_w , h_w and r_s counter side. . . .	69
7.3	Spectrum as was applied to the DMO half-V welded cruciform specimens. The right-most column is the spectrum for a Rayleigh distribution without modification. The column left of that contains the spectrum that was applied to the specimen, and indicates the removal of low stress range cycles.	81
7.4	Optimised parameters	92
7.5	Linear spectrum as applied by Zhang and Maddox	96
7.6	Fatigue life scatter index per dataset of the VA fatigue database. Yellow boxes indicate a scatter index between 1:1.10 and 1:1.20, orange is 1:1.20 and above.	98
7.7	Expected values of the fatigue life ratio for the VA fatigue database. Yellow boxes indicate a deviation of 5 to 10% from the ideal mean of 1.00, orange is 10% and above.	99
7.8	Optimal θ_{VA} configuration per dataset	100
7.9	Weighted means of the three θ_{VA} parameters, separated by the dominant stress range level of the spectra. The labels 'Mid-High' and 'Low' indicate the interpretation of the stress range level of the majority of the cycles in the spectrum.	102
7.10	Comparing the expected damage value for the LDAM and of the optimised θ_{VA} set for the NLDAM	104
7.11	NSC and ENSC results for the cruciform samples from [63]	104
7.12	Comparing the optimal six parameters of the GRFL based on stress ranges for both the 38 CA specimens from Klippstein and Schilling as used by Leonetti et al. and for the 1806 specimens as collected by Qin et al..	104
7.13	Comparing the NSC- and ENSC-based fatigue life predictions. The values of N_{pred} correspond to the intersections of the horizontal lines and S-N curves in figure 7.39. The ratio is equal to $N_{pred}(NSC)/N_{pred}(ENSC)$. The expected value of the critical damage is equal to 1.57 (the expected value of the critical damage in the NSC assessment according to Leonetti et al.) times the ratio.	105
7.14	Summarising research results. n is the number of parameters as used by the model.	106
A.1	Research results from Hectors and de Waele for two-stage block loading for a combination of H-L and L-H sequences. Each value is given as an expression of $D_{crit} = N_{predicted}/N_{experiment}$. . .	146

Abbreviations

6PRFLM	6 Parameter Random Fatigue Limit Model	LI	Load Interaction
AIC	Akaike Information Criterion	LS	Load Sequence
BIC	Bayesian Information Criterion	MC	Monte Carlo
BRFL	Bilinear Random Fatigue Limit	MCF	Medium Cycle Fatigue
CA	Constant Amplitude	MF	Membershipfunction
CAT	Fatigue CATegory	MLE	Maximum Likelihood Estimate
CDM	Continuum Damage Mechanics	MSC	Macroscopic Stress Concentration
COV	Coefficient of Variation	NLC	Non-load carrying
DCA	Damage Curve Approach	NLCD	Non-linear Continuous fatigue Damage
DDCA	Double Damage Curve Approach	NLDAM	Non-linear Damage Accumulation Model
DLDT	Double Linear Damage Theory	NSC	Nominal Stress Concept
DMO	Defence Materiel Organisation	OL	Overloads
ENSC	Effective Notch Stress Concept	ORFL	Ordinary Random Fatigue Limit
FAT	Fatigue Class	PPL	Parameter Profile Likelihood
FE	Finite Element	RAO	Response Amplitude Operator
FFE	Fatigue Fracture Entropy	RFL	Random Fatigue Limit
FLS	Fatigue Limit State	RLDM	Relative Linear Damage Model
FORM	First Order Reliability Method	RMS	Root Mean Square
FSS	Full Scale Specimen	RVE	Representative Volume Element
GRFL	Generalised Random Fatigue Limit	SCF	Stress Concentration Factor
HCF	High Cycle Fatigue	SIF	Stress Intensity Factor
HSS	High Strength Steel	SSS	Small Scale Specimen
HSSSC	Hot Spot Structural Stress Concept	TSC	Total Stress Concept
IACS	International Association of Classification Societies	UL	Underloads
LC	Load carrying	ULS	Ultimate Limit State
LCF	Low Cycle Fatigue	VA	Variable Amplitude
LDAM	Linear Damage Accumulation Model		
LEFM	Linear Elastic Fracture Mechanics		

1

Introduction

Fatigue is a governing limit state for maritime structures [19], including naval ones. Welded joints are typically critical. Balancing the resistance with the demand of the fatigue equation is a challenge when large uncertainties are in place, in particular for naval ships. The estimated and actual operational profile based demand might diverge up to a factor of 2 [133] solely from a difference in usage rate. Beside that, sailing areas for the future are unsure. At the same, the performance of fatigue assessment concepts range from low effort-low accuracy (e.g. **Nominal Stress Concept**) to high effort-high accuracy (e.g. **Total Stress Concept**) as a result of involving either an intact or cracked geometry parameter, incorporating local or global information, etc. and define the resistance uncertainty. A reliability analysis involving the demand and resistance uncertainty provides safety factors, increasing the navy ship hull structural member scantlings (i.e. structural weight).

In this chapter the motivation for this research is presented and elaborated upon (Section 1.1). It is followed by the outline of the report (Section 1.2).

1.1. Motivation

For the new generation M-frigates the **Defence Materiel Organisation (DMO)** is facing the challenge to reduce the structural weight, without a reduction of fatigue strength and preventing at the same time for increased production and maintenance efforts. Since fatigue is a governing limit state for maritime structures [19], a reduction of the (demand and) resistance uncertainty seems an opportunity to reduce structural weight without a reduction of fatigue strength.

The most recently used fatigue standard at **DMO** is the NEN2063 [99], a Dutch national standard from 1988. Application covers a range of arc-welded joint configurations. The NEN2063 standard adopted the **Nominal Stress Concept (NSC)** and the linear Palmgren-Miner damage accumulation model. However, because of the relatively large plate thickness of ± 30 (mm) used for the fatigue test specimens to develop the fatigue resistance (i.e. S-N) curves, the poorly documented fatigue test data and the significantly larger fatigue strength of tested samples taken from the HMS Tromp strength deck, the validity of the NEN2063 standard today for fatigue design of the new generation M-frigates is questioned. At the same time, the NEN2063 norm has been withdrawn since November 2010. Many fatigue assessment developments have been made since.

The follow-up of the NEN2063 standard, the Eurocode 3, as well as dedicated maritime industry (class) standards [27, 55] allow to use fatigue assessment concepts involving more local information in comparison to the nominal stress concept. However, the linear Palmgren-Miner fatigue damage accumulation model is still adopted. Besides that, the critical value for the accumulated damage under this linear accumulation rule varies widely: from 1.0 [27], to 0.75 (**DMO** practise), 0.5 [54] and 0.2 (for fluctuating mean stresses [54]). This critical value has a linear relation with the predicted fatigue life, proving the significance of the uncertainties in the damage accumulation.

Naval ships did not necessarily have a class notation in the past. For the design of new ones classification societies will be involved, meaning classification standards will be imposed although classification societies allow to deviate in case sufficient proof is provided. Naval ships predominantly transport people (rather than

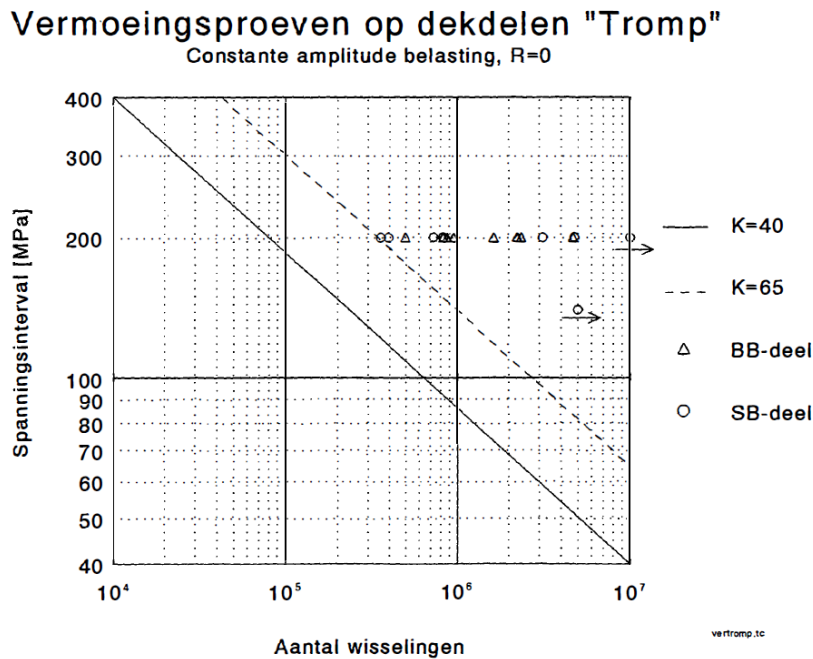


Figure 1.1: Fatigue tests of deck samples of the HMS Tromp after approx. 20 years of service [78]. The tests are performed on samples without initial cracks, and indicate significant conservatism w.r.t. the NEN 2063 norm for a K-40 detail. The tests are conducted on the detail at **Constant Amplitude (CA)** and $R = 0 = F_{\min}/F_{\max}$. The assumed reason for the longer fatigue life of the test samples is the redistribution of the residual stresses due to the frigates operations. Secondly, it is speculated that the small plate thicknesses (ca. 9 mm) of the samples provide a longer fatigue life compared to the norm. The weld quality is concluded to be poor after a visual inspection: this is thus not further considered as a reason.

cargo) and provide service. The ship structure is typically thin walled - plate/shell thickness t_p 10 [mm] [133]- in contrast to typical offshore structures involving t_p values in the range of 20 to 90 [mm] [101]. The fatigue assessment concept to be selected should be capable to deal with plate/shell thickness effects.

The possibility to adopt other fatigue assessment methods requires an investigation to decide which one is best. Recent fatigue damage accumulation model developments pose good potential for weight reduction, ideally in combination with State-of-the-Art fatigue assessment concepts.

1.2. Report outline

The report starts with a definition of the problem, based on the standpoint of the initiating party of this research, **DMO** (Chapter 2). After this the report is separated into three parts: I) Literature review, II) Modelling and III) Judgement and future work. Part I presents the relevant scientific research on both fatigue assessment concepts (Chapter 3) and fatigue damage accumulation models (Chapter 4): the two elements of the fatigue assessment method that are subject of this thesis. Chapter 5 presents the analysis of the scientific knowledge gap and the proposed method to reduce this gap thereafter.

In Part II the modelling is separated into the **Constant Amplitude (CA)** and **Variable Amplitude (VA)** analysis. The first is subject of chapter 6, and discusses the validity of fatigue data and S-N curves from class, as well as fatigue data from scientific literature for the fatigue assessment of **DMO**. In chapter 7 the **VA** fatigue models are presented in detail, as well as the research results.

Last but not least, Part III presents the evaluation of the results (Chapter 8), followed by the recommended implementation strategies (Chapter 9).

2

Problem definition

To specify the problem that motivates this research (see Section 1.1), this chapter concerns the definition of the problem as is posed by DMO, as well as the context and implications of this stated problem. Note that the analysis of this problem in the scientific context, as well as the formulation of the research question based on the identified knowledge gap, will be the content of chapter 5.

At first the context for the problem is presented. This is done in relation to the identified main sources of uncertainty in fatigue assessment (Section 2.1), in relation to an analysis of the fatigue assessment of frigates (Section 2.2). This is followed by the problem statement (Section 2.3), research question (Section 2.4), scope (Section 2.5), goal (Section 2.6) and the implications of the research (Section 2.7).

2.1. Uncertainty in fatigue assessment

To assess the expected fatigue life-time of a structure, reality is simplified and captured into models. Figure 2.1 shows a diagram that captures the transition of the physical world to the modelled world, and indicates in red the sources of uncertainty that arise from this transition. The central question is whether the calculated total damage is representative for the real-world case.

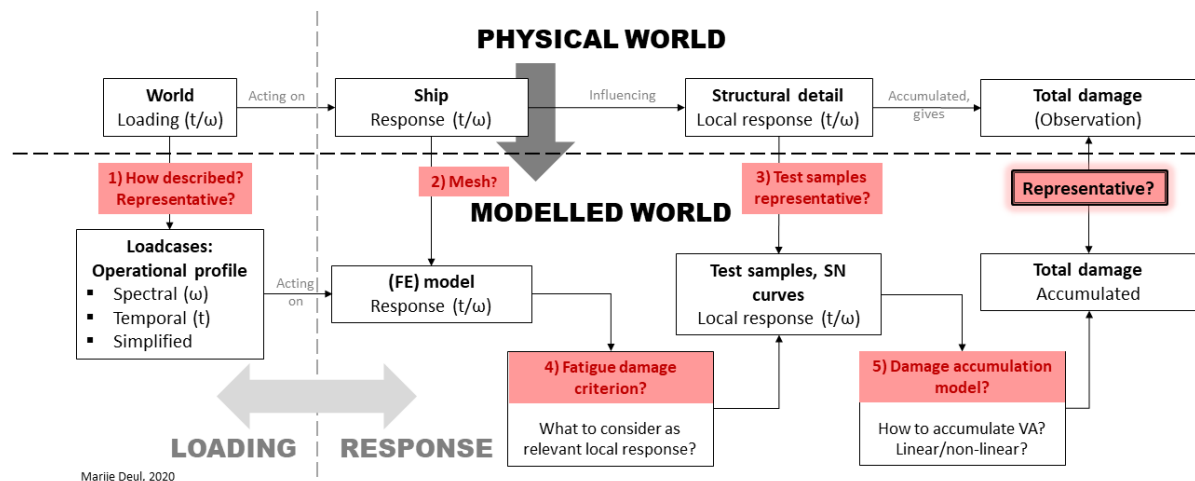


Figure 2.1: Mapping the uncertainty in fatigue assessment. The numbers in the red boxes indicate the separate sources of uncertainty.

The identified sources of uncertainty are (as indicated in red), with the numbers that will be used for further reference to the sources:

Source 1: Fatigue loading & response conditions

This includes the quality of the estimated operational profile (usage factor, operational area, etc.) and possible simplifications.

Source 2: FE model uncertainty

The modelling parameters of the FE model of the total ship are a source of uncertainty as different settings influence the outcome.

Source 3: Fatigue resistance

The fatigue resistance covers the representivity of the tested samples of the structural details. That includes **Constant Amplitude (CA)/ Variable Amplitude (VA)** and size effects (which is relevant, depending on the applied fatigue assessment concept).

Source 4: Fatigue damage criterion

This comprises the selection of the fatigue assessment concept. The literature review on the fatigue assessment concepts is content of chapter 3.

Source 5: Fatigue damage accumulation

The linear Palmgren-Miner sum of 1 (as stated by the DNV-GL rules [27]) is typically reduced based on engineering judgement. This reduction includes conservatism. Non-linear models are also proposed and offer a choice in concepts. The literature review on the fatigue damage accumulation models is content of chapter 4.

2.2. Fatigue assessment of frigates

Answering to the question of the sponsor of this research (DMO), the focus is on naval applications. Before the presentation of the research goal (section 2.6) the link to the naval applications and the assessment of their current state is presented here. This is what provides the motivation for this research.

2.2.1. Research motivation

The TNO report from 1995, with figure 1.1, indicates that the 20 year old samples have a longer life-time than the NEN2063 prescribes for the respective nr. 204 detail (see figure 2.2).

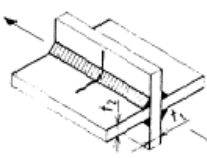
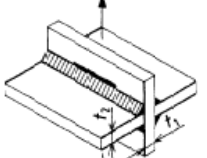
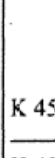
nr.	omschrijving	$\Delta\sigma_y$	$\Delta\sigma_x$	$\Delta\tau_{xy}$
204	Hoeklassen (flanklassen)			
	$t_2 \leq 3 t_1$			
	$t_2 > 3 t_1$	K 50	K 35	K 40

Figure 2.2: The double sided cruciform joint that assessed in [78], which is a K 40 detail according to the NEN2063 tables [99].

It should be noted that figure 1.1 compares the 95% confidence bound for 95% probability of survival, with the actual measured data. For a fair comparison this measured data should be compared to the mean values. For this comparison, see figure 2.3. The transformation of the 95% confidence to the 50% confidence level is done using equation (2.1), assuming a normal distribution. Here $\sigma = 0.2$, $m = 3$ and $C_{95\%} = N_{95\%} S^m$ according to the Basquin relation.

$$N_{50\%} = 10^{(\log C_{95\%} + 1.96\sigma) - m \log S} \quad (2.1)$$

It is observed that the line that all datapoints provide a significantly longer fatigue life that what is used as the mean stress criterion. This deviation can mean the following:

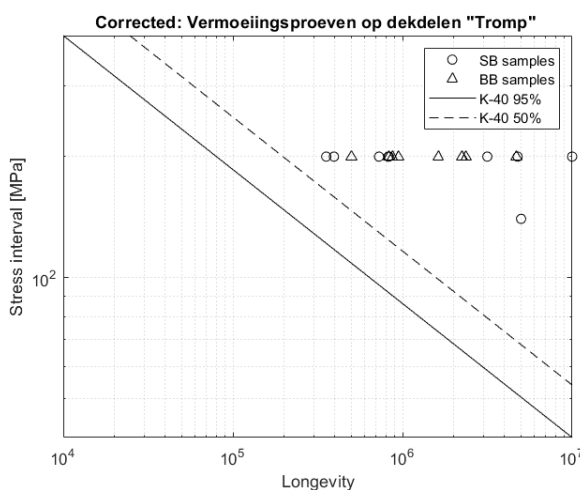


Figure 2.3: Corrected comparison of the tested samples from the HMS Tromp to the K-40 detail from NEN2063. The lines show the mean stress curve and lower confidence bound of the K-40 criterion.

1. Either the detail is considered as K40 and the classification of the detail includes (excessive) conservatism. However, the conservatism of the K 40 detail is already expressed in its confidence and probability of survival. This hypothesis is rejected.
2. Or, the 20 years of service were beneficial for the detail and actually increased its lifetime so that the lifetime after the 20 years is more than it was at the start. Operating from the assumption that fatigue damage can not be undone, this hypothesis is rejected.
3. Or, there are principles in place that were not part of the assessment. TNO lists the redistribution of residual stresses and a limited plate thickness as aspects that are beneficial but not accounted for. Another affecting property is multi-axiality. Multi-axiality is however excluded from the scope to propose a feasible research.

It is assumed that reality is governed by the third reason [78]. The TNO report discusses the beneficial nature of highly tensile loads in the beginning of the lifetime, resulting in a redistribution of the production induced residual stresses throughout the material [78]. Residual stresses pose a shift of the mean stress, but do not affect the stress amplitude. A positive residual stress (tensile) increases the mean stress and is thus unfavourable for the fatigue life. Apart from that a negative stress (compressive) might pose a net negative stress on the hot spot. In the case of a net negative stress a microcrack can hardly grow [121]. Because the amplitude is not affected by the residual stress, cyclic slip is still nucleating microcracks. Typically the residual stresses are high at the welds right after production. The advice of TNO [78] is to not consider a decrease of the residual stresses due to a lack of information on this characteristic. It is speculated that the residual stresses reduce over the life time and that a high load (i.e. heavy weather) during the trials positively affect the fatigue life time. The article by Lee et al. [68] reports for welded specimens at different stress levels a 250% increase in life-time when not accounting for residual stresses. This indicates that the redistribution of residual stress has a significant influence on the predicted life-time.

The second aspect that is not accounted for is the limited plate thickness. The NEN2063 poses a correction factor for plate thicknesses above 30 mm that reduces the life time; extrapolating this to lower plate thicknesses yields the hypothesis that thinner plates have a longer fatigue life. It should be noted that all these considerations are for the **Nominal Stress Concept**, which does not account for the size effect. Applying a damage criterion that accounts for the size effect (like the **Effective Notch Stress Concept** or **Total Stress Concept**) solves this. A detailed explanation of the stress concepts (fatigue damage criteria) is included in chapter 3.

2.2.2. Engineering practise at Damen Schelde Naval Shipbuilding

Damen Schelde Naval Shipbuilding is the common contractor for frigates of the Royal Netherlands Navy. They follow the requirements of the customer, and indicate to commonly use for the fatigue assessment the DNV-GL Class Guideline DNVGL-CG-0129 "Fatigue Assessment of Ship Structures" [27]. This guideline allows the use of the **NSC**, **HSSSC** and **ENSC**, and Damen Schelde adopts the **HSSSC**. This is done to ensure practical engineering applicability: the **HSSSC** can be determined from only a shell model of the total vessel to determine the far field stress for each detail.

The **HSSSC** does not explicitly account for the thickness effect, but allows a correction for thicker plates. For thinner plates the potential advantage from the thickness effect is unused. Secondly the DNVGL-CG-0129 points to the Rules: DNVGL-RU-SHIP-Pt3Ch9, for general ship types list a design life of 25 years, during which $D_{crit} \leq 1$. **DMO**, as a customer of Damen Schelde, requires $D_{crit} \leq 0.75$. This reduction is based on the fatigue life reduction related to the occurrence of slamming. Besides that, as is confirmed in [111], the **HSSSC** does not reduce the conservatism, but merely the uncertainty as incorporated in the fatigue assessment. However, as the uncertainty determines the scatterband, the mean is not affected, but the 95% probability of survival bound is. The problem of the conservative fatigue life estimate as is shown in figure 2.3 still holds.

2.3. Problem statement

Originating from the report of the fatigue tests of samples of the HMS Tromp, as presented in figure 2.3, the problem is stated as:

PROBLEM STATEMENT

*The **current fatigue assessment method**, as used to assess the fatigue lifetime of frigates, incorporates excessive conservatism due to an accumulation of conservative assumptions and uncertainty. This needs to reduce to avoid excessive structural weight.*

In this statement the **current fatigue assessment method** indicates the use of the Haibach modification of the **LDAM** by Palmgren and Miner (DNV-GL-CG-0129, Damen Schelde practise) with a critical damage sum of 0.75 (**DMO** requirement) on a vessel that is evaluated using the **HSSSC**.

The observation is that there is excessive conservatism in the current assessment methods, which can be reduced by including more insight in the State-of-the-Art fatigue assessment concepts, together with an effective choice of fatigue damage accumulation method. More hypotheses are formulated and will be addressed in section 5.2.

2.4. Research question

Following the problem statement, the central research question in this thesis is stated as:

RESEARCH QUESTION

*How can State-of-the-Art fatigue damage criteria and fatigue damage accumulation models be applied, combined, and updated, to provide a balance between accuracy and complexity whilst reducing the uncertainty of the fatigue assessment methods **as currently presented** in design codes?*

To answer the research question, the following sub-questions are answered. The sources of uncertainty to which a reference is made are from section 2.1 and figure 2.1.

1. **Source 3** What is the validity of the S-N curves generated with the samples that are used in Commercial Fatigue codes for the naval-specific detail?
2. **Source 4** Which fatigue damage criterion from literature provides the most suitable balance between accuracy and cost?
3. **Source 5** What is the validity of the **LDAM** for random **VA** loads when using the **HSSSC**?
4. **Source 4** What is the validity of the **LDAM** for random **VA** loads when incorporating more local information into the fatigue assessment (**ENSC**)?
5. **Source 5** What are feasible alternatives for the **LDAM**?
6. **Source 5** If possible, how can the selected alternatives from Q5 be improved?
7. **Source 4 and 5** What combination of State-of-the-Art Fatigue damage criteria and damage accumulation models has the largest potential?
8. **Source 4 and 5** What is the improvement of the novel selected combination from Q7 compared to the use of the **HSSSC** with the **LDAM**?
9. **Source 4 and 5** What is the effect of the spectrum type on the validity of the fatigue life prediction, using the novel selected combination from Q7?
10. **Source 4 and 5** What is the effect of the mean stress on the validity of the fatigue life prediction, using the novel selected combination from Q7?

2.5. Research scope

To propose a feasible study, some limitations are imposed on the scope. The imposed limitations are deemed sufficient to attain the goal of this thesis, which is to propose and validate a novel fatigue life model (with the focus on the damage accumulation and fatigue damage criterion) for naval ship applications.

The research is limited to **steel** (excluding RVS, and other metals of which the similarity in fatigue mechanisms is not certain), to **welded joints** and to **uniaxial loading**.

There are five general origins of conservatism identified, as presented in figure 2.1. To improve the fatigue assessment method, the selection of the **fatigue damage criterion (source 4) in combination with a State-of-the-Art damage accumulation model (source 5)** is investigated in depth in this research.

2.6. Research goal

To rewrite the problem into something that can be achieved by actions, it is formulated in the form of a goal. The goal is bi-fold and is formulated as follows:

GOAL

- 1) *To deliver recommendation for the fatigue assessment method, fit for naval applications, based on State-of-the-Art fatigue work on VA damage accumulation and fatigue damage criteria, to reduce the conservatism of the fatigue assessment.*
- and
- 2) *To validate the recommended method against experimental data and to compare the novel model to the current assessment method.*

This research will be called successful if the implementation of a State-of-the-Art fatigue assessment method (for which either the fatigue assessment concept, a damage accumulation model, or both is/are used) has proven to provide a less conservative and at least equally accurate estimate of the fatigue life, compared to the current practise. The conservatism is compared by the Log-Likelihood of the fatigue life predictions and the accuracy is expressed by the scatter index of the calculated and experimental fatigue life fractions.

2.7. Research implications

The implications of this research, both practical, scientific and societal, have to be acknowledged beforehand to provide a proper context and ethically just considerations in the research process.

2.7.1. Practical

The practical implication of this research is what affects the practise at DMO. The motive for this research is the deviations of the measured samples compared to the NEN2063, which was approximately 30 years ago. Standards and methods have developed since then. This thesis offers a summary of the relevant research and considerations with regards to the reduction of uncertainty in the fatigue assessment.

The research works towards the development of a novel Naval Fatigue Standard, and resulting to engineering practises. The novel standard should have a scope covering the specific thin-walled structures and have the objective to design the structure to meet the lifetime requirement without being overly conservative, which focuses on the interests that differ from commercial ships.

2.7.2. Scientific

This research aims to promote the practical implementation of scientific material. Many papers are presented in chapter 4 that present a modified or novel damage accumulation model, whereas all class codes still only use the Haibach modification of the Palmgren-Miner model. The developments towards the formulation of a Naval Fatigue Standard based on State-of-the-Art research results promotes the use of novel models. The added scientific value of this research lies in the combined insights in developments in fatigue damage criteria and damage accumulation models. This is discussed in more detail in section 5.1.

2.7.3. Societal

The research is sponsored by DMO, who is responsible for the structure design of the new generation M-frigates for the Royal Netherlands Navy. Therefore this research will contribute to the development of vessels that can operate in war. The ethics and political considerations of the operations of the frigate are not part of this research, but the contribution and context of a frigate is to be acknowledged. This research will focus on the reduction of excessive safety margins as incorporated in the fatigue assessment, and as such either reduce the weight or the costs related to weld quality demands. Both contribute the the success of the new-

built frigate, but do not change its mission.

Reduction of safety factors comes with the requirement so firmly substantiate the reduction. The frigate has to provide a safe platform for the crew and the structural integrity should not compromise its missions.

I

Literature review

3

Fatigue assessment concepts

As was presented in figure 2.1, the fatigue assessment concept is one of the identified blocks that influences the level of uncertainty in the fatigue life estimate. This chapter provides the explanation and relation, based on a literature review, of five of the main concepts from literature and their place in the class codes and recommended practises that are applicable for frigates. Chapter 4 provides the literature review of the other source of uncertainty that is part of the scope of this thesis: the damage accumulation model.

Different fatigue damage criteria (also called fatigue assessment concepts) are presented in literature and are summarised in figure 3.1 using a classification based on [19]:

- Global or local information
- An intact or cracked geometry
- Stress, strain or energy based
- Point, line or area/volume based

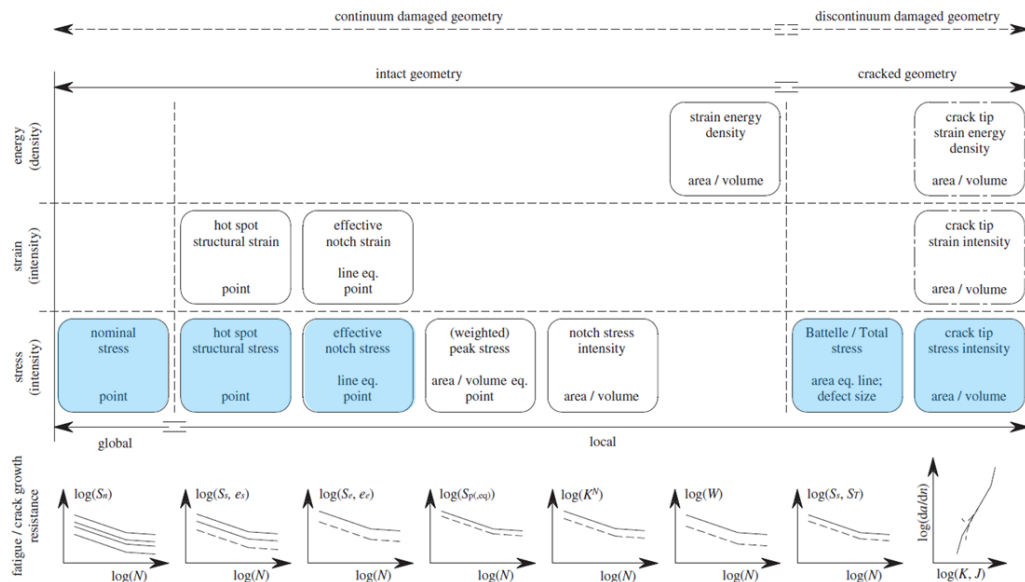


Figure 3.1: Fatigue assessment concepts overview [19], placing each concept on a global-local scale, considering intact or cracked geometries, in the stress/strain/energy domain. The bottom figures indicate the required S-N curve. The concepts that are discussed in this thesis are highlighted in blue.

The ones discussed in this thesis are the **Nominal Stress Concept (NSC)**, the **Hot Spot Structural Stress Concept (HSSSC)**, the **Effective Notch Stress Concept (ENSC)** and the **Total Stress Concept (TSC)** (including the **Stress Intensity Factor (SIF)**). The first three concepts are selected as these are commonly applied in engineering standards and guidelines [27, 99, 100, 111]. The SIF is not studied independently, but is incorporated in the TSC. The **Total Stress Concept (TSC)** is not yet widely applied in engineering, but is included to also assess a cracked geometry method that has the promising feature of having one S_T -N curve to consider all structural details, with less scatter than the **ENSC**.

A comparison between the **NSC**, **HSSSC**, **ENSC** and the **TSC** is provided in the work by Qin et al. [111]. The figures from this paper are used in this chapter to illustrate the respective benefits and differences.

The first three concepts (**Nominal Stress Concept (NSC)**, **Hot Spot Structural Stress Concept (HSSSC)** and **Effective Notch Stress Concept (ENSC)**) are continuum domain fatigue damage criteria. The **SIF** and **TSC** are fracture domain criteria. This is shown in figure 3.1. Chapter 4 presents novel damage accumulation models in this subdivision alike.

Fatigue hot spots can typically be separated into three categories [27], see figure 3.2.

- Type A Being notches at the weld end, perpendicular to the weld seam. The specimen will develop a crack in the through-thickness direction of the base plate.
- Type B Being notches at the weld end, parallel to the weld seam. The specimen will develop a crack over the full width of the plate, along the weld seam.
- Type C Being notches in the joint cross section, along the weld seam. The specimen will develop a crack in the through-thickness direction of the base plate.

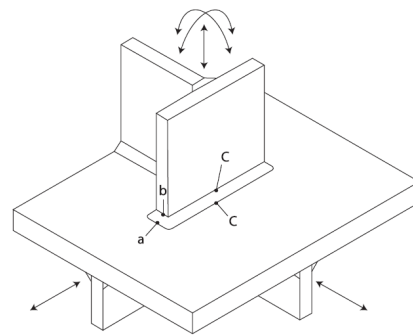


Figure 3.2: HS Type sketch from DNVGL-CG-0129 [27]

3.1. Nominal Stress Concept

For the resistance of a welded joint in the **Medium Cycle Fatigue (MCF)** and **High Cycle Fatigue (HCF)** range, the most basic criterion is the nominal stress range [19]. This is a point criterion, meaning the nominal stress at only one point in the structural detail is used, to express the reference stress of the detail by means of a linear intact geometry parameter. Figure 3.3 shows the nominal stress for a T-joint as σ_n . The distribution through the base plate thickness is assumed to be linear. This means that the nature (i.e. shape and size) of the specimen should be accounted for in the selected S-N curve. For further analysis $S_n = \Delta\sigma_n$ is used.

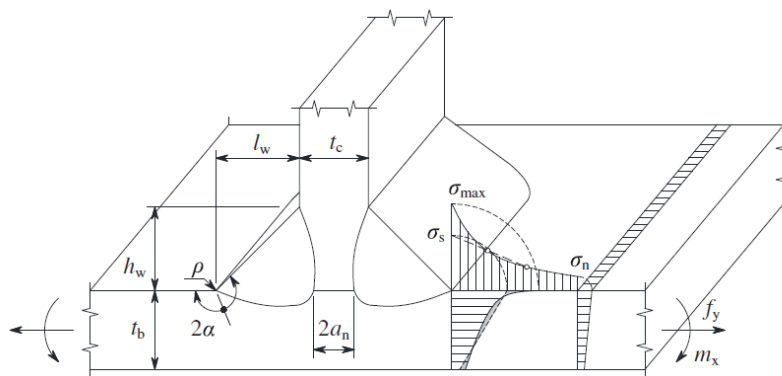


Figure 3.3: A double sided T-joint with fillet welds, indicating the nominal stress and structural hot spot stress, figure from [19].

Figure 3.4 shows for the **NSC** the scatter in the datapoints, plotted in different subdivisions. It should be noted that the difference between thin ($< 20\text{mm}$) and thick plates (figure 3.4b) is clear. When combining all datapoints bluntly, the standard deviation σ is 0.32 and the strength scatter range index $T_{\sigma S} = 1 : (S_{10}/S_{90})$ [113] is

1:2.29. It should be noted that some of this scatter is reduced when using the designated **FAT** classes.

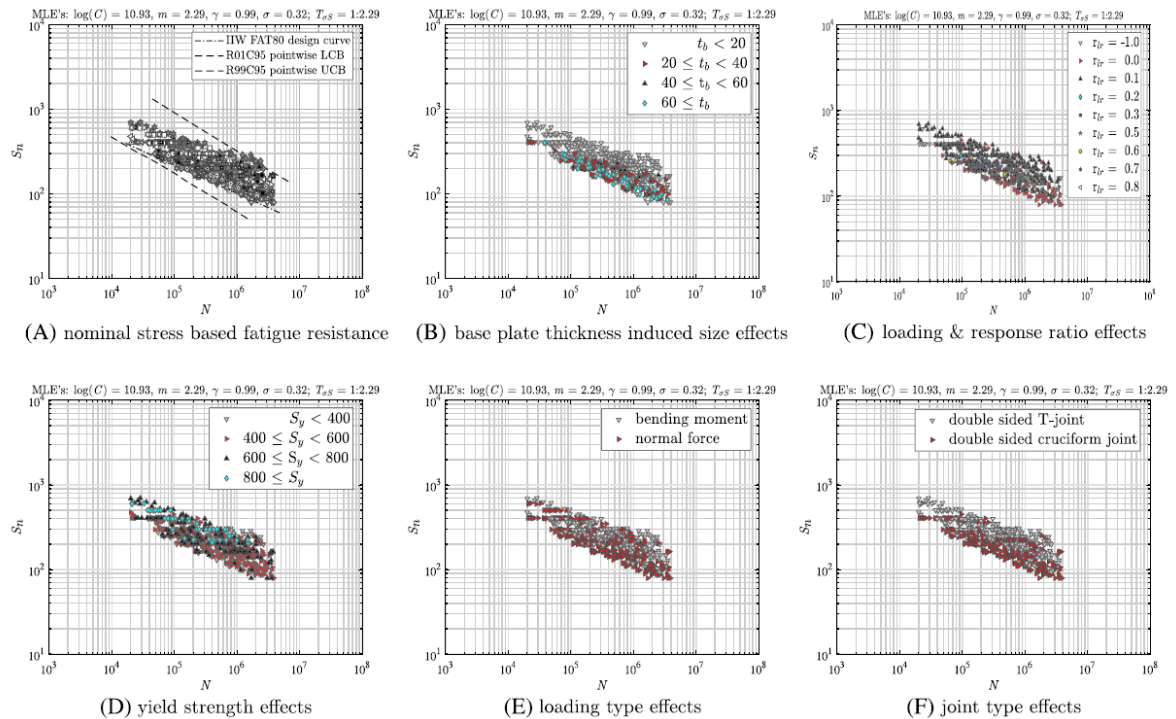


Figure 3.4: Nominal stress based fatigue resistance and influence factors, figure from [111]

Pros and cons of the method

To summarise, the pros and cons of the **Nominal Stress Concept** are:

- + If the analysis fits within the **FAT** or **CAT** description, computational effort is limited and the complexity of the method is low. This is also the reason that this method is often used in the industry.
- Local dimensional variations are not explicitly included, reducing the accuracy of the calculated resistance.
- Size effects¹ are not explicitly taken into account, and have to be corrected for.
- Complications increase if the local S_n has to be extracted from a **Finite Element (FE)** model.
- Large amount of **FAT** classes are needed to be valid for a large range of structure types.

3.2. Hot Spot Structural Stress Concept

The **HSSSC** is, like the **NSC**, an intact geometry concept, but in contrary to the **NSC** it includes local information about the structural detail. The **HSSSC** implicitly models the simplified shape of the specimen, allowing to significantly reduce the amount of S-N curves compared to the **NSC**. Figure 3.3 shows the hot spot structural stress for a T-joint as σ_s . The distribution through the base plate thickness is linearised. This concept models the force- and moment equilibrium of the actual stress distribution at the notch. It, however, does not model the actual geometry of the notch and the size of the components. For further analysis $S_s = \Delta\sigma_s$ is used. Several options for this linearisation exist in literature, being [21]:

- **Linear surface extrapolation**, typically through two points at respectively 1.0 and 0.4 t_p distance from the notch.
- **Non-linear surface extrapolation**, typically through three points at respectively 1.4, 0.9 and 0.4 t_p distance from the notch.
- **Virtual node below the surface**, typically the stress is read out at approximately 0.1 t_p [21] below the surface, at the location of the notch.

¹The effect where, for geometrically similar components with notches, the fatigue strength of larger components is different/lower than that of smaller components.

- **Through-thickness linearisation** of either the nodal forces and moments of a shell model, or the structural field stress components of the elements in the through-thickness direction based on force and moment equilibrium in the cross-section of a solid model. This method is typically used to verify the linear or non-linear surface extrapolation.

The appropriate method to determine this structural stress depends on the geometry and hot-spot type at hand.

For this method a distinction is made between **Load carrying (LC)** and **Non-load carrying (NLC)** details [54] as an engineering solution to limit the amount of SN-curves to consider. The **LC** and **NLC** curves present the extremes, and the engineer has to decide whether the detail at hand is carrying the load or not, and to what extent. There is no explicit rule that decides if a detail is **LC** or **NLC**. The weld load carrying level of the detail is influenced by two mechanisms: stiffness that attracts the load path, and an enforced load path (which is the case for non-penetrative welds).

Figure 3.5 shows for the **HSSSC** the scatter in the datapoints, plotted in different subdivisions. When combining all datapoints, the standard deviation σ is 0.33 and the strength scatter range index $T_{\sigma S} = 1 : (S_{10}/S_{90})$ is 1:2.41. An interesting observation is the existence of two fronts in both the plate thickness (figure 3.5B) and the joint type (figure 3.5F) plots. The first one is most likely due to the fact that the size effect is not explicitly accounted for in the **HSSSC**: hence the clear separation in plot B. The separation in the double sided T and double cruciform joint is presumably due to the existence of another parallel loadpath for the cruciform joint: reducing the load carrying level per hot spot, but increasing the amount of fatigue sensitive locations. "Except the loading type effect (figure 3.5B), the influence factors show hardly any difference in comparison with the nominal stress based results (figure 3.4)" [111].

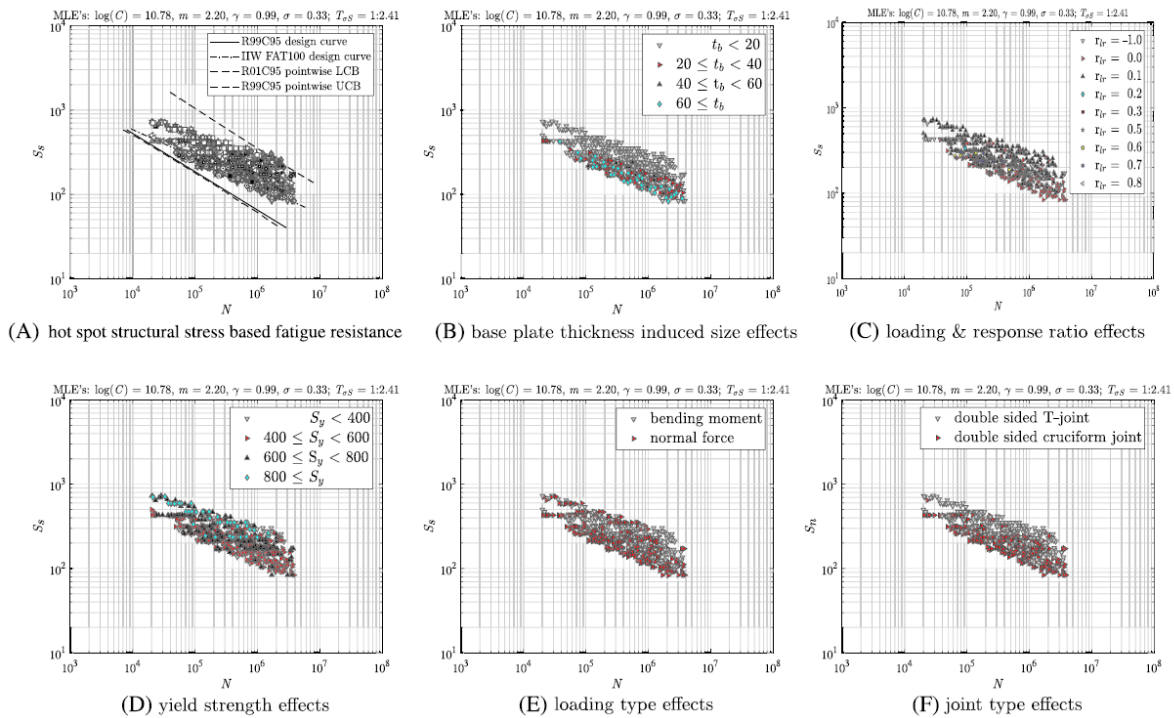


Figure 3.5: Hot spot structural stress-based fatigue resistance and influence factors, figure from [111]

Pros and cons of the method

To summarise, the pros and cons of the **Hot Spot Structural Stress Concept** are:

- + Only two **FAT** classes are needed: a **LC** and **NLC** line.
- + Local dimensional variations are included.

- Engineering judgement needed - this creates user variations.
- Increased complexity compared to NSC.
- Size effects are not explicitly taken into account, and have to be corrected for.

3.3. (Averaged) Effective Notch Stress Concept

Whereas the HSSSC does not account for size effects, the ENSC explicitly accounts for the size and shape of the detail. The concept models the actual weld geometry and the resulting through-thickness weld notch stress distribution. To do this, either the actual geometry is modelled with solids, or the actual through-thickness weld notch stress distribution (based on a semi-analytical expression of this distribution) is averaged over a characteristic depth. This concept therefore answers to all of the objections to the original NSC, at the cost of increased model complexity and efforts.

The presence of a notch in the structural detail creates the notch effect: the effect that increases the stress concentration. This poses a singularity, when modelling the idealised weld geometry. "The (as) weld(ed) notch radius is typically small ($\rho \rightarrow 0$) and the theoretical stress concentration is not fully effective, meaning a (local) peak stress as fatigue damage criterion $S_{max} = \Delta\sigma_{max}$ would be too conservative." [19]. There are two main proposals to determine the micro-structural notch:

1. The stress averaging approach adopts the averaged notch stress distribution along a presumed crack path over a distance that is characteristic for the material; the micro- and meso- structural length ρ^* :

$$\sigma_{av} = \frac{1}{\rho^*} \int_0^{\rho^*} (\sigma_n) dr \quad (3.1)$$

2. The critical distance approach by Peterson [110] adopts the stress value at a distance from the notch that is the micro- and meso- structural length ρ^* .

Results by Qin et al. support the choice of the stress averaging approach, when taking advantage of the analytical weld notch stress formulations.

Concluding, the effective notch stress is a combination of the peak stress (zone 1) and notch stress gradient (zone 2), allowing to account for the size effect. Figure 3.6 shows for the ENSC the scatter in the datapoints, plotted in different subdivisions. When combining all datapoints, the standard deviation σ is 0.23 and the strength scatter range index $T_{\sigma S} = 1 : (S_{10}/S_{90})$ is 1:1.52. For each of the five considered influence factors the distribution over the data scatter band has improved compared to the NSC and HSSSC.

Pros and cons of the method

To summarise, the pros and cons of the Effective Notch Stress Concept are:

- + Only one S-N curve needed: using a reference notch radius.
- + Local dimensional variations are included.
- + Size effects are taken into account.
- Increased complexity compared to NSC and HSSSC.

3.4. Total Stress Concept

The TSC [19, 23] has been proposed by den Besten in his PhD thesis. It is an elaborated version of the ENSC, aiming for even more fatigue strength similarity. This method comprises a total stress damage criterion in the form of S_t , being an area-equivalent line criterion. It is developed to capture fatigue resistance in one single curve. The difference with the ENSC is that this is a cracked geometry and stress intensity (SIF) based criterion, compared to an intact geometry.

The SIF is a cracked geometry based factor that expresses the fatigue life as a function of the crack length development. It is a zone 2 (notch stress gradient) parameter, relating to the assumption that for arc-welded marine structures the majority of the life-time is spent in the crack-growth region [19]. It is assumed that defects in the welds consume the initiation phase. The SIF K captures the magnitude of the linear elastic stress at an infinitely sharp crack tip (this thus leads to a singularity). At weld toe notches (infinitely sharp

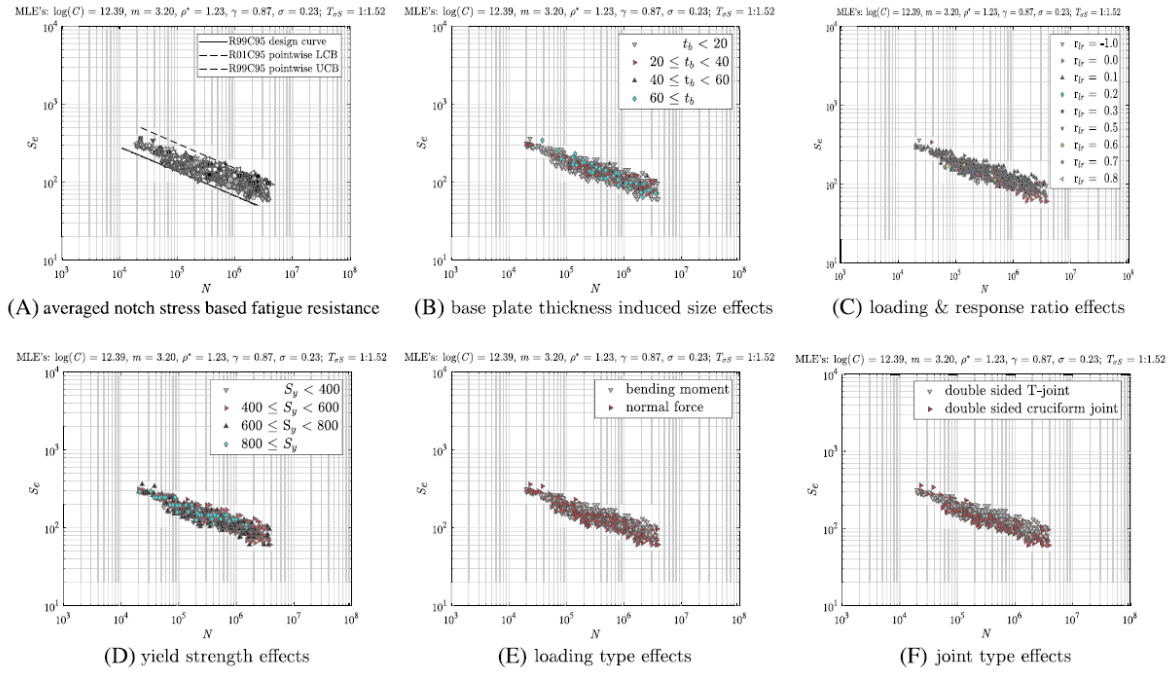


Figure 3.6: Averaged effective notch stress-based fatigue resistance and influence factors, figure from [111]

cracks) this is expressed as (3.2) with K the stress intensity factor, Y_n and Y_f respectively the notch and far field factor depending on the crack length a .

$$K = \sigma Y_n(a) Y_f(a) \sqrt{\pi a} \quad (3.2)$$

The comparison between the four methods is presented in [23, 111], showing the reduced scatterband when using the **TSC** compared to the more assessment concepts that use less local information.

Figure 3.7 shows for the **TSC** the scatter in the datapoints, plotted in different subdivisions. When combining all datapoints the standard deviation σ is 0.22 and the strength scatter range index $T_{\sigma,S} = 1 : (S_{10}/S_{90})$ is 1:1.47.

Pros and cons of the method

To summarise, the pros and cons of the **Total Stress Concept** are:

- + Only one S-N curve needed.
- + Local dimensional variations are included.
- + Size effects are taken into account.
- Increased complexity compared to **NSC**, **HSSC** and **ENSC**.

3.5. Fatigue resistance curves (CA)

As was stated before: fatigue is a governing limit state for maritime structures [19], amongst which naval frigates. Fatigue is about cyclic loading induced crack development (initiation, propagation and growth up to fracture) in materials and structures, typically characterised in four dimensions:

1. Environment (i.e. non-mechanical loading). Temperature, electro-chemical, etc.
2. Mechanical loading & structural response. This is captured in a transfer function between the loading on the structure (imposing stress) and its response (deflection), which can be regarded as the stiffness. This mechanical loading can be induced by the environment in the form of waves. Part of the mechanical loading & response are third and fourth dimension that influence this transfer function:
3. Geometry - Blunt points, stress concentrations, etc.
4. Material - Properties

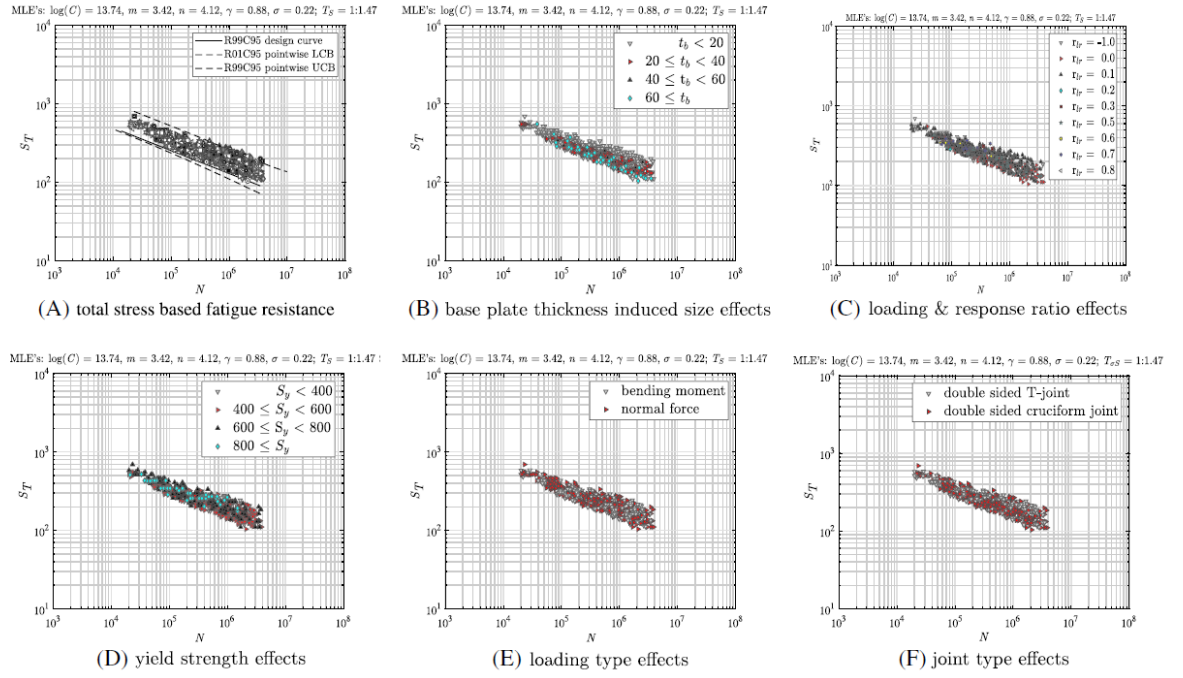


Figure 3.7: Total stress-based fatigue resistance and influence factors, figure from [111]

Limit states, like the **Ultimate Limit State (ULS)** and **Fatigue Limit State (FLS)** relate demand and resistance. This relation is present in each of the four fatigue dimensions from the previous list. A typical manner to express the demand (i.e. longevity) and resistance (i.e. integrity) is by means of a stress-cycle curve (S-N curve, first proposed by Wöhler [138]) for CA data.

3.5.1. Linear fatigue resistance

For the log-log linear part at the **MCF** range (single slope, Basquin type) the expression of the Wöhler curve is as presented in (3.3). Here N is the amount of cycles (life time), m is the slope of the relation and $\log C$ provides information about the endurance (i.e. the curve intercept). S is the fatigue damage criterion of the selected fatigue assessment concept (nominal stress, structural hot spot stress, total stress, etc.).

$$\log N = \log C - m \log S \quad (3.3)$$

$$N = \frac{C}{10^{m \log S}} = \frac{C}{S^m}$$

Research indicates that the amplitude variability (i.e. VA data) affects predominantly the fatigue strength $\log(C)$, but hardly affects the slope m of the curve [22].

By adopting novel methods that provide increased accuracy the complexity and related computational costs typically increase accordingly. Research strives to balance accuracy and complexity (linked to costs) [19].

3.5.2. Random fatigue limit models

For CA load histories the fatigue limit is a stress amplitude that indicates the threshold stress: for CA loads with amplitudes below this threshold no damage is accumulated. Several proposals for formulations of the **MCF-HCF-fatigue limit** fatigue resistance curves are presented in scientific literature, as is summarised in [74, 112]. In this thesis the more descriptive versions of the models from [112] are used. Figure 3.8 presents the four models in relation to one another, for the same set of function parameters.

Ordinary Random Fatigue Limit (ORFL) The five-parameter ORFL model by Pascual and Meeker [106] is formulated as a version of the non-linear S-N curve formulation from Strohmeyer [129], but with the fatigue limit S_∞ expressed as a random variable.

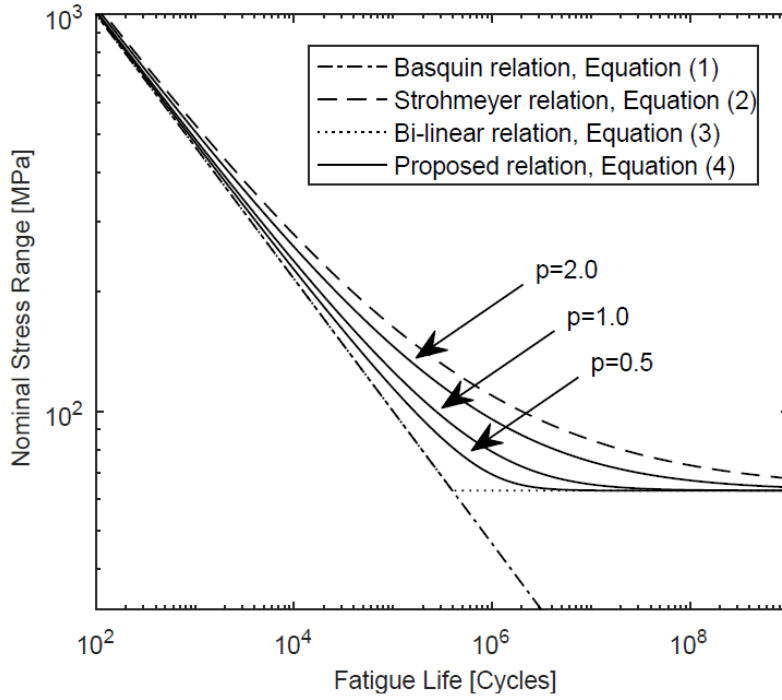


Figure 3.8: S-N curves resulting from for the Basquin-, ORFL- (i.e. based on Strohmeier), BRFL-, and GRFL (or 6PRFLM, here the proposed relation) relations having the same parameters. For the GRFL model the effect of the parameter p (ρ_{S_∞}) on the curvature is shown. The figure is from [74].

$$\log N = \log C - m \log(S - S_\infty(\mu, \sigma)) \quad (3.4)$$

Bilinear Random Fatigue Limit (BRFL) The five-parameter BRFL model by D'Angelo and Nussbaumer [17] has a better alignment [112] with the class guidelines and standards [24, 54, 100]. Here $H(\dots)$ is the Heaviside Step Function to capture the piece-wise continuous transition of the MCF to the HCF domain.

$$\log N = \log C - \frac{m \log(S)}{H(S - S_\infty(\mu, \sigma))} \quad (3.5)$$

Generalised Random Fatigue Limit (GRFL) The six-parameter GRFL by Leonetti et al. [74] is the first model to adopt a non-fixed formulation of the MCF-HCF transition. The transition-curvature is expressed by the parameter ρ_{S_∞} . The name "generalised" indicates the generic and flexible nature of the formulation.

$$\log N = \log C - m \log(S) - \rho_{S_\infty} \left(1 - \frac{S_\infty(\mu, \sigma)}{S} \right) \quad (3.6)$$

Due to its generalised nature the GRFL (also called the 6PRFLM [74]) is used in this thesis.

3.6. Codes, guidelines and recommended practises

The fatigue codes and recommended practises that are relevant for the frigates of DMO are discussed in this section.

NEN2063

The NEN2063 [99] compared to experimental results of the samples of the HMS Tromp, was the trigger for this project and is therefore part of this consideration. It has been withdrawn as of 2010, and is officially replaced by the Eurocode 3 [100]. The scope of the norm includes details that are:

- As welded and stress relieved by post weld heat treatment
- Arc welded details
- No failing in the LCF region
- Not operating in aggressive environments, e.g. seawater (which is interesting, as this standard was applied to assess previous frigates)
- Not of High Strength Steel (HSS) (which is in the NEN2063 defined as a yields stress exceeding 355 MPa)
- Not exceeding plate thicknesses of 30 mm; for thicker details a correction factor is required

Within this scope the norm states to use the Palmgren-Miner model to accumulate the VA damage, with a critical damage of 1. It accounts for the modification as proposed by Haibach [48] that separates the slope of the S-N curve for the MCF en HCF. For double sided T-joints, the stress should be determined at the weld based on the stresses in the base material (NSC). There is a fatigue limit at 0.55 times the stress at $N = 10^7$ on the respective S-N curve.

Eurocode 3

The Eurocode 3 [100] is the document that follows up on the NEN2063, and this does include the Hot Spot Structural Stress Concept (HSSSC), based on the Stress Concentration Factor (SCF) that enlarges the nominal stress at the weld based on the shape of the detail. There is a fatigue limit and the accumulation up until this limit is to be done with the Haibach modification of the Palmgren-Miner model and a critical damage of 1.

Both the NEN2063 and the Eurocode 3 are applicable to a large variety of steel structures, implicitly including the structural details in a frigate.

IACS

IACS is the International Association of Classification Societies that sets the minimum requirements, such as unified requirements, for all classification societies. The requirement of IACS: No. 56 [55] is to use the Palmgren-Miner cumulative damage model with a critical damage of 1. IACS allows both the NSC, HSSSC and ENSC and considers S-N curves with the Haibach modification.

DNV-GL Rules for Classification of Naval Ships

The DNV Class Guidelines [27] (DNVGL-CG-0129) for fatigue recommend the use of the Palmgren-Miner model with a critical damage as is indicated in the rules. For frigates this indicates the Rules for Classification of Naval Ships, Part 3 Surface Ships, Chapter 1 Hull structures and ship equipment [25]. For the use of the ENSC the Class Guideline directs to the Oil and Gas Recommended Practice DNVGL-RP-C203 [26].

The DNV-GL rules prescribe for welded joints the Palmgren-Miner model with $D_{crit} = 1$. The rules indicate to conduct the fatigue analysis with an amount of cycles of $N_{max} = 5(10^7)$ for a straight-line spectrum (which includes typical stress ranges of seaway-induced stresses), for 25 years of service with 230 days at sea per year. Modified operational profiles are to be agreed upon with the naval administration.

IIW Fatigue recommendations

The IIW Fatigue Recommendations by Hobbacher [54] recommend the use of the Palmgren-Miner summation and set the D_{crit} to 0.5 to 1.0. The 0.5 is recommended for VA loading based on recent research (Hobbacher provides no direct references), whereas for a load with a fluctuating mean stress even 0.2 is recommended.

Table 3.1 provides the four main documents for fatigue assessment of the DMO vessels, along with the respective fatigue assessment concepts and the probability of survival and confidence of the respective S-N curves.

Table 3.1: Summary of class codes and recommended practises. DS = Double sided, SS = Single sided confidence interval

Document	Concepts	S-N Probability of survival	S-N Confidence
NEN2063	NSC	95%	DS 95%
Eurocode 3	NSC, HSSSC	95%	DS 75%
DNV-GL 0129	NSC, HSSSC, ENSC	97.7% (i.e. $\mu - 2\sigma$)	DS 75% ⁽¹⁾
IIW	NSC, HSSSC, ENSC	95%	DS 75% or SS 87%

⁽¹⁾ DNV-GL adopts a confidence bound of 75% as [Ronold and Lotsberg \[117\]](#) links 75% confidence to a probability of failure of 10^{-4} in the last year of a 20 year lifetime.

Table 3.1 shows the inherent relative conservatism of the NEN2063: by using the 95% double sided confidence bound, the analysis is more conservative than by using the 75% bound.

3.7. Concluding remarks

This chapter presents the four commonly applied and promising fatigue damage criteria for steel maritime structures, in order of increasing complexity. The SIF was discussed as it influences the fracture domain models from chapter 4 and appendix A, but not further used as a separate criterion because this is a stable crack growth criterion that is commonly employed to assess the residual fatigue life based on the observation of a present crack. For the assessment of the fatigue life the NSC and HSSSC have a limited complexity at the cost of a limited accuracy. The scatter related to this limited accuracy is restraining the quality of the fatigue life prediction. The ENSC and TSC provide both only one S-N curve for all structural details combined. The TSC offers the highest accuracy. However, to propose a best practise that fits within the limited time frame of the current assessment, the ENSC (with a scatter index only 3.4% below that of the TSC) is deemed the best choice in relation to the problem statement.

This ENSC is not accounted for in the NEN2063 and Eurocode 3. However the DNV-GL-CG-0129 has adopted the artificial notch radius approach to the ENSC. The stress-averaging approach is not yet approved or adopted by any of the class societies.

4

Fatigue damage accumulation models

The second block of uncertainty that is part of this research is the uncertainty related to the damage accumulation model. The first one (fatigue assessment concepts) was addressed in chapter 3. This current chapter provides the problems related to the current method, the LDAM, and presents the most dominant models from scientific literature that have been proposed. This is done by a separation into three domains: continuum, fracture and (continuum) damage mechanics.

4.1. Variable amplitude loading and response

For a CA load history the similarity of each tested sample is not tarnished by the quality of the damage accumulation. Determining the fraction of consumed fatigue life is straight-forward: Adopting the Wöhler-type S-n curve of CA fatigue data, the critical amount of cycles (N) per fatigue damage criterion (stress level σ) is known. The fraction of the consumed fatigue life n/N equals 1 at fracture and provides a linear relation of the consumed cycles and the residual fatigue-life. For a VA load history, however, the process of accumulating damage is more complex as data-point similarity is more challenging than for CA loads.

If the load history is of the (random) Variable Amplitude type, two main options are at hand: analysing the fatigue damage per reversal/cycle (temporal approach), or by means of an (energy) spectral approach. The first method is computationally expensive, but typical for a fracture mechanics analysis. The second simplifies the load history and loses information. Both methods are cycle-by-cycle, as the information of what happens within a cycle is not taken into account. A cycle-by-cycle approach is to date the only well developed available model [22]. For a maritime structure typically a spectrum of the wave loads is available.

4.1.1. Cycle definition

From the Ramberg-Osgood relation [114] it is known that one cycle generates a closed hysteresis loop, introduced by the loading and unloading of the specimen. Therefore the counting of hysteresis loops equals the counting of fatigue cycles. Herewith one cycle is defined as two reversals. Figure 4.1 shows the definition of the maximum, minimum and mean stress of a CA load history. For the cycle counting procedure of a VA load history the hysteresis loops are used.

The description of a loading and response cycle requires two parameters: the mean and the amplitude of the cyclic motion. This is captured in the R_{lr} (in literature also R , r or r_{lr}), which is expressed as the minimum over the maximum of loading amplitude. Assuming for the NSC that the stresses in the notch affected region are highly tensile and close to yield due to welding induced residual stresses, it is justified to not explicitly consider the r_{lr} (i.e. = 0) [19]. However, in literature the test results are commonly translated to $r_{lr} \approx 0.5$ by means of a mean stress correction. Typically the mean stress correction by Walker et al. [134] is used.

4.1.2. Temporal approach

Cycle counting techniques including Rainflow

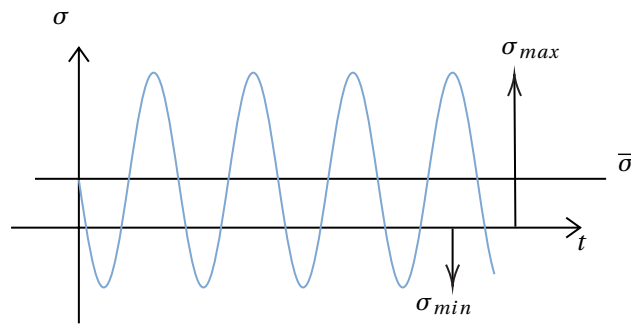


Figure 4.1: Definition stress cycle

Definitions

Loading and response ratio:

$$R_{lr} = \frac{\sigma_{min}}{\sigma_{max}}$$

Stress range:

$$\Delta\sigma = \sigma_{max} - \sigma_{min}$$

A typical procedure to translate a temporal load history to a spectral one is the rain flow counting technique by [Matsuishi and Endo](#) [32, 92]. It is used in modern (maritime) fatigue codes [27, 54, 55, 100].

Figure 4.3 shows an example of the rain flow counting procedure for a VA load history. In the rain flow counting procedure information of the load history is lost, being:

- Sequence effects (the effect of the order of the stress blocks¹) is not taken into account. [Schijve](#) [121] suggests that for a long term random VA load this effect is not relevant as it is averaged out.
- Frequency effects, the influence of the testing frequency is not taken into account. As [Cui](#) explains: "Many experiments [40] have shown that over the frequency range 1–200 Hz, the fatigue limit or strength after a long period of time [...] remains constant for all practical purposes, although there is, [...], a slight increase with increasing test speed. At higher testing speeds, the fatigue limit continues to increase with testing speed up to frequencies of about 2kHz, but beyond this frequency, the experimental data do not agree." [16]
- The shape of the cycle, which can be saw-tooth/sinusoidal/etc., is not taken into account. That is, the method is cycle-by-cycle.
- In the example from figure 4.3, the mean stress is not part of the information in the histogram. To include the mean stress a two-parameter counting technique should be applied. Such techniques are outside of the scope of this thesis.

Despite the loss of this information, it is the most common counting procedure in the (maritime) literature [9, 39, 61]. The ISSC document of 2018 explicitly focuses on the effect of whipping, and concludes: "For the time series that have been investigated [61], rainflow counting and the Palmgren-Miner hypothesis are suitable to estimate the fatigue damage for stress histories with and without (whipping) vibrations. The Committee did not come across research results with opposite conclusions."

The focus of this research is, in line with the conclusions from the ISSC Committees of 2015 [9] and 2018 [39], not on improving the counting procedure. The rain flow counting procedure is adopted. However, for reference the other methods as suggested in industry standards are listed. For this the ASTM Standard Practise [6] is used. It should be noted that the scope of this standard practise is not specifically maritime applications, but fatigue analysis in general. ASTM lists the following:

- **Level crossing counting**
This counts the occurrences at which a preset value is exceeded.
- **Peak counting**
This counts the occurrences of a peak (derivative = 0 and second derivative < 0) within a certain stress bin.
- **Range counting**
This counts the occurrence of a stress range within a stress bin.

¹A stress block is a repetition of cycles with the same mean and amplitude.

The rain flow counting procedure translates a VA load history (figure 4.2) to a histogram with amount of cycles per stress range. As an example the time-history from [69] is used.

Step 1: Rotate time-history 90°

To employ the analogy with rain flowing from a pagoda roof, the figure is rotated, see figure 4.2a to 4.2b.

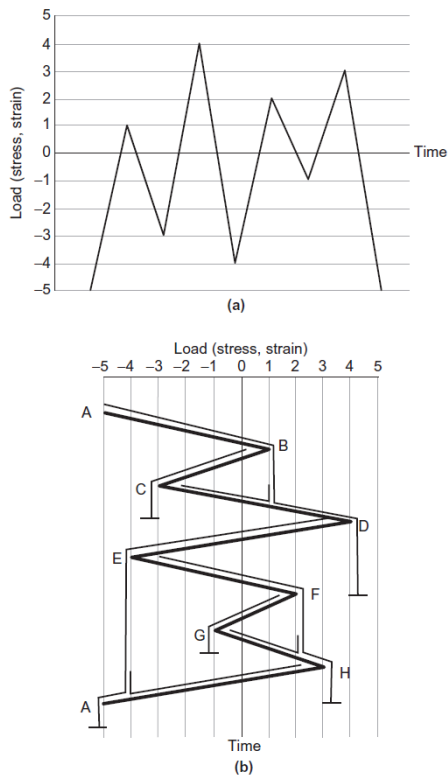


Figure 4.2: Load time history, figure is taken from [69]

Step 2: Count reversals

The counting criteria, in a downwards direction and to both sides, are applied:

- If a valley of greater magnitude is encountered
- If a rain drop merges with a flow that started from an earlier peak
- If the end of a peak-valley sequence is reached

Step 2 yields table 4.1 with all reversals.

Table 4.1: Counted reversals

No. of reversals	From	To	From	To	Range	Mean
1	A	D	-5	4	0	-0.5
1	D	A	4	-5	9	-0.5
1	B	C	1	-3	4	-1
1	C	B	-3	2	4	-1
1	E	H	-4	3	7	-0.5
1	H	E	3	-4	7	-0.5
1	F	G	2	-1	3	0.5
1	G	F	-1	2	3	0.5

Step 3: List cycles

Table 4.1 is then translated to capture the cycles instead of the reversals, see figure 4.2.

Table 4.2: Counted cycles

No. of cycles	From	To	From	To	Range	Mean
1	A	D	-5	4	0	-0.5
1	B	C	1	-3	4	-1
1	E	H	-4	3	7	-0.5
1	F	G	2	-1	3	0.5

Step 4: Produce histogram

The cycles are plotted in a histogram for further processing, see figure 4.3.

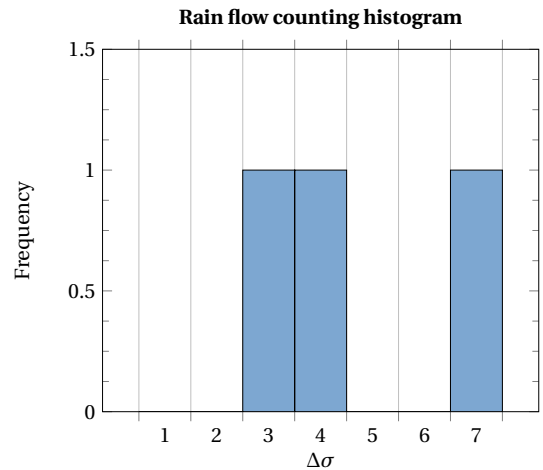


Table 4.3: Histogram that results from the rain flow counting procedure applied to the load history from figure 4.2a

Figure 4.3: Rain flow counting procedure example. Explanation based on [22, 69]

The rain flow counting procedure combines the information of the peak and range counting methods. All three methods in this section are less advanced than the rain flow counting procedure.

4.1.3. Spectral approach

Using standardised spectra including the Gassner curve

Following the proposal by Palmgren in 1924 [104] to accumulate fatigue damage under VA loading by dividing the sequence into CA blocks, Gassner [43] was in 1939 the first to propose a systematic method of testing under VA loading, by means of an eight-step block load as shown in figure 4.4 to represent a Gaussian-like distributed load.

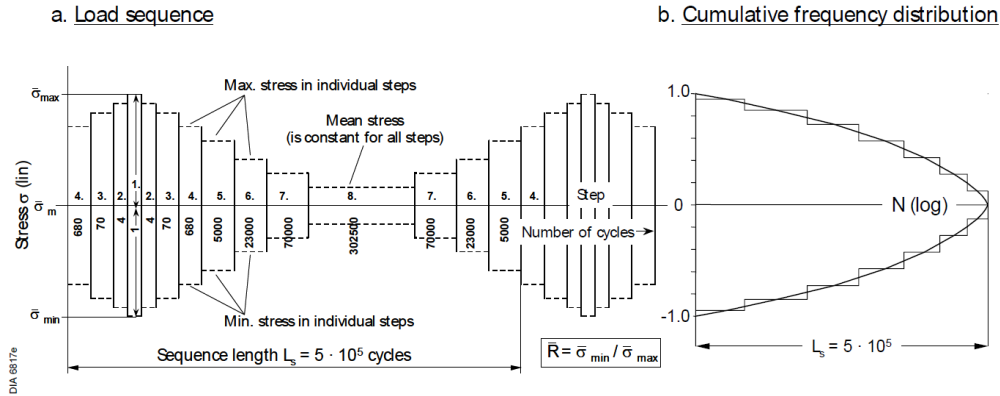


Figure 4.4: The Gassner eight-step block loading sequence [43] translated to a cumulative frequency distribution, figure from [127]

The Gassner-curve is a VA equivalent of the CA S-N curve, and is obtained by calculating the damage per repetitive spectrum sequence, according to Palmgren-Miner.

$$\sum \left(\frac{n}{N} \right)_i = D_{spec} \quad (4.1)$$

The real damage is calculated by correcting for the spectrum length L_s (i.e. number of cycles per repeated sequence) and measured longevity \bar{N}_{exp} of the sample.

$$D_{real} = \frac{D_{spec}}{L_s} \cdot \bar{N}_{exp} \quad (4.2)$$

The Gassner 8-block load spectrum closely resembles a normal (or Gaussian) distribution. A more general procedure to describe spectra is by means of the Weibull distribution. A normal distribution can be closely modelled by a Weibull distribution.

Weibull distribution

Typical for the load spectrum of a maritime structure is the use of the Weibull distribution [27], see (4.3). It is one of the extreme value distributions that fits perfectly to fatigue phenomena since fatigue life time is the time to failure of the weakest link [20].

$$f(x; \lambda, k) = \frac{k}{\lambda} \left(\frac{x}{\lambda} \right)^{k-1} e^{-(x/\lambda)^k} \quad (4.3)$$

Here λ is the scale parameter, which refers to the modification of the scale of the abscissa. As the area under the curve is unchanged the peak will be higher for lower scale parameters. k is the shape parameter, which refers to the slope of the graph in a probability plot. The shape parameter is subject to discussion.

To illustrate the sensitivity of the longevity calculation to the Weibull shape parameter, the closed form damage estimate for two-slope S-N curves and Weibull distribution from DNV-GI [27] is plotted in figure 4.5. The detail is the NEN 2063 K-40 detail, which is approximately a type F S-N curve of DNV-GL and a FAT71. The largest reference stress is set to 80 MPa at 10^3 cycles for all shape factors. According to the DNV-GL Class Guideline the Weibull scale factor is a function of the reference stress, the occurrence of this reference stress

and the shape factor ξ . The damage is presented for the in-air condition.

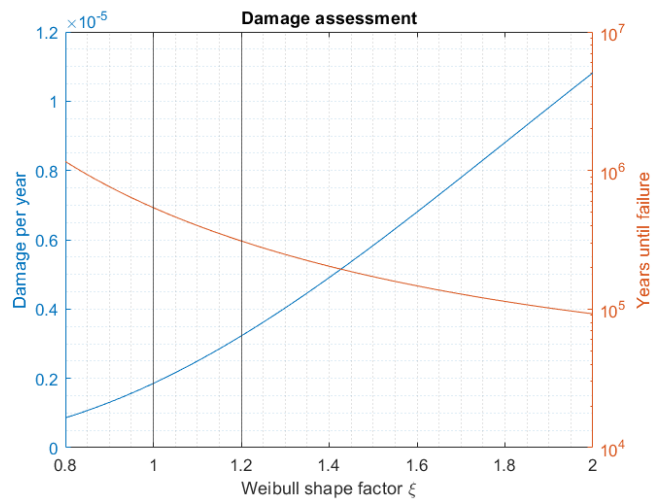


Figure 4.5: DNV-GL Class Guideline calculation of the longevity per shape factor ξ for a K-40 detail.

The variation of a ξ of 1 to 1.2 yields a longevity reduction of 43% for the illustrative case in figure 4.5.

The meaning of this shape factor for the stress spectrum is explained in [38, 64]:

$\xi = 0.8$

Concave distribution, interpretation as log-normal distribution possible: gusts of wind over an extended period.

$\xi = 1.0$

Exponential distribution which forms a straight line in a semi-logarithmic plot: This distribution can be interpreted as a mixture of different normal distributions, for instance, during the measurement of stresses due to a rough sea over an extended period. This is the SLD of figure 4.6.

$\xi = 2.0$

Standard or normal distribution which forms a parabola in a semi-logarithmic plot: Frequency distribution from a stationary Gaussian random process; measurement of stresses due to a rough sea or measurement of the vertical forces on a motor vehicle on a specific roadway without driving manoeuvres. This is the LSD of figure 4.6.

$\xi = 4.0$

Convex distribution: Typical for crane and bridge construction.

$\xi \rightarrow \infty$

Rectangular spectrum (constant amplitude).

For maritime structures it is thus expected to have a shape factor between 0.8 and 2.0.

Now the fatigue life is dependent on the spectrum shape, as is illustrated by figures 4.5 and 4.6. The type of variable amplitude loading is of great significance to determining the fatigue life time. For maritime structures it is common to use a Weibull distribution for the long-term calculation [27, 55], whereby the shape parameter of the distribution has a large influence on the calculated fatigue life. IACS and DNV-GL both present a formula as a function of the ship length as initial estimate of this shape parameter. For a vessel of 120 m (\approx length of the current M-frigate) this yields a respective value of 1.077 and 1.087 for IACS and DNV-GL.

The approach by Gassner is still a linear hypothesis, as the damage that is done by previous cycles does not influence the damage rate in the future. However, Load Interaction (LI) and Load Sequence (LS) effects (more explanation on these effects is included in section 4.2.2) are implicitly taken into account by means of the experimental data, the Gassner curve is closely related to the RLDM by Schütz [123] as it incorporates experimental data based on the actual in-service load in the LDAM. More on the model by Schütz is included in section A.1.

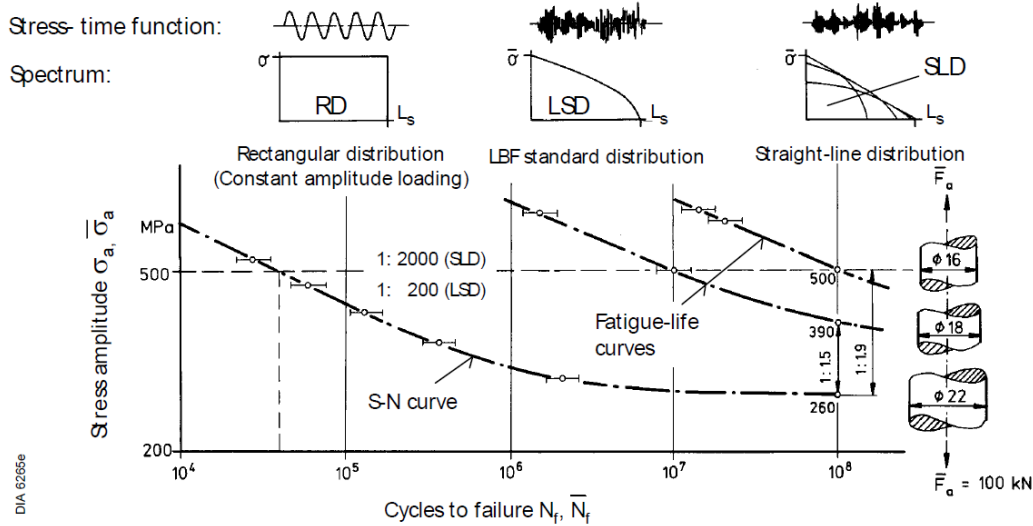


Figure 4.6: Gassner curve dependency on spectrum type as presented by Sonsino [127]

The method by Gassner requires a repetitive nature to separate a time signal into equal block-sequences. Schijve states that for a valid VA test there should be at least five to ten repetitions of this sequence Schijve [121]. Sonsino suggests that the repetition of sea-states might answer to this [127], whereas for a frigate with changing operations this is questioned. Svensson et al. [131] points out that the method of selecting a spectrum puts a choice on the engineer: "To use all possible spectra for estimation and accept large safety factors, or choose a reference set of spectra that can be judged to comply with the specific application, giving more accurate predictions."

Sonsino [128] even claims that a prediction of fatigue life under this complex loading is not possible by any cumulative damage (CA data based) hypothesis. He proposes systematic testing with decent reporting according to his paper [128], for a wider variety of spectra than only the spectrum as proposed by Gassner.

4.2. The LDAM by Palmgren-Miner

The first model that was proposed to translate the stress-histogram to fatigue life is the Linear Damage Accumulation Model. This is also the model that is included in each of the considered class codes and recommended practises.

4.2.1. Definition and origin

Most often used in practise (and in all of the considered relevant codes and standards), partially due to its simplicity [57, 97, 119, 121], is the Palmgren-Miner Linear Damage Accumulation Model (LDAM).

It was proposed in 1924 by Palmgren as a method to predict the life-time of ball bearings [104] and was primarily based on his intuition. It is to date used in modern fatigue codes [27, 54, 55, 100] to accumulate the damage under a VA load. The model is given by (4.4) with k = the amount of stress levels, n_i = the amount of cycles per stress level and N_i = the number of cycles to failure per stress level, i.e. per histogram under the S-N curve, see figure 4.7.

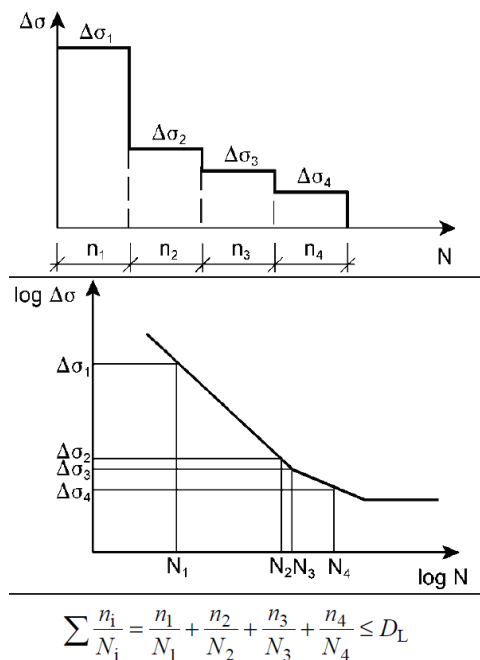


Figure 4.7: Explanation of the Palmgren-Miner model, from Eurocode 3 [100]

$$\text{for } \Delta\sigma \geq \Delta\sigma_{th}$$

$$D = \sum_{i=1}^k \frac{n_i}{N_i} \leq D_{\text{crit}} = 1 \quad (4.4)$$

It is also called the **LDAM** as the damage is linearly related to the cycle ratio. This model by **Palmgren** became more popular upon the physical derivation by **Miner** [95]. **Miner** based his derivation on the assumption that a constant amount of work is absorbed per cycle [95]. For the derivation, see appendix B.1. Another derivation proves the consistency of the **LDAM** with fracture mechanics (that is, with **LEFM**), and is included in appendix B.2.

The assumptions in the Palmgren-Miner model are [95, 155] that the rate of damage accumulation is constant, that the S-N curve represents a line of 100% fatigue damage and that below a certain threshold (called: fatigue limit) no damage is accumulated. For an S-N curve with a **FAT** class the curve represents 2.5% chance of failure for a double sided confidence interval of 95%: 100% damage does not mean failure, but a critical probability of failure.

Due to its linear and simplified nature, the validity of the Palmgren-Miner model for (random) **VA** loading is questioned and called "often unsatisfactory" [34] as it is not able to capture the effects related to variable amplitudes properly. It is proven to not be absolutely valid under **VA** loading [34, 49, 61, 121]. However, the conclusions by the ISSC 2018 [39] committee indicate that Palmgren-Miner might suffice for maritime typical loads.

4.2.2. Limitations

By assuming no damage below the fatigue limit, the **LDAM** neglects the **Load Interaction (LI)** and **Load Sequence (LS)** effects. The **LI effect** is that the fatigue damage increments induced by load cycles depend on the damage as caused by previous cycles. It is due to notch root plasticity, which leads to a redistribution of residual stresses, affecting the fatigue damage contribution of subsequent cycles [121]. Part of the **LI effect** (see figure 4.9) is the influence of the sequence of stress blocks, the **LS effect**. Experimental evidence of completely reversed loading conditions indicates $D > 1$ for a low-to-high (L-H) loading sequence, and $D < 1$ for a high-to-low (H-L) loading sequence [34, 93].

Figure 4.8a illustrates the **LI effect** of the loading history on the fatigue life to failure: the sample with an **Underloads (UL)** before the change to the low-amplitude stress block has a shorter fatigue life than the sample with the overload before the block-transition. Figure 4.8b illustrates for an unnotched specimen the following: it confirms the H-L versus L-H sequence statement from [34, 93], and it shows that for a multitude of similar block loads the sequence effect (for unnotched specimens) is negligible. This is presumably because the beneficial and harmful effects of the sequence cancel one another out. A stochastic signal does not pose **LS effects** [121] following the same reasoning.

It should be noted that the explanatory figures from [121] as presented in figure 4.8 are for an Al-alloy specimen. Typically an Al-alloy does not have a significant crack propagation phase. However, the trends that are sketched are valid for steels.

The **LS** and **LI** effects are linked to two phenomena: **Overloads (OL)** and **Underloads (UL)**. **OL's** are instantaneous high peak loads that impose large retardation in the measured crack length development [35, 121]. This retardation is typically attributed to plasticity induced crack closure at the relative "unloading" after the respective overload [31, 121]. An **UL** is a large negative amplitude load that can slightly increase the crack growth rate (and thus reduce the life-time to full-fracture). It can also reduce the effect of the aforementioned overloads [121]. "In general the positive interaction effects overrule the negative ones during crack growth. As a result, non-interaction predictions for fatigue crack growth under **VA** loading will usually give conservative results." [121]

The work by **McEvily et al.** [93] discusses the causes of deviation from the Palmgren-Miner model for three different **VA** block load histories. The paper concludes:

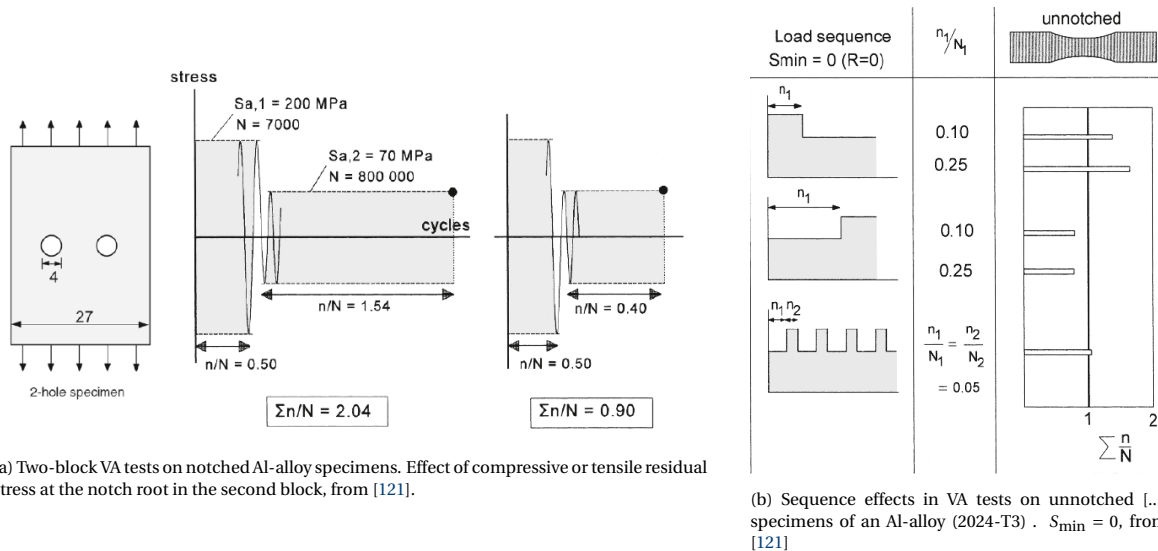


Figure 4.8: Explanatory figures LI and LS effects, from [121].

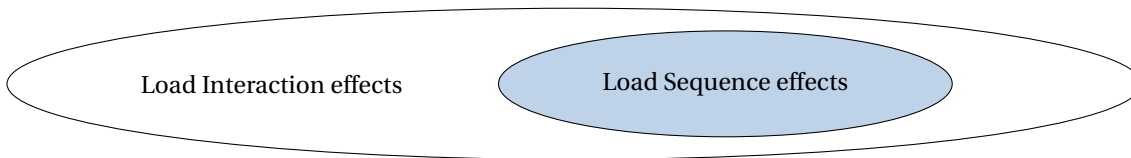


Figure 4.9: LS effects as subset of LI effects.

- For a two-step test (two sequential blocks both between the yield stress and the fatigue limit) - confirmed by [34]
 - A high-low (H-L) sequence yields a $D_{crit} < 1$
 - A L-H sequence yields a $D_{crit} > 1$
- For multiple two-step tests (two alternating blocks, the lower amplitude below the fatigue strength and the higher one below the yield stress but above the fatigue limit) a large effect of the lower stress level can be to reduce the crack closure level; allowing a faster crack growth rate at the higher stress level.
- When considering OL's and UL's, McEvily et al. conclude: An OL typically retards the crack growth due to lateral contraction of the material, whereas an UL typically accelerates the process due to a reduced crack closure level.

The final conclusion of McEvily et al. is that for many VA loads the fatigue lifetime prediction based on crack growth provides a more rational and accurate than the LDAM by Palmgren and Miner, due to the temporal approach that covers the effects related to the previous cycles (Load Interaction). This is in agreement with the statements by Schijve [121].

The work by Gurney [46] discusses the variations in Palmgren-Miner damage sums for different random VA load histories. The main conclusions are:

1. Under tensile loading a wide band spectrum consistently gave values of $D_{crit} \leq 1$, while narrow band loading gave $D_{crit} \geq 1$.
2. At $R_{lr} = -1$, however, the difference between the two types of loading was much smaller, although wide band loading still gave $D_{crit} \leq 1$ and was more damaging than narrow band.
3. In terms of life, narrow band loading gave a longer life at $R_{lr} = 0$ than at $R_{lr} = -1$, for both block lengths. Under wide band loading the opposite was true. It should be noted that this analysis was done using the NSC, which by nature does not account for the loading and response level.

Agerskov and Ibsø [2] pose a formula of the critical damage as a function of the irregularity factor I , which is the number of rising zero crossings divided by the number of peaks:

$$\sum \frac{n}{N} = 2I - 1 \quad (4.5)$$

Petersen et al. [109] suggests to use for offshore structural details that are loaded at $R_{Ir} = 0$ to use I between 0.7 and 1.0. The main contribution from [2] is to define a critical damage as a function of the irregularity of the respective spectrum.

Gurney [45–47] provides in chapter 7 of his book the overview of the Palmgren-Miner sums for typical random loading conditions in offshore environments is provided, based on the research from [1, 3] and the British offshore test programme. It hereby does not add data to the list, but offers insight in the variation in the LDAM critical values. This distribution is presented in figure 4.10.

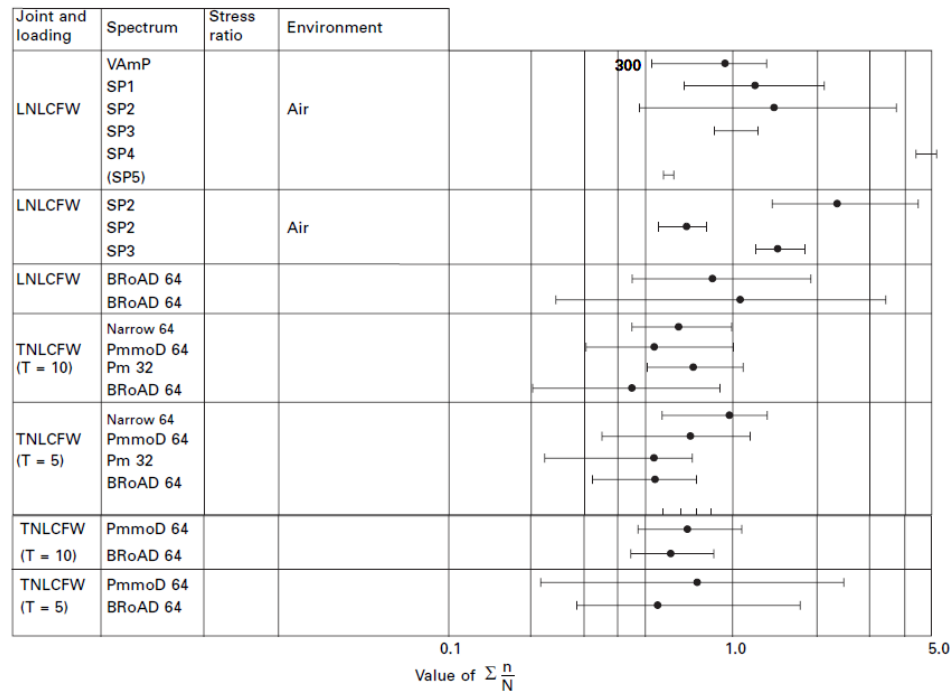


Figure 4.10: Research results of the Nordic offshore programme, from Gurney

Summarising the shortcomings of the Palmgren-Miner model [121]:

- The rate of damage accumulation is constant ($\frac{dD}{dn} = \frac{1}{N_i} = \text{cst}$), which is contradicted by the different damage rates for large and small cracks [121].
- The S-N curve is assumed to be a line of constant damage, whereas for lower stress levels the resulting crack will be shorter than for higher stress levels. Schijve suggests that this shortcoming is not significant, as the majority of the lifetime is spent in the crack initiation and microcrack growth period [121].
- No damage accumulated below the fatigue limit, which is a material constant. This neglects Load Interaction (LI) and resulting Load Sequence (LS) effects and is contradicted by [82–84] which indicate the load amplitude-sequence dependence of the fatigue limit.

Elementary Palmgren-Miner model

To tackle the objection that no damage is accumulated below the fatigue limit, the Elementary Palmgren-Miner model linearly extends the S-N curve beyond the fatigue limit. This removes the fatigue limit and poses a linear relation between S and N for all stress levels. This adds conservatism to the basic Palmgren-Miner model. However, the exact slope of the curve (the linear extension of the S-N curve) lacks a physical basis [64].

4.2.3. Engineering practise

If the equivalent VA data fits the CA scatterband, the Palmgren-Miner model with $D_{\text{crit}} = 1$ can be adopted [22]. This method is common in engineering practise [133], although in literature different definitions of the

equivalent stress amplitude $\Delta\sigma_{eq}$ are proposed. $\Delta\sigma_{eq}$ can be the maximum stress [38, 127], or a value derived from the spectrum [54, 100, 128] (the derivation is included in appendix C.1.1). The conclusion of validity of the LDAM for VA loading only holds if the equivalent stress as derived in the appendix is used, due to the nature of the derivation. If the data does not fit the scatterband an engineering cut-down factor (reducing the D_{crit}) is adopted [22]. The selection of this factor is based on engineering judgement of fatigue data from literature according to the Relative Linear Damage Model (RLDM) by Schütz, which is discussed in section A.1.

The relevant codes and standards [27, 54, 55, 100] incorporate the LDAM with the extension below the fatigue limit as proposed by Haibach [48]. The critical damage in [27, 55, 100] is 1.0 for all load spectra. The IIW [54] suggests $D_{crit} = 0.5$ for VA loads.

D_{crit} distribution in literature

For reliability analyses the distribution of the stochastic variables is input. From the standards [27, 54, 55] already a variation of $D_{crit} = 0.2$ to 1.0 is present, and measurements [34, 49, 61, 121] also do not provide a distinctive and absolutely valid D_{crit} value. This paragraph assesses several proposed distributions.

The work by Folsø et al.[36] compares five damage-distribution models, of which the Wirsching model [135] is the only one that presents a distribution for the damage sum for offshore structures. The scope of the work by Folsø et al. is Ship Structures, and it selects for further use the log-normal distribution with mean 1.0 and a CoV of 0.3 according to [90, 135].

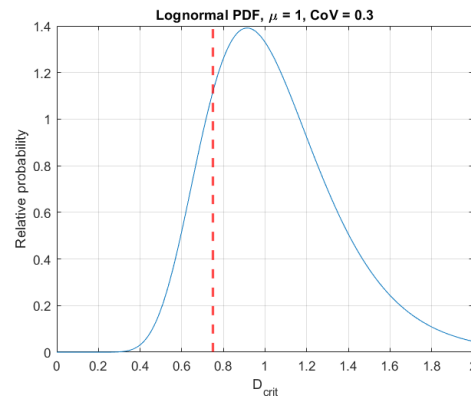


Figure 4.11: Lognormal distribution of the D_{crit} , in red the DMO limit of 0.75 is indicated

DNV-GL [24] prescribes a usage factor D_{crit} of 1.0 and recommends for the calculation of the probability of fatigue failure a log-normal distribution with median 1.0 and CoV equal to 0.30. The scope of the DNV-GL guidelines is Ship Structures.

Slamming

The reason for DMO to incorporate a D_{crit} of 0.75 is to account for slamming [133]. For a log-normal distribution this means that 16.9%² of the cases that match with the literature distribution are below the DMO threshold. The DNV guidelines propose to use the mean (= 1.0) of this distribution.

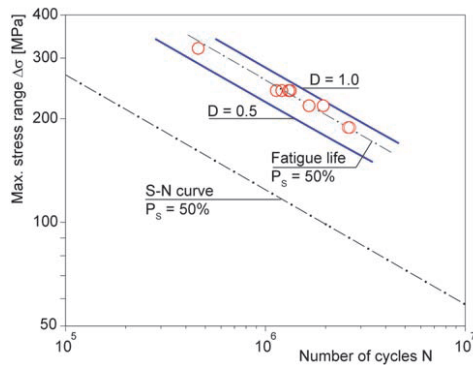
Wave loads and slamming loads acting on the ship's hull pose a superposition of low-frequency wave-induced stresses and high-frequency stresses from whipping as well as springing effects [61]. For frigates, with a length of approximately 120 m springing is not a critical excitation state: due to the relatively stiff structure of the vessel the first eigenfrequency is higher than the typical wave excitation frequencies.

The comparison within the VALID project, lead by MARIN, of the long term spectral fatigue calculation with and without the inclusion of the whipping factor (the total fatigue damage due to the total stress history over the wave frequent fatigue damage) allowed to conclude that the long term whipping contribution increases the fatigue damage with 6% [29]. Upon processing more data this was even concluded to be 7% [30]. This conclusion yields a recommended D_{crit} of 0.935 (=100%/107%) for the considered US Coastguard vessels and their respective operational profiles.

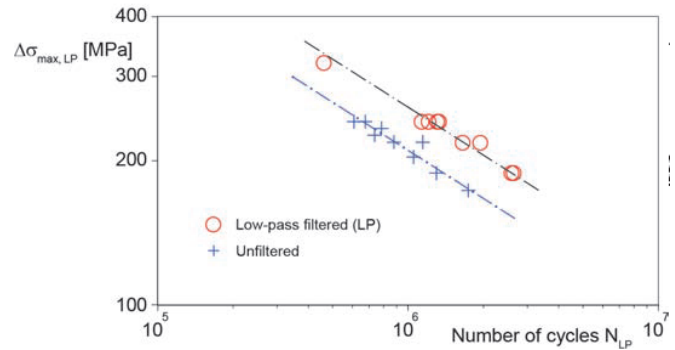
The thesis by Tuitman [132] reports for the M-frigate measurements a reduction of 10% of the life time for a sailing speed of 12 knts and a reduction of 16% for the 17.5 knts case. Besides the effect of slamming, this also shows the effect of encounter-frequency (i.e. sailing speed) on fatigue damage.

²MATLAB: `logncdf(0.75, log(1), log(0.3)) = 0.169`

The work by Kahl et al. [61] covers whipping effects and concludes that the inclusion of whipping results in 20% more damage in a typical 30 minute time-frame for a container-vessel of > 250 m length, when containing a whipping event. The work also concludes for this vessel type that a D_{crit} of 0.5 to 1.0 is justified. The results of Kahl et al. are presented in figure 4.12.



(a) Fatigue lives from variable-amplitude tests with low-pass filtered (< 0.4Hz) 30-minute stress history and life prediction based on mean S-N curve, from [61].



(b) Fatigue lives from variable-amplitude tests with unfiltered and low-pass (LP) filtered 30-minute stress history, both based on $\Delta\sigma$ and N for LP filtered history, from [61].

Figure 4.12: Research results from Kahl et al., concluding the D_{crit} range of 0.5 to 1.0

Care should be taken to extrapolate these results to other cases: the added damage due to slamming is highly influenced by the operational profile and hull shape. Secondly, the involved fatigue resistance relation might differ in cut-off limit and bi- or uni-linear nature.

4.3. State-of-the-Art fatigue damage accumulation models

To determine the fatigue life time of a structure under VA loading, the stress level (fatigue damage criterion) histogram at the hot spot is translated to a damage indicator, which is accumulated over time up to a critical value (typically 1) like in the LDAM that was discussed in section 4.2. Literature presents multiple proposals to calculate and accumulate this damage with the aim to overcome the shortcomings of the LDAM, which are discussed in this chapter. However, at the moment no generally applicable solution with satisfactory accuracy is presented [97, 119, 131, 150, 152].

The focus in this chapter is, within the scope (Section 2.5), on research that a) strongly influenced later work, b) is of the last 5 years or c) is used in the current fatigue assessment of the DMO frigates.

This chapter distinguishes three categories of damage accumulation models, with a basis in:

- Continuum Mechanics: The material is modelled as a continuum (i.e. intact geometry, section A.1). The indicative property is the **amount of cycles** n_i .
- Fracture Mechanics: The sample is modelled as a cracked geometry (Section A.2). The indicative property is the **crack length** a_i .
- Damage Mechanics: The material is modelled as a deteriorating continuum (Section A.3). The indicative property is typically the **Young's modulus** E_i .

In each of the three model categories a non-dimensional damage parameter D can be formulated by dividing the current indicative property over its critical value. It should be noted that the damage rate dD might not be constant.

The starting point is the LDAM from Palmgren and Miner. The characteristics of this model are summarised in the box below.

Theory:	<i>Linear Damage Accumulation Model (LDAM)</i>	
Theory by:	PALMGREN-MINER	year: 1924 - 1945
Type:	Phenomenological (Palmgren) & Physics-based (Miner), linear, continuum, spectral	
Typical application:	Variety of steel (and other materials) welded joints and base materials under (random) VA loads.	

Recall that the Palmgren-Miner model is given as:

$$\text{for } \Delta\sigma \geq \Delta\sigma_{th}$$

$$D = \sum_{i=1}^k \frac{n_i}{N_i} \leq D_{\text{crit}} = 1 \quad (4.6)$$

Each model is classified as being (partially):

Empirical An empirical model is constructed by fitting trends through experimental data. It is based on measurements/observations alone, without considering the system and available theories. Due to this experimental nature, extrapolation is not recommended.

Phenomenological A phenomenological model captures trends in phenomenal and mimics these phenomena and observed processes, but it does not consider the underlying physics. As it models phenomena, extrapolation is typically possible.

Physics-based A physics-based model is derived from first principles (axioms) and does not include observations or observed processes.

In total 30 proposed models are subject to discussion in this thesis. Because the model as proposed by Leonetti et al. (based on the proposal by Hirt and Kunz) is selected for further analysis (see section 4.4) it is discussed here. The description of the 28 other models that were considered is presented in appendix A.

Theory:	<i>Damage limit concept</i>	
Theory by:	HIRT-KUNZ	year: 1999
Type:	Phenomenologic, non-linear, fracture, semi-temporal	
Typical application:	Fatigue assessment of steel bridges	

The damage limit concept by [Hirt and Kunz](#) [52] defines a threshold stress range, derived from LEFM, below which no damage is accumulated. This threshold stress range lowers as the fatigue damage accumulates. [Hirt and Kunz](#) express the accumulated fatigue damage in the fracture mechanics domain as the crack length.

The fatigue life is calculated in the same manner as for the LDAM, with the exception that the accumulated damage affects the threshold stress per historical step h . The expression for the fatigue life is given by (4.7). In this equation $N_{i,h}$ is the allowable fatigue life at stress level i at damage increment h , expressed by a Basquin-type relation. The fatigue limit is reduced according to (4.10) over the development of the damage from 0 to 1.

$$\text{for } \Delta\sigma \geq \Delta\sigma_{th,h}$$

$$N = \frac{1}{\sum_{h=1}^{h_{tot}} \left[\sum_i \frac{n_i}{N_{i,h}} \frac{n_i}{\sum_i n_i} \right]} \quad (4.7)$$

To calculate the threshold stress [Hirt and Kunz](#) propose (4.10), with $\Delta\sigma_{th}$ the threshold stress range for fatigue damage accumulation, $\Delta\sigma_0$ the fatigue limit, Y the geometrical correction function for the SIF a_{ini} the initial crack depth, a the current crack depth, D the accumulated fatigue damage and m the slope of the S-N curve. For structural steels this m is typically 3 in the MCF range.

The threshold stress intensity factor for long fatigue cracks $\Delta K_{th,lc}$ is defined as:

$$\Delta K_{th,lc} = Y(a)\Delta\sigma_{th}\sqrt{\pi a} \quad (4.8)$$

This allows to write the definition (4.9) to the threshold equation (4.10) by [Hirt and Kunz](#). The damage is defined in analogy of the development of a crack to a through-thickness crack.

$$\Delta\sigma_0 = \frac{\Delta K_{th,lc}}{Y(a_{ini})\sqrt{\pi a}} \quad (4.9)$$

The derivation of (4.9) by [Hirt and Kunz](#) follows the same scheme as used for the model by [Leonetti et al.](#) [75] as is expressed in appendix B.4. The only differences is that the model by [Leonetti et al.](#) employs the RLDM to scale the critical damage, and multiplies the threshold SIF with the SIF intensification factor $M_w(a)$.

$$\begin{aligned} \Delta\sigma_{th} &= \Delta\sigma_0 \frac{Y(a_{ini})\sqrt{\pi a_{ini}}}{Y(a)\sqrt{\pi a}} \\ &= \Delta\sigma_0 \left(1 - \frac{D}{D_c}\right)^{1/(m-2)} \end{aligned} \quad (4.10)$$

$$\text{Which, for structural steels with } m = 3 \text{ yields, } = \Delta\sigma_0 \left(1 - \frac{D}{D_c}\right)$$

This damage limit model is, due to the assumptions in the derivation, valid under the following conditions [52, 75]:

1. The crack is a long fatigue crack.
2. The stress range level is high enough for a crack to propagate in the Paris regime.

The damage limit, below which no fatigue damage is accumulated, is thus a function of the damage that has accumulated before. The damage limit concept thus has a link to the damage mechanics, but it models the damage in the fracture instead of the continuum domain.

Summarizing the benefits and downfalls of the Kunz model:

- + Accounts for the non-linear, damage-dependent damage development
- Does not account for unstable crack growth region. However, as this typically only consumes a small fraction of the fatigue life, this downfall is not of significance in relation to the fatigue life prediction.
- Does not consider the different threshold conditions of long and short fatigue cracks.

Theory:	<i>Non-linear damage accumulation model: Modified Hirt-Kunz</i>	
Theory by:	LEONETTI	year: 2020
Type:	Phenomenological, non-linear, fracture, semi-temporal (due to integration steps h in recursive formulation)	
Typical application:	Nominal stress of welded joints in (random) VA loading conditions. Typically applied to steel bridges.	

The model by Leonetti et al. [75] proceeds from the damage limit concept by Hirt and Kunz. The modifications are:

- The integration of the 6PRFLM (also called the GRFL in the expression of the fatigue life. The fatigue resistance is also a function of the propagating fatigue damage.
- The implementation of the SIF intensification factor $M_w(a)$ as a function of the weld geometry.
- Implementing the RLDM to describe the critical damage not strictly as 1, but as a fitted distributed parameter.

The SIF intensification factor ($M_w(a)$) originates from [53]. It is shown in (4.11).

$$M_w(a) = \max\left(C_\alpha \left(\frac{a}{T}\right)^\alpha, 1\right) \quad (4.11)$$

The threshold stress intensity factor ($\Delta K_{th,lc}$) for long fatigue cracks is defined as (4.12) with $M_w(a)$ as given in (4.11) in which T is the plate thickness, and C_α and α are a function of the weld geometry. $Y(a)$ is a geometrical correction factor. This equation is valid for fatigue cracks that grow from the weld toe.

$$\Delta K_{th} = M_w(a) Y(a) \Delta \sigma_{th} \sqrt{\pi(a_0 + a)} \quad (4.12)$$

This yields the stress-threshold equation in (4.13).

$$\Delta \sigma_{th} = \Delta \sigma_0 \frac{M_w(a_{ini}) Y(a_{ini}) \sqrt{\pi(a_0 + a_{ini})}}{M_w(a) Y(a) \sqrt{\pi(a_0 + a)}} \quad (4.13)$$

$$\text{Of which the first order approx. is: } = \Delta \sigma_0 \frac{M_w(a_{ini}) Y(a_{ini}) \sqrt{a_{ini}}}{M_w(a) Y(a) \sqrt{a}}$$

Further derivation by Leonetti et al., based on the Forman-Mettu relation (instead of the Paris relation) for the crack growth rate in the near-threshold region at a fixed stress ratio, eventually yields the relation of the stress range and the threshold stress:

$$\Delta \sigma_{th,h} = \Delta \sigma_0 \left(1 - \frac{D_h}{D_{cr}}\right)^\zeta \quad (4.14)$$

With:

$$\zeta = f(\alpha, m) = \frac{\alpha + 1/2}{1 - m(\alpha + 1/2)} \quad (4.15)$$

See appendix B.4 for the derivation of the above formulations.

This expression for ζ captures the low-stress cycles: the "tail" of the S-N curve, which determines the damage of low-stress cycles, is included as a function of the weld geometry. Combining the expected value of the damage (4.17), with the formulation of the 6 Parameter Random Fatigue Limit Model (6PRFLM) [74], yields the expression of the amount of cycles to failure (4.18). Leonetti et al. determines the parameters by inference of CA and VA data. It should be noted that the model by Hirt and Kunz defines $\zeta = 1$. $\zeta = 0$ poses the LDAM by

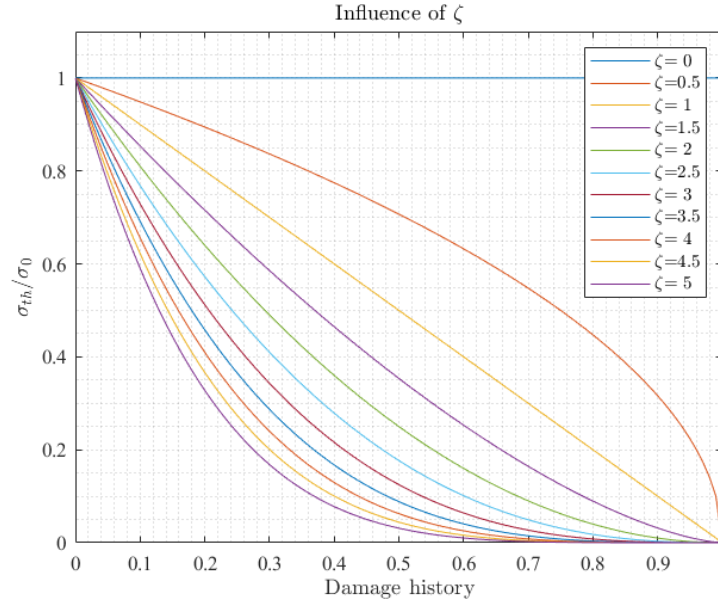


Figure 4.13: Influence of the ζ parameter on the damage accumulation

Palmgren and Miner. Figure 4.13 shows the effect of the ζ on the relation between the damage history (0 is at the beginning of the life and 1 equals failure) and the threshold stress.

Assuming that the load history is ergodic³, the fatigue life can be determined by :

$$N = \int_0^{D_{\text{crit}}} E[\dot{D}] dD \quad (4.16)$$

For which the expected value of the damage rate, identical to the expression in the **LDAM**, is given by:

$$E[\dot{D}] = \sum_i \frac{n_i}{N_i} \frac{n_i}{\sum_i n_i} \quad (4.17)$$

The integration of the **GRFL** yields the final expression for the fatigue life.

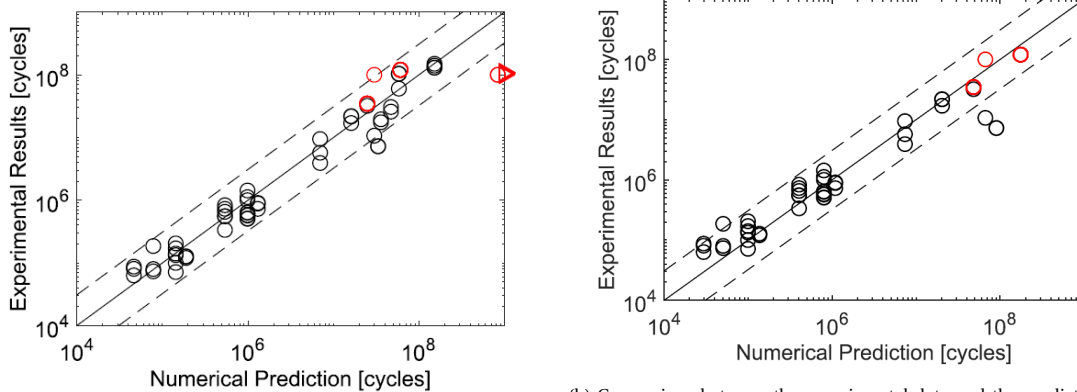
for $\Delta\sigma \geq \Delta\sigma_{th,h}$

$$\begin{aligned} E[\dot{D}] &= \sum_{h=1}^{h_{\text{tot}}} \left[\sum_i \frac{n_i}{N_{i,h}} \frac{n_i}{\sum_i n_i} \right] \\ &= \sum_{h=1}^{h_{\text{tot}}} \left[\sum_i \frac{n_i}{10^{\beta_0 + \beta_1 \log_{10}(\Delta\sigma_i) - p \log_{10}\left(1 - \frac{\Delta\sigma_{th,h}}{\Delta\sigma_i}\right)}} \frac{n_i}{\sum_i n_i} \right] \\ &= \sum_{h=1}^{h_{\text{tot}}} \left[\sum_i \frac{n_i}{\frac{\beta_0(\Delta\sigma_i)^{\beta_1}}{\left(1 - \frac{\Delta\sigma_{th,h}}{\Delta\sigma_i}\right)^p}} \frac{n_i}{\sum_i n_i} \right] \end{aligned} \quad (4.18)$$

$$\text{allowing } N = \frac{D_{\text{crit}}}{E[\dot{D}]}$$

6PRFLM The **6PRFLM** expresses the S-N curve not as one line, but as a distribution of curves of different percentiles (confidence level). In the damage assessment as proposed by **Leonetti et al.** the S-N curve is a function of the damage state (expressed as a vector from 0 to 1, increasing over time) D/D_{cr} .

³An ergodic process is a subset of stochastic processes. A process is said to be ergodic if the time averages of a section of the signal are equal to the time averages of the total signal. Or, as Wikipedia puts it: "a stochastic process is said to be ergodic if its statistical properties can be deduced from a single, sufficiently long, random sample of the process."



(a) Comparison between the experimental data and the prediction obtained by the proposed model. The black points represent the failure data, whereas the red points represent the runout data. If the predicted fatigue life is finite, the resulting point is a circle, otherwise it is a triangle positioned at 10^9 cycles. From [75].

(b) Comparison between the experimental data and the prediction obtained by Model 1 (Eurocode-3) [...] The black markers represent the experimental failure data, whereas the red markers represent the runout data. If the predicted fatigue life is finite, the resulting marker is a circle, otherwise it is a triangle positioned at 10^9 cycles. The dashed lines bound the mean prediction and are derived as $\log_{10}(N) \pm 1.64$. From [75].

Figure 4.14: Research results from Leonetti et al., showing the improved fit of the numerically predicted amount of cycles with the experimental data, compared to the Eurocode 3.

The conclusion of Leonetti et al. for the dataset from Klippstein and Schilling is that the Eurocode 3 predicts a (slightly) longer life times than the novel model. At the cost of some increased conservatism Leonetti et al. provides a more accurate prediction.

As the paper by Leonetti et al. uses inference to fit the parameters of the damage calculation, it would benefit from a dataset with less scatter. By using the NSC the dataset is valid for the S-N curves of samples with an identical FAT class, but inference has to be performed per FAT class to have a general validity. A suggested improvement is to include more local information (i.e. use the ENSC instead of the NSC) to reduce the data scatter and to deliver a generally applicable model.

Summarizing the benefits and downfalls of this model:

- + Shows promising results for the tested dataset.
- + Expected benefit of including local information is large as the scatterband determines the scatter in the output.
- Provides (slightly) more conservative results than the Eurocode 3. However, it is better to have more accurate results if research results substantiate the novel method. The conservatism is also a function of the fatigue damage criterion that is applied and the manner in which the mean stress correction is applied.
- The method requires representative (preferably full-scale) VA test results, which is expensive, but it is a database that expands rapidly. The VALID III project (a JIP in which DMO partakes) is an example.

4.4. Variable amplitude fatigue damage database

To test the validity of the selected damage accumulation models for (random) VA loading, a database is compiled. This database is for steel samples within the research scope (see section 2.5). Each of the databases is introduced and summarised (table 4.4) in this section. Section 7.3 presents the analysis of the specimens from this table.

The papers that are cited are all for steel welded joints of various yield strength. Qin et al. proved that the yield strength hardly (and to a decreasing extent with increased local information) affects the fatigue resistance for the NSC, HSSSC, ENSC and TSC. Stainless steels are excluded from the database as the research into the respective damage mechanisms (i.e. crack initiation and propagation behaviour) involved is not part of this research.

The papers that are cited are all for random VA loading, and are listed below. The aim is to compile a list with an even variation over hot spot types, geometries, spectra and plate thicknesses. This is to, in line with

the work in [111], be able to assess the influence of these variations and to assess if the novel method is independent of these variations.

- Klippstein and Schilling [63] studied the CA and VA fatigue behaviour of transverse stiffener welds. The welds are 6.35 mm (throat height) fillet welds. The random loading was applied according to the Rayleigh distribution.
The VA test data comprises 10 datapoints of which the minimum, maximum and the Miner effective stress ($0.538(S_{\max} - S_{\min})$) are presented. The material is ASTM A572 Grade 50 weathering steel, with a yield strength of 50 ksi = 345 MPa to present the data for a typical medium-size bridge structural steel. The respective hotspot is of type C.
- Agerskov et al. [3] tested a HSS, as is typical for offshore structures for a modified Pierson-Moskowitz spectrum. The tested samples are a cruciform that is loaded on the base-plate with a hot spot type C, and a plate with a longitudinal attachment on both sides with a hot spot type A. The analyses were performed using the NSC and the LDAM. It should be noted that only the results of the larger specimens (larger versions of the smaller specimens, but still SSS) are used, based on the recommendation by Agerskov et al. and their critical attitude towards the smaller specimen results.
- Ota et al. [103] present the fatigue data of a butt-welded joint under a Rayleigh spectrum load. The experiments are performed at two loading and response levels and runout data is excluded from the analysis.
- Zhang and Maddox [147] present the values of the Palmgren-Miner damage sum for welded joints of longitudinal attachments of the hot spot type A and B, subject to Gaussian loads. The material is a regular structural steel with a yield strength of 418 MPa. The paper presents the results for three variations of the Gaussian load: cycling up and down from a constant mean stress, and cycling around a constant mean stress.
- Zhang and Maddox [148] present the results of full-scale tests of welded SCR pipe details subject to maritime VA loads. The details are butt-welds with a base material that yields at 519 MPa.
- DMO has performed four VA experiments as part of the assessment of the quality of half-V cruciform joints in relation to class rules.

The papers by Yoo et al. [143] and Osawa et al. [102] assess the influence of storm loads, under the assumption that the peak loads from storms pose the largest part of the fatigue damage. The SSC-466 from the Ship Structure Committee [125] presents an overview of CA and VA fatigue test results up to 2013. The presented database in this section is a combination of the random VA data from [125] and of other authors.

A summary of the results that will be used to assess the validity of the LDAM and the novel assessment method that will be the result of this research is presented in table 4.4.

Table 4.4: Database summary of random VA spectrum loading of steel welded joints

Source	Geometry	HS Type	Spectrum	Number
Klippstein and Schilling [63]	PP DS Cruciform joint	Type C	Rayleigh	10
Agerskov et al. [3]	PP DS Longi. plate attachment	Type A	BROAD64	16
Agerskov et al. [3]	FP DS Cruciform joint	Type C	PMMOD64	10
Agerskov et al. [3]	FP DS Cruciform joint	Type C	BROAD64	12
Ota et al. [103]	FP DS Butt joint	Type C	Rayleigh	14
Zhang and Maddox [147]	PP DS Longi. plate attachment	Type A	Linear/Gaussian	10
Zhang and Maddox [147]	PP DS Longi. edge attachment	Type B	Linear/Gaussian	6
Zhang and Maddox [148]	FP DS Butt joint	Type C	Log-linear	7
DMO	FP DS Cruciform joint	Type C	Rayleigh	4

An observation with regards to table 4.4 is that only 6 hot-spot type B samples are included. HS Type-B is the category of notches at the weld end, parallel to the weld seam. It are typical notches at frame-stiffener connections. This will be subject for discussion in chapter 8.

4.5. Concluding remarks

This chapter provides an overview of the most promising damage accumulation models for fatigue under VA loading. For further assessment several demands are listed:

- To allow an accurate assessment of the consumed fatigue life time the model should account for the non-linear nature of the fatigue damage accumulation.
- To fit in the short timeframe that is typically available at a shipyard to perform the assessment, it should operate in the spectral instead of the temporal domain.
- The model has to be properly validated for random loading histories.

Ideally, to promote a fruitful implementation in the yard-practise, it has a physical foundation.

Table 4.5 presents the summary of the comparison of the presented models, highlighting in green the ones that tick three times "yes" to the criteria above. The model by Subramanyan has only been validated for base materials, not for welded joints, and is thus not selected. The models by Corten and Dolan and by Chaboche and Lesne are excluded from further analysis as respectively the physical nature and validity for complex loads (i.e. many OL's and UL's in a highly stochastic signal) are compromised.

In yellow the four models are listed that propose a linear accumulation, whereas the spectral approach and validity for random (stochastic) VA loads is confirmed. This is done because the linear nature of a model is not a strict requirement: that is, the model will be combined with a fatigue damage criterion (see chapter 3) and the combination of the fatigue damage criterion and damage accumulation model provides the assessment method. Only when reducing the total damage D to a value below 1 the non-linearity is a requirement.

The model that complies the best with the total list of demands is the fracture domain model by Hirt and Kunz as implemented by Leonetti et al. [75]. The paper was published in 2020 and will be considered as an alternative for the LDAM in this research. The improvement potential of this method is subject of section 5.1. The method by Leonetti et al. is strictly speaking in the temporal domain (hence the **yes*** in table 4.5). However, because this temporal domain refers to integration steps in a recursive equation, instead of the temporal analysis of the loading history, the analysis is not excessively intensive and still deemed suitable for yard-implementation.

For reference, the more advanced State-of-the-Art method of Leonetti et al. is compared to the Palmgren-Miner model with the Haibach extension. The deterministic RLDM by Schütz is excluded from the analysis as it is highly dependent on the input spectrum. It is however incorporated in the model by Leonetti et al., but the probabilistic nature of this method allows the use of the RLDM.

Table 4.5: Table to summarise the comparison of the presented fatigue damage accumulation models. Green boxes indicate full compliance (three times a "yes") and yellow boxes indicate models that are not strictly non-linear, but comply with the demands for spectral calculations and validity for stochastic VA loads.

Model by	Non-linear accumulation	Spectral domain	Validated for stochastic VA	Note
CONTINUUM				
Palmgren-Miner [95, 104]	no	yes	yes	Large scatter
Corten and Dolan [15]	yes	yes	yes	Physically incorrect
Marco and Starkey [91]	yes	yes	no	Only multi-level loads
Manson [89]	no	yes	yes	Bi-linear accumulation
Haibach [48]	no	yes	yes	See Palmgren-Miner
Subramanyan [130]	yes	yes	yes	Only for base-materials
Schütz [123]	no	yes	yes	Requires identical test
Leipholz [70]	no	yes	no	Multi-level block loads
Ben-Amoz [7]	yes	yes	no	Only two-step block loads
Mesmacque et al. [94]	yes	no	yes	Extends well to multi-axial
Naderi et al. [98]	yes	no	yes	Entropy based
Zhu et al. [150]	no	yes	no	Multi-level block loads
Gao et al. [42]	yes	yes	no	Only for base-materials
Zuo et al. [155]	yes	yes	no	Two-level block loads
Rege and Pavlou [115]	yes	yes	no	Two-level block loads
Pavlou [107]	yes	yes	no	Two-level block loads
Zhu et al. [153]	yes	yes	no	Multi-level block loads
Liu et al. [77]	yes	no	no	Multi-level block loads
FRACTURE				
Paris and Erdogan [105]	yes	no	yes	Crack-growth model
Manson and Halford [87]	yes	no	no	Multi-level loads
Hirt and Kunz [52]	yes	yes*	-	Not strictly accumulation
Kwofie and Rahbar [66]	no	no	yes	Piece-wise linear
Gao et al. [41]	yes	no	no	Multi-level loads
Leonetti et al. [75]	yes	yes*	yes	Integration steps: temporal
DAMAGE				
Xiaode et al. [139]	yes	yes	no	Two-level block loads
Chaboche and Lesne [11]	yes	yes	yes	Inadequate for complex loads
Lemaitre et al. [73]	yes	no	no	Multi-level block loads
Shang and Yao [124]	yes	yes	no	Multi-level block loads
Dattoma et al. [18]	yes	no	no	Multi-level block loads
Yuan et al. [144]	yes	no	no	Multi-level block loads
Zhang et al. [146]	yes	no	yes	Only for base-materials

5

Method

The analysis of the literature on fatigue damage criteria (Chapter 3) and VA damage accumulation models (Chapter 4) is presented before. This chapter provides a detailed analysis of the problem at hand. It is closely related to chapter 2 where the problem is stated. This chapter provides the scientific justification of the research.

This chapter presents the analysis of the knowledge gap (Section 5.1) and the statement of the hypotheses to test (Section 5.2).

5.1. Knowledge gap

The identified knowledge gap that this research will fill is depicted in table 5.1. It shows that, whereas several proposals are present in literature for fatigue assessment concepts (properly summarised in [19, 111]) - determining the stress type to compare - and for the damage accumulation separately, a combination of both solution paths is thin.

As more local information (increasing in downward direction in table 5.1) implies more accuracy at the cost of more efforts and complexity, but the scatter index of the TSC compared to the ENSC is only 3.4% less, the TSC is not employed in this research. To benefit from the fact that the ENSC operates on only one S-N curve and has an improved scatter of 37.0%, the method by Leonetti et al. will be tested for improvement when using the ENSC.

Table 5.1: Knowledge gap visualisation. The references show the known research and class efforts. The grey marked cells indicate the combinations of fatigue damage criteria and damage accumulation models that are not yet made in literature. The last column contains the hypotheses of proportionality between the complexity and scatter reduction. The three roman numbers indicate the cases that are compared in this paper.

		LDAM [95, 104]	NLDAM [75]
increased accuracy, complexity and efforts	NSC	i.a. [27, 55, 99, 100, 111]	[75]
	HSSSC	I) i.a. [27, 55, 100, 111]	Limited scatter reduction
	ENSC	II) i.a. [26, 55, 111]	III) Complexity \propto scatter reduction
	TSC	[23, 111]	Complexity \geq scatter reduction [111]

5.2. Hypotheses

The hypotheses to test in this research are:

- H1. The current approach of DMO, to use the HSSSC in combination with the LDAM with $D_{crit} = 0.75$, provides a conservative fatigue life prediction.

This hypothesis originates from the motivation of this research and will be rejected or accepted based on the LogNormal mean value of the N_{exp}/N_{calc} of the VA database for the DMO approach. It should

be noted that the effect of slamming should be divided out of the 0.75, in accordance with the results of the slamming factor from literature, to provide a fair comparison.

- H2. The model as postulated by [Leonetti et al.](#) and the [LDAM](#) improve¹ when incorporating more local information in the fatigue damage criterion.

This hypothesis originates from the use of the 95% probability of survival bound as is typical for the S-N curves. For a smaller standard deviation this bound is closer to the mean and the conservatism reduces accordingly. This hypothesis is linked to the research results by [Qin et al.](#) [111], who proves the reduction of scatter for fatigue damage criteria with more local information.

- H3. The model by [Leonetti et al.](#) in combination with the [ENSC](#) provides a better² prediction of the fatigue life than the model by [Miner](#), [Palmgren](#) in combination with the [ENSC](#).

This hypothesis originates from the fact that the model by [Leonetti et al.](#) models the fatigue damage accumulation as non-linear: this complies with the observed development of fatigue damage and the analogy with fracture mechanics. The use of a linear fatigue damage accumulation model overestimates the influence of cycles at the beginning of the fatigue lifetime (crack initiation), which is stochastic and scattered. Also, the [LDAM](#), in contrary to the [NLDAM](#) does not account for the effect of low stress range amplitudes below the fatigue limit. This makes the estimation of the fatigue life in the crack propagation phase conservative, here the specimen is more sensitive to fatigue damage accumulation due to the locally reduced material strength.

- H4. The model by [Leonetti et al.](#) in combination with the [ENSC](#) provides a better² prediction of the fatigue life than the model by [Miner](#), [Palmgren](#) in combination with the [HSSSC](#).

This hypothesis is confirmed if the other hypothesis are confirmed and superposition is valid. The different elements in the fatigue assessment do interact, which might challenge the validity of superposition. However, the [NLDAM](#) uses the mean stress according to the [ENSC](#) to determine the S-N curve. This curve is subject to scatter from both the [CA](#) fatigue limit and the value of the critical damage: both do not interfere with the calculation of the fatigue damage criterion.

Table 5.2 presents a visualisation of the four hypotheses in relation to one another.

Table 5.2: Visualisation of the four hypotheses and their relation. The letters in [brackets] are used to refer to each combination, whereas the H# indicates the hypotheses.

	Palmgren-Miner [95, 104] with Haibach [48] extension	Leonetti [75]
HSSSC	[A] H1: [A] is conservative	[B]
ENSC	[C] H2: [C] better than [A]	[D] H2: [D] better than [B] H3: [D] better than [C] H4: [D] better than [A]

The conclusion of the research will present a rejection or acceptance of each hypothesis.

5.3. Methods to assess damage accumulation models

Acknowledging the two-dimensional variation in this research, see table 5.1, the typical scientific methods to assess the improvements in both axes are discussed separately. As was done in the paper by [Qin et al.](#) [111] the improvements of using a more complex fatigue damage criterion was studied using a database of [CA](#) fatigue data, and by assessing the geometry of the underlying samples with each of the four concepts. The standard deviation and strength scatter range index provide a mean to objectively assess the improvement in accuracy.

¹i.e. incorporate less conservatism, provide more accurate fatigue life predictions

² i.e. incorporates less conservatism and provides a more accurate fatigue life predictions

Novel damage accumulation models, like the ones postulated in [75, 89], are assessed for a compiled VA fatigue database and compared to the fatigue life prediction from the LDAM.

For this research a hybrid solution is proposed: firstly to select and assess a novel damage accumulation model with the HSSSC using the compiled VA fatigue database and secondly, to vary the S-N curve for these damage accumulation models by implementing a more complex fatigue damage criterion (i.e. the ENSC). The ENSC is selected in line with the research results from [111].

The model by Leonetti et al. [75] is selected and is deemed to benefit from more accuracy in the fatigue damage criterion. This is because the method uses curve fitting/statistical inference to formulate the criterion: less scatter means better (i.e. more accurate) fitting/inference. The ENSC is the first method on the scale of increasing efforts and cost that compiles one S-N curve for all structural details. This makes the method more prone to implementation and improves the inference as the total fatigue database can be used for the inference.

The AIC will be used to assess the difference in quality of the fit of the different combined fatigue assessment methods. This is as was done in [75].

5.4. Research roadmap

To summarise the research, figure 5.1 presents a visual overview of the research steps and their relation to the main question.

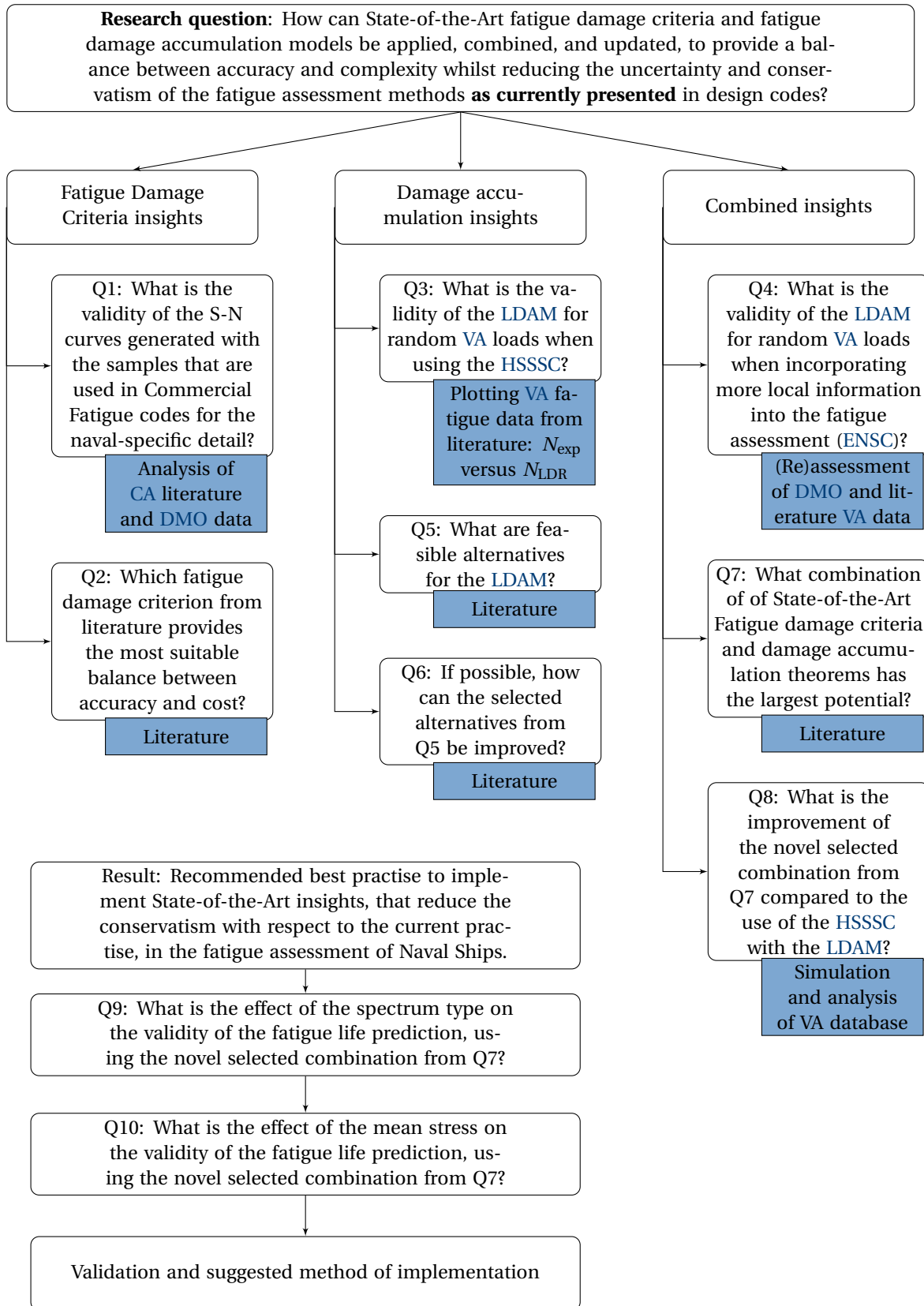


Figure 5.1: Research roadmap. The blue boxes indicate the means that are used to formulate the answer to the respective questions.

II

Modelling

6

Constant Amplitude analysis

*In chapter 3 the literature in relation to the fatigue damage criteria was presented. In this current chapter the considered fatigue damage criteria are used to assess the **Constant Amplitude (CA)** fatigue life of the specimens.*

This chapter presents the analyses and considerations with respect to the constant amplitude fatigue resistance that form the input for the variable amplitude damage accumulation models. The two fatigue damage criteria that are used are, in line with the scope, the **Hot Spot Structural Stress Concept** (Section 6.1) and the **Effective Notch Stress Concept** (Section 6.2). These fatigue damage criteria are used to establish the fatigue strength of the **DMO** cruciform joint samples (Section 6.3). After that, the **Generalised Random Fatigue Limit (GRFL)** is introduced (Section 6.4) to model the **MCF** and **HCF** resistance. Section 6.5 contains the **SCF** analysis of the **CA** specimens that are also presented in the articles the contain the **VA** data.

6.1. Hot Spot Structural Stress Concept

In line with the typical yard practise, the analysis of the hot spot structural stress is performed according to DNVGL-CG-0129 "Fatigue assessment of ship structures" [27]. The hot spot structural stress is based on the assumption of a linear stress variation over the thickness of the plate, which typically shows an enhancement of the nominal stress due to the presence of the notch. The structural stress is the equilibrium equivalent stress distribution at the notch location.

DNVGL-CL-0129 allows both a shell and a solid model for the analysis. The only argumentation to use solid elements is "for complex cases", without specification of what these are. As a result typically a shell model (without modelled welds) is used to assess the hot spot structural stress. This is computationally less expensive than a solid model, and thus provides for a fast analysis. The use of a shell model without a model of the weld suffices for the **HSSC** if "the structural discontinuity is small, and if no bending is introduced in the vicinity of the weld" [21]: due to the non-symmetry of the half-v weld at one side of the cruciform, and the weld-load-carrying nature of the attachment, this is not the case for the **DMO** samples.

DNV-GL offers two methods of analysis: method A poses a linear extrapolation to the location of the hot spot of the effective stress at $t_p/2$ and $3t_p/2$ from the hot spot - method B poses to multiply the effective stress at $t_p/2$ from the hot spot with a factor of 1.12. One has to realise that both methods are simplifications of reality, and will likely have some deviation. To determine which one is the best fit, both methods can be compared to the through-thickness linearisation as proposed by **Dong** [28]. By its nature this will provide the exact answer, independent of the mesh size. The method by **Dong** is based on (normal) force and moment equilibrium over the cross section, and is given by (6.1) for a solid model.

$$\begin{aligned}
 s_s &= s_m + s_b \\
 &= \frac{\sum f_i}{t_p} + 6 \left(\frac{\sum_i (f_i r_i) - \frac{\sum f_i}{t_p} (t_p/2)}{t_p^2} \right)
 \end{aligned} \tag{6.1}$$

Method B from DNVGL-CG-0129 only uses one source of information (stress at $t_p/2$ from the notch) in contrary to method A, where also the stress at $3t_p/2$ is input, enabling the (linear) estimation of a slope. Including the most information within the DNV-GL rules, method A is used for the comparison of the **DMO CA** samples to the DNV-GL S-N curve.

DNV-GL presents the following formulae to compute the effective stress at each considered node [27], based on the principal stresses:

$$\Delta\sigma_1 = \frac{\Delta\sigma_{\perp} + \Delta\sigma_{\parallel}}{2} + \frac{1}{2}\sqrt{(\Delta\sigma_{\perp} - \Delta\sigma_{\parallel})^2 + 4\Delta\tau_{\parallel}^2} \quad (6.2)$$

$$\Delta\sigma_2 = \frac{\Delta\sigma_{\perp} + \Delta\sigma_{\parallel}}{2} - \frac{1}{2}\sqrt{(\Delta\sigma_{\perp} - \Delta\sigma_{\parallel})^2 + 4\Delta\tau_{\parallel}^2} \quad (6.3)$$

$$\sigma_{Eff} = \left(c \cdot \max \left\{ \begin{array}{l} \sqrt{\Delta\sigma_{\perp}^2 + 0.81\Delta\tau_{\parallel}^2} \\ K_p \cdot \Delta\sigma_1 \\ K_p \cdot |\Delta\sigma_2| \end{array} \right\} \right) \quad (6.4)$$

In the above formulations $c = \{1, 1.12\}$ for method {A, B}, and $K_p = 0.9$ to account for a manual welding process. The values of $\Delta\sigma_{\perp}$, $\Delta\sigma_{\parallel}$ and $\Delta\tau_{\parallel}$ are extracted from the **FE** model. The orientations are with respect to the expected fatigue crack. This calculation of the effective stress accounts for the principal stresses, which are both calculated according to the formulations as expressed by Mohr's circle. The principal stress directions are, by definition, those in which no shear stress is present.

The first formulation ($\sqrt{\Delta\sigma_{\perp}^2 + 0.81\Delta\tau_{\parallel}^2}$) originates from the paper by **Lotsberg [79]**. The β (0.81) formulation per type of sample is constructed by fitting **CA** fatigue test data under different stress angles to the DNV-GL C203 S-N curves [26]. For the combination of a D curve (FAT 90, for **NLC HSSSC** assessments) in the stress direction normal to the weld toe, and a C2 curve ("S-N category C2 may be used for continuous shear stress in a full penetration weld according to DNV-RP-C203" [79]) for the stress direction parallel to the weld, this yields a value of 0.81 [26, 79, 80]. It is thus a capture of the angle between the two stresses. This formulation resembles a weighted Pythagorean calculation of the stress under an angle.

As for the relevant **FAT** class to compare the test results to: "For welded details, the D-curve is the reference curve for the hot spot stress method" [27]. The D-curve equals the **FAT90** (i.e. $S_s = 90$ MPa at $N = 2 \cdot 10^6$).

6.2. Effective Notch Stress Concept

To calculate the effective notch stress, the stress-averaging approach is used (see [23, 111, 112] for the derivations). The stress-averaging approach comprises an analytical through-thickness weld notch stress distribution (σ_n) which is averaged, see (6.5), over the material-characteristic micro-structural support length ρ^* .

The structural stress (from the **HSSSC**) is the input for a local analysis of the welded detail by means of the **ENSC**: ideally even without a **FE** model. The **FE** model will ideally only be used for verification of the analytical solution.

For reference, the **DMO** sample resistance is compared to a **CA** database with 1804 datapoints of a variety of weld types, plate thicknesses, loading and response ratios (r_{lr}), yield strengths and loading types as presented by **Qin et al. [112]**.

The effective notch stress is a function of:

$$\sigma_e = \frac{1}{\rho^*} \int_0^{\rho^*} \sigma_n(r) dr \quad (6.5)$$

$$2\sigma_e = S_e = f(\rho^*, t_p, s_s, r_s, C_{bw}, \beta, \alpha)$$

With:

- ρ^* Micro-structural support length: the stress is averaged over this depth
- t_p Plate thickness in the direction of the developing crack
- s_s Structural far-field stress
- r_s Structural bending stress ratio $r_s = s_b/s_s$
- C_{bw} Weld load carrying stress coefficient
- β Stress angle
- α Half of the notch angle

Here C_{bw} is considered as a curve-fitted function of the weld leg height (h_w), weld leg length (l_w), {connecting, cross, cover} plate thickness (t_c) and the base plate thickness (t_b), first presented in [111, 112].

Figure 6.1 presents the parameters in a sketch of a T-joint and a cruciform joint. This figure is from [111].

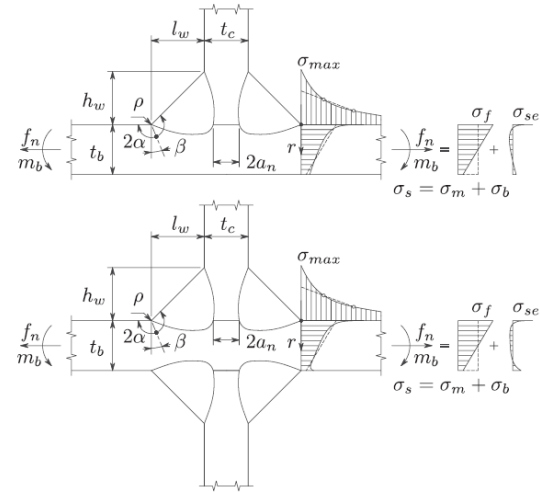


Figure 6.1: Sketch of the relevant parameters in the semi-analytical ENSC assessment of welded joints in a T- and cruciform joint respectively [112].

For a one-on-one comparison of fatigue test results at different loading and response ratios, the mean stress should be corrected for. This is typically done with the Walker mean stress correction [134]. The structural far field stress and bending stress ratio are obtained from the the hot spot structural stress distribution. However, in this semi-analytical approach the s_s and r_s are not taken from the DNVGL-CL-0129 approximations, but from the through-thickness linearisation by Dong [28]. This is because the method by Dong provides the exact solution independent of the mesh size. A second argument for the method by Dong is that the semi-analytical formulation will be compared to the converged FE results in a plot: therefore the data required for the method by Dong is extracted either way.

6.3. CA analysis of the DMO specimens

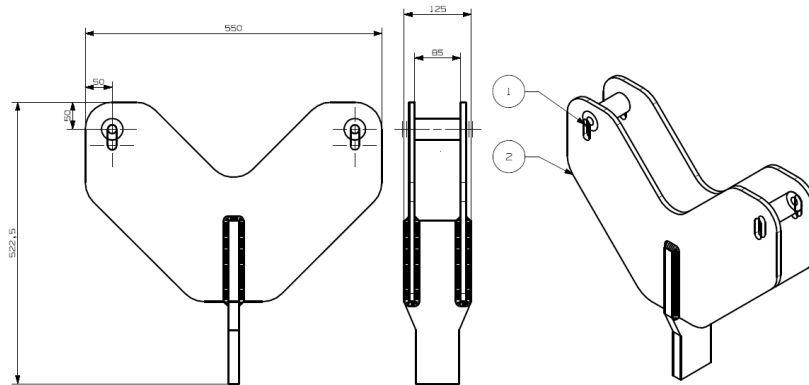
DMO has conducted CA fatigue tests of a cruciform joint with on one side a full-penetration half-V weld, and on the other side a FP double-K weld, see figure 6.3. The test setup enables a three-point bending load. The goal of the comparison is to assess the difference in results between the DMO samples and the samples as used to construct the S-N curves in the DNV-GL-0129. The hypothesis is that, by having a more specific scope and by using rutile welding material - which ideally poses a smoother welding surface -, the DMO samples have a better fatigue resistance (i.e. longer fatigue life) than suggested by the class [27] S-N curves. This section provides a test of this hypothesis. To this extent the parameters of the Basquin relation with the maximum likelihood based regression analysis are attained with the Matlab `fmincon` optimization procedure.

The DMO CA test data is used to showcase in detail the methods to determine the nominal, hot spot structural and effective notch stress.

6.3.1. Experiment setup

For the tests a separate specimen grip (accessory) was designed, as is shown in figure 6.2a. This accessory ensures a fixed distance between the two supporting points, at equal distance from the attachment. The accessory is greased at the contact locations between the grip and the specimen to minimise the friction forces acting on the specimen. The accessory and sample are clamped into the machine. This setup enables the maximum moment of the sample to be at the same location for each test, as the active pulling action is on the plate that is attached by means of the half-V weld. This also ensures that each of the samples is placed in the same orientation. A variation in results might however be due to the difference between the drawing and the actual weld.

The welds meet the minimum requirements by the welding procedure specification, but the as-welded ge-



(a) Drawing of the accessory as used to insert the specimen in the testing setup.



(b) Photo of the testing setup, including the accessory.

Figure 6.2: Layout of the test setup and the accessory.

ometry has in all locations a larger weld leg length and weld leg height. The analysis is based on the as-welded weld dimensions, with the idealised fillet shape. This is to capture the actual shape of the weld implicitly in the resistance curves, enabling the designer that uses these curves to model the idealised shape for calculations. The FE model has the dimensions as presented in figure 6.3.

The free body diagram of the sample is presented in figure 6.4. This resembles the FE model that is used in the analyses of the model with the roll bearing constraint (more on this in section 6.3.2). The sample width has some scatter with a mean of 72 mm from the manual cutting procedure. For the analysis per datapoint in the S-N curve the actual sample width is used.

6.3.2. FE 2D solid model

As was mentioned before, a non-modified¹ shell model does not suffice due to the local discontinuity and the introduced bending moment due to non-symmetry from the half-V weld. The cruciform detail is modelled by means of 2D solid elements. The DNV-GL method as employed is by means of 4 node isoparametric elements with 2 degrees of freedom at each node (PLANE42 in ANSYS).

With respect to the boundary conditions the load is applied on top of the attachment on the side of the half-V weld. The reaction forces at the interface between the sample and the accessory can be modelled in several ways:



Assuming there is no friction, the interface can be represented by a simply supported rolling connection. That means: only the translation in y direction (perpendicular to the base plate) is prevented.



Assuming the friction is infinite, the interface can be represented by a simply supported hinge connection. That means: the translations in x and y direction are prevented.



Assuming the friction is finite, the interface can be represented by a simply supported rolling connection with a force in x direction to represent the friction at the joint. That means: the translation in y direction is prevented and the translation in x direction is counteracted. Because the sample is greased the assumption is made that the friction force per side is 5% of the total force applied to the specimen.

¹When manually introducing misalignments in the shell model to capture the local discontinuities and introduced bending moments this statement does not hold. However, this is a labour-intensive and engineering-judgement sensitive procedure.

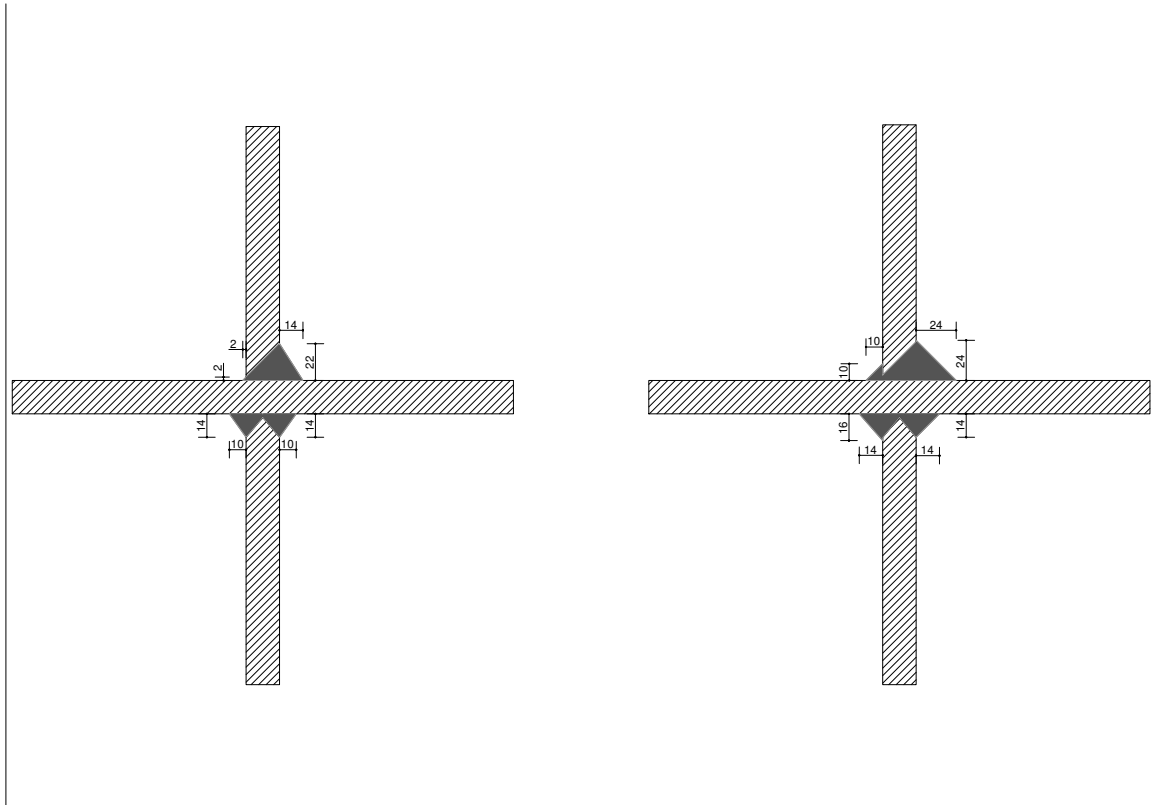


Figure 6.3: Idealised actual weld geometries. Left: FP half-V joint (top attachment) - called the "normal configuration", right: FP half-V joint with counter weld at the root (top attachment) - called the "double configuration"

This is related to the static friction coefficient of lubricated and greased steel-on-steel $\mu_{\text{static}} = 0.16$ [33]. As the normal force is half of the active force the friction force per side is 8% of the applied force. However, as fatigue is a cyclic process the static friction coefficient might over-estimate the friction. That is, the static friction is what the object has to overcome to move, whereas the kinetic friction is what the object has to overcome to keep moving. Engineering judgement leads to an estimated friction force of 5% the applied force per side.

All three of the modelling options are considered and will be subject for comparison and discussion in this section.

6.3.3. Fatigue damage criteria

The load that is applied to the cruciform joint specimens is $\approx 10\text{kN}$. The analysis in this section is performed at a load of 10kN, applied to the top of the attachment. The result at this load-level is used to linearly scale the results to the other load levels that the specimen has endured. In this section the SCF's are presented for four calculations: at the normal and double welded geometry (see figure 6.3) and for both sides of the attachment of the half-V weld (top side in figure 6.3). The side of the half-V weld is called "Half-V side" and the opposed side is called "Counter side". This separation in four notches is to use the actual SCF at the location that failed.

6.3.3.1. Nominal Stress Concept

The nominal stress is the stress in the material, without considering the notching element: hence, the base-plate subject to three-point bending. As the three-point bending load case has a linear increase and decrease of the bending moment towards and from the center, the bending moment is a function of the weld leg length l_w and thus different for each of the two positively loaded hotspots.

The nominal stress for the roller-boundary condition yields:

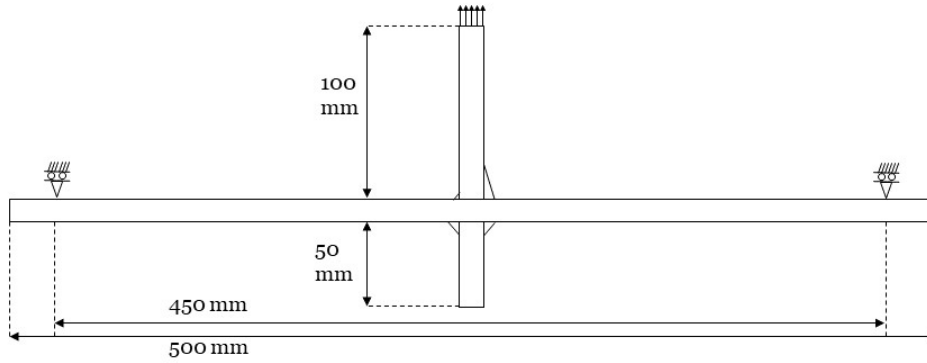


Figure 6.4: Free body diagram of the cruciform joint sample as tested by order of DMO. For illustration purposes this figure displays the roller boundary condition at the specimen-accessory interface.

$$\sigma_{\text{nom}}(x) = \sigma_b(x) + \sigma_n = \frac{M(x)y}{I} = \frac{Pr(x)y}{4I} = \frac{P((L - t_c)/2 - l_w)}{4I} \quad (6.6)$$

For the hinge-boundary condition the sample is statically indeterminate. For the friction case, the friction force perpendicular to the base plate induces a bending moment equal to the friction force times the arm of half the base plate thickness. This adds, for a friction force per side of 5%, a bending stress of:

$$\sigma_{b,fric} = 0.05P \frac{(t_b/2)^2}{I} \quad (6.7)$$

The data is compared to the DNV-GL [27] requirements, see figure 6.5. For a weld angle of 45° this yields a nominal FAT86 class.

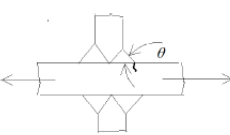
No.	Geometry	Description of joint	K factor	FAT N/mm ²
4		Cruciform joint or double sided transverse attachment with non-load carrying transverse attachment with thickness t. With full penetration or fillet weld. $K_{ms} = 1.12^{(4)}$, $K_{me} = 1.0$, $\theta = 45^{\circ(4)}$ $t \leq 25$ mm $t > 25$ mm	1.05 1.19	86 76

Figure 6.5: FAT class from DNV-GL-CG-0129

For a weld angle $\neq 45^\circ$, DNV-GL poses the correction to the FAT class of $1/c$. The K factor for the HSSC should be multiplied by this c coefficient:

$$c = \frac{1}{1.2} (0.6 + 0.6 \tan(\theta)^{1/4}) \quad (6.8)$$

$$c(71^\circ) \approx 1.05$$

This yields a NSC FAT class of 82 MPa. DNV-GL uses the 97.7% probability of survival bound at the 75% confidence level [26]. A fair comparison is thus to be made to a MLE fit of the fatigue data at this same probability of survival bound and confidence level.

6.3.3.2. Hot Spot Structural Stress Concept

The structural stress at the hot spot is calculated as was explained in section 6.1. As was stated the method A (linear extrapolation to the hotspot) is used. For reference, also the structural stress at the hot spot according to method B and Dong are calculated. These are presented in the second to fourth row of tables {6.2, 6.3, 6.4} for the {roller, hinge, 5% force} boundary conditions. The Dong method in row 4 is based on the full actual thickness (thus including potential added thickness due to the K-weld on the bottom side of the specimen).

The results of the analysis for method A and B are included in appendix D.1.

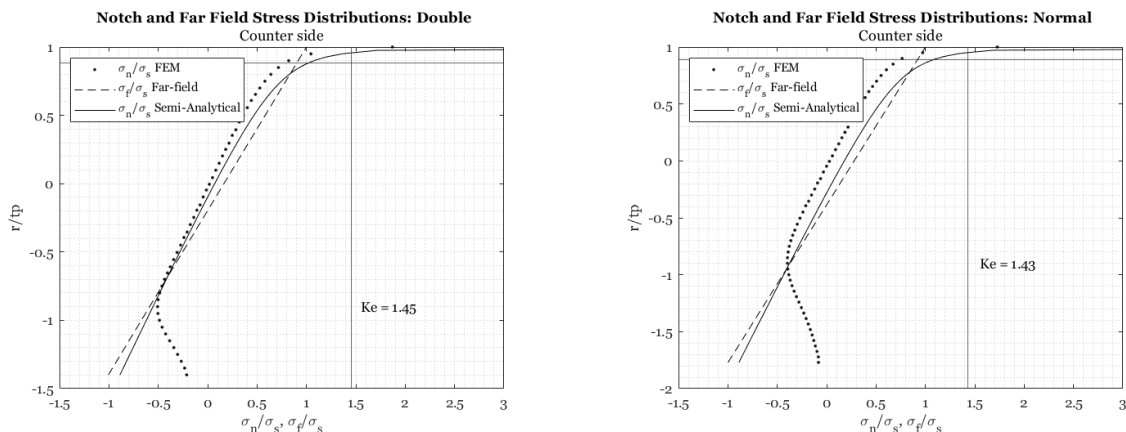
6.3.3.3. Effective Notch Stress Concept

For the calculation of the effective notch stress, the structural far-field stress s_s and structural bending stress ratio r_s are obtained from the linearisation of the numerical FE through-thickness weld notch stress distribution [28]. This method is selected (in contrary to the method A and B by DNV-GL) as it is mesh independent, and enables to distinguish between the far field stress due to different parts of the material (by selecting a part of the nodal forces f_i at corresponding distance from the neutral axis r_i).

In this sub-structuring approach the structural far-field stress s_s is applied to a 2D solid model of the welded detail, including the actual idealised weld geometries. The method is thus semi-analytical: the input for the analytical formulation of s_e is numerical.

s_s and r_s for the counter-welds The structural stress following the method by Dong in the fourth row of tables {6.2, 6.3, 6.4} is for the total actual thickness (including material from a counterweld with a longer weld leg length than the considered weld). For the assessment of the effective notch stress, the fit of the linear s_s to the numerical data is of great importance. Figure 6.6 shows the comparison of the analytical solution, as a function of the numerical results over the total thickness. It shows the poor fit, which is due to the presence of the extra material, causing a discontinuity in the stress distribution. This discontinuity influences the linear structural stress distribution as the force and moment equilibrium are used.

In figure 6.6 the analytical formulation is based on the FE through-thickness weld notch stress distribution in all elements that are below the respective notch. For the counter-welds this includes elements on the other side of the base plate, from the K-weld on the bottom attachment. When excluding the weld material of the K-welds the force and moment equilibrium will make the shift of neutral axis manifest as a membrane stress component.



(a) Double weld configuration: the specimen is welded on both sides of the attachment (right drawing in figure 6.3).

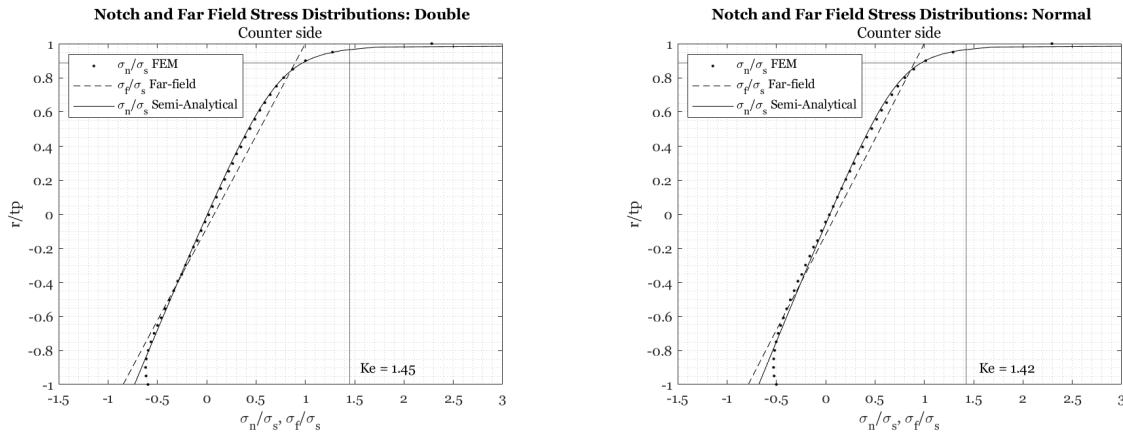
(b) Normal weld configuration: the specimen is welded on one side of the attachment (left drawing in figure 6.3).

Figure 6.6: Through-thickness weld notch stress distributions based on the structural stress over the total material thickness at the notch location. Example for the roller case. The numbers at the vertical axes indicate from -1 to 1 the base plate, and below -1 the amount of weld-material in line with the cross-section.

However, when excluding the discontinuity due to the bottom welds from the s_s formulation, and thus also from the s_e formulation, the fit is significantly improved (see figure 6.7). In figure 6.7 the analytical formulation is based on the FE through-thickness weld notch stress distribution only in the base plate.

As a conclusion, the structural stress will be based on the base plate thickness.

Observation K_e factor in relation to s_s The K_e factor (σ_e/σ_s) is hardly influenced by the change in structural stress input for the analytical formulation of σ_e . This is due to the fact that the σ_e is a function of the input of s_s and its distribution. As figure 6.6 compared to 6.7 shows, the slope of the stress distribution is hardly affected. This is quantified in table 6.1 where the difference in r_s (bending stress over far-field stress) is \mathcal{O}



(a) Double weld configuration: the specimen is welded on both sides of the attachment (right drawing in figure 6.3).

(b) Normal weld configuration: the specimen is welded on one side of the attachment (left drawing in figure 6.3).

Figure 6.7: Through-thickness weld notch stress distributions based on the structural stress over the base plate thickness at the notch location. Example for the case with the roller boundary condition.

10%. The effective notch stress is integrated over zone 1 and 2 of the weld notch stress distribution: this zone is governed by the peak stress and the notch stress gradient, and not by the far-field stress.

Table 6.1: r_s values for the counter welds, for the structural stress as calculated over only the base plate or the total thickness (including the counterweld contribution). See figure 6.3 for the drawing of the double and normal weld configurations.

	Double weld config.			Normal weld config.		
r_s over:	Base plate	Full thickness	Proc. diff.	Base plate	Full thickness	Proc. diff.
Figure	6.7a	6.6a		6.7b	6.6b	
Roller	0.89	1.00	12%	0.92	1.00	9%
Hinge	1.17	1.22	4%	1.18	1.23	4%
5% friction	0.89	1.00	12%	0.92	1.00	9%

For the hinged case the $r_s \leq 1$ because the membrane stress acts in the opposite direction, reducing the structural stress at the respective notch.

6.3.4. Results

The resulting σ_n , σ_s and σ_e are presented in table {6.2, 6.3, 6.4} for the {roller, hinge, 5% force} boundary condition. The calculated K_e factors are presented by means of a corresponding plot comparing the FE through-thickness weld notch stress distribution with the analytical in Appendix {E.1.1, E.1.2 and E.1.3}.

The governing notch is the half-V weld of the normal configuration (column 3). All fatigue damage criteria for this notch exceed the values at the other locations and configurations. This is in line with expectations as this location has the sharpest notch.

The 5% case is used for further analysis. This assumption is subject for discussion in section 6.3.5.

Observations SCFs The observations made with respect to the SCFs, and the explanation for the observed phenomena, are listed in this section.

1. The HSSSC method by Dong presents smaller stresses than both method A and B by DNV-GL.

This is because all three concepts work with a different definition of the structural stress, and all three concepts present an estimation of this stress. By implementing the through-thickness weld notch stress distribution, the method by Dong [28] is less sensitive to the peak stress than the methods by DNV-GL which only use the surface stresses (zone 1).

2. The presence of the counter-weld (K-weld on the bottom side) poses a different through-thickness weld notch stress distribution.

Table 6.2: Stress in N/mm^2 at 10 kN load applied to the specimen, per fatigue damage criterion, using a roller connection. "Double" refers to the sample with a counter weld at the root, see figure 6.3.

	Counter-weld	Half-V weld	Counter-weld (double)	Half-V weld (double)
NSC (σ_n)	220	210	214	199
HSSC (σ_s) DNV-GL Solids method A	228	240	221	233
HSSC (σ_s) DNV-GL Solids method B	247	256	237	247
HSSC (σ_s) by Dong [28]	212	215	204	210
$K_s = \sigma_{s,DNV(A)}/\sigma_n$	1.03	1.14	1.03	1.17
Over the base plate thickness (excluding counter-weld contribution):				
HSSC (σ_s) by Dong [28]	160	215	167	210
$K_s = \sigma_{s,Dong}/\sigma_n$	0.73	1.03	0.78	1.05
$K_e = \sigma_e/\sigma_s$	1.43	1.50	1.45	1.45
ENSC ($\sigma_e = \sigma_s K_e$)	228	323	242	305

Table 6.3: Stress in N/mm (per unit sample width) at 10kN load applied to the specimen, per fatigue damage criterion, using a hinged connection. "Double" refers to the sample with a counter weld at the root, see figure 6.3.

	Counter-weld	Half-V weld	Counter-weld (double)	Half-V weld (double)
NSC (σ_n)	statically indeterminate			
HSSC (σ_s) DNV-GL Solids method A	116	120	115	114
HSSC (σ_s) DNV-GL Solids method B	120	121	117	115
HSSC (σ_s) by Dong [28]	116	112	109	108
$K_s = \sigma_{s,DNV(A)}/\sigma_n$	statically indeterminate NSC			
Over the base plate thickness (excluding counter-weld contribution):				
HSSC (σ_s) by Dong [28]	75	112	83	108
$K_s = \sigma_{s,Dong}/\sigma_n$	statically indeterminate NSC			
$K_e = \sigma_e/\sigma_s$	1.42	1.52	1.46	1.47
ENSC ($\sigma_e = \sigma_s K_e$)	107	171	121	158

This is because, for the through-thickness weld notch stress distribution, the force and moment equilibrium over the total thickness are used to determine the structural stress. The presence of a counter-weld on the bottom side adds load-carrying material (decreases membrane stress) and moves the actual neutral axis down (increasing the bending stress at the notch).

3. The K_e factor (s_e/s_s) is hardly influenced by the nature of the boundary condition at the interface between the accessory and the specimen.

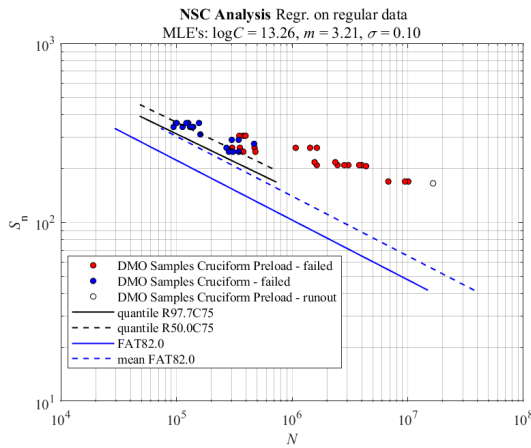
This is because the s_e is calculated in the zone 1 and 2, both of which are hardly influenced by the far field stress and are governed by the peak.

Table 6.4: Stress in N/mm (per unit sample width) at 10kN load applied to the specimen, per fatigue damage criterion., using a 5% force connection. "Double" refers to the sample with a counter weld at the root, see figure 6.3.

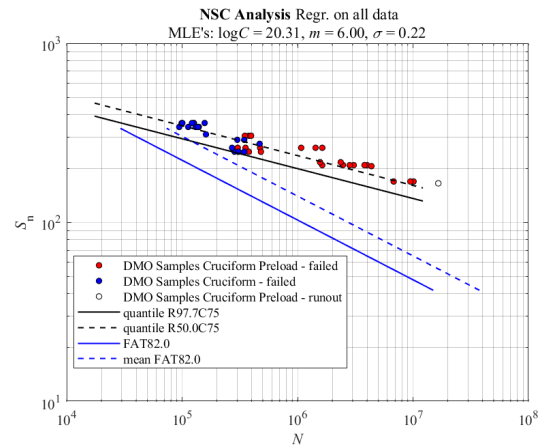
	Counter-weld	Half-V weld	Counter-weld (double)	Half-V weld (double)
NSC (σ_n)	222	211	216	201
HSSSC (σ_s) DNV-GL Solids method A	229	242	223	234
HSSSC (σ_s) DNV-GL Solids method B	248	258	239	249
HSSSC (σ_s) by Dong [28]	214	217	201	211
$K_s = \sigma_{s, DNV(A)} / \sigma_n$	1.03	1.15	1.03	1.16
Over the base plate thickness (excluding counter-weld contribution):				
HSSSC (σ_s) by Dong [28]	161	217	168	211
$K_s = \sigma_{s, Dong} / \sigma_n$	0.73	1.03	0.78	1.05
$K_e = \sigma_e / \sigma_s$	1.42	1.50	1.45	1.45
ENSC ($\sigma_e = \sigma_s K_e$)	229	325	244	307

The results from figure 6.8 implicate that the experimental data has a longer fatigue life than is predicted by the S-N curve by DNV-GL. It should however be noted that this can not be attributed to weld quality, but rather to the limitations of the assessment. Figure 6.9a presents the comparison when the datapoints are corrected for the r_{lr} level of the DNV-GL D curve, which is 0.5. DNV-GL presents one S-N curve for all HSSSC assessments, whereas IIW presents two curves: a LC and NLC curve at respectively FAT90 and 100. The specimen is classified as a NLC detail, yielding the comparison in figure 6.9b. It can be concluded that the DMO specimens do not possess of a better quality than the ones used for the class S-N curves.

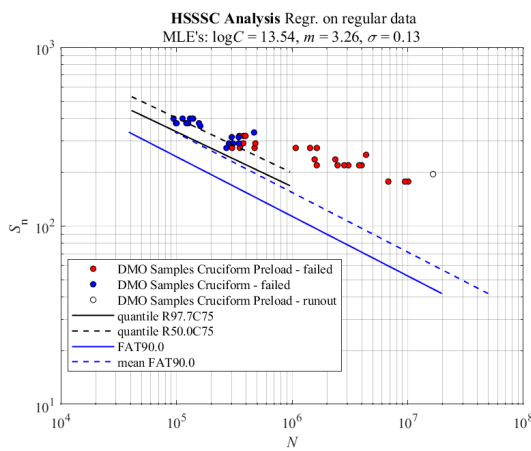
In this section the word "preloaded" is used to indicate specimens that are subject to an initial overload.



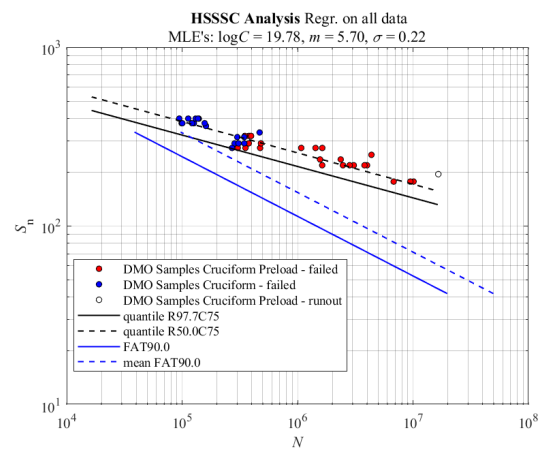
(a) NSC analysis of the regular (non-preloaded) samples



(b) NSC analysis of all samples

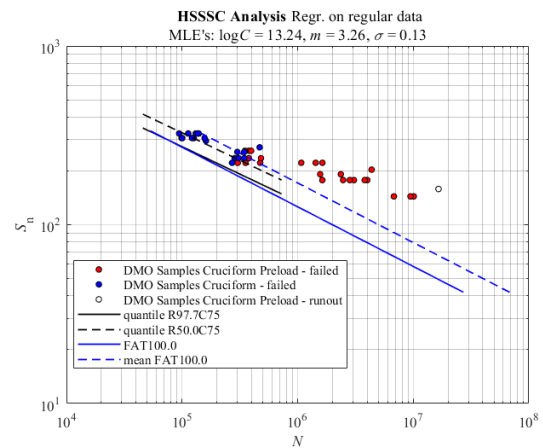
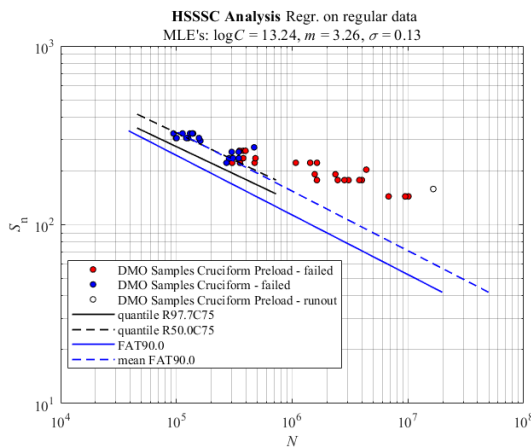


(c) HSSSC analysis of the regular (non-preloaded) samples



(d) HSSSC analysis of all samples

Figure 6.8: MLE regression results per fatigue damage criteria on only the regular (non-preloaded) samples and the complete DMO CA dataset, respectively.



(a) HSSSC analysis of the regular (non-preloaded) samples, compared to the (b) HSSSC analysis of the regular (non-preloaded) samples, compared to the DNV-GL D curve, including the Walker mean stress correction to the $r_{II} = 0.5$ NLC FAT100 curve, including the Walker mean stress correction to the $r_{II} = 0.5$ level of the curve.

Figure 6.9: MLE regression results per fatigue damage criteria on only the regular (non-preloaded) samples. The experimental data is compared to both the DNV-GL D curve [27] and the FAT100 [54].

Observations MLE S-N curves The observations made with respect to the MLE S-N curves, and the explanation for the observed phenomena, are listed in this section.

1. There is an increase in scatter when using more local information.

This is because by increasing the amount of local information, the samples are separated by actual failure location and its properties. It should be noted that this is not in disagreement with the demonstration in [111] that more local information reduces scatter: that statement still holds when comparing multiple datasets. As this assessment only considers one dataset, the increased in scatter is not due to the fatigue damage criterion, but due to the increased level of detail.

2. The change in slope seems to correspond to the separation in datasets that did and did not receive an initial overload.

This is deemed to be the result of the overload: an overload relieves a part of the production-induced residual stresses as are included in the material. As the net stress level is reduced the fatigue life is increased: presenting as a shift to the right in the diagram.

Figure 6.10 presents the datapoints from [112] of 1804 tested specimens of a variety of weld types, plate thicknesses, loading and response ratios (r_{lr}), yield strengths and loading types. The red and blue points indicate the tested DMO specimens.

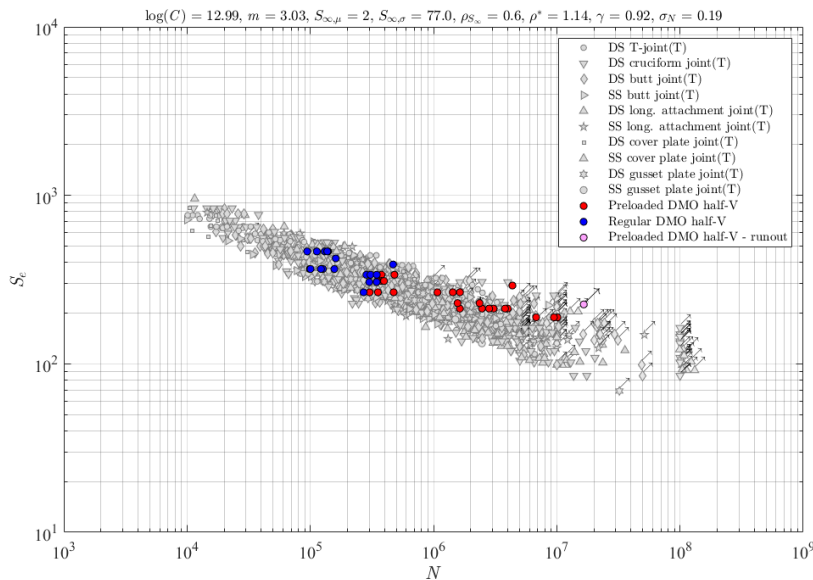


Figure 6.10: Data is the courtesy of Yanxin Qin, it was presented in his paper [112].

Conclusion Based on the findings in figure 6.8 there is no indication that the DMO CA specimens have a significant better fatigue resistance than the specimens as used to construct the DNV-GL $S_s - N$ FAT90 curve (i.e. D curve). The difference can be attributed to the (conservative) choice of DNV-GL to not distinguish between LC and NLC specimens, in contrary to IIW.

Unfortunately the datasets that can be compared are limited to the not-preloaded sets. For the DMO samples this is only in the MCF region, and has a limited confidence near the HCF region when extrapolated. On the other hand, the dataset does support the hypothesis that applying an overload at the beginning of the lifetime has some beneficial effect on the fatigue life. This is in line with the conclusions of the TNO report [78] in which the specimens from the HMS Tromp were analysed.

There is also no indication that the DMO specimens have a significant better fatigue resistance than the data-cloud as presented in [112] for the ENSC assessment of 1804 datapoints from literature. See figure 6.10.

6.3.5. Discussion

As was indicated, the dataset by DMO does not allow for an absolute conclusion as to whether the fatigue resistance is better or worse than the ones used to construct the DNV-GL S-N curves. This is mainly due to the limited domain of the non-preloaded specimens.

A second source of uncertainty lies in the boundary condition at the interface between the accessory and the specimen. This can be modelled in extremes by a roller joint or a hinged connection. In reality there is a finite friction force: due to the lubrication the condition is closer to that of a roller, but it is hard to quantify the actual counteracting force. A solution would be to provide all specimens with a strain gauge to measure the strains (and translate these to the stress) at the $t_p/2$ and $3t_p/2$ locations. The analysis showed limited significance of the nature of the connection, although in reality the boundary condition poses a friction force opposing the motion of the specimen: for the loading and unloading cycle this is thus not a constant.

Summarising, the validity of the conclusion is limited due to:

1. The dataset that did not receive an initial overload has a limited domain and does not allow for a confident extrapolation to the MCF and HCF regions.
2. The (dynamic) boundary condition at the interface is uncertain. This has however a limited effect on the results of the analysis, as was proven with the static friction coefficients.

6.4. Generalised Random Fatigue Limit

To estimate the fatigue life of a specimen, the point-cloud of data-points has to be expressed in terms of a mean or a bound at a certain level of confidence and probability of survival. As the data-points considered in this thesis cover the MCF and HCF domain, the selected S-N curve formulation has to be valid for both. As was explained in section 3.5.2, the GRFL is used in this thesis.

This model was first presented by Leonetti et al. under the name "6 Parameter Random Fatigue Limit Model (6PRFLM)". Due to the generic nature and flexibility of the formulation the more descriptive name Generalised Random Fatigue Limit (GRFL), as proposed by [112], is used in this thesis.

The fatigue resistance curve as proposed by Leonetti et al. reads:

$$\log_{10}(N) = \beta_0 + \beta_1 \log_{10}(\Delta S) - p \log_{10} \left(1 - \frac{\Delta S_0}{\Delta S} \right) \quad (6.9)$$

Where $\Delta S_0 = \text{Normal}(10^{\mu_v}, \sigma_v)$. The re-formulation by Qin et al. reads:

$$\log(N) = \log(C) - m \log(S) - \rho_{S\infty} \log \left(1 - \frac{S_{\infty}(\mu, \sigma)}{S} \right) \quad (6.10)$$

In line with the original formulation by Leonetti et al. the natural logarithms are exchanged for the \log_{10} . This has no effect on the outcome as is shown in and proven by appendix C.2.

$$\log_{10}(N) = \log_{10}(C) - m \log_{10}(S) - \rho_{S\infty} \log_{10} \left(1 - \frac{S_{\infty}(\mu, \sigma)}{S} \right) \quad (6.11)$$

It should be noted that the formulation is the same as by Leonetti et al., but with different parameter names. To find the optimum set of the six parameters $\{\log C, m, \sigma, \rho_{S\infty}, \mu_{S\infty}, \sigma_{S\infty}\}$ an optimization by means of the Matlab function `fmincon` is used to find the maximum log-likelihood². The log-likelihood is defined as:

$$\mathcal{L} = \sum_{j=1}^n \delta_j \cdot \log(f_w(\theta)) + (1 - \delta_j) \cdot \log(1 - F_w(\theta)) \quad (6.12)$$

Here:

$$\delta_j = \begin{cases} 1, & \text{for a failure} \\ 0, & \text{for a run-out} \end{cases} \quad (6.13)$$

²For computational reasons the log-likelihood is used instead of the likelihood.

The problem then concludes to the following optimization problem. Strictly speaking it is not a constrained, but a bounded optimization problem.

$$\begin{aligned} \min_{\theta} f &= -\mathcal{L}(\theta) \\ \text{subject to: } &(\theta_{LB} \leq \theta \leq \theta_{UB}) \end{aligned} \quad (6.14)$$

In [112] the comparison is made between the values of the AIC for a fit when considering the distributions of the fatigue life given the fatigue limit $w|v$ and the fatigue limit v as either a Normal or Weibull distribution. For a dataset of 1804 points that are analysed using the ENSC the minimal AIC was found for a Normal distributed fatigue life, and a Weibull distributed fatigue limit.

In line with the research outcome from [112], in this thesis the fatigue life is of the (log) Normal distribution type.

$$\begin{aligned} f_{w|v} &= \frac{1}{\sqrt{2\pi}\sigma} \cdot \exp\left(-\frac{(w-\mu)^2}{2\sigma^2}\right) \\ F_{w|v} &= \frac{1}{2} \left(1 + \operatorname{erf}\left(\frac{w-\mu}{\sigma\sqrt{2}}\right)\right) \end{aligned} \quad (6.15)$$

In the paper by Leonetti et al. the fatigue limit is of the (log) Normal distribution type:

$$\begin{aligned} f_v &= \frac{1}{\sqrt{2\pi}\sigma} \cdot \exp\left(-\frac{(v-\mu)^2}{2\sigma^2}\right) \\ F_v &= 1 - \exp\left(-\exp\left(\frac{v-\mu}{\sigma}\right)\right) \end{aligned} \quad (6.16)$$

Here μ is the mean of the fatigue limit distribution: given as the fourth entry in θ . σ is the fifth entry in θ and represents the respective standard deviation.

In the paper by Qin et al. the fatigue limit is of the (log) Weibull extreme value distribution type:

$$\begin{aligned} f_v &= \frac{1}{\sigma} \cdot \exp\left(\left(\frac{v-\mu}{\sigma}\right) - \exp\left(\frac{v-\mu}{\sigma}\right)\right) \\ F_v &= \frac{1}{2} \left(1 + \operatorname{erf}\left(\frac{v-\mu}{\sigma\sqrt{2}}\right)\right) \end{aligned} \quad (6.17)$$

The mean μ is the unbiased ($\mu = \mu_i + \gamma \frac{\sqrt{6}}{\pi} \sigma_i$) mean of the Weibull extreme value distribution and σ is the unbiased ($\sigma = \frac{\sqrt{6}}{\pi} \sigma_i$) standard deviation.

The fatigue life is of the Extreme Value Distribution (type 1) type.

$$\begin{aligned} f_w &= \int_{-\infty}^S f_{w|v}(w|v, \theta) \cdot f_v(v, \theta) dv \\ F_w &= \int_{-\infty}^S F_{w|v}(w|v, \theta) \cdot f_v(v, \theta) dv \end{aligned} \quad (6.18)$$

For verification the optimization is used on the dataset from [112]. Table 6.5 shows for an analysis based on the amplitudes of the effective notch stress, the optimal values found by [112] and by the author of this thesis.

Table 6.5: Based on amplitudes - not ranges, for comparison with the results from [112]

Param. Leonetti	Param. Qin	Qin [112] (2021)	MDe (2021) ⁽¹⁾
β_0	$\log C$	12.02	12.08
β_1	$-m$	-3.04	-3.03
σ	σ	0.20	0.19
μ_v	$S_{\infty}(\mu)$	$\log_{10}(39) = 1.59$	1.59
σ_v	$S_{\infty}(\sigma)$	$\log_{10}(2.15) = 0.33$	0.35
p	$\rho_{S_{\infty}}$	0.57	0.65
\mathcal{L}	\mathcal{L}	190.8	190.8

- (1) The small difference between the results in [112] and in this thesis has a numerical origin: the input for [112] is rounded. Also, the optimization algorithm and its termination criteria from [112] are not known.

In line with formulations by class however, it is more common to use a fatigue damage criterion based on the range: this reflects the cyclic nature of the fatigue phenomenon. The optimal values for the analysis based on the stress ranges are presented in table 6.6.

Table 6.6: Optimum six parameters of the GRFL based on stress ranges

Param. Leonetti	Param. Qin	MDe
β_0	$\log C$	12.99
β_1	$-m$	-3.03
σ	σ	0.19
μ_v	$S_{\infty}(\mu)$	1.89
σ_v	$S_{\infty}(\sigma)$	0.35
p	ρS_{∞}	0.65
\mathcal{L}	\mathcal{L}	190.8

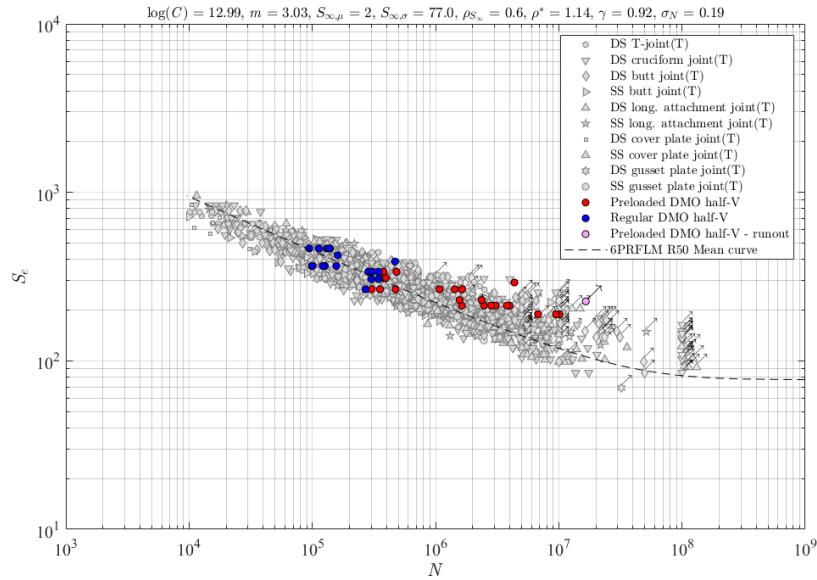


Figure 6.11: ENSC CA fatigue data from [112] -expressing the stress range-, with the GRFL (6PRFLM) from [75] fitted and plotted as a dashed line.

Stress amplitude to stress range The change of stress amplitudes to stress range only affects the $\log C$ and μ_v . This observation is in line with expectations as the change of amplitudes to shift only poses a vertical shift of the curve. Both shifts ($S_{\infty, range}(\mu) = 0.30 + S_{\infty, amp}(\mu)$ and $\log_{10}(C_{range}) = 0.91 + \log_{10}(C_{amp})$) can be derived as well from the logarithmic relations:

$$\begin{aligned}
 S_{\infty, range}(\mu) &= 2S_{\infty, amp}(\mu) \\
 \log_{10}(S_{\infty, range}(\mu)) &= \log_{10}(2S_{\infty, amp}(\mu)) \\
 &= \log_{10}(2) + \log_{10}(S_{\infty, amp}(\mu)) \\
 &\approx 0.30 + \log_{10}(S_{\infty, amp}(\mu))
 \end{aligned} \tag{6.19}$$

Assuming a Basquin relation:

$$\begin{aligned}
\log_{10}(C_{range}) &= \log_{10}(N) + m \log_{10}(2S_{\infty,amp}(\mu)) \\
&= \log_{10}(N) + m (\log_{10}(2) + \log_{10} S_{\infty,amp}(\mu)) \\
&= m \log_{10}(2) + \log_{10}(N) + m \log_{10} S_{\infty,amp}(\mu) \\
&\approx 3.03 \cdot 0.30 + \log_{10}(C_{amp}) \\
&\approx 0.91 + \log_{10}(C_{amp})
\end{aligned} \tag{6.20}$$

Lastly the likelihood is identical for both analyses: the relation between the datapoints and the curve has not changed.

6.5. CA analysis of the VA database specimens

With the exception of the database by [Zhang and Maddox \[148\]](#), all references for the VA database also contain CA fatigue test results. These test results are used to assess whether the potential conservatism is due to the accumulation model, a VA effect, or due to the nature of either the specimens or the SCF assessment. The database of CA fatigue tests from the VA references, that is assessed in this section, is summarised in table 6.7.

Table 6.7: Database summary of CA fatigue tests of steel welded joints, equal to the specimens that form the VA database

Source	Geometry	HS Type	Number
Klippstein and Schilling [63]	PP DS Cruciform joint	Type C	12
Agerskov et al. [3]	PP DS Longi. plate attachment	Type A	14
Agerskov et al. [3]	FP DS Cruciform joint	Type C	13
Ota et al. [103]	FP DS Butt joint	Type C	7 (down) + 14 (up)
Zhang and Maddox [147]	PP DS Longi. plate attachment	Type A	6
Zhang and Maddox [147]	PP DS Longi. edge attachment	Type B	5

6.5.1. SCF results

The SCF's for all specimens in the VA database are calculated to assess the hot spot structural and effective notch stress per nominal stress contribution. To this extent the DNV-GL HSSSC calculations are presented in appendix D.2 and the through-thickness weld notch stress distributions and the analytical plot of the notch stress are presented per specimen-type in appendix E.2. Appendix F contains the FE models as used to extract the through-thickness weld notch stress distribution. Table 6.8 contains the SCF's per dataset and per fatigue damage criterion.

Table 6.8: Stresses corresponding to 100kN load in total (50kN on both sides), rounded to MPa.

	Type	Nominal		Structural		Effective notch		
		NSC	HSSSC (σ_s) (⁵) DNV-GL method A	K_s	HSSSC (σ_s) by Dong [28]	K_s	K_e	ENSC
Cruciform [63]	N	83	97 ⁽¹⁾	1.16	83 ⁽²⁾	1.	1.39	115
Cruciform [3]	N	35	38 / 37 ⁽⁴⁾	1.08 / 1.06	35 ⁽²⁾	1.	1.35	47
Long. attach (A) [3]	N	52	65	1.24	76	1.46	1.60	109
Butt joints [103]	N	50	56.5	1.13 ⁽¹⁾	50 ⁽²⁾	1.	1.40	70
Long. attach (A) [147]	N	27	34	1.26	38	1.43	1.50	58
Long. attach (B) [147]	N	40	43	1.09	53	1.32	1.39	74
Butt joints [148]	N	31	35	1.13 ⁽¹⁾	31	1.00	1.22	38
Long. attach (A) [118]	N	33	43	1.30	47	1.42	1.62	77
Cruciform (DMO)	3B ⁽³⁾	211	242	1.15	217	1.03	1.50	325

With:

N indicating a normal load, in contrary to 3B: 3-point bending

- (1) According to DNV [27] method B with a correction factor, equal to the DNV prescribed K_s factor for the weld type, should be applied for simple cruciforms and butt joints.
- (2) No structural stress increase w.r.t. nominal stress under the assumption of a linear through-thickness weld notch stress distribution of the (hot spot) structural stress and a symmetrical detail.
- (3) The 3-point bending loadcases are given for a 10kN load.
- (4) Here respectively the half-v and counter side SCF's are presented.
- (5) See appendix D.2 for the FE models.

6.5.2. Comparison of the CA scatterband

To assess the potential conservatism as incorporated in the specimens, the CA scatterbands are compared to the scatter of the respective S-N curves. At first the HSSSC is used. See figure 6.12. Especially the HS type B specimens from Zhang and Maddox exceed the expected scatterband. This set was tested at a relatively high r_{lr} level, which is currently not corrected for. To address this, the Walker mean stress correction [134] is applied.

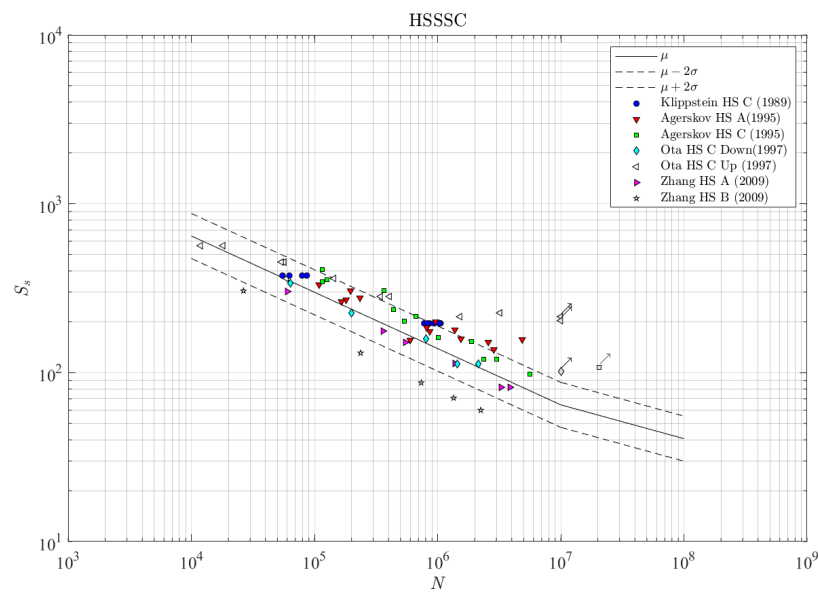


Figure 6.12: HSSSC CA assessment of the VA database specimens: comparing the CA scatterband from the DNV-GL D curve to the CA fatigue tests.

The use of the Walker mean stress correction indeed affects the amount of (non-) conservatism for the HS type B specimens from Zhang and Maddox, see figure 6.13. The scatter of all specimens combined has also reduced. The last step is to use the ENSC to assess all CA fatigue test results, and to compare them to the scatterband as published by Qin et al..

As figure 6.14 portrays, the specimens show a good overlap with the scatterband of the 1804 specimens as analysed in [112]. Some exceptions are observed:

- The HS type A specimens from Zhang and Maddox are positioned on the upper side of the scatterband. These specimens are reported to have lower residual stresses than the HS type B specimens as assessed in the same paper. The residual stresses are reported to be about 67% of the yield stress, compared to stresses approaching the yield for the HS type B specimens. Lower residual stresses pose a reduced r_{lr} level, which is beneficial for the fatigue life. This benefit is not quantified, but considered as part of the phenomenological scatter in fatigue.
- The HS type C specimens from Agerskov et al. are positioned on the lower side of the scatterband. These specimens are, due to the non-symmetrical nature of the half-V weld prone to welding-induced

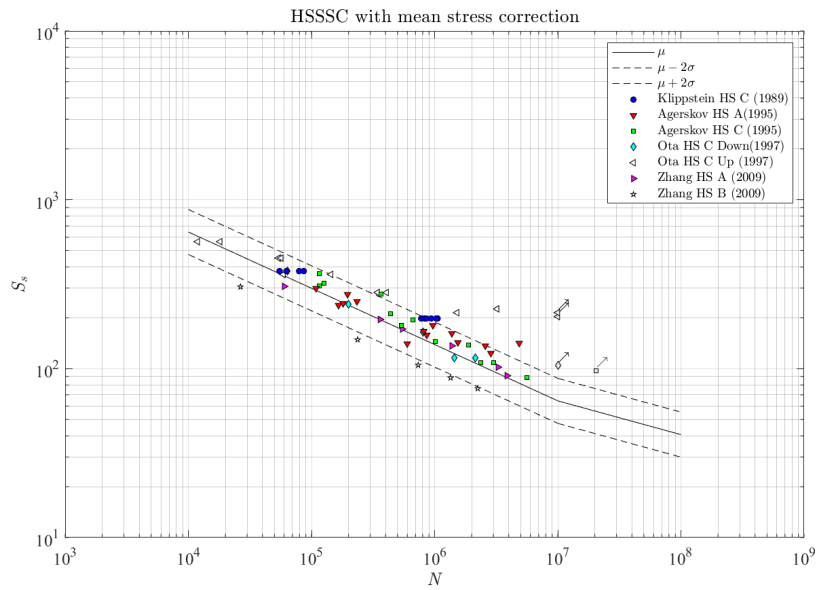


Figure 6.13: HSSSC CA assessment of the VA database specimens: comparing the CA scatterband from the DNV-GL D curve to the CA fatigue tests, including the mean stress correction.

angular deformations. The authors have measured the actual stresses, which are the ones that are reported. However, the angular deformations are not reported, which is why the SCF calculations do not account for these deformations. The deformations are likely to affect the specimens in a negative manner: increasing the stress concentration factors, and positioning the data in the scatterband.

The other datasets show a good overlap with the scatterband from [112].

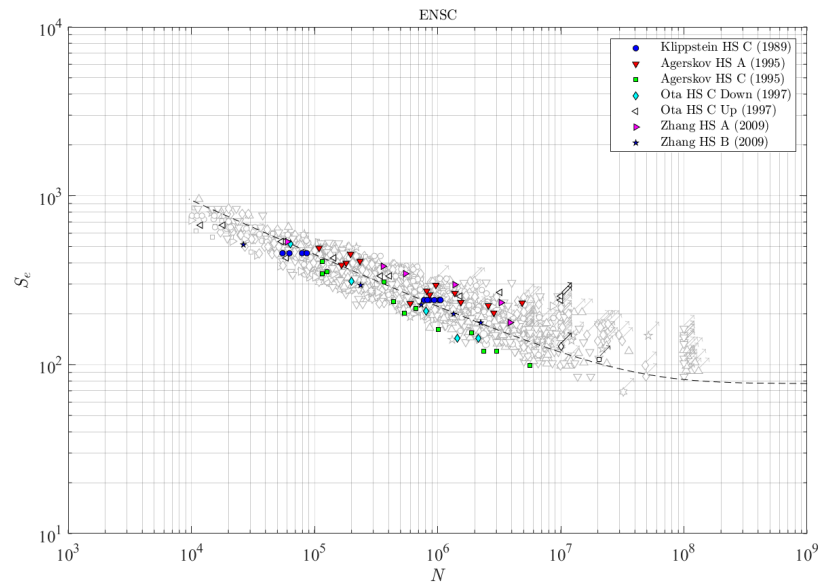


Figure 6.14: ENSC CA assessment of the VA database references: comparing the CA scatterband from [112] to the CA fatigue tests from the references that provide the VA datasets.

6.6. Concluding remarks

In this chapter, next to the S-N curve D from DNV-GL, the GRFL curve is defined, as plotted in figure 6.11, to express the relation between the fatigue life N and the stress range $\{S_s, S_e\}$ for the {HSSC, ENSC}.

The analysis of the half-V cruciform specimens (as tested by order of DMO) allowed to conclude that the dataset, although limited, does not indicate a significant deviation from both the DNV-GL S-N curves and the data-points from literature [112]. This conclusion also holds for the CA fatigue test data of the VA database references. The exceptions are 1) the HS type A specimens from [147], 2) the down-cycling HS type C specimens from [103] and 3) the HS type C specimens from [3]. Exception 1) is due to lower residual stresses than anticipated in the calculation, 2) is presumably due to lower residual stresses, but this can not be verified in the paper and 3) is due to angular deformations which are not explicitly, but only implicitly, listed in the paper. It is expected that 1) and 2) are of limited influence on the fatigue life prediction under VA loading histories: the presence of occasional high peak loads will reduce the residual stresses and is accounted for per cycle with the Walker mean stress correction. The angular deformations from 3) are not quantified in [3], it is however expected that for the ENSC the fatigue life predictions are on the unconservative side: due to the deformations the actual effective notch stress range is higher than what is accounted for in this chapter.

Relating back to figure 2.1, the translation of the local structural response to the S-N curves at hand is not identified as a main source of uncertainty. The focus in this thesis is on uncertainty originating from the fatigue damage criterion and damage accumulation models.

7

Variable Amplitude analysis

In chapter 4 the literature in relation to the damage accumulation models was presented. In this current chapter the considered damage accumulation models are used to assess the *Variable Amplitude (VA)* fatigue life of the specimens.

This chapter contains the VA analysis. At first the two damage accumulation models are discussed in detail: the LDAM in section 7.1 and the NLDAM in section 7.2. Section 7.3 presents the analysis of the fatigue resistance and loading conditions for all specimens in the VA database. The resulting fatigue life predictions are presented in section 7.4. Last but not least, section 7.5 provides a reflection on the physical nature of the State-of-the-Art NLDAM.

Two types of resistance curves are used in this chapter, number 1 is the base case and number 2 is based on the research efforts in [74, 112]:

1 - [HSSSC] DNV-GL D curve For welded joints, analysed with the HSSSC, DNV-GL prescribes the D curve as fatigue resistance curve. This D curve is expressed as a piecewise continuous bi-linear Basquin relation:

$$\begin{aligned} \log(N) &= \log(C) - m \log(S) \\ &= \begin{cases} 12.164 - 3 \log(S), & N \leq 10^7 \\ 15.606 - 5 \log(S), & N > 10^7 \end{cases} \end{aligned} \quad (7.1)$$

Here S is the HSSSC stress range $S_s = \Delta\sigma_s$. The D curve is presented at the P97.7C75 level. The mean curve is the D curve plus 2 times the standard deviation 0.2. The fatigue life time is assumed to be normally distributed.

2 - [ENSC] Six-parameter GRFL model by Leonetti et al. This model is discussed in section 6.4. It provides the distribution of the fatigue life $\log N$, accounting for the random nature of the fatigue limit S_∞ :

$$\log(N) = \log(C) - m \log(S) - \rho_{S_\infty} \log\left(1 - \frac{S_\infty(\mu, \sigma)}{S}\right) \quad (7.2)$$

Here S is the ENSC stress range $S_e = \Delta\sigma_e$. The P97.7C75 level is calculated from the first quartile of the 97.7 percent probability of survival samples of the Monte Carlo analysis. This is the method as proposed in [75].

7.1. LDAM by Palmgren and Miner

The **Linear Damage Accumulation Model (LDAM)** typically provides the damage as a function of the number of cycles. It is rewritten to extract the predicted fatigue life N (total number of cycles as experienced by the structure), given a certain resistance curve and critical damage. The \hat{n}_i denotes the normalised spectrum. Hence, $\hat{n}_i = n_i / \sum_{i=1}^k n_i$. That yields:

$$D_{\text{crit}} = 1 = \sum_{i=1}^k \frac{n_i}{N_i} = N \sum_{i=1}^k \frac{\hat{n}_i}{N_i} \quad (7.3)$$

$$N = \frac{D_{\text{crit}}}{\sum_{i=1}^k \frac{\hat{n}_i}{N_i}} = \frac{D_{\text{crit}}}{E[\dot{D}]}$$

The damage rate (\dot{D}) is the damage per cycle, at a certain stress level S_i .

In this model, the stress ranges below the fatigue limit (assuming that above $N = 10^8$ DNV defines the fatigue limit, this is at $\Delta\sigma_h = 33.2$ MPa) do not contribute to the fatigue damage. In the Matlab code this is represented by a maximum fatigue life N_i at these stress levels of ∞ .

7.2. NLDAM by Hirt and Kunz, modified by Leonetti et al.

The Non-linear Damage Accumulation Model (NLDAM) by Leonetti et al. is formulated as:

$$N = \frac{D_{\text{crit}}}{\sum_{h=1}^{h_{\text{tot}}} \left[\sum_{i=1}^k \frac{\hat{n}_i}{N_{i,h}} \right]} = \frac{D_{\text{crit}}}{E[\dot{D}]} \quad (7.4)$$

This resembles the formulation by Palmgren and Miner (see (7.3)), with the exception that the expected fatigue life $N_{i,h}$ per stress level S_i is now calculated per damage increment h . The contributions per damage increment are accumulated to obtain the total lifetime. The hat indicates the use of a normalised spectrum (\hat{n}_i). The novelty of the model by Hirt and Kunz, as is adopted by Leonetti et al., lies in the double summation over both the spectrum i and the damage history h , this was explained in section 4.3, along with a detailed explanation of the NLDAM in relation to the LDAM. The derivation of the model is presented in appendix B.4.

Adopting the GRFL as the formulation of the resistance curve yields:

$$E[\dot{D}] = \sum_{h=1}^{h_{\text{tot}}} \left[\sum_{i=1}^k \frac{n_i}{10^{\beta_0 + \beta_1 \log_{10}(\Delta\sigma_i) - p \log_{10}\left(1 - \frac{\Delta\sigma_{th,h}}{\Delta\sigma_i}\right)}} \frac{n_i}{\sum_i n_i} \right] \quad (7.5)$$

$$= \sum_{h=1}^{h_{\text{tot}}} \left[\sum_{i=1}^k \frac{n_i}{10^{\beta_0 + \beta_1 \log_{10}(\Delta\sigma_i) - p \log_{10}\left(1 - \frac{\Delta\sigma_{th,h}}{\Delta\sigma_i}\right)}} \hat{n}_i \right]$$

In this model the threshold stress per damage increment $\Delta\sigma_{th,h}$ is given by:

$$\Delta\sigma_{th,h} = \Delta\sigma_0 \left(1 - \frac{D_h}{D_{\text{crit}}} \right)^\zeta \quad (7.6)$$

Following the random fatigue limit $S_\infty(\mu, \sigma)$, the critical damage D_{crit} is modelled as a Log-Normal distribution with mean μ_D and standard deviation σ_D ¹. To find the most likely parameters for $\theta_{VA} = (\mu_D, \sigma_D, \zeta)$, the log-likelihood is maximised (MLE) in a Matlab routine. Figure 7.1 presents a schematic overview of this optimisation routine and its entries. ζ determines the sensitivity of the damage accumulation process to low stress range cycles. If $\zeta = 0$ the formulation equals the LDAM. $\zeta = 1$ provides the model as suggested by Hirt and Kunz. The modification by Leonetti et al. allows to modify the ζ value. If $\{\zeta > 1, \zeta < 1\}$ the damage accumulation is {convex, concave}, see figure 4.13.

Verification For verification of the model, the optimum θ_{VA} values for the data as used by Leonetti et al. are compared to the research results from his paper [75]. Table 7.1 presents the outcome of the most likely parameters. The data originates from [63] and is for the NSC analysis of PP cruciform joints. Considering the equal optimum values and Log-Likelihood for the verification case and according to Leonetti et al., the model is verified.

¹Notice the parallel with the proposed Log-Normal distribution as given in [24, 135, 136].

Table 7.1: Results for the cruciform samples from [63] for verification of the constructed model with the results from [75]

Parameter	Leonetti et al. [75] (2020)	Verification (2021)
μ_D	1.61	1.61
σ_D	0.23	0.23
ζ	1.14	1.14
\mathcal{L}	6.96	6.96

A large amount of Monte Carlo samples is required to account for the random nature of the fatigue limit and the critical damage. The quality of the results is a function of the amount of samples. This is because by taking a finite number of random samples of a distribution, a non-smooth objective surface is created. If more samples are used, the surface becomes more smooth, which is beneficial for the optimisation algorithm. Leonetti et al. mention that at least 10^5 MC samples are required to obtain converged maximum likelihood parameter estimates. These 10^5 samples are also used in the verification casus.

7.3. SCF- and spectrum analysis of the VA database

For the validation, a database of VA fatigue data is compiled for a variety of hot spot types, spectrum types, mean stress levels and geometries (see table 4.4). This section provides the preparatory analysis of these datapoints to use in the VA assessment in section 7.4. Per datapoint the following information is required for the VA assessment:

- Total number of cycles until failure (i. e. experimental lifetime)
- Data type: failure (completed test) or run-out (censored data)
- Nominal stress range histogram/spectrum or a time trace
- Loading and response ratio r_{lr} per stress contribution (can be per cycle, or per block, depending on the nature of the signal)
- SCF's for DNV-GL HSSSC method A (see section 6.5)
- SCF's for the analytical stress-averaging ENSC analysis (see section 6.5)
- Loading type: normal force or bending moment (see section 6.5)
- Geometry parameters
- Failure location: weld toe or weld root

Table 7.2 contains the geometry and loading characteristics of the specimens that are used in the analysis. These are discussed in the following sections in this same order. The resulting equivalent r_{lr} values and SCF's are presented in table 6.8.

Table 7.2: Specimens and characteristics: plate width w_p , base plate thickness t_b , attachment/ cross-plate thickness (i.e. height) t_c , weld leg length l_w and height h_w , whether it is symmetrical (δ) and the bending stress ratio r_s . All dimensions are in mm. For non symmetrical cruciforms two weld dimensions and r_s values are given: l_w , h_w and r_s half-V side / l_w , h_w and r_s counter side.

Specimen	HS Type	Source	w_p	t_b	t_c	l_w	h_w	δ	r_s
PP DS Cruciform joint	C	[63]	63.5	9.5	9.5	9	9	1	0
FP DS Cruciform joint	C	[3]	90	16	10	4/2	14/2	1	0
PP DS Longi. plate attach.	A	[3]	80	12	39	8.5	8.5	1	0
FP DS Butt joint	C	[103]	50	20	n.a.	10	3	1	0
PP DS Longi. plate attach.	A	[147]	150	12.5	38	8	6	1	0
PP DS Longi. edge attach.	B	[147]	125	20	12	8	8	1	0
FP SS Butt joint	C	[148]	80	20	n.a.	10	3	0	0.1
FP DS Cruciform joint	C	DMO	72	20	20	14/12	22/2	1	1.00/0.89
FP DS Cruciform joint	C	DMO	72	20	20	24/10	24/10	1	1.00/0.92

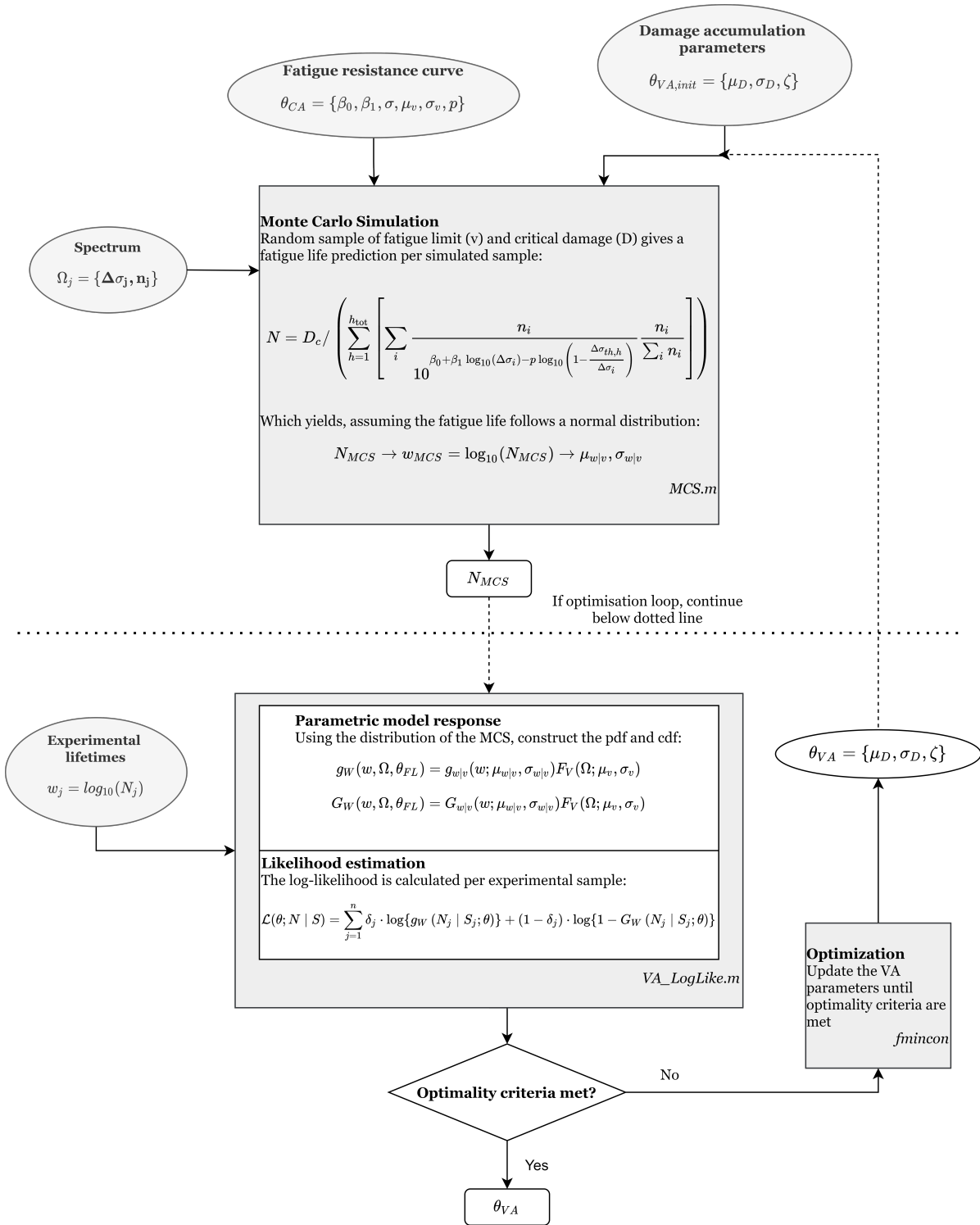


Figure 7.1: Optimisation routine for the GRFL combined with the damage accumulation by [52], as proposed by Leonetti et al.

7.3.1. Cruciform HS Type C from [63]

Dataset:	PP DS Cruciform joint HS Type C	year: 1989
Author:	KLIPPSTEIN and SCHILLING	$r_{I_r} \approx 0.1$ (avg.)
Amount:	10 failure, 0 runout	
Spectrum:	Truncated Rayleigh	
Notes:	Loading type is a normal force. all failures are weld toe failures. Crack initiation occurs over a range of locations in the specimen width direction.	

The specimens as tested by [63] are in-plane loaded 45-degree fillet-welded simple cruciforms, see figure 7.2. The throat height of all welds is ≈ 6 mm, making the weld leg length and height both $\sqrt{2} \cdot 6 \approx 8.5$ mm. Klippstein and Schilling report the out-of-flatness of all specimens, and conclude: "Based on the data shown, there appears to be no evidence that the out-of-flatness, as experienced in the specimens tested, consistently significantly affected the fatigue life." [63]. The out-of-flatness is therefore not accounted for in this assessment.

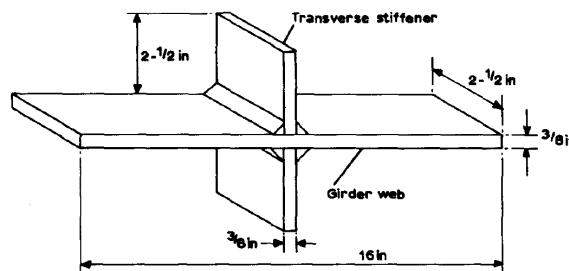


Figure 7.2: PP DS Cruciform as tested by Klippstein and Schilling [63].

The DNV-GL method A can not be applied to calculate the hot spot structural stress of simple cruciform joints [27]. This is because method A requires a stress gradient between the two points. For simple cruciforms the structural stress is approximately equal to the (nominal) far field stress. The gradient is thus approximately zero, yielding an extrapolated value equal to the base values. To circumvent this, DNV-GL proposes to use method B (1.12 times the effective stress at $t_p/2$), multiplied with the K_s factor for the respective geometry (being 1.05 for an in-plane loaded cruciform).

Discussion The FE analysis of a shell model (figure D.1 in the appendix) shows that the maximum first principal stress is found at the plate edges. Klippstein and Schilling indicate that failure occurs at locations scattered over the width of the specimen. That means that the calculated structural stress, at the centre of the specimen, is not accurate and relevant for all failures. This could have been circumvented by the use of decently designed dogbone specimens or by rounding the edges. As the authors have equipped the specimens with strain gauges at the centerline of the specimen (in width direction), they did not further analyse the effect of edge- and centre failures. They did however report in what region (separated in four quadrants) the failure initiated. This information is not used in the VA database, in line with the strain gauge measurements and research conclusions by Klippstein and Schilling.

Spectrum The spectrum that is applied to the specimens is a 500-cycle time trace with the minimum stress of 13.8 MPa, a maximum stress of {294, 250, 192} MPa and a stress range histogram compliant with a Rayleigh distribution. Each stress cycle returns to the minimum level. The pdf of the respective Rayleigh distribution (made non-dimensional) is given as [122] $p' = 1.011x' \exp(-\frac{1}{2}x'^2)$, with:

- x' Non-dimensional stress range ($x' = (S_r - S_{r,min}) / S_{r,d}$)
- S_r Stress range
- $S_{r,min}$ Minimum stress range
- $S_{r,d}$ Modal stress range ($S_{r,max}/2 - S_{r,min}$)

Figure 7.3 shows both the histogram, obtained from the pdf (probability density function) and a part of the time signal obtained by random sampling the peaks from the pdf.

The mean r_{I_r} value is obtained by calculating the mean of the r_{I_r} per cycle. The mean r_{I_r} value, over the 500 cycles, is ≈ 0.1 . For the fatigue assessment the r_{I_r} value per cycle is required, allowing to weight the contributions of larger and smaller stress cycles fairly. This is done and results in a stress range vector of length 500.

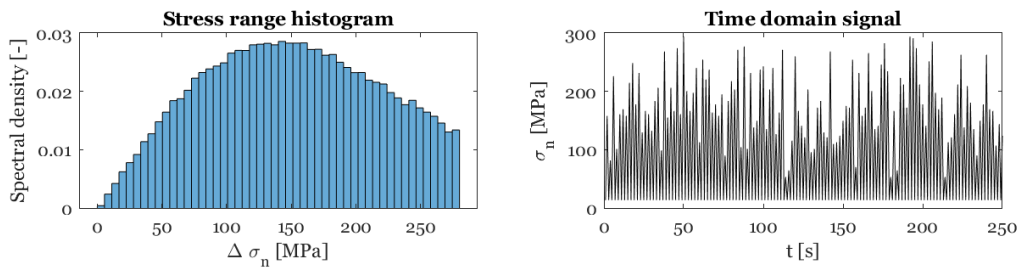


Figure 7.3: The histogram is compiled over 100 000 points. The frequency at which the time signal is plotted is 1 Hz.

7.3.2. Cruciform HS Type C from [3]

Dataset:	<i>FP DS Cruciform joint HS Type C</i>	
Author:	PETERSEN et. al.	year: 1995
Amount:	10 failure, 0 runout (PMMOD64) and 12 failure, 0 runout (BROAD64)	$r_{lr} \approx -1$ (avg.)
Spectrum:	PMMOD64 (Pierson-Moskowitz) and BROAD64 (Gaussian white-noise)	
Notes:	Loading type is a normal force. All failures are weld toe failures.	

The first specimen type as tested by [Agerskov et al.](#) is a full penetration half-V welded double sided cruciform, see figure 7.4. As the half-V weld poses a non-symmetry, the hot spot structural stress should be assessed by means of a solid model. By using a solid model to capture the effect of the non-symmetry, the use of Method A suffices. By modelling the attachment as a plate with a physical thickness the stress concentration is introduced. Two specimens of this type are tested: a larger and a smaller one. [Agerskov et al.](#) report a critical attitude towards the quality of the smaller specimens, which is why only the larger specimens are added to the VA database.

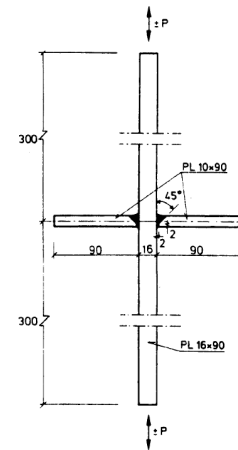


Figure 7.4: FP DS Cruciform joint as tested by [Agerskov et al.](#) [3].

Spectra The first spectrum is a modified² Pierson-Moskowitz spectrum. As the peaks are generated without a mean stress, the mean r_{lr} is ≈ -1.0 . The spectrum is given in the frequency domain, see the left part of figure 7.5. To obtain a pdf of the stress ranges this is first translated to the temporal domain (right side of figure 7.5), to use a rainflow counting procedure to find the stress ranges and r_{lr} values.

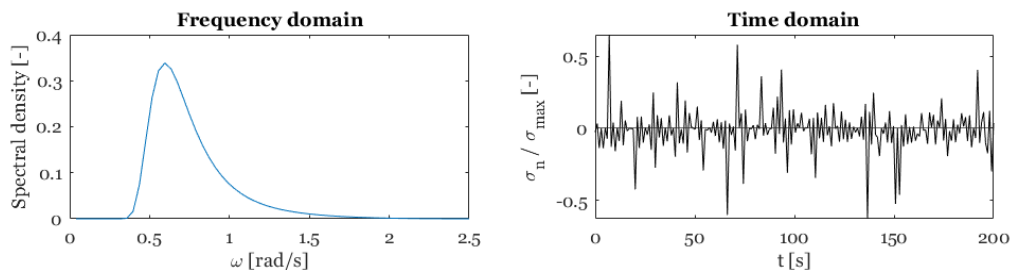


Figure 7.5: Frequency and time domain plot of the modified Pierson-Moskowitz spectrum as used in the experiments from [3].

The formulation of the spectrum, as commonly used is:

²The spectrum is in the analysis from [3] modified to fit the Markov matrix formulation. The modification entails the addition of the k factor.

$$S_{PM}(\omega|H_s, T_z) = \left(\frac{H_s^2}{4\pi}\right) \left(\frac{2\pi}{T_z}\right)^4 \omega^{-5} \exp\left(-\frac{1}{\pi} \left(\frac{2\pi}{T_z}\right)^4 \omega^{-4}\right) \quad (7.7)$$

However, [Agerskov et al.](#) present the formula as:

$$S_{load}(\omega|T_z) = \frac{4}{\pi} \sigma^2 \left(\frac{2\pi}{T_z}\right)^4 \omega^{-5} \exp\left(-\frac{1}{\pi} \left(\frac{2\pi}{T_z}\right)^4 \omega^{-4}\right) \quad (7.8)$$

Equating both formulations yields the conclusion that $4\sigma = H_s$, which is consistent with the typically accepted estimate of the significant wave height as a function of the variance [62].

For the modified version this spectrum is multiplied with the factor $k(\omega) = \exp\left(-\left(\frac{\omega}{\omega_t}\right)^8\right)$.

This k factor poses a sharp but continuous truncation of the spectrum at the angular truncation frequency ([Agerskov et al.](#) use 3 times the peak frequency). In the formulation of the Pierson-Moskowitz wave spectrum the significant wave height H_s and wave period T_z pose an absolute multiplication of the spectrum. The H_s and T_z values are not reported. To mitigate this uncertainty the normalised spectrum (excluding the H_s and T_z multiplications) is used, and multiplied with the reported equivalent stress values.

It should be noted that by using the wave spectrum as input for the loads acting on the structural detail, the assumption is made that the [Response Amplitude Operator \(RAO\)](#) is equal to one for all frequencies: this does not comply with reality and is an assumption that limits the applicability of the results. However, as the goal of this thesis is to test the spectrum dependency of the validity of the fatigue life prediction, this spectrum can be used for further considerations.

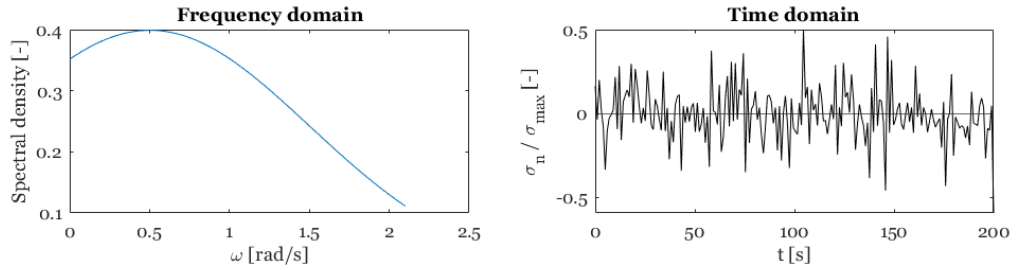


Figure 7.6: Frequency and time domain plot of the white-noise based spectrum as used in the experiments from [3].

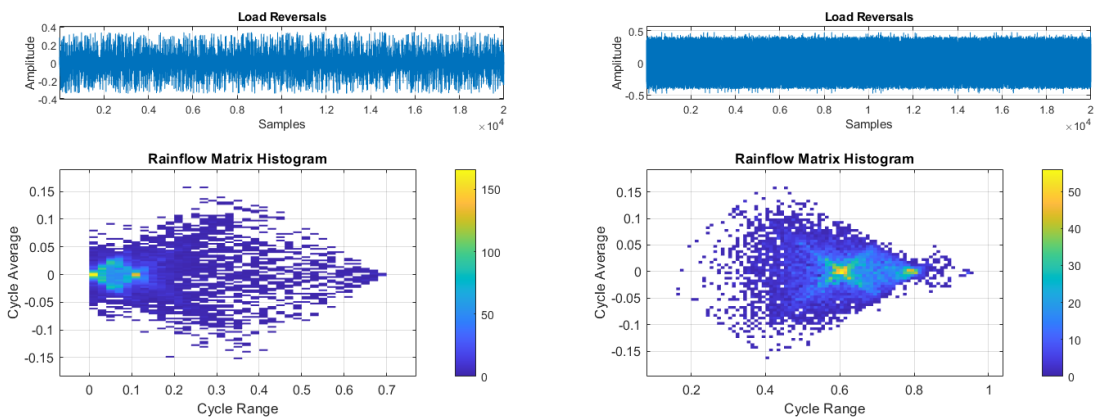


Figure 7.7: Rainflow histogram of 20000 peaks of the PMMOD64 distribution.

Figure 7.8: Rainflow histogram of 20000 peaks of the BROAD64 distribution.

As the spectral domain formulation is known, the inverse Fourier transform gives the complex transformed notation Z_i , of which the amplitude $A_i = |Z_i|$ and phase angle $\phi_i = \text{atan2}(\Im(Z_i)/\Re(Z_i))$ can be calculated. Per frequency (64 in total) a time signal is constructed according to:

$$S_{PM,i}(t) = A_i \cos(\omega_i t + \phi_i) \quad (7.9)$$

Summing the contributions of all frequencies results in the net time signal, which is normalised. A rainflow counting procedure provides the stress range histogram (figure 7.7). It should be noted that the actual r_{lr} per cycle is not a constant value of -1. The loading and response ratio r_{lr} is calculated per cycle of a 5000 cycle time-trace separately. The fatigue life (or inverse: fatigue damage) is calculated per cycle and accumulated to the total result. An important note here is that the sequence effect is not introduced here: this is implicitly accounted for in both the LDAM and the NLDAM. The order of the cycles is not important here.

The second spectrum is a white-noise based broad band spectrum composed of 64 frequency signals, called BROAD64. For a white noise spectrum the spectral density is expressed as a normal distribution. In this case with a mean equal to the normalised mean stress. The Fourier transformation is identical to the procedure applied to the modified Pierson-Moskovich spectrum. Figure 7.8 presents the histogram of the stress ranges, and figure 7.6 presents both the frequency and time domain (over 200 seconds) plot of the signal. Like for the PMMOD64 spectrum, the actual r_{lr} per cycle is not a constant value of -1. The loading and response ratio r_{lr} is calculated per cycle of a 5000 cycle time-trace.

7.3.3. Longitudinal attachment HS Type A from [3]

Dataset:	PP DS Longitudinal attachments HS Type A	
Author:	PETERSEN et. al.	year: 1995
Amount:	16 failure, 0 runout	$r_{lr} \approx -1$ (avg.)
Spectrum:	BROAD64	
Notes:	Loading type is a normal force. All failures are weld toe failures.	

The second specimens as tested by Agerskov et al. are in-plane loaded specimens with a DS longitudinal attachment, see figure 7.9. The specimens are produced with 45-degree fillet welds. The use of fillet welds means that the attachment is only connected to the base plate by means of the welds. As was done for the HS type C specimens, two variations are tested: a larger and a smaller one. Agerskov et al. report a critical attitude towards the quality of the smaller specimens, which is why only the larger specimens are added to the VA database.

Spectrum The spectrum as applied by Agerskov et al. is, like for the longitudinal attachments, a modified Pierson-Moskovich spectrum (figures 7.6 and 7.8). As the peaks are generated without a mean stress, the mean r_{lr} is ≈ -1.0 . As was described before: the actual r_{lr} per cycle is calculated to accumulate the contributions per cycle.

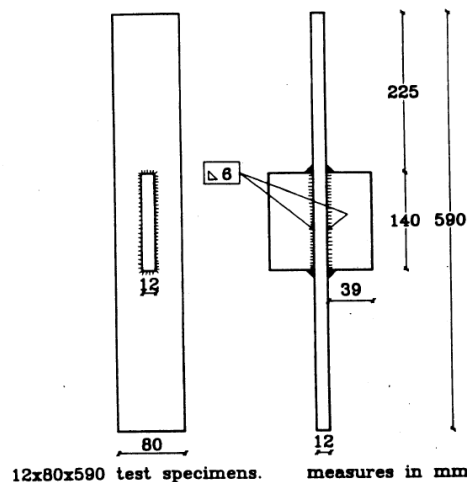


Figure 7.9: PP DS Longitudinal attachment as tested by Agerskov et al. [3].

7.3.4. Butt joints HS Type C from [103]

Dataset:	FP DS Butt joint HS Type C	
Author:	OTA et. al.	year: 1997
Amount:	11 failure, 0 runout	$r_{lr} \approx \{0.85, 0\}$ (avg.)
Spectrum:	Rayleigh up (4x) and down (7x)	
Notes:	Loading type is a normal force. all failures are weld toe failures.	

The specimen as tested by Ota et al. is a girth welded transverse butt joint. The only information in the article is that SMAW was used and the geometry is depicted by figure 7.10. Whether the specimen is symmetrical or not is not explicitly included in the paper. Based on figure 7.10, which shows that the weld was made from two sides, the assumption is made that it is a simple butt joint, without ground caps. As the model is symmetrical, the plate FE analysis does not show a notch at the weld. DNV-GL proposes to use method B (1.12 times the effective stress at $t_p/2$), multiplied with the K_s factor for the respective geometry (being 1.13 for an in-plane loaded transverse butt joint welded from both sides, of type No. 3 [27]).

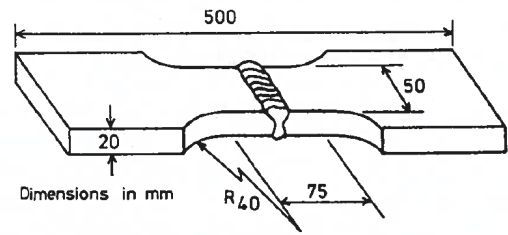


Figure 7.10: FP DS Butt joint as tested by Ota et al. [103].

Spectrum The stress ranges are distributed according to the formulation by Rayleigh, like in [63]. However, Ota et al. use this distribution to form two different load histories:

1. Cycling down from the yield stress (579 MPa), with varying r_{lr} values per stress block, see figure 7.11
2. Cycling up from zero, and thus $r_{lr} = 0$, see figure 7.12

Per specimen the applied specimen meets the Rayleigh formulation. As the spectrum is simplified and expressed in a maximum of 9 blocks, the exact block formulation per specimen is used for the analysis. The r_{lr} is calculated per stress block.

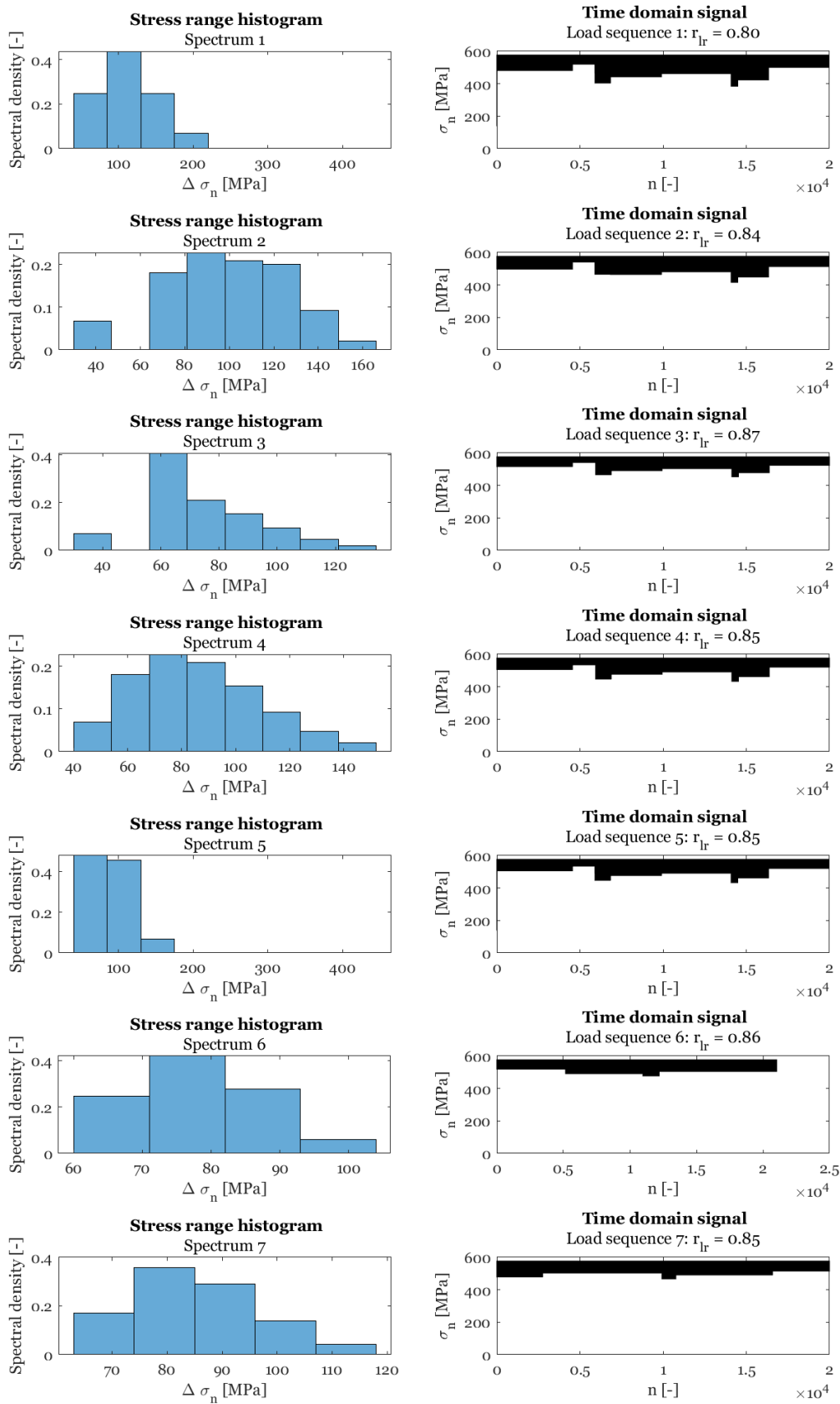


Figure 7.11: Spectra as applied to the butt jointed joints [103], cycling down from the yield stress. The presented r_{Ir} values represent the weighted mean over all cycles. This is not the value that is used in the calculations.

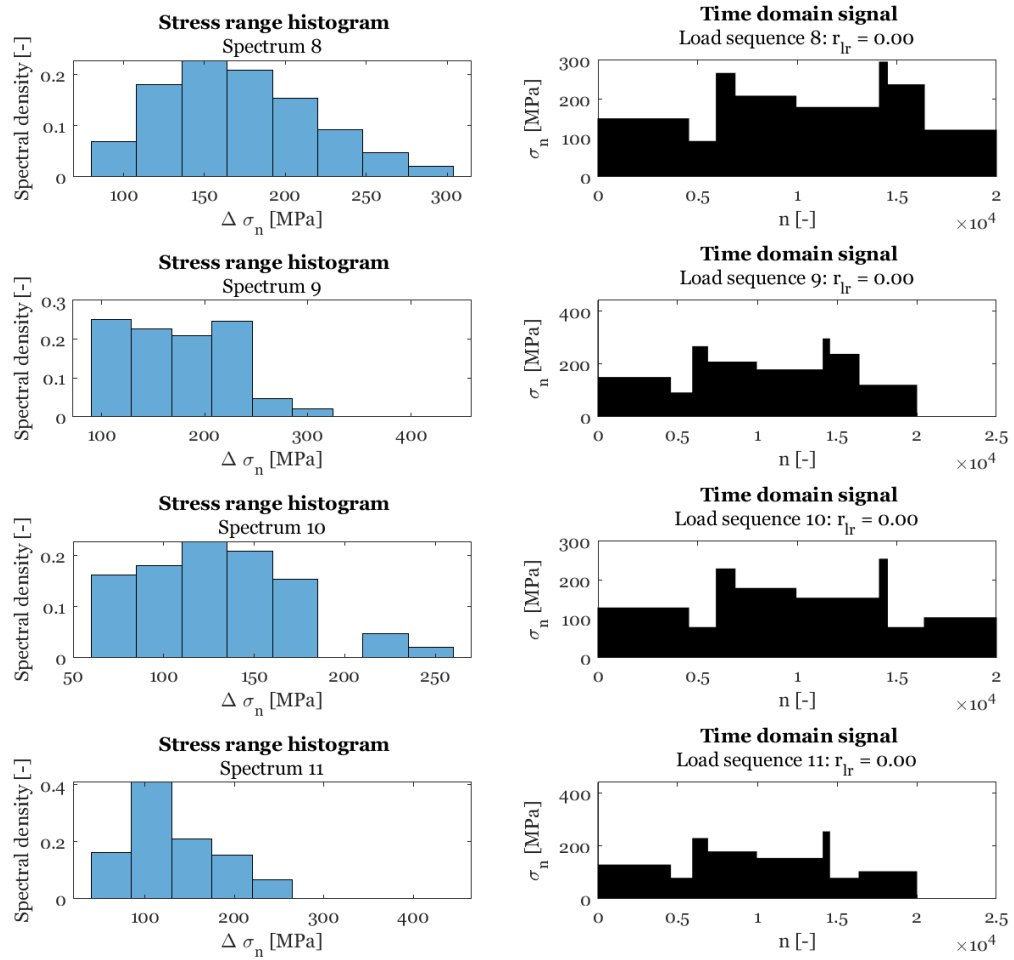


Figure 7.12: Spectra as applied to the butt jointed joints [103], cycling up from $\sigma_n = 0$.

7.3.5. Longitudinal attachment HS Type A from [147]

Dataset:	<i>PP DS Longitudinal plate attachment HS Type A</i>	year: 2009
Author:	ZHANG and MADDOX	r_{lr} : various
Amount:	10 failure, 0 runout	
Spectrum:	Concave-up	
Notes:	Loading type is a normal force. All failures are weld toe failures.	

The first specimen as tested by Zhang and Maddox has a fillet-welded double sided longitudinal attachment. The specimen is symmetrical, see figure 7.13.

Spectrum Zhang and Maddox imposed a concave-up spectrum on the specimens. That means that the relation between the relative stress range and the minimum and maximum stress is close to log-linear. The authors made three variations on this spectrum:

1. Sequence 1: Cycling down from a maximum stress of 280 MPa
2. Sequence 2: Cycling symmetrically around a mean stress of 175 MPa
3. Sequence 3: Cycling up from a minimum stress of 70 MPa

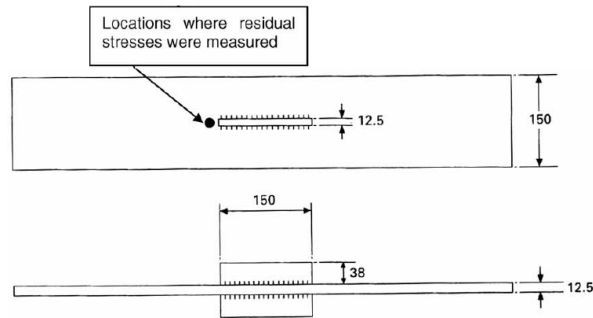


Figure 7.13: PP DS Longitudinal plate attachment as tested by Zhang and Maddox [147]

The lower truncation bound of the spectrum differs per specimen (all are normalised after truncation). For each of the variations the effective r_{lr} is calculated per cycle from the time trace, see figure 7.14. An important note is that sequence 2 cycles up and down at the same amplitude per cycle. The start of each cycle is thus at 175 MPa, by which the mean stress is constant. Figure 7.14 only shows 100 cycles, to visually present the nature of the time signal in line with the previous formulations. The actual spectrum is defined in 14 blocks, of which the values are presented in [147].

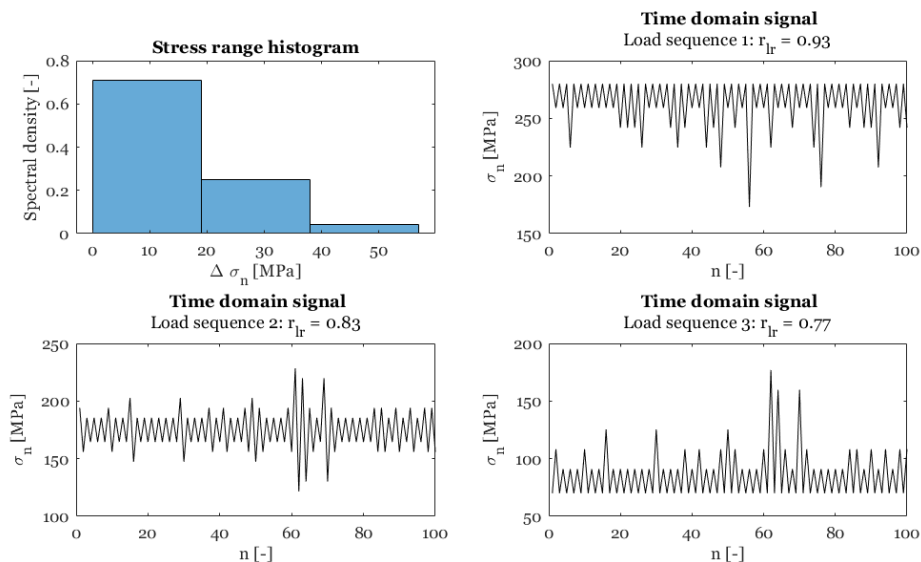


Figure 7.14: Example for the first three bins of the stress range histogram and corresponding time traces for the three variations as tested by [147].

7.3.6. Longitudinal attachment HS Type B from [147]

Dataset:	<i>PP DS Longitudinal edge attachment HS Type B</i>	year: 2009
Author:	ZHANG and MADDOX	\bar{r}_{I_r} : various
Amount:	6 failure, 0 runout	
Spectrum:	Concave-up	
Notes:	Loading type is a normal force. All failures are weld toe failures.	

The second specimen as tested by Zhang and Maddox has a fillet-welded longitudinal attachment that poses a HS type B on both sides of the base plate. The specimen is symmetrical. The local geometry of the weld that connects the attachments with the base plate is uncertain and part of the inherent scatter in fatigue. The stresses are extracted from a FE shell model.

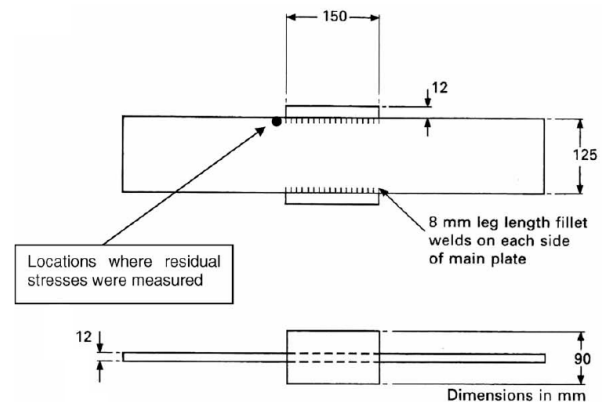


Figure 7.15: PP DS Longitudinal edge attachment as tested by Zhang and Maddox [147]

Spectrum The spectrum is the same as discussed in the previous section for the longitudinal attachment with HS type A from [147]. The lower truncation bound of the spectrum differs per specimen (all are normalised after truncation). For the specific values see [147].

7.3.7. Butt joints HS Type C from [148]

Dataset:	<i>FP SS Butt joint HS Type C</i>	year: 2014
Author:	ZHANG and MADDOX	$\bar{r}_{I_r} \approx 0.71$ (avg.)
Amount:	9 failure, 9 runout	
Spectrum:	Log-Linear	
Notes:	Loading type is a normal force. All failures are weld root failures (i.e. the bottom side of the weld).	

The specimens that were tested by [148] are used to eventually assess the fatigue life of a girth-welded full scale specimen. To do this, a small scale specimen of a dog-bone shaped strip specimen is loaded. The structural detail is a single sided full penetration butt-welded joint as in figure 7.16.

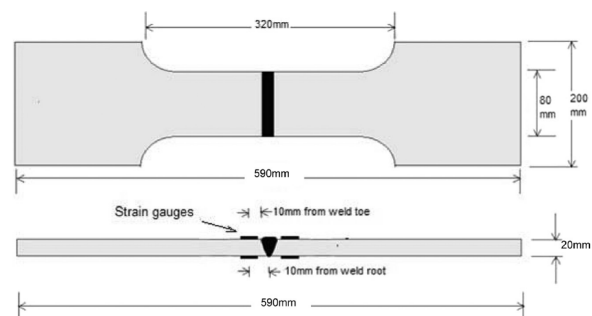


Figure 7.16: FP DS Butt joint as tested by Zhang and Maddox [148]

Spectrum Zhang and Maddox impose a log-linear spectrum on the full-scale girth welded specimens. That means that the relation between the minimum stress and the probability of occurrence is linear on the logarithmic scale. The maximum stress is the same for each of the six variations. The minimum stress of the spectrum differs. Figure 7.17 presents per spectral variation the stress range histogram and corresponding time trace. The time trace is obtained in the same manner as Sequence 2 in [147], which was explained in section 7.3.5.

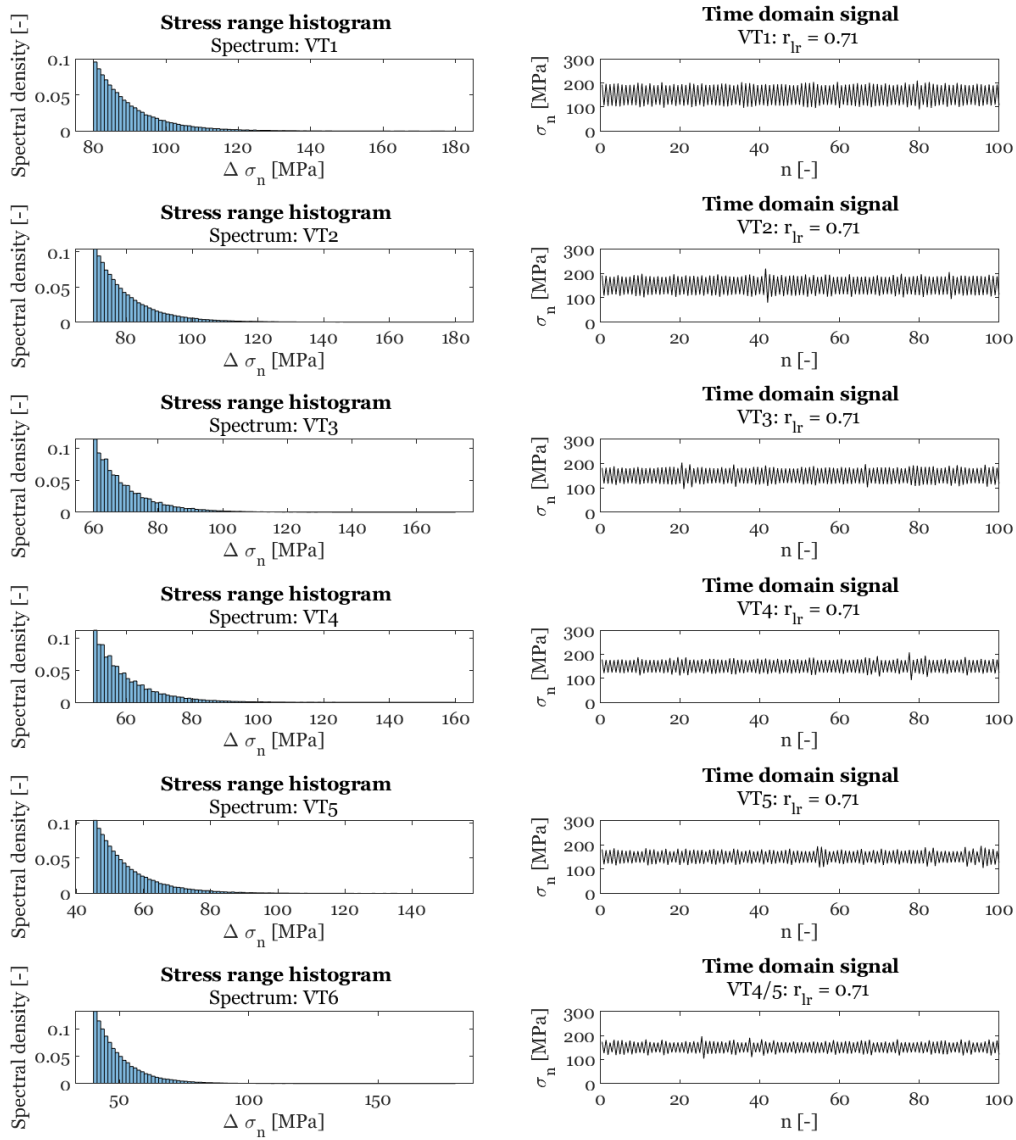


Figure 7.17: Stress range histograms and corresponding time traces for the six spectra as tested by [148]. VT6 is actually the spectrum between VT4 and VT5.

7.3.8. Cruciform HS Type C from DMO (2020)

Dataset:	<i>FP DS Cruciform joint HS Type C</i>	
Author:	DMO & Femto Engineering	year: 2020
Amount:	4 failure, 0 runout	$r_{lr} = 0.1$
Spectrum:	Rayleigh	
Notes:	Loading type is a three-point bending moment, applied to the centre of the specimen. The spectrum was applied as a block-load. All four specimens failed on the side of the half-V weld at the weld toe.	

As part of the fatigue tests that **DMO** ordered, four **VA** fatigue tests were done. The analysis of these specimens is the subject of chapter 6. The spectrum is according to a Rayleigh distribution and is separated into six load levels, which are randomly applied to the specimen to create a signal of 1000 cycles divided over 100 blocks, which is repeated until failure. All blocks are applied at a r_{lr} level of 0.1. Table 7.3 presents the six stress blocks and their probability of occurrence, expressed as amount of cycles in a 1000 cycle time history.

Table 7.3: Spectrum as was applied to the **DMO** half-V welded cruciform specimens. The right-most column is the spectrum for a Rayleigh distribution without modification. The column left of that contains the spectrum that was applied to the specimen, and indicates the removal of low stress range cycles.

Range ΔF_N [N]	Range $\Delta \sigma_n$ [MPa]	Cycles Rayleigh mod.	Cycles Rayleigh
5599	145	180	290
7722	200	350	310
9652	250	220	200
11583	300	130	100
13513	350	80	70
15926	412	40	30

7.4. Results

This section contains the results of the combined fatigue damage models and fatigue damage criteria as presented in chapter 5.

7.4.1. LDAM by Palmgren and Miner with the HSSSC

Due to the linear nature of the Palmgren-Miner model, the only parameter D_{crit} has a linear and positive relation with the predicted fatigue life. Serving as the base-case, the **LDAM** with the **HSSSC**, according to the methods as proposed by DNV-GL [27], is first used to estimate the fatigue life per specimen. Figure 7.18 provides the comparison between the experimental and estimated fatigue lives. The dashed lines indicate the $\pm 2\sigma$ variations. Figure 7.19 compares the **SSS VA** scatterband to the **SSS CA** scatterband, and makes use of the equivalent stress formulation:

$$S_{eq} = \sqrt[m]{\sum_{i=1}^k \left(\frac{n_i}{N}\right) S_i^m} \quad (7.10)$$

The derivation of this equivalent stress formulation is included in appendix C.1.1. The comparison of the **VA** and **CA** scatterbands shows that the specimens typically fall outside of the $\pm 2\sigma$ bounds, either on the conservative or non-conservative side. That means that the use of $D_{crit} \leq 1$ does not seem to be a sufficient criterion.

Figure 7.20 presents the histogram of the experimental over the calculated fatigue lives. This figure shows that the mean critical damage for all specimens is around 1 for the mean S-N curve formulation as was used. However, two peaks are observed, corresponding with the separation in HS type A and B compared to HS type C.

The scatter of the data is expressed by dividing the 90% percentile over the 10% percentile of the log-fatigue life ratio. This provides the scatter index in the form of 1 : (90%percentile/(10%percentile)). This is an expression that is typically used to express the scatter in fatigue strength (e.g. [111]), but is used here to express the scatter in the resulting fatigue life predictions. The fatigue life scatter index is $1 : 1.28$ and the Log-Likelihood of the fit is approximately 22.2 .

As was mentioned before, the **Akaike Information Criterion (AIC)** is used to assess the relative quality of the fit with the experimental data of a model. The model is not regression-based but deterministic. Therefore the **AIC** is simply twice the negative of the Log-Likelihood:

$$\begin{aligned} \text{AIC} &= -2 \sum \log(\mathcal{L}) + 2n \\ &= -2 \cdot 22.234 + 2 \cdot 0 \approx -44.5 \end{aligned} \quad (7.11)$$

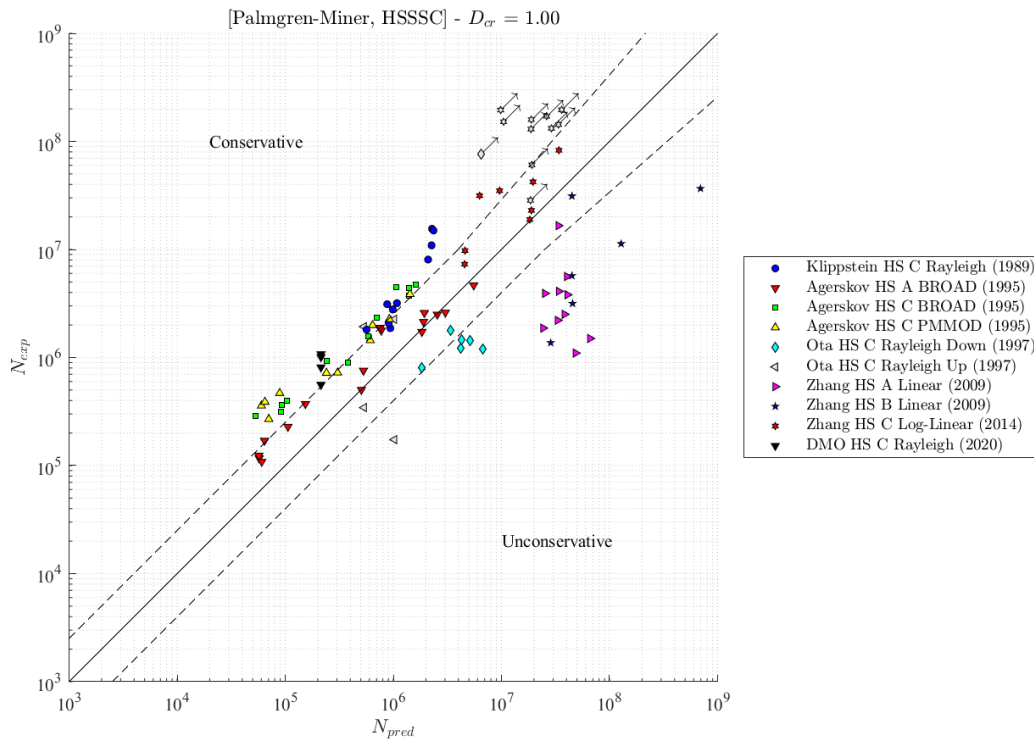


Figure 7.18: Comparison of the experimental and predicted fatigue life from the **LDAM** in combination with the **HSSSC** (base-case). The critical damage is fixed on a value of $D_{\text{crit}} = 1$, in line with the original formulation [95, 104].

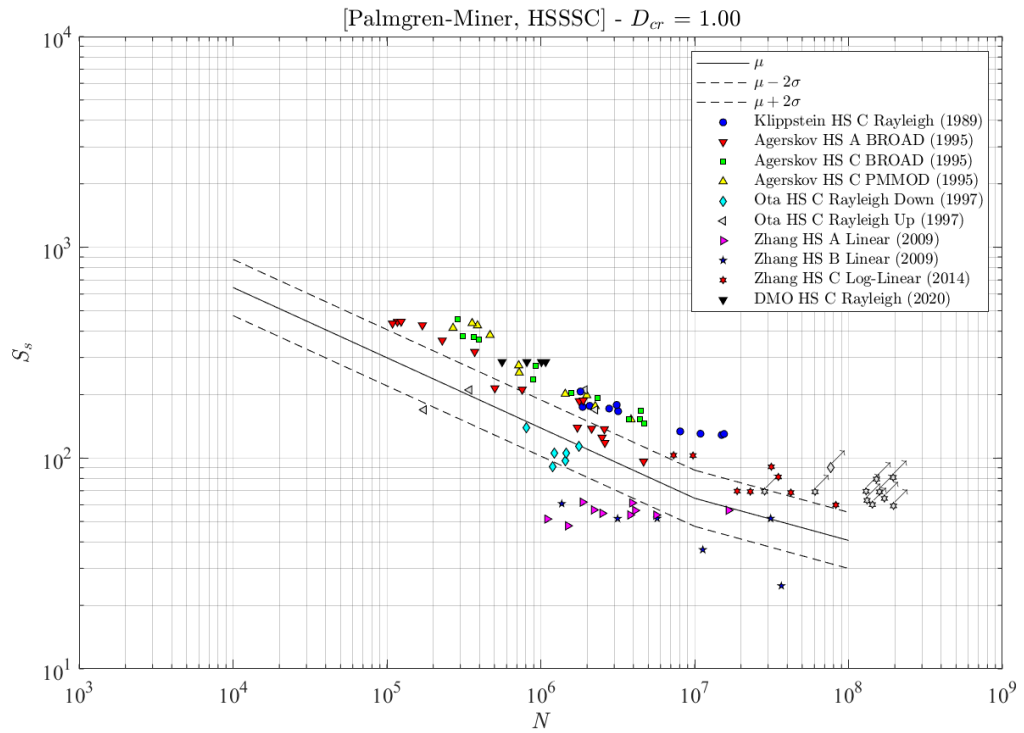


Figure 7.19: Comparison of the experimental and predicted fatigue life from the LDAM in combination with the HSSSC (base-case). The critical damage is fixed on a value of $D_{crit} = 1$, in line with the original formulation [95, 104]. For each of the tested specimens the equivalent stress is calculated and plotted on the ordinate.

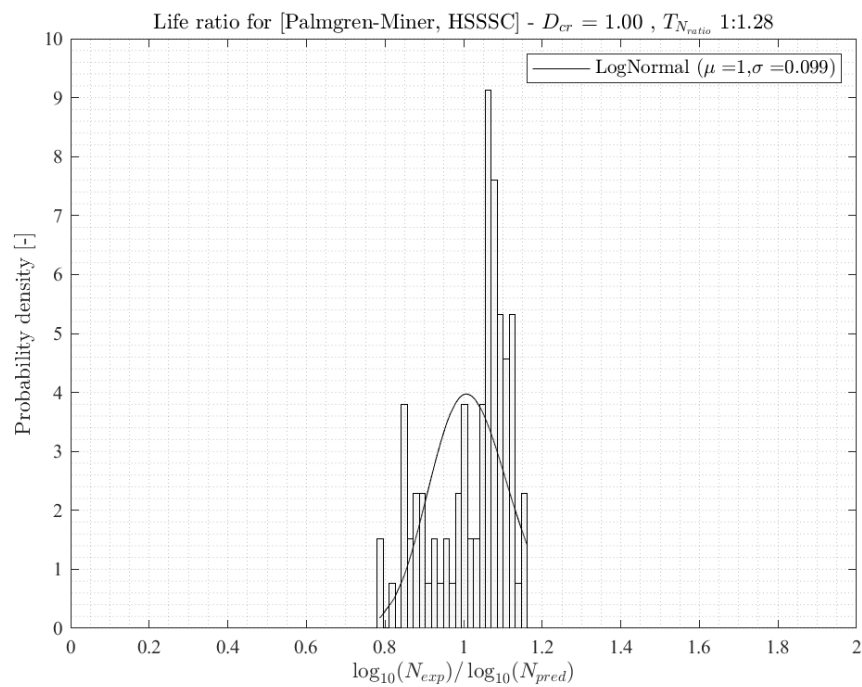


Figure 7.20: Scatter histogram of the log10 of the experimental fatigue life over the calculated fatigue life for the LDAM in combination with the HSSSC (base-case).

There are some observations with regards to the presented results in the figures above, being:

- With the exception of the specimens from [Agerskov et al.](#), the estimated fatigue lives of the HS type A and B specimens are non-conservative (see figures 7.18 and 7.19): the calculated fatigue life is larger than the experimental lives. The HS type C specimens are generally on the conservative side. The difference between HS type A and B compared to HS type C should reduce when using the [ENSC](#), as the actual local geometry will be accounted for. The peak stress for HS type A and B specimens is typically higher due to the hard point that is introduced. This is not accounted for in the [HSSSC](#).
- The exception of the specimens from [Agerskov et al.](#) (HS Type A subject to a BROAD64 spectrum) can most likely be attributed to the relatively low amount of low stress range cycles, which means that the sensitivity near the fatigue limit has a limited effect on the predicted fatigue life. The HS type A and B specimens from [147] are subject to linear spectra, which are governed by low stress range loads. This statement can be confirmed by applying a non-linear damage accumulation model, which accounts for the influence of low stress ranges on the total fatigue life (e.g. the [NLDAM](#) by [Leonetti et al.](#), as used in this thesis).
- The predicted fatigue life of the specimens from [103], subject to the Rayleigh Down load, are also non-conservative. This is presumably due to the relatively high r_{lr} level at which the specimens are tested. This explanation is substantiated in the next section, where the inclusion of the r_{lr} correction moves the specimens to the conservative domain; into the scatterband of the other HS type C specimens.
- On average the fatigue life estimate with this method is conservative. The best fit of a LogNormal distribution provides a mean of 1 and a standard deviation of 0.099. The expected value of that distribution equals $E[x] = \exp(\log(1) + 0.099^2/2) \approx 1.01$. It is assumed that a LogNormal distribution of the fatigue life also poses a LogNormal distribution of the error of the prediction of this fatigue life. It should be noted that this conservatism can also be attributed to conservatism in the DNV-GL D-curve. The conclusions of chapter 6 support this hypothesis.
- The fraction of the log10 of the experimental and calculated fatigue life poses two peaks. This is related to the first observation of the separation between HS type A and B from HS type C result.

7.4.2. LDAM by Palmgren and Miner with the HSSSC and mean stress correction

The scatter of the data reduces by implementing the Walker mean stress correction, cycle-by-cycle. The observed scatter reduction from 1:1.28 to $\boxed{1 : 1.22}$ is in line with the findings in section 6.5. The Log-Likelihood is approximately $\boxed{22.5}$, which is an improvement of approximately 0.3 (absolute value of the difference in Log-Likelihood) in relation to the assessment without the mean stress correction. The resulting [AIC](#) yields:

$$\begin{aligned} \text{AIC} &= -2 \sum \log(\mathcal{L}) + 2n \\ &= -2 \cdot 22.478 + 2 \cdot 0 \approx -45.0 \end{aligned} \tag{7.12}$$

As was expected, the implementation of the cycle-by-cycle Walker mean stress correction has reduced the scatter. The non-conservative specimens are now only the specimens that are subject to the linear spectrum in [147]: the limited sensitivity of the [LDAM](#) to low stress ranges is presumably responsible for the observed difference. The tendency of the total fatigue life prediction to be on the conservative side could be mitigated by finding the [MLE](#) of the critical damage.

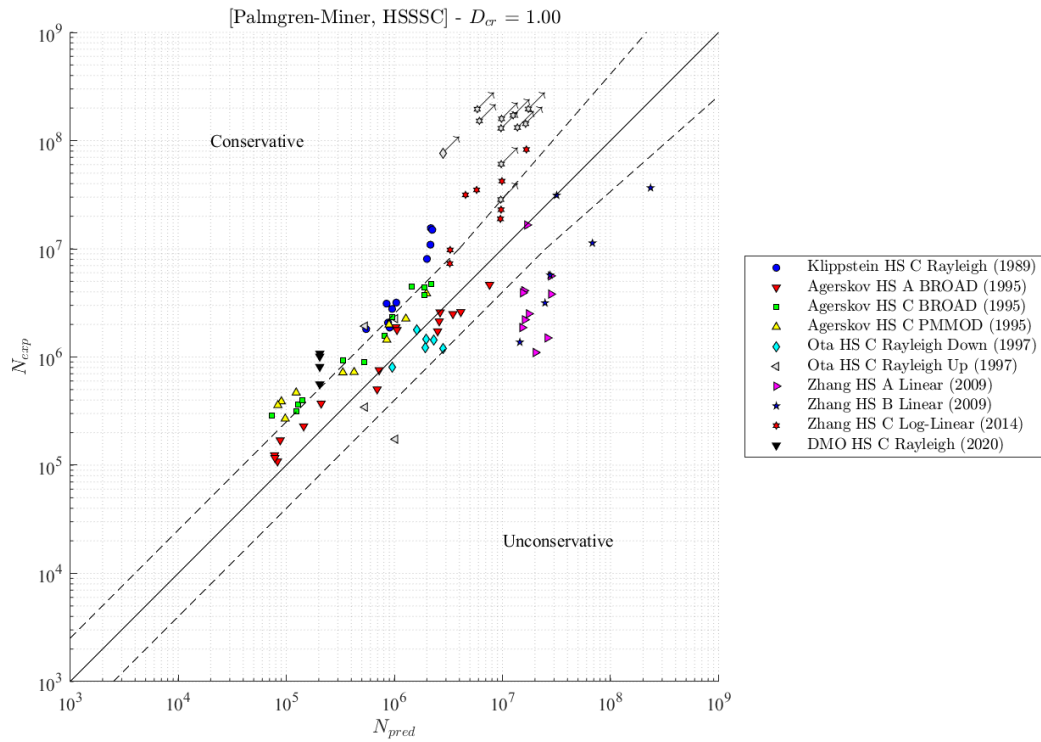


Figure 7.21: Comparison of the experimental and predicted fatigue life from the LDAM in combination with the HSSSC (base-case). The critical damage is fixed on a value of $D_{crit} = 1$, in line with the original formulation [95, 104].

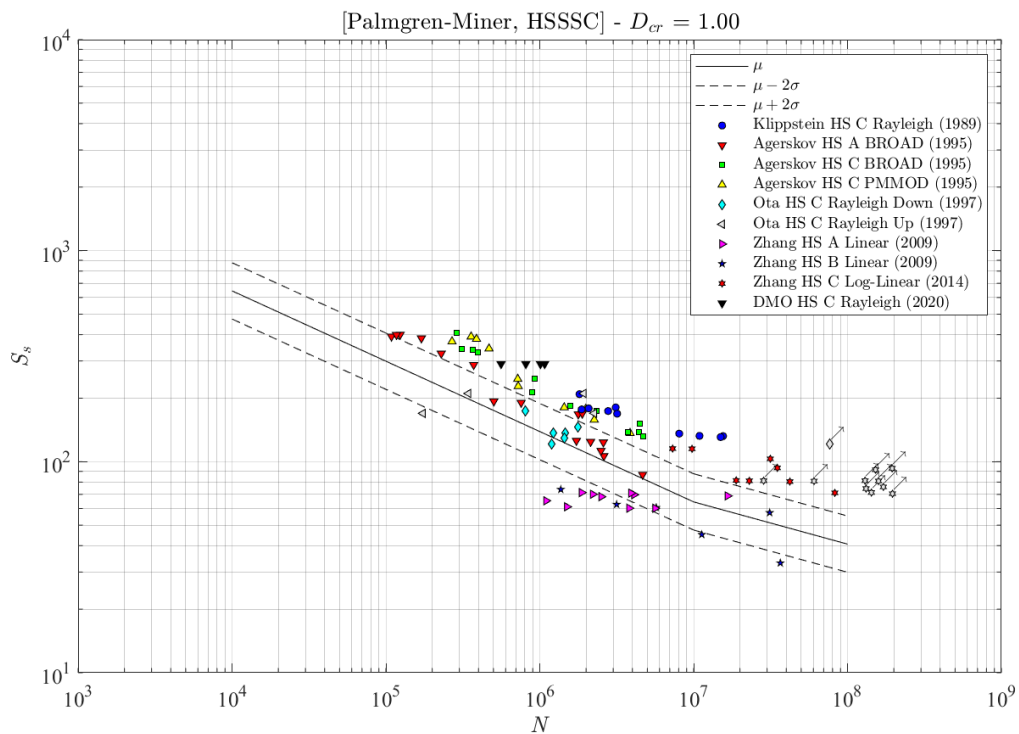


Figure 7.22: Comparison of the experimental and predicted fatigue life from the LDAM in combination with the HSSSC (base-case). The critical damage is fixed on a value of $D_{crit} = 1$, in line with the original formulation [95, 104]. For each of the tested specimens the equivalent stress is calculated and plotted on the ordinate.

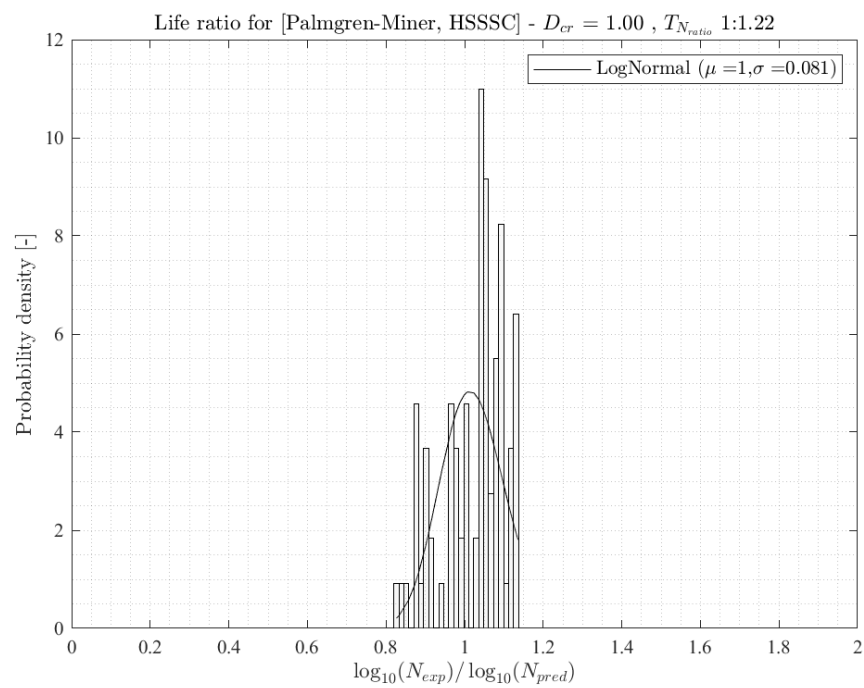


Figure 7.23: Scatter histogram of the log10 of the experimental fatigue life over the calculated fatigue life for the LDAM in combination with the HSSSC (base-case).

7.4.3. LDAM by Palmgren and Miner with the ENSC

The second deviation from the base-case is the use of the **ENSC** in combination with the **LDAM**. As was explained in the previous section, the hypothesis is that this reduces the difference between the HS type A, B and C specimens significantly.

Figure 7.5 presents the diagonal comparison between the experimental and calculated fatigue lives. It shows that indeed the difference between HS type A, B and C is reduced (arguably even negligible). Figure 7.25 compares the **SSS VA** and **CA** scatterbands and makes use of the equivalent stress formulation:

$$S_{eq}^m \left(1 - \frac{S_{\infty}(\mu, \sigma)}{S_{eq}} \right)^{\rho_{S_{\infty}}} - \sum_{i=1}^k \frac{n_i S_i^m \left(1 - \frac{S_{\infty}(\mu, \sigma)}{S_i} \right)^{\rho_{S_{\infty}}}}{N} = 0 \quad (7.13)$$

An algorithm like `fzero` can be used to obtain the equivalent stress that complies with the above formulation. The derivation of this equivalent stress formulation is included in appendix C.1.3. Figure 7.26 shows the scatter histogram of the fraction of the log10 of the fatigue lives. This figure clearly indicates only one peak, at around $D_{crit} = 1$. The scatter is reduced from 1:1:28 for the **HSSSC** with the **LDAM** without the mean stress correction to $[1 : 1.16]$ for the **ENSC** with the **LDAM**. The Log-Likelihood is approximately $[37.3]$. Considering the **AIC** the model has 6 regression-parameters (the six parameters from the **GRFL**) the **AIC** yields:

$$\begin{aligned} AIC &= -2 \sum \log(\mathcal{L}) + 2n \\ &= -2 \cdot 37.3243 + 2 \cdot 6 \approx -62.6 \end{aligned} \quad (7.14)$$

A lower **AIC** is found for a model that has a better fit, accounting for a penalty on the amount of variables. Therefore, it can be concluded that the use of the **ENSC** provides a significant improvement in the fatigue life prediction compared to the **HSSSC**, both in combination with the **LDAM**.

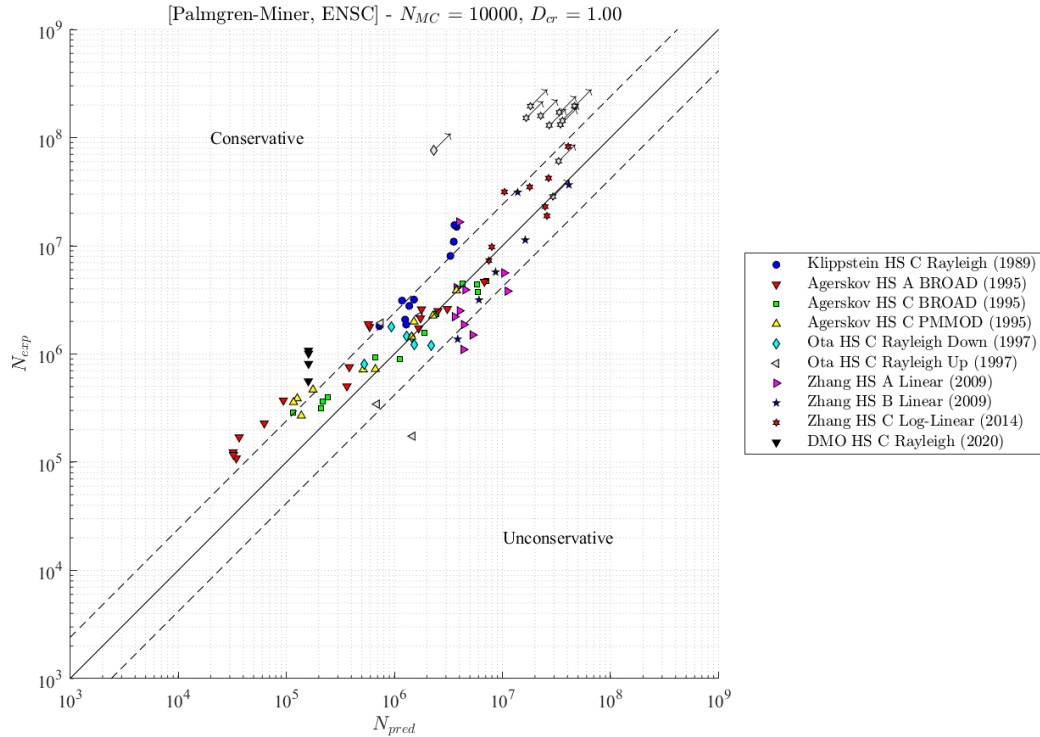


Figure 7.24: Comparison of the experimental and predicted fatigue life from the **LDAM** in combination with the **ENSC**. The critical damage is fixed on a value of $D_{crit} = 1$, in line with the original formulation [95, 104].

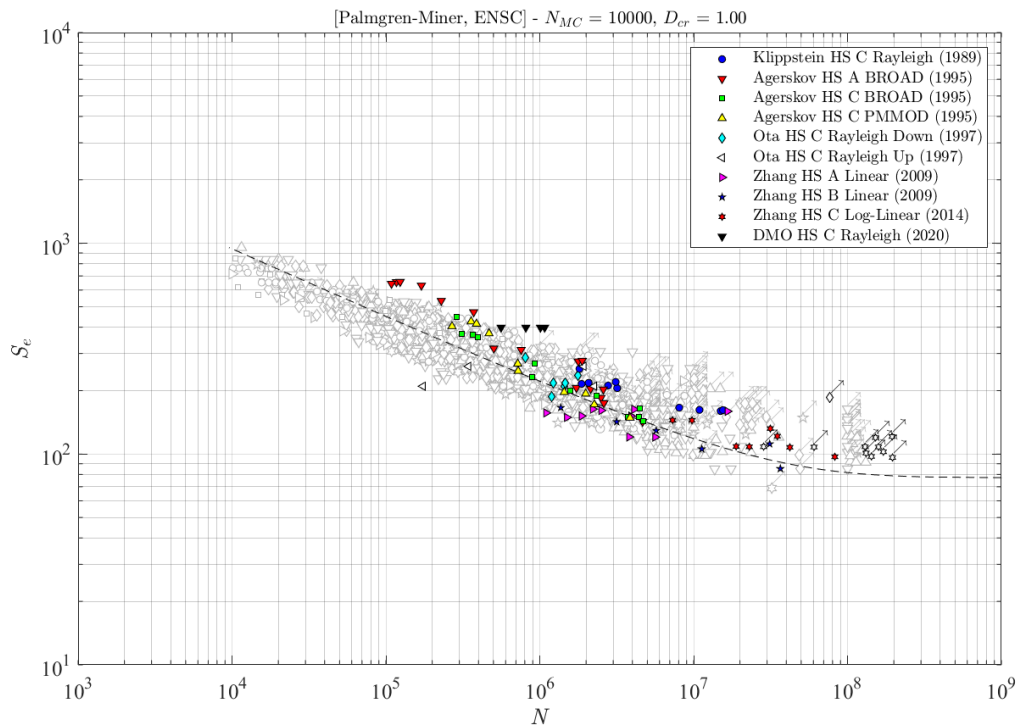


Figure 7.25: Comparison of the experimental and predicted fatigue life from the LDAM in combination with the ENSC. The critical damage is fixed on a value of $D_{crit} = 1$, in line with the original formulation [95, 104]. For each of the tested specimens the equivalent stress is calculated and plotted on the ordinate.

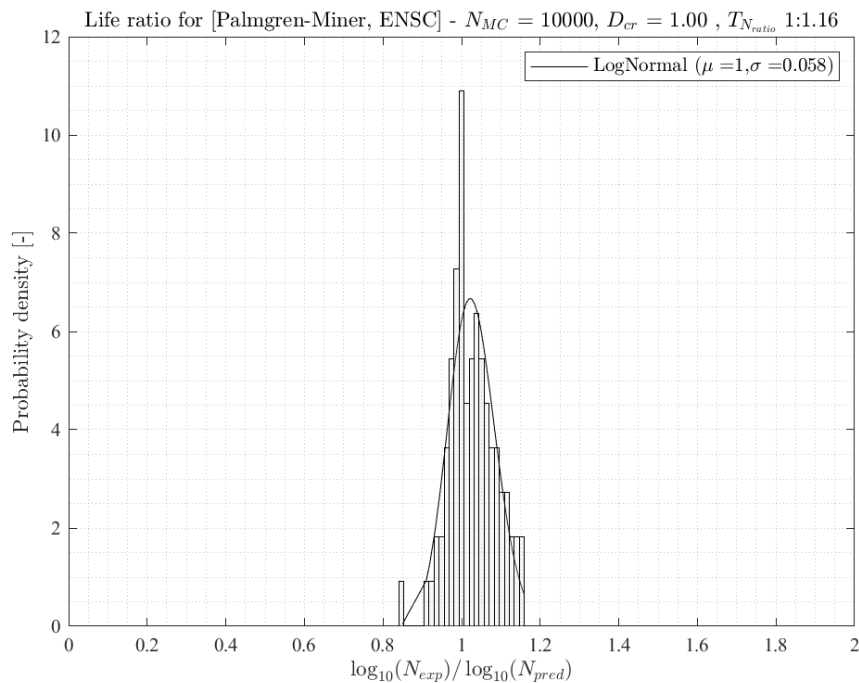


Figure 7.26: Scatter histogram of the log10 of the experimental fatigue life over the calculated fatigue life for the LDAM in combination with the ENSC.

There are some observations with regards to the presented results in the figures above, being:

- As was expected, there is no clear difference between the fit of the HS type A, B and C specimens. This is to be attributed to the local information in the [ENSC](#).
- The conservatism and scatter per dataset shows a correlation with the shape of the spectra:
 - The Rayleigh, Log-Linear and BROAD64 spectra are typically on the conservative side. These are relatively broad spectra, with a majority of medium stress range cycles. The conservatism might be due to the limited validity of the $D_{\text{crit}} \leq 1$ criterion.
 - The PMMOD64 and Linear (concave-up) spectra provide results on the unconservative side. That means that the model over-estimates the fatigue lives. These spectra are governed by low stress range cycles, which are - when below the fatigue limit - not contributing to the modelled damage.

[Fricke et al.](#) concludes that the critical damage value is spectrum dependent [38]. This is assessed by means of the Gassner-curves for specimens subject to different spectrum loads. This conclusion by [Fricke et al.](#) is supported by the findings in this section. The hypothesis is that the use of a fatigue damage accumulation model that accounts for the influence of low-stress cycles reduces the scatter further, by reducing the estimated (calculated) fatigue life of the specimens with spectra that are governed by low stress range cycles.

In general the [SSS VA](#) and [SSS CA](#) scatterbands overlap. That means that for the mean stress curve ([GRFL](#)) as used, the design criterion of $D_{\text{crit}} \leq 1$ is sufficient for most datapoints.

7.4.4. NLDAM by Hirt and Kunz, modified by Leonetti et al.

The third deviation from the base-case is the use of the [ENSC](#) with the [Non-linear Damage Accumulation Model \(NLDAM\)](#) by [Leonetti et al.](#). Because this model is formulated with the [GRFL](#) (called [6PRFLM](#) in [74, 75]) as the S-N curve, the model requires an S-N curve in this form. The base-case ([HSSSC](#) by [DNV-GL](#)) is formulated as a Basquin-type relation, and is thus not fit for the model by [Leonetti et al.](#). The [NLDAM](#) is only analysed for the [ENSC](#).

The damage accumulation model by [Leonetti et al.](#) requires a fit of the three parameters of the expression for the threshold stress range $\Delta\sigma_{th,h}$, below which no damage is accumulated. This threshold stress range is determined per damage increment and is expressed as:

$$\Delta\sigma_{th,h} = \Delta\sigma_0 \left(1 - \frac{D}{D_{\text{crit}}}\right)^\zeta \quad (7.15)$$

With:

$$\zeta = f(\alpha, m) = \frac{\alpha + 1/2}{1 - m(\alpha + 1/2)} \quad (7.16)$$

If the threshold stress increases, less damage is accumulated and the fatigue life increases accordingly. All parameters in the equation are positive [75]. To assess the influence of the parameters (μ_D , σ_D and ζ), their respective first derivatives are calculated. As the critical damage D_{crit} is expressed as a distribution with mean μ_D and standard deviation σ_D , only one derivative is calculated.

$$\begin{aligned} \frac{d}{d\zeta} \Delta\sigma_{th,h} &= \Delta\sigma_0 \left(1 - \frac{D}{D_{\text{crit}}}\right)^\zeta \ln\left(1 - \frac{D}{D_{\text{crit}}}\right) \\ \text{sign}\left(\frac{d}{d\zeta} \Delta\sigma_{th,h}\right) &= \text{sign}(\ln(0 < x < 1)) = \text{negative} \end{aligned} \quad (7.17)$$

$$\begin{aligned} \frac{d}{dD_{\text{crit}}} \Delta\sigma_{th,h} &= \Delta\sigma_0 \zeta \frac{D}{D_{\text{crit}}^2} \left(1 - \frac{D}{D_{\text{crit}}}\right)^{\zeta-1} \\ \text{sign}\left(\frac{d}{dD_{\text{crit}}} \Delta\sigma_{th,h}\right) &= \text{positive} \end{aligned} \quad (7.18)$$

The equations above show that the relation between ζ and $\Delta\sigma_{th,h}$ is negative: a lower ζ yields a higher $\Delta\sigma_{th,h}$ and thus a longer fatigue life. The relation between the critical damage D_{crit} and $\Delta\sigma_{th,h}$ is as expected positive: a higher critical damage means a higher $\Delta\sigma_{th,h}$ and thus a longer fatigue life.

ζ is given as a function of α (geometry dependent constant) and m (slope of S-N curve). When using the **ENSC** and the related **GRFL** for this fatigue damage criterion, the geometry and slope should be already accounted for, and identical for all specimens. This also means that the extent to which the **ENSC** captures the geometry information as required for the **VA** fatigue life can be tested by this parameter. This hypothesis is confirmed if the ζ is approximately identical for all datasets.

To assess which of the parameters (D_{crit} or ζ) is governing, their first derivatives are divided and the fraction is analysed for different values of the developing damage D .

$$\begin{aligned} \frac{\frac{d}{d\zeta} \Delta\sigma_{th,h}}{\frac{d}{dD_{crit}} \Delta\sigma_{th,h}} &= \frac{\left(1 - \frac{D}{D_{crit}}\right)^\zeta \ln\left(1 - \frac{D}{D_{crit}}\right)}{\zeta \frac{D}{D_{crit}^2} \left(1 - \frac{D}{D_{crit}}\right)^{\zeta-1}} \\ &= \frac{D_{crit}^2}{\zeta D} \left(1 - \frac{D}{D_{crit}}\right) \ln\left(1 - \frac{D}{D_{crit}}\right) \\ &= \frac{D_{crit}}{\zeta} \left(\frac{D_{crit}}{D} - 1\right) \ln\left(1 - \frac{D}{D_{crit}}\right) = \mathcal{O} \frac{D_{crit}}{\zeta} \end{aligned} \quad (7.19)$$

For D approaching D_{crit} the critical damage is governing. The extent to which ζ is governing in the lower damage regions is dependent on the value of the fraction D_{crit}/ζ . The influence of ζ decreases when the damage D increases. The standard deviation of the critical damage, σ_D does not influence the magnitude of the fatigue life. It does however improve the quality of the fit (measured by the log-likelihood) with experimental data, and reflects the scatter that is included in the fatigue data.

To find the maximum likelihood of the model, an optimisation procedure is used.

7.4.4.1. Optimisation algorithm selection

Considering the roughness of the objective surface (which reduces if more **MC** samples are used), the optimisation algorithm should be a fit for non-differentiable functions. A suitable option is found in the Genetic Algorithm. This algorithm generates a population, of which the "fittest" members are used to reproduce. The use of an evolving population makes the algorithm robust, and also suitable for discontinuous functions. The robustness is obtained by the scatter of the first generation over the design space.

7.4.4.2. Numerical considerations

Due to the high amount of data that is processed in the model, the computational costs (time) are high. In total there are five main parameters that influence the computational costs:

- **Length of time trace = 500**

This parameter sets the amount of cycles to represent each loading history. If the time trace is too short the high loads with a relatively low probability of occurrence might not be accounted for in the analysis. This effect will be the same for all function evaluations, as the seed is programmed before the optimisation. Therefore: for the optimisation of the θ_{VA} parameters this is less important than for the calculation of the fatigue life of a given spectrum. The length of the time traces has a linear relation with the function evaluation time. After the overhead time this means that for double the length of each time trace the calculation takes the overhead³ time plus twice the direct time.

A sensitivity analysis of the length of the time trace is performed. For each time trace the mean and standard deviation of the stress range is computed. The criterion is expressed as the mean over ten time traces, of the mean divided by the maximum value of the $\{\mu, \sigma\}$. The variation is the difference between the current and previous result. Figure 7.27 shows the convergence results. Sufficient convergence is

³See the parallel with economical formulations: the costs are the overhead costs (typically fixed) + the direct costs.

defined at at maximum variation of 0.5% in the mean and 1.0% in the standard deviation. This first occurs at a time trace maximum of 500 cycles. The convergence limits are selected whilst taking into account the costs of an increase in the amount of cycles.

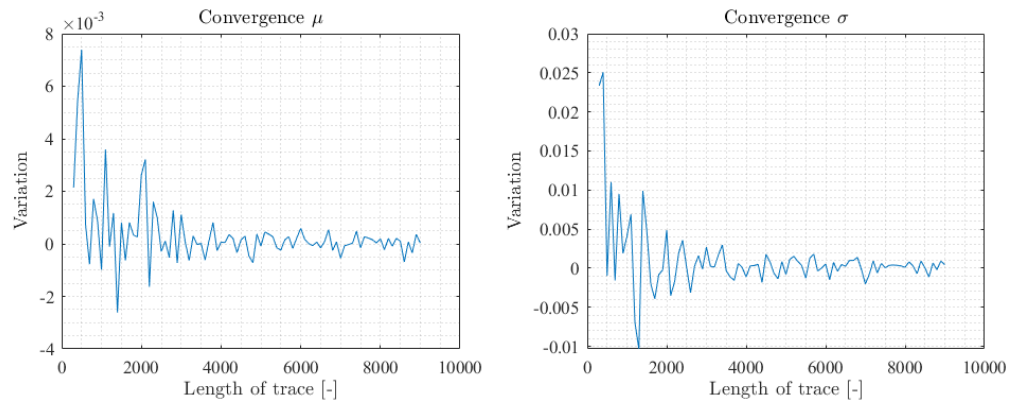


Figure 7.27: Convergence study on the length of the time trace.

- **Monte Carlo samples**

The amount of Monte Carlo samples influences the smoothness of the objective surface, and is of great importance for the optimisation algorithm. If the amount of samples is too low, the objective surface is rough and the algorithm might find local optima. Ideally the objective function is not dependent on the amount of Monte Carlo samples (convergence). The parameter has a linear relation (minus the overhead time) with the calculation time.

An infinite number of MC samples would provide a perfectly smooth objective function. Leonetti et al. calculated that for 10^5 MC samples the estimation of the likelihood function converges and the order of magnitude of the sampling error is one below that of the tolerance of the optimisation procedure [75]. This high resolution is indeed required when employing a gradient based optimisation algorithm. When using a swarm-based algorithm this is less sensitive.

It should be noted that a limited amount of MC samples does not pose an absolute error, but merely an uncertainty. Accounting for the available computational power, both the optimisation is and the final analysis of the fatigue lives at the most likely parameters are performed with 1000 MC samples. The effect of this is that the solution might not be fully converged to the second digit. However, the nature of the design space (see the next section) ensures that the attained optimum is in close proximity of the actual optimum.

For the optimisation of the θ_{VA} parameters a Genetic Algorithm is applied. MATLAB provides the function as `ga`, with parameters:

- **Population size = 50**

The MATLAB default is to set a population of 50 for a problem with up to five variables. This default is adopted.

- **Function tolerance = 1e-3**

The MATLAB default is 1e-6. However, the variation in the input parameters (see the convergence study in the previous part) is in the order of 1 percent. The function tolerance is selected on one order below the order of variation in the input distributions.

- **Maximum number of generations = 50**

The amount of generations is linked to the convergence of the solution. If the function tolerance is not met, the optimisation is aborted after 300 generations. The MATLAB default is to set the maximum number of generations to 100 times the number of variables. Considering the nature of the objective surface this is deemed to extensive: which is supported by observations of the convergence behaviour. The algorithm models 50 generations.

7.4.4.3. Design space exploration

The first step in the strategy is to determine the nature of the optimum. Both the mean of the D_{crit} and ζ are monotonic with the predicted fatigue life, as was calculated above respectively monotonic increasing and decreasing. However, they are not monotonic with the log-likelihood. This is a measure of the quality of the fit with all experimental data. For both parameters the objective function (log-likelihood) is convex: in a minimisation procedure this yields a concave objective space. Due to the counteracting effect of both parameters the objective surface is most likely shaped like an oval, with the major axis in the direction of the diagonal between both parameters.

7.4.4.4. Optimised NLDAM

The MLE's of the θ_{VA} parameters, as found with the genetic algorithm (ga) are presented in table 7.4. The resulting fatigue life and equivalent stress estimates are plotted in figures 7.28 to 7.29. It should be noted that the resulting figures are obtained for a run with a cycles length of 500 and an average over 3 cycles to calculate the damage. 1000 MC samples were used. This is done to assess the more accurate actual fatigue lives at the roughly obtained, most-likely sub-optimal, θ_{VA} parameters.

Table 7.4: Optimised parameters

Parameter	Value
μ_D	1.95
σ_D	0.39
ζ	8.13
\mathcal{L}	52.157

The AIC for this method yields:

$$\begin{aligned} \text{AIC} &= -2\log(\mathcal{L}) + 2n \\ &= -2 \cdot 52.157 + 2 \cdot 9 \approx -86.3 \end{aligned} \tag{7.20}$$

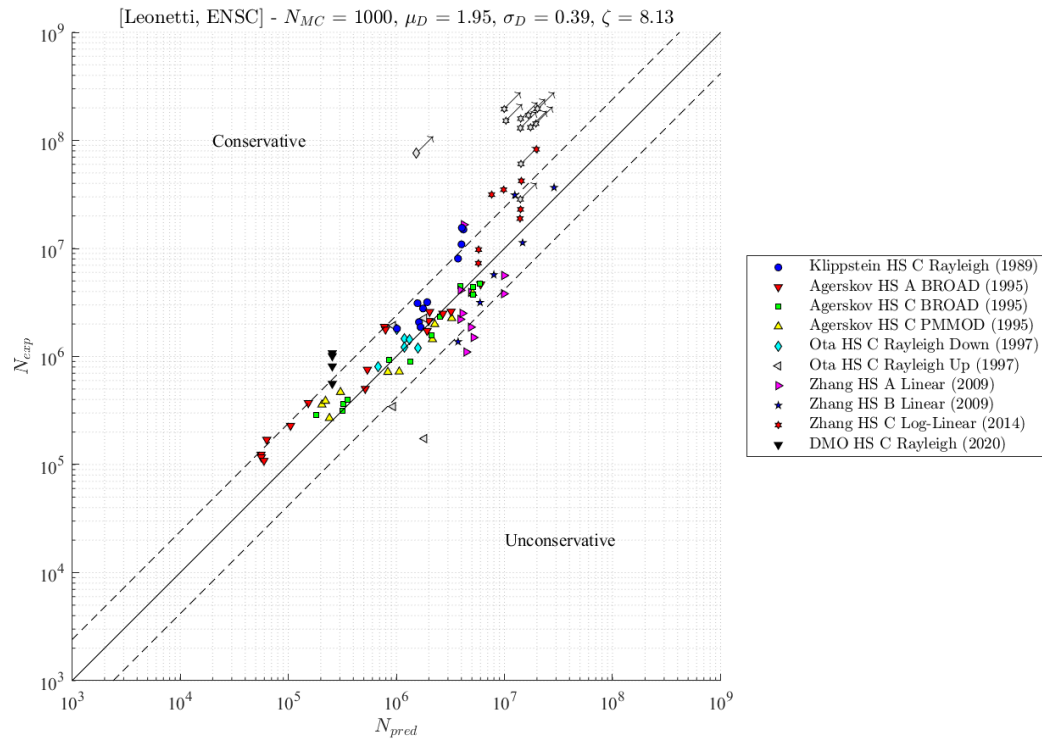


Figure 7.28: Comparison of the experimental and predicted fatigue life from the **NLDAM** in combination with the **ENSC**.

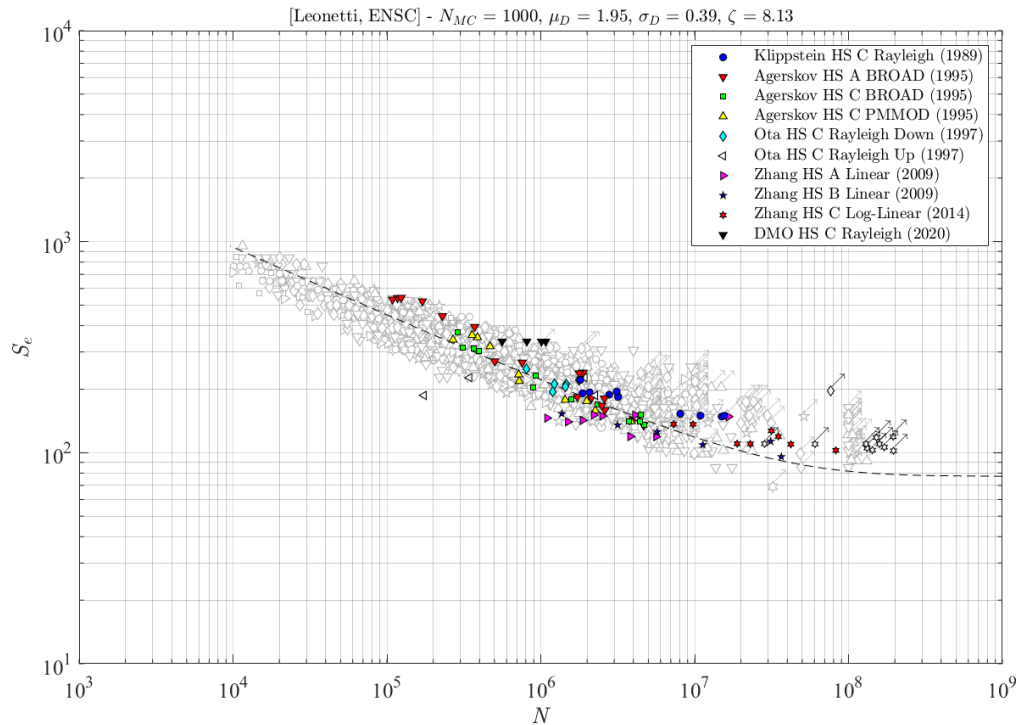


Figure 7.29: Comparison of the experimental and predicted fatigue life from the **NLDAM** in combination with the **ENSC**. For each of the tested specimens the equivalent stress is calculated and plotted on the ordinate.

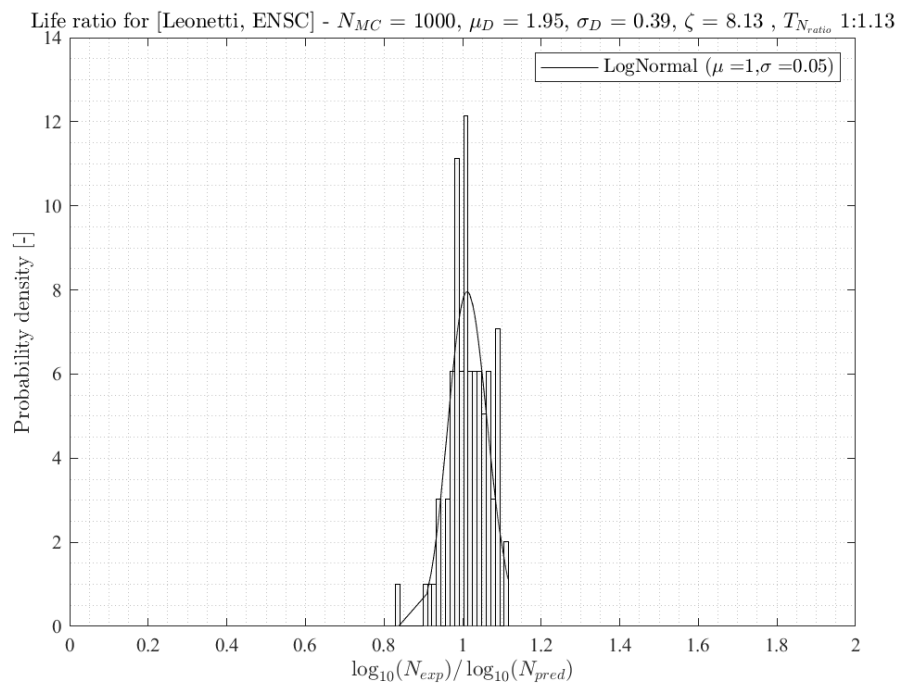


Figure 7.30: Scatter histogram of the \log_{10} of the experimental fatigue life over the calculated fatigue life for the NLDAM in combination with the ENSC.

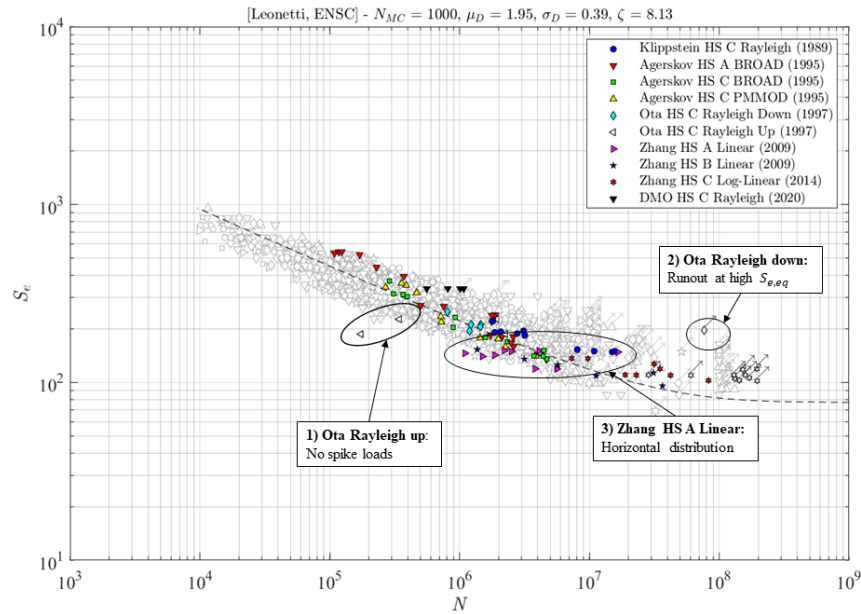


Figure 7.31: Indication of the results that fall outside of the expected scatterband or trend

Figure 7.31 indicates the fatigue test data which exceeds the expected scatterband, or otherwise raises questions. The following three outliers are discussed:

- 1) **Ota Rayleigh up** This indicates two specimens of which the fatigue life is over estimated. The two specimens of the Rayleigh-up sequence are not subject to a peak load ("spike loads" in [103]) of 441 MPa at the beginning of each cycle. This is in contrary to the two points of this dataset that are subject to a periodic peak load: these have a higher predicted fatigue life and fall well in the expected scatterband. The peak loads reduce the processing-induced residual stresses in the material which are tensile at the notch: the net stress level is thus reduced. This is reflected by the difference in observed fatigue lives: the specimens that did not receive overloads have lower fatigue lives. It can be assumed that for this loading history the process-induced residual stresses are not relieved, which is limiting the observed fatigue lives. *Ota et al.* did not use strictly random spectra, but applied a preset block loading to the specimens. That means that if the loading history as prescribed does not exceed the yield stress at any moment in time, the benefit of residual stress relieve is negligible. All other authors have used spectra with a tail in the high stress region, allowing a sparse high amplitude. This outlier is further discussed in section 7.4.4.6 and figure 7.37.
- 3) **Ota Rayleigh down** The specimen from *Ota et al.* that has a scatterband-exceeding experimental fatigue life is a censored datapoint. *Ota et al.* explain that for the respective load history only 6.2% of the blocks exceed the initial fatigue limit $\Delta\sigma_0$: it is expected that the experimental fatigue life of that specimen is high. This one out-lyer did not weigh strongly enough on the MLE of the θ_{VA} values to have a higher predicted fatigue life. Secondly, fatigue as a phenomenon is prone to scatter and uncertainty, a occasional run-out (i.e. censored datapoint) is within the line of expectation, and the CA scatterband.
- 3) **Zhang HS A Linear** The HS type A dataset from *Zhang and Maddox* has nearly the same predicted fatigue life for all load histories, when using the NLDAM. This dataset is plotted separately in figure 7.32, indicating the three different loading histories (A cycles down, B cycles around the mean stress and C cycles up). The observed trend of nearly identical predicted fatigue lives is predominantly observed in the specimens as loaded by the Type A loading history. Specifying even further, the datapoints are obtained for different spectra. *Zhang and Maddox* have varied the minimum stress range in the load history, and the labels in figure 7.32 indicate the respective minimum stress ranges. Table 7.5 presents the spectrum formulation.

The observed trend in figure 7.32 is that the datapoints with higher minimum stresses have lower experimental fatigue lives, whereas the predicted fatigue life is hardly a function of the spectrum type.

Table 7.5: Linear spectrum as applied by Zhang and Maddox

Relative stress range (p_i)	Stress range (MPa)	Cycles	Exceedance
1.00	210.0	1	1
0.90	189.0	3	4
0.80	168.0	6	10
0.70	147.0	12	21
0.60	126.0	23	44
0.50	105.0	48	92
0.40	84.0	109	202
0.30	63.0	296	498
0.25	52.5	544	1042
0.20	42.0	1125	2167
0.15	31.5	2815	4982
0.10	21.0	9500	14,482
0.06	12.6	43,981	58,463
0.04	8.4	148,438	206,901

This can be explained by two counter-acting phenomena:

- When using the [NLDAM](#), the specimens that are loaded predominantly by low stress range cycles (thus having a lower minimum stress) are more strongly affected by the ζ term. Their predicted fatigue life is reduced.
- The specimens that are loaded by higher stress ranges on average (thus having a higher minimum stress) are subject to higher loads, and thus have (even when considering the [LDAM](#)) lower predicted fatigue lives.

Combining the two phenomena yields approximately equal predicted fatigue lives. The effect of the lower predicted fatigue lives is dominant.

Besides the observed out-lyers, there are some other observations with regards to the results:

- The optimised ζ tends to 8, which means that the low stress cycles are rapidly of a large influence on the fatigue life prediction. To compensate for the resulting fatigue life reduction in all specimens, the mean of the critical damage is found to be ≈ 1.95 . This finding indicates that linear damage accumulation does not model the fatigue damage accumulation with sufficient accuracy to capture the fatigue phenomena. It should however be noted that the most likely parameter selection is highly influenced by the low stress range datapoints by [Ota et al.](#)

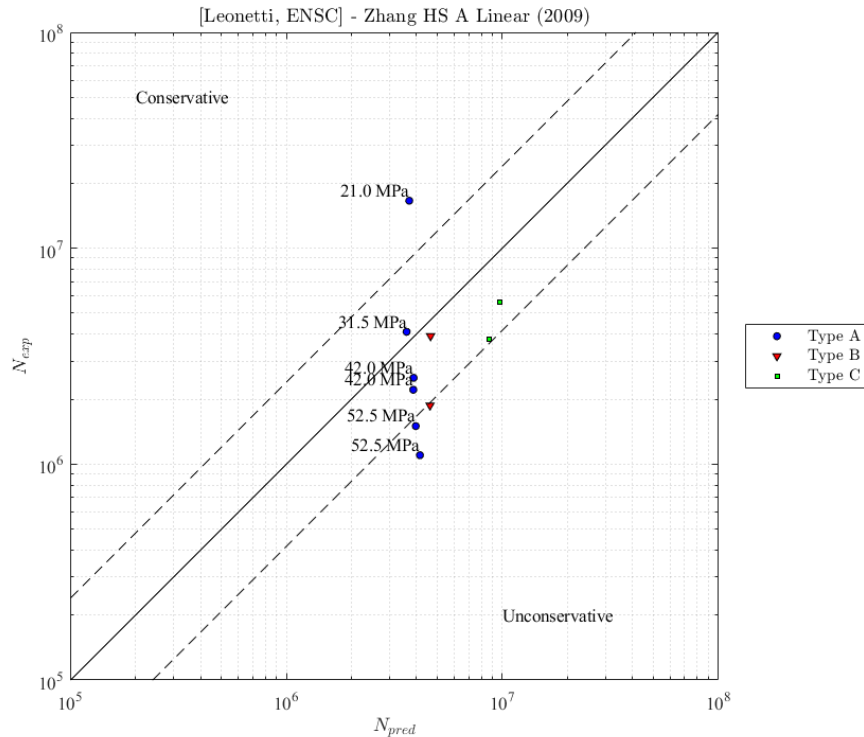


Figure 7.32: Assessing the variations in the predicted and experimental fatigue lives of the HS type A specimens as tested by Zhang and Maddox.

7.4.4.5. Analysis per dataset

Upon finding the MLE of the θ_{VA} parameters for all datasets combined, the data is post-processed to assess the quality of the θ_{VA} parameters and the resulting fatigue life predictions per dataset. Table 7.6 contains the scatter index for all sets separately. Every cell in the table contains four values: the {first, second} is for the HSSSC-LDAM {without, with} mean stress correction, the third is for the ENSC-LDAM and the fourth is for the ENSC-NLDAM.

Scatter With regards to table 7.6, the results from Ota et al. pose the largest scatter. This is in line with the observations and analyses from section 7.4.4.4. The spectra that are governed by medium stress range cycles (Rayleigh, BROAD64 and PMMOD64) provide good and limited scatter results. The linear and log-linear spectra, which are governed by the low stress range cycles reduce in scatter when including more local information. The improvement in scatter is limited when using the NLDAM instead of the LDAM.

Expected value of the ratio Table 7.7 presents the expected value of the LogNormal distribution that is fitted through the scatter histogram per dataset. It is observed that the datasets from Ota et al. deviate significantly. Besides the datasets from Ota et al. the Rayleigh, BROAD64, PMMOD64 and Linear spectra all provide an expected value near 1. The improvement of the NLDAM compared to the LDAM is not clearly visible in this table. That might be due to the results from Ota et al., that influence the MLE 's of θ_{VA} . The step from the HSSSC to the ENSC proves to reduce conservatism significantly.

Table 7.6: Fatigue life scatter index per dataset of the VA fatigue database. Yellow boxes indicate a scatter index between 1:1.10 and 1:1.20, orange is 1:1.20 and above.

Specimen	Rayleigh up	Rayleigh down	BROAD64	PMMOD64	Linear	Log-Linear
PP DS Cruciform [63]	1:1.06					
	1:1.06					
	1:1.06					
	1:1.07					
PP DS Long. attach [3]			1:1.09			
			1:1.09			
			1:1.11			
FP DS Cruciform [3]			1:1.10			
			1:1.06			
			1:1.06			
			1:1.05			
FP DS Cruciform [3]				1:1.09		
				1:1.09		
				1:1.08		
				1:1.08		
FP DS Butt joint [103]		1:1.43				
		1:1.32				
		1:1.26				
		1:1.26				
FP DS Butt joint [103]	1:1.32					
	1:1.30					
	1:1.31					
	1:1.30					
PP DS Long. attach [147] (A)					1:1.21	
					1:1.18	
					1:1.10	
PP DS Long. attach [147] (B)					1:1.10	
					1:1.20	
					1:1.19	
					1:1.16	
FP SS Butt joint [148]					1:1.16	
					1:1.28	
					1:1.27	
FP DS Cruciform (DMO)					1:1.16	
	1:1.05					
	1:1.05					
	1:1.05					

Table 7.7: Expected values of the fatigue life ratio for the VA fatigue database. Yellow boxes indicate a deviation of 5 to 10% from the ideal mean of 1.00, orange is 10% and above.

Specimen	Rayleigh up	Rayleigh down	BROAD64	PMMOD64	Linear	Log-Linear
PP DS Cruciform [63]	0.92					
	0.92					
	1.00					
	0.96					
PP DS Long. attach [3]			0.97			
			0.99			
			1.00			
			0.97			
FP DS Cruciform [3]			0.91			
			0.93			
			1.10			
			1.00			
FP DS Cruciform [3]				0.91		
				0.94		
				1.10		
				1.00		
FP DS Butt joint [103]		1.20				
		0.85				
		1.00				
		0.95				
FP DS Butt joint [103]	1.00					
	1.00					
	1.10					
	1.10					
PP DS Long. attach [147] (A)					1.10	
					1.10	
					1.10	
					1.00	
PP DS Long. attach [147] (B)					1.10	
					1.10	
					1.10	
					1.00	
FP SS Butt joint [148]						0.94
						0.91
						1.00
						0.92
FP DS Cruciform (DMO)	0.98					
	0.94					
	1.00					
	0.96					

7.4.4.6. Optimisation per dataset

Further analysis is done to assess the optimal θ_{VA} configuration per dataset. The results are listed in table 7.8.

Table 7.8: Optimal θ_{VA} configuration per dataset

Nr.	Dataset	μ_D	σ_D	ζ	n specimens
1	PP DS Cruciform Rayleigh [63]	3.43	0.22	7.18	10
2	PP DS Long. attach. BROAD64 [3]	4.43	0.07	6.07	16
3	FP DS Cruciform BROAD64 [3]	1.92	0.16	8.99	12
4	FP DS Cruciform PMMOD64 [3]	1.60	0.18	8.41	10
5	FP DS Butt joint Rayleigh down [103]	2.27	0.19	9.60	7
6	FP DS Butt joint Rayleigh up [103]	2.42	0.10	9.47	4
7	PP DS Long. attach. A Linear [147]	0.95	0.36	9.78	10
8	PP DS Long. attach. B Linear [147]	1.31	0.20	8.76	6
9	FP SS Butt joint Log-Linear [148]	2.91	0.11	7.75	18
10	FP DS Cruciform Rayleigh mod. DMO	4.97	0.05	0.19	4

The plots of the CA and VA scatterband and predicted versus experimental fatigue lives, considering the set-specific θ_{VA} configurations, are presented in appendix G. Almost all sets provide a good overlap between the CA and VA scatterbands, despite the limited amount of specimens in some datasets. Two sets (number 2 and 6) provide non-symmetrical results, and are presented and discussed in more detail here. Both sets tend to the unconservative side (the fatigue life is over-predicted, yielding an under-predicted equivalent stress level).

Dataset 10, the FP DS Cruciform joints subject to a modified Rayleigh spectrum, can not be used to judge the quality of the optimal values. This is because this datasets contains only four points, all tested at the same spectrum. Therefore, the only conclusion that can be drawn on the basis of this set is that it overlaps with the CA scatterband and VA scatterband of the other datasets (see figure 7.29).

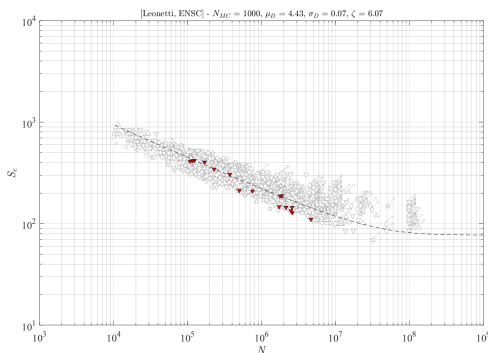


Figure 7.33: Comparison of CA and VA scatterband of the PP DS Longitudinal attachments, subject to the BROAD64 spectrum from Agerskov et al. (set 2)

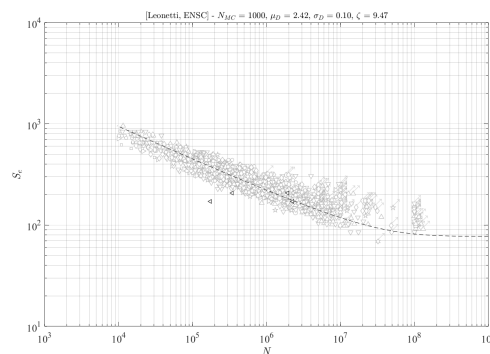


Figure 7.34: Comparison of CA and VA scatterband of the FP DS Butt joints, subject to the Rayleigh up load from Ota et al. (set 6)

Dataset 2

Figure 7.33, and corresponding figure 7.35 show that the fatigue life of the PP DS HS type A specimens from Agerskov et al. tend to the unconservative (i.e. overpredicted fatigue life) side. This is not an indication of a poorly converged solution, but of a dis-balance between the GRFL-curve and the CA specimens from the report [3]. Figure 6.14 shows that the CA specimens are on the higher side of the CA scatterband, indicating a better experimental fatigue strength than predicted by the generalised curve. To compensate for this difference the algorithm finds a relatively high value for μ_D . Besides that, this configuration aligns very well with the GRFL-curve in figure 7.33 in the higher strength region, this enables this configuration to pose the maximum likelihood.

Dataset 6

In part, the same reasoning holds for figure 7.34 and corresponding figure 7.36: the attained configuration of

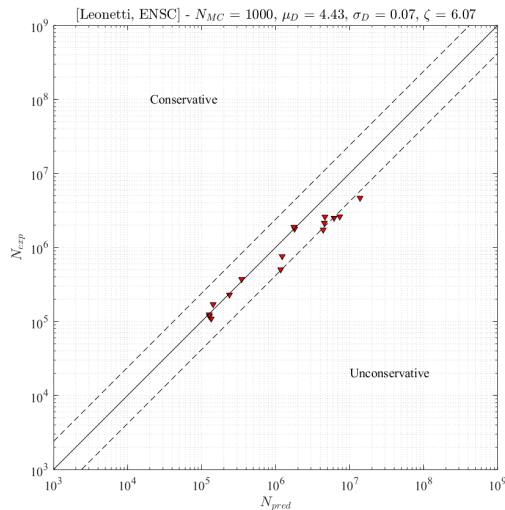


Figure 7.35: Comparison of predicted and experimental fatigue lives of the PP DS Longitudinal attachments, subject to the BROAD64 spectrum from Agerskov et al. (set 2)

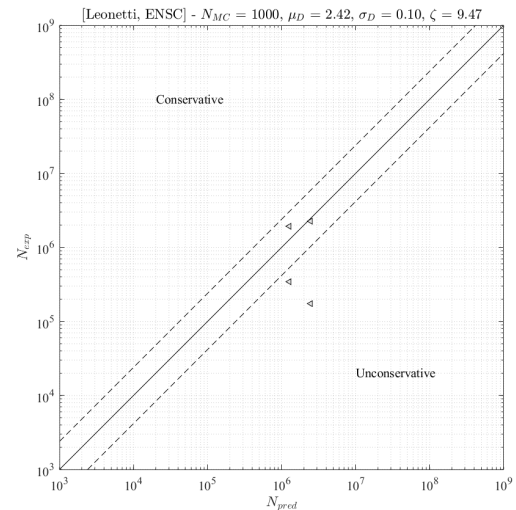


Figure 7.36: Comparison of predicted and experimental fatigue lives of the FP DS Butt joints, subject to the Rayleigh up load from Ota et al. (set 6)

θ_{VA} provides a good fit with the specimens that are subject to an occasional peak stress. This is because these two specimens are close together. It should be noted that the amount of specimens on which the inference is performed is limited to only four. Of these four, two are considered as outliers, see figure 7.37. The difference between the outliers and the two datapoints that overlap with the CA scatterband is that the latter are subject to a peak load of 441 MPa every $5e5$ cycles. Therefore, what these results show is the influence of the residual stress relief on the fatigue life. It is debatable whether the two specimens 01 and 02 are part of the research scope, as the subject of this work is "(random) variable amplitude loading". All other specimens are subject to a spectrum of which the bins are not predefined, allowing an occasional peak stress in the right-tail of the spectrum. The 01 and 02 specimens from figure 7.37 only exceed the initial fatigue limit in 6.2% of the cycles and have a maximum stress range to endure of respectively 296.8 and 255.4 MPa. The material as tested has a yield strength of 490 MPa. Assuming that the welding-induced residual stress levels are close to the yield strength, the maximum cycles will not significantly relieve the residual stress levels. This explains the lower experimental fatigue lives of these specimens. However, despite the outliers, it complies well with the other mid-high stress dominated spectra. This is a coincidence as the optimum is strongly affected by the two peak-stress loaded specimen.

A high peak load has a different effect on the experimental and predicted fatigue lives. For the fatigue life prediction it is assumed that the material has constant properties (that is, when not considering continuum damage mechanics). The effect of the peak loads will thus not affect the damage rate via the specimen properties in the manner that it does for the experiments. The effect of the peak loads is limited to the damage that is attributed to the one cycle with a high stress range.

Trends in optimum configurations

To distinguish trends in the optimum configurations per dataset, the datasets are combined in two groups: predominantly subject to 1) mid-to-high stress ranges [Rayleigh, Broad-band and the inverse Log-Linear spectra] and 2) low stress ranges [Linear and Pierson-Moskowitz]. Dataset 2 and 10 are excluded from this analysis because respectively the optimum is tarnished (see figure 7.33) and the dataset is only for 1 equivalent stress level and four datapoints. The weighted means of the optimal values are presented in table 7.9, and visualised in figure 7.38. This shows that there is a more distinct difference in the formulation of the distributed critical damage than in the ζ exponent.

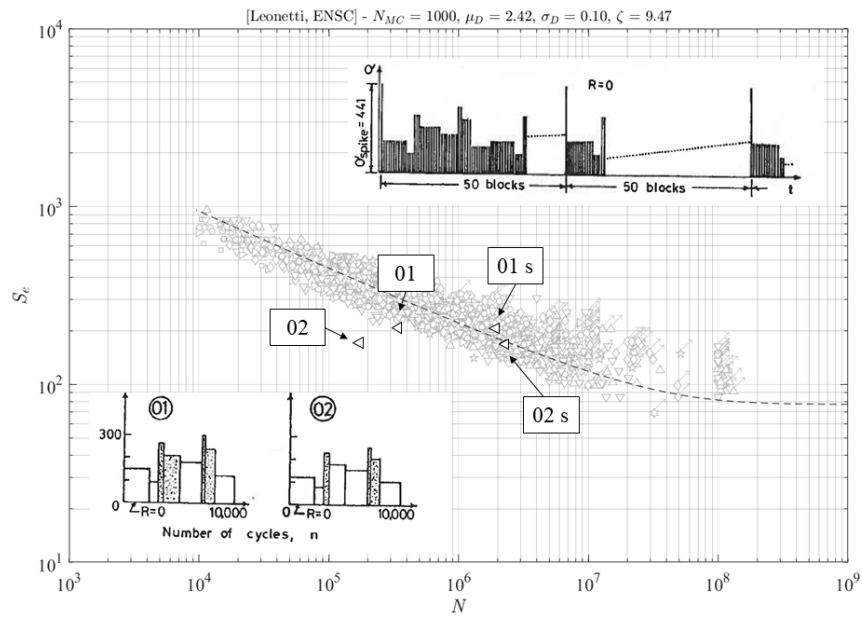


Figure 7.37: The datapoints that are labeled with an "s" are subject to a peak stress of 441 MPa every 50 blocks (= 5e5 cycles) as is indicated for the 01 sequence in the top-right corner of the figure. The bottom-left corner of the figure contains respectively the 01 and 02 sequence blocks.

Table 7.9: Weighted means of the three θ_{VA} parameters, separated by the dominant stress range level of the spectra. The labels 'Mid-High' and 'Low' indicate the interpretation of the stress range level of the majority of the cycles in the spectrum.

Datasets	μ_D	σ_D	ζ
Mid-High stress dominated: (1,3,5,6,9)	2.65	0.16	8.31
variation	+0.78, -0.74	+0.07, -0.06	+1.28, -1.14
Low stress dominated: (4,7,8)	1.28	0.26	9.02
variation	+0.32, -0.33	+0.11, -0.07	+0.76, -0.61

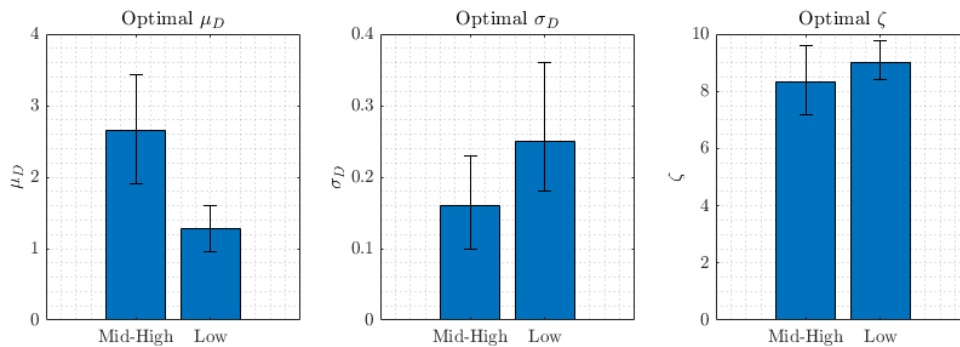


Figure 7.38: Bargraph containing the mean and error-bars of the optimal three θ_{VA} parameters, separated by the dominant stress range level of the spectra. The labels 'Mid-High' and 'Low' indicate the interpretation of the stress range level of the majority of the cycles in the spectrum.

The distinct difference in critical damage distributions is attributed to the nature of the spectra: as is observed in figure 7.25 (capturing the **ENSC** in combination with the **LDAM** with a critical damage value of 1), the fatigue life of the mid-to-high-spectra are typically under-predicted. For the low-stress range spectra the life is typically over-predicted by the **ENSC-LDAM** model. This is due to the limited extent to which the **LDAM** accounts for the influence of low stress cycles. It is assumed that the model is in general under-estimating the fatigue life, whereas this effect is counteracted by low stress range cycles. Due to the limitations of the **LDAM** the damaging effect of those cycles is underestimated, yielding an over-predicted fatigue life for specimens that are predominantly subject to low stress cycles. The **NLDAM** uses statistical inference to determine the critical damage. This means that the respective over- and underprediction of the fatigue life will be corrected for, per dataset. This trend is indeed observed: yielding the higher critical damage for the previously under-estimated fatigue lives of specimens subject to mid-to-high-stress spectra than for the low stress range spectra.

For all spectra the ζ exponent is strongly deviating from the value of zero, as used in the **LDAM** (see figure 4.13). This indicates that the fatigue limit has a limited validity when applying a **VA** load, for these specimens. The difference between the exponent ζ for both spectrum types (mid-high and low) is not very clear, but is typically higher for spectra that are dominated by low stress ranges. This indicates that the influence of lower stress cycles is higher for the low-stress dominated spectra, which is in line with expectations. It should be noted that this weighted mean is only for illustration purposes, to find truly generic values, the datasets should be combined as listed in table 7.9 and collectively optimised.

7.5. Model interpretation

The **NLDAM** optimisation has, in the plot where the experimental and predicted fatigue lives are compared, two degrees of freedom: linear translation and rotation. The translation is obtained from the critical damage distribution and the rotation from the ζ exponent. The ζ exponent has the highest influence on the specimens subject to lower stress-ranges, hence the translation in the diagram. All optimisation results show that, in relation to the **LDAM** ($\mu_D = \ln(1) = 0, \sigma_D = 0, \zeta = 0$), all three parameters are increased. The **LDAM** configuration yields an expected damage of 1, whereas the combined optimisation (table 7.4) has an expected value of 2.10. A comparison between figure and 7.28 shows that this has a beneficial influence on the fatigue lives of the highly-loaded specimens in the **MCF** range: these specimens shift to the right in the diagram, closer to the diagonal. On the other hand, from approximately $S_{e,eq} = 150$ and below (i.e. $N = 4e6$ and up), the fatigue life is reduced instead of increased. This is the effect that the ζ exponent has on these **HCF** range specimens.

PHYSICAL INTERPRETATION

The physical interpretation of the model parameters in the **NLDAM** yields:

D_{crit} The critical damage value is expressed as a LogNormal distribution (= $\text{LogNormal}(\mu_D, \sigma_D)$). This captures the stochastic nature of the fatigue life, which is in part due to the phenomenological fatigue life scatter, and enables a probabilistic instead of deterministic calculation of the fatigue life.

ζ The exponent ζ originates from the fracture mechanics formulation of the stress intensity factor, which is used to derive the relation between the initial and current fatigue limit $\Delta\sigma_0$ and $\Delta\sigma_{th}$. It captures the non-linear nature of the fatigue crack growth rate da/dn , as is given in the Forman-Mettu relation. The use of this exponent assumes a valid crack-growth analogy for the total fatigue life and hereby neglects the crack initiation phase.

The observation that the parameters of the **LDAM** and optimised for the **NLDAM**, see table 7.10, strongly diverge indicates that the **LDAM** is not a good fit for all considered datasets. The high value of ζ indicates that the fatigue limit is of limited value when considering a **VA** load, for these specimens.

To assess the quality of the optimal values, and their physical meaning, a detailed analysis is performed on the results from **Leonetti et al.** and from the previous section for the dataset by **Klippstein and Schilling**. That is, a comparison is made between the optimum θ_{VA} for two analyses:

1. The 38-specimen based **GRFL** for the **NSC** as inferred by **Leonetti et al.**, translated to **ENSC**-level by means of the **SCF**'s.
2. The 1806-specimen based **GRFL** for the **ENSC** as originally inferred by **Qin et al.** (the values here are divergent from the solution in [112] as the stress range in contrary to amplitude is used).

Table 7.10: Comparing the expected damage value for the LDAM and of the optimised θ_{VA} set for the NLDAM

Parameter	LDAM	Optimised with the NLDAM
μ_D	1	1.95
$\ln(\mu_D)$	0	0.67
σ_D	0	0.39
$E[D] = \exp(\ln(\mu_D) + \sigma_D^2/2)$	1	2.10

To enable a comparison between the optimal θ_{VA} according to Leonetti et al. and the more generalised analysis in this chapter, the ENSC GRFL is adopted for the generalised analysis. This generalised curve is based on 1806 datapoints, whereas the analysis by Leonetti et al. is based on 38 points. The NSC-equivalent GRFL-curve is obtained by dividing the ENSC-based curve by the SCF ($K_s \cdot K_e$). It should be noted that this is not the typical manner to assess the NSC fatigue life. However, because this analysis is based on the mean curves and the ENSC is generalised, this evaluation is valid and sound. Table 7.11 provides the optimal configuration of θ_{VA} according to both analyses. A first glance shows a significant difference in all three parameters. Table 7.12 contains the considered GRFL parameters.

Table 7.11: NSC and ENSC results for the cruciform samples from [63]

Parameter	NSC [75] (2020)	ENSC (2021)
μ_D	1.61	3.43
σ_D	0.23	0.22
ζ	1.14	7.18
\mathcal{L}	6.96	8.09

The NSC results from Leonetti et al. are based on the CA GRFL-curve, fitted to 29 failures and 9 run-outs as reported by Klippstein and Schilling. Figure 7.29 shows, however, that the estimated fatigue life from the generic model (fitted to the 1806 datapoints from [112]) is conservative for this dataset. This is related to the CA GRFL-curve differences. Figure 7.39 presents the NSC curves for the 38 points from Klippstein and Schilling, as well as the NSC equivalent of the mean curve of the ENSC assessment of 1806 CA fatigue tests as done by Qin et al.. It should be noted that it is not in line with expectations that the NSC analysis is less conservative than the ENSC analysis: this is in this case attributed to the (non)-generic nature of the datapoints on which the GRFL-curve is inferred.

Table 7.12: Comparing the optimal six parameters of the GRFL based on stress ranges for both the 38 CA specimens from Klippstein and Schilling as used by Leonetti et al. and for the 1806 specimens as collected by Qin et al..

Param. Leonetti	Param. Qin	NSC, $n = 38$ [63, 75]	ENSC, $n = 1806$ [112]
β_0	$\log C$	14.8	12.99
β_1	$-m$	-3.99	-3.03
σ	σ	7.33e-2	0.19
μ_v	$S_\infty(\mu)$	2.10	1.89
σ_v	$S_\infty(\sigma)$	3.83e-2	0.35
p	ρ_{S_∞}	0.44	0.65

Table 7.13 provides the numerical analysis of figure 7.39.

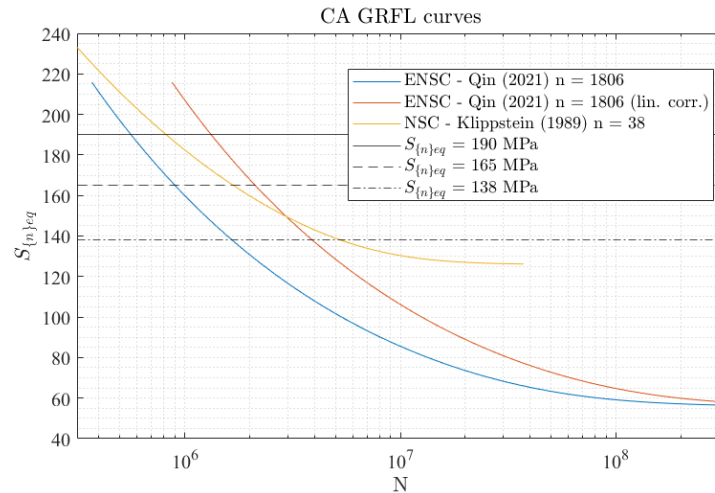


Figure 7.39: The **ENSC** is multiplied with $(1/1.39)$ ($= 1/(K_s \cdot K_\rho)$) to represent the **NSC** level. The horizontal lines indicate the three equivalent stress levels at which the specimens are tested, according to the inference on the 38 **CA** specimens. The figure shows the conservative nature of the estimate with the generalised **ENSC** curve for these specimens.

Table 7.13: Comparing the **NSC**- and **ENSC**-based fatigue life predictions. The values of N_{pred} correspond to the intersections of the horizontal lines and S-N curves in figure 7.39. The ratio is equal to $N_{pred}(\text{NSC})/N_{pred}(\text{ENSC})$. The expected value of the critical damage is equal to 1.57 (the expected value of the critical damage in the **NSC** assessment according to Leonetti et al.) times the ratio.

$S_{(n)eq}$	n specimens	$N_{pred}(\text{NSC})$	$N_{pred}(\text{ENSC})$	Ratio	$E[D_{crit}]$
209	1	8.20e5	5.63e5	1.46	2.29
176	5	1.67e6	9.01e5	1.86	2.92
133	4	5.31e6	1.66e6	3.20	5.03

The weighted average of expected value of the critical damage, for the corrected optimal configuration of the **NSC**-based analysis, yields 3.31. The expected value of the optimal configuration of the generalised **ENSC**-based analysis (right column in table 7.11) yields 3.51. This allows to conclude that the shift in the mean of the critical damage can, at least to a significant extent, be attributed to the difference in conservatism in the parameters that are used to infer the **GRFL** curves. However, the effect of the fatigue life reduction due to a higher ζ exponent is not yet accounted for in this comparison. The expected value of the critical damage is given as:

$$E[D_{crit}] = \exp(\mu_D + \sigma_D^2/2) \quad (7.21)$$

With regards to the increase in the ζ parameter, see table 7.11, this is both attributed to the difference in fatigue limit level and the correction for the linear increase in critical damage. An increased ζ value yields a lower equivalent fatigue limit, and thus a reduced fatigue life for specimens that are subject to cycles below the (initial) fatigue limit. In turn, a reduced predicted fatigue life corresponds to a higher equivalent stress level.

- **Difference in fatigue limit** For the **GRFL** parameters based on the 38 samples from Klippstein and Schilling 38.5% of the cycles are below the initial fatigue limit of 125.9 MPa. For the **ENSC** equivalent formulation based on the 1806 specimens as combined by Qin et al., only 8.86% is below the initial fatigue limit of 55.8 MPa. This means that the formulation based on the 38 samples is more sensitive to the ζ parameter: a smaller increase yields the same fatigue life reduction. To correct for that the **ENSC**-bases assessment has to significantly increase the ζ to reduce the fatigue lives in the lower stress region: this in part explains the increase from $\zeta = 1.14$ to 7.18.
- **Linear correction for log-linear relation** An increase in the expected value of the critical damage yields a linear increase of the predicted fatigue lives of all specimens. However, the algorithm maximises the likelihood on the basis of the log of the fatigue life. That means that a linear increase in the fatigue life has to rate a larger influence on the log-life of the specimens subject to a lower equivalent stress

level. These specimens are also more sensitive to the ζ parameter, as for a lower equivalent stress level a larger part of the cycles is below the initial fatigue limit. To correct for this effect the algorithm finds a higher value for ζ .

To link the above statements to figure 7.39, an increased ζ parameter tilts the corrected **ENSC** curve (red) counter-clockwise: yielding an improved fit with the **NSC** curve (yellow). This explains the increase in the ζ parameter when using the generalised **ENSC** curve (corrected to **NSC** level) instead of the **NSC** curve based on 38 datapoints.

The last parameter that is different in both analyses is the standard deviation of the critical damage, σ_D . This parameter has reduced when using the generalised **ENSC** formulation. This parameter connects the formulation of the LogNormal mean and standard deviation with the expected value of the critical damage as presented in equation (7.21). This means that the parameter is only driven by the shape of the LogNormal distribution: considering the fact that all parameters are fitted on the log-scale, the increase in the parameter μ_D is accompanied by a decrease in the standard deviation σ_D . This is because the log-scale provides to a larger extent the logarithmic nature of the formulation, which reduces the optimal standard deviation of the Log-Normal critical damage in this domain.

To conclude, the differences between the two optima are predominantly attributed to differences in the **GRFL** formulation and the datasets that are used for the inference.

7.6. Concluding remarks

In this section the three model variations on the fatigue life prediction with the **HSSSC** and **LDAM** are considered. Table 7.14 presents the summary of the results per model. It is observed that the inclusion of the cycle-by-cycle mean stress correction reduces the scatter index, but only slightly increases the (log-)likelihood. A significant improvement is found when using the **ENSC** in combination with the **LDAM**: both the scatter index and the (log-)likelihood improve. The (log-)likelihood increases by 66%. It is observed that the fit improves even further when using the **ENSC** in combination with the **NLDAM**. The (log-)likelihood increases by 37%. These before-mentioned results are for a generalisation of all datapoints. When maximising the likelihood per dataset it is observed that different configurations of the θ_{VA} are optimal for low and mid-to-high stress dominated spectra. This finding is attributed to the fracture-mechanics nature of the damage accumulation model. A fracture-mechanics model assumes that the crack initiation phase is already consumed by the surface roughness as a result of the welding process. However, for specimens that are predominantly subject to low stress range cycles the crack initiation phase can not be neglected. This means that, when separating the low and mid-to-high stress range dominated spectra, the improved parameters in table 7.14 will be even better for the **ENSC-NLDAM** combination.

Table 7.14: Summarising research results. n is the number of parameters as used by the model.

Model	$\sum \log(\hat{\mathcal{L}})$	n	AIC	Scatter index
HSSSC-LDAM	22.2	0	-44.5	1:1.28
HSSSC-LDAM (mean stress corrected)	22.5	0	-45.0	1:1.22
ENSC-LDAM	37.3	6	-62.6	1:1.16
ENSC-NLDAM (optimised)	52.2	9	-86.3	1:1.13

III

Judgement and future work

8

Evaluation

The conclusions are drawn, based on the answer to the sub-questions that were posed in section 2.4. After this, the hypothesis are revisited and either rejected or accepted. The answers to the sub-questions and the research question are:

1) What is the validity of the S-N curves generated with the samples that are used in Commercial Fatigue codes for the naval-specific detail?

This question is answered in section 6.3. By comparing the tested fatigue results, as analysed with the NSC and HSSSC, as described by DNV-GL [27], to the class S-N curves the answer to this question is that no significant deviation is observed. However, due to a limited domain of the not-preloaded specimens (the preloaded specimens are not used to draw conclusions as the resulting reduction of the residual stresses was unknown for these specimens), the conclusion is that the considered dataset does not indicate a significant deviation in fatigue resistance compared to the class S-N curves.

2) Which fatigue damage criterion from literature provides the most suitable balance between accuracy and cost?

This question is answered in chapter 3. The Effective Notch Stress Concept (ENSC) is selected as it is on a scale of increasing complexity and effort the first fatigue damage criterion that uses only one S-N curve for all details and has a scatter index only 3.5% below that of the Total Stress Concept (TSC) (more complexity and effort required, also one S-N curve). Also, as the ENSC allows the analytical stress-averaging approach, the calculation is significantly less expensive than for the HSSSC, which requires an FE model.

3) What is the validity of the LDAM for random VA loads when using the HSSSC?

This is answered in section 7.4.1. It quantifies the answer by dividing the \log_{10} of the experimental and calculated fatigue lives, and assessing the scatter in this ratio. The scatter index (90% over 10% bound) for this base-case is 1:1.28 with a LogLikelihood of 22.2 (AIC = -45.0) and the histogram of the ratio's shows two peaks: one corresponding to the specimens of which the fatigue life estimate is conservative (typically the HS type C specimens) and one corresponding to the specimens of which the fatigue life estimate is unconservative (typically the HS type A and B specimens). This difference in fit is attributed to the limited extend to which the HSSSC accounts for the local nature of the HS type A and B stress concentrations.

4) What is the validity of the LDAM for random VA loads when incorporating more local information into the fatigue assessment (ENSC)?

This is answered in section 7.4.3. As was done to answer subquestion 3, the ratio of the \log_{10} of the experimental and calculated fatigue life is used to quantify the outcome. The scatter index is reduced to 1:1.16 with a LogLikelihood of 37.3 (AIC = -62.6). The ratio histogram shows one peak around a ratio of 1, compared to the two peaks for the HSSSC case. This confirms the expected effect of the ENSC, which accounts for the local

effects of each hotspot, and hereby reduced the difference between HS type A, B and C fatigue life estimates. The scatter that is left is attributed to the fullness of the spectrum, and the amount of low stress range cycles in the sequence. Low stress range cycles below the fatigue limit do not add to the accumulated damage, according to the LDAM by Palmgren and Miner.

5) What are feasible alternatives for the LDAM?

This question is answered in chapter 4. Of the 30 studied models the Double Linear Damage Theory (DLDT) by Manson and Halford [87] and the Non-linear Damage Accumulation Model (NLDAM) by Leonetti et al. [75] are selected based on a consideration of the required non-linear nature and proven validity for stochastic VA load histories.

6) If possible, how can the selected alternatives from Q5 be improved?

This question is answered in chapter 5, and more specifically in section 5.3. The quality of the two selected alternatives for the LDAM are both a function of the implicit conservatism of the fatigue damage criterion and respective fatigue resistance curve. By including more local information in the fatigue damage criterion (i.e. use the ENSC instead of the HSSSC), accounting for the local (idealised) geometry of the welded detail, the implicit scatter is reduced (see [111]). By reducing the scatter, the 97.7% probability of survival and 75% confidence curve (P97.7C75) is closer to the mean: hence less conservative.

Secondly, both the Double Linear Damage Theory (DLDT) by Manson and Halford [87] and the Non-linear Damage Accumulation Model (NLDAM) by Leonetti et al. [75] use fitted parameters to define the fatigue damage accumulation behaviour. The DLDT typically uses fixed values for the y_1 and y_2 parameters: a MLE of these parameters based on the compiled VA database will provide the assessment of the quality of these typical parameters. This provides an improvement with respect to the implementations of the DLDT as are known in literature [57, 87].

7) What combination of State-of-the-Art Fatigue damage criteria and damage accumulation models has the largest potential?

The model by Manson and Halford poses a bi-linear damage accumulation model, whereas the one by Leonetti et al. is fully non-linear. Secondly, the model by Leonetti et al. is the only reported model that accounts for the stochastic nature of both the CA fatigue limit and the VA critical damage.

8) What is the improvement of the novel selected combination from Q7 compared to the use of the HSSSC with the LDAM?

This question is answered in section 7.4.4. The ratio of the \log_{10} of the experimental and calculated fatigue life is used to quantify the outcome. The scatter index is reduced to 1:1.13, compared to 1:1.28 for the HSSSC with the LDAM. The Log-Likelihood is increased from 22.2 to 52.2, with a related AIC of -44.5 to -86.3. Both conclude to significant improvements.

9) What is the effect of the spectrum type on the validity of the fatigue life prediction, using the novel selected combination from Q7?

This question is answered in section 7.4.4.4. The use of the NLDAM, compared to the LDAM does reduce the differences between the quality of the fatigue life predictions for specimens subject to different spectra. However, the optimisation of each dataset separately, and the analysis of the optimal configurations of θ_{VA} shows a difference in configuration for broad spectra (mid-to-high stress dominated) and slim spectra (low stress dominated). This difference is attributed to the assumptions in the NLDAM. The NLDAM is a damage accumulation model in the fracture mechanics domain. It is therefore not able to capture the crack initiation sufficiently, which is reflected by the deviating results for low stress range spectra. For these spectra it is observed that the optimal configuration tends to the LDAM with an S-N curve that does not have a fatigue limit.

With the exception of the two block-loaded specimens from Ota et al., which are attributed to the absence of

residual stress relief, all VA datapoints overlap with the CA scatterband.

10) What is the effect of the mean stress on the validity of the fatigue life prediction, using the novel selected combination from Q7?

As was shown in the comparison between the HSSSC-LDAM assessment with and without the cycle-by-cycle mean stress correction (figures 7.19 and 7.22), the difference between datasets with high and low (mean) r_{lr} levels is negligible upon implementing the Walker mean stress correction. The implementation of the ENSC and NLDAM does not influence the nature of the mean stress correction. The conclusion is thus that the mean stress effect is accounted for in the proposed fatigue life prediction procedure.

The limitation of this conclusion is posed by two significant out-lyers: specimens tested at load histories that cycle down from a stress level close to the yield, and specimens tested at load histories that do not exceed the initial fatigue limit. The first out-lyer is attributed to the effect of residual stress relief at high stress levels, whereas the second has no residual stress relief in the fatigue life at all (in contrary to specimens tested for random spectrum loads with occasional high stress range cycles that relieve the residual stresses to some extent). The experimental fatigue lives of the first case are higher than predicted, whereas for the second case they are lower than predicted.

8.1. Conclusions

The conclusions of this research are formulated with respect to the research question and the hypotheses from section 5.2.

RESEARCH QUESTION

How can State-of-the-Art fatigue damage criteria and fatigue damage accumulation models be applied, combined, and updated, to provide a balance between accuracy and complexity whilst reducing the uncertainty of the fatigue assessment methods as currently presented in design codes?

A combination of the research efforts in the domain of fatigue damage criteria and damage accumulation models provides a significant reduction of the scatter in the fatigue life. Scatter is translated to conservatism by the use of the lower prediction (95% / 97.7%) bound as a design curve. The State-of-the-Art ENSC is combined with the NLDAM for the best result. The findings are summarised and linked to the four hypotheses:

- There is no reason to assume that the welded details as produced by order of DMO have a quality that deviates significantly from those in scientific literature.
- The experimental fatigue life of the specimens as tested by DMO is better than what is estimated by the HSSSC as prescribed by DNV-GL. This is not attributed to the weld quality, but to two other sources:
 - The DNV-GL D curve [27] is used for all structural details: LC and NLC. IIW [54] on the other hand recommends a FAT100 for NLC details and a FAT90 for LC details. The benefit of the NLC detail as tested by DMO is thus not used when only considering the DNV-GL D curve.
 - The assessment method by DNV-GL does not account for differences (and potential benefits) in the loading and response ratio r_{lr} . To pose a conservative fatigue life estimate the D curve is proposed at a r_{lr} level of 0.5. If the cycle is partially compressive the fatigue life is typically improved, which poses an unused benefit: the DMO specimens were tested at r_{lr} levels of 0.1 and 0.3. The Walker mean stress correction is proposed to account for the difference in loading and response ratio.

Considering that the mean of the LogNormal distribution in figure 7.20 and 7.23 is both 1, at a critical damage of 1, a critical damage or 0.75 provides a conservative analysis. This finding confirms part of the first hypothesis: **Accepted: "H1. The current approach of DMO, to use the HSSSC in combination with the LDAM with $D_{crit} = 0.75$, provides a conservative fatigue life prediction."** The use of $D_{crit} = 0.75$ instead of 1 adds to the conservatism, as is confirmed by the distribution of the fatigue ratio scatter, which has a mean of 1 for both a Normal and a LogNormal distribution when using $D_{crit} = 1$. Depending on the HS type, however, the estimate is conservative or unconservative. On average, the fatigue life with $D_{crit} = 1$ is suitable and any reduction¹ would incorporate conservatism.

¹With the exception of reductions related to external factors like slamming.

- In combination with the LDAM the ENSC provides a less scattered fatigue life estimate, on which the influence of the HS type is negligible. When using the P97.7C75 bound, the fatigue life estimate will be less conservative than for the HSSSC. This is reflected by the reduction of the scatter index from 1:1.28 to 1:1.16 and is in line with the research findings in [23].
As the estimation of the fatigue life for both models is a function of the mean S-N curve parameters and the respective scatter, this finding confirms the second hypothesis: **Accepted: "H2: The model as postulated by Leonetti et al. and the LDAM improve when incorporating more local information in the fatigue damage criterion."**
- The use of the NLDAM by Leonetti et al. poses an improved fatigue life estimate compared to both the ENSC and HSSSC in combination with the LDAM. This allows the acceptance of the last two hypotheses: **Accepted: "H3: The model by Leonetti et al. in combination with the ENSC provides a better prediction of the fatigue life than the model by Miner, Palmgren in combination with the ENSC."** and **Accepted: "H4: The model by Leonetti et al. in combination with the ENSC provides a better prediction of the fatigue life than the model by Miner, Palmgren in combination with the HSSSC."**

The goal of this thesis (see the box below) is therefore considered to be met.

GOAL

1) To deliver recommendation for the fatigue assessment method, fit for naval applications, based on State-of-the-Art fatigue work on VA damage accumulation and fatigue damage criteria, to reduce the conservatism of the fatigue assessment.

and

2) To validate the recommended method against experimental data and to compare the novel model to the current assessment method.

The research was to be called successful if the implementation of a State-of-the-Art fatigue assessment method (for which either the fatigue assessment concept, a damage accumulation model, or both is/are used) has proven to provide a less conservative and at least equally accurate estimate of the fatigue life, compared to the current practise. The scatter has reduced from a scatter index of the fatigue life from 1:1.28 to 1:1.13 - providing a more accurate, and less conservative 97.7 or 95% lower prediction bound. The accuracy has improved from a LogLikelihood of 22.2 to 52.2. This LogLikelihood increase supports the claim of reduced scatter. The research is concluded to be successful.

8.2. Discussion

The research results as are presented in chapter 7 provide a promising analysis of the ENSC as a method to reduce the scatter due to different hot spot types, and the NLDAM as a mean to reduce the scatter due to different spectrum shapes.

To reflect on the results, the conclusions are compared to the research results of others. Revisiting the findings from section 4.2.2, Gurney [46] shows that narrow banded loads consistently provide longer fatigue lives, compared to broad banded load spectra. This means that an inferred value of the critical damage can be lower. Secondly, Ibsø and Agerskov [56] proposed a relation between the irregularity factor and the critical damage ($D_{crit} = 2I - 1$). This irregularity factor (number of positive zero crossings divided over the amount of cycles) is reported to be {0.745, 0.817, 0.987} for {broad banded, Pierson-Moskowitz, narrow banded} spectra; indicating a trend of a higher irregularity factor I for low-stress dominated spectra. This higher I yields a higher experimental D_{crit} , substantiating again that an inferred value of the critical damage can be lower. Both statements [46, 56] are in line with the results from section 7.4.4.6, where the low-stress dominated spectra have lower inferred critical damage values than the mid-to-high-stress dominated spectra. The nature of the NLDAM allows to reduce, but not remove, the differences between spectrum types by means of the ζ value. This is linked to the nature of the derivation that lies at the basis of the NLDAM. This derivation assumes that a fracture mechanics approach is valid for the fatigue life prediction. However, for spectra that are governed by low-amplitude stresses the crack initiation is more scattered. Schijve explains this as: *"Although surface damage can accelerate crack initiation, the high stress amplitude cycles can also generate crack nuclei early in the fatigue life, and the assistance of surface damage is less important for the initiation process. However, if the design life is large in numbers of cycles, the significance of adverse surface effects should be recognised. The high sensitivity for surface effects at low stress amplitudes and the relatively low sensitivity*

for surface effects at high stress amplitudes can lead to more scatter of the fatigue life at low amplitudes and less scatter at high amplitudes." [121]. This citation explains that for low-stress amplitudes spectra the crack initiation is more dominant than high-stress amplitude spectra: making the derivation of [Hirt and Kunz](#) and [Leonetti et al.](#) less valid for the low-stress range governed spectra.

The minimum (phenomenological) amount of scatter in the fatigue data can be attributed to differences in weld quality (e.g. undercuts, incomplete penetration, etc.), failure criteria (what crack length is deemed long enough to terminate the experiment) and process-induced residual stress levels. When considering the [ENSC](#) in combination with the [NLDAM](#) there is also some scatter related to the spectrum type: within the [CA](#) scatterband, the [VA](#) data of the spectra that are dominated by low stress range cycles are on the non-conservative side, whereas the wide spectra that are dominated by mid- to high- stress range cycles are on the conservative side. The observed scatter reduction from 1:1.16 to 1:1.13 proves that the use of the [NLDAM](#) does improve the data fit, but is not sufficient to remove all spectrum-induced scatter.

The analysis of the "out-lyers" as presented in figure 7.31 showed that the specimens that are subject to a load that is cycling up from a stress level of zero, without occasional peak stresses, exceed the [CA](#) scatterband. This is attributed to the -absence of- relief of the process-induced residual stresses. Unfortunately these stresses are not always reported in literature, and hard to quantify in practise. In a laboratory the use of strain-gauges during the production of the specimens allows to quantify the residual stresses at the notch, but this is too expensive and not practical to apply to all (types of) welds in a frigate.

The research question contains the line "to provide a balance between accuracy and complexity". This balance should be considered by the engineer or rule-maker, and might differ depending on the considered fatigue prediction problem. To assess a total vessel it can be beneficial to apply the [ENSC](#) in combination with the [LDAM](#), this might already provide a sufficient fatigue life prediction. When the fatigue life is very critical, the accuracy is of greater importance and the used can opt for the [ENSC](#) in combination with the [NLDAM](#), as is concluded in this thesis.

Lastly, the assessment has some limitations, being:

- The [VA](#) fatigue database has only one dataset, of 6 specimens, of HS type B. By incorporating at least one set of HS type B, the effect of this is limited. The comparison of the [HSSSC](#) and [ENSC](#), both with the [LDAM](#), has shown that the [ENSC](#) sufficiently accounts for the differences between several HS types.
- The databases from [3] are tested for the PMMOD64 and BROAD64 wave spectra. This implicitly assumes, wrongfully, a constant [RAO](#) of 1 over the full frequency domain. However, the analysis of the [VA](#) database with the [NLDAM](#) has shown that the θ_{VA} parameters can be generalised for all considered spectra.
- The optimisation might not be fully converged, due to limitations in the available computational power. The nature of the design space and resulting objective surface however guarantees that the attained optimum is in close proximity of the global optimum. The global optimum can be obtained by increasing the amount of [MC](#) samples to 10^5 , and by prolongation of the assessed time traces.

8.3. Recommendations

Following the finding of a separation between mid-to-high and low stress dominated spectra, the first recommendation is to work on a damage accumulation model that accounts for the differences in crack initiation and crack propagation that lead to the observed differences between low-stress and mid-to-high-stress dominated spectra. As was explained in the previous section, the [NLDAM](#) is a fracture-mechanics based model. That means that the model models crack propagation, but not crack initiation. When welded joints are considered it can be assumed that the crack initiation phase is already consumed by the surface defects from the welding process. However, the research findings indicate that this assumption is of limited validity for low-stress range dominated spectra. The recommendation is to assess the combination of the [Total Stress Concept \(TSC\)](#) in combination with the [LDAM](#), considering the [TSC](#) combines the crack initiation and crack propagation stage in the fatigue damage criterion. This recommendation is in line with the indicated trend in [19] where fatigue damage criteria developments can develop in the direction of complete strength, total

life and multi-scale. The results of this thesis indicate that the total life development is of value for the fatigue life prediction under VA loading histories. However, this does not improve the validity of the damage accumulation model internally, only of the combination between the fatigue damage criterion and damage accumulation model.

The second recommendation is to also, next to the NLDAM by Leonetti et al., analyse the respective benefits of the DLDL by Manson and Halford. This model accumulates the fatigue damage in a bi-linear manner, and is deemed to be less complex to analyse and to implement than the NLDAM. However, this model would need a validation of the respective parameters y_1 and y_2 .

Thirdly, it is recommended to expand and use the compiled VA database for future assessments of fatigue life prediction models, subject to (random) VA loads. The author did not find such a database in literature. Expanding the database should at first be done with the datasets from Kahl et al. [61] and Rörup and Petershagen [118]. Considering that for both datasets not all data is contained in the articles ([61] presents the results only in figures, and [118] provides limited information with regards to the cycle-by-cycle mean stresses), a further assessment and correspondence with the authors is required for a sound analysis. The time constraint on this thesis has lead these datasets to be excluded from the presented analyse. Upon including the datasets from [61, 118], the database should be expanded with novel experiments (when conducted), complying with the measured operational profiles of vessels and the respective load spectra (rainflow spectra, including the mean stress). It should be noted that the database expansion might also slightly influence the MLE's of the θ_{VA} parameters in the NLDAM: the optimisation should be performed again.

This thesis has reviewed and showed the beneficial effect of relieved residual stresses (see [103] and chapter 7) due to overloads. To make use of this beneficial effect, the critical details in a vessel can be subject to a post-weld treatment. One example is laser shock peening, which imposes large compressive stresses on the structure. If used correctly this relieves the process-induced tensile residual stress at the notch. A recommendation is to look into the mechanisms of this method to assess how it should be applied. After that it should be assessed how sensitive this method is to the capabilities of the user. If it is not used correctly the compressive stresses cause self-equilibrating tensile stresses in another location: limiting the benefits of the laser shock peening process.

The last recommendation is with regards to the total fatigue assessment procedure. A fellow graduation student, Martijn Witvoet, is working on the comparison between the time-domain and spectral-domain assessment of the stress ranges [137]. All models as are presented in chapter 7 are performed on rainflow spectra. That means that the cycle-by-cycle information of the mean stress should be known. A solution is to always report the time traces (which can be generated from spectra by adding random phases). However, in determining the stresses as a function of the sea states, research shows a significant difference between the spectral and temporal approach. This is, amongst other sources, attributed to the assumption of respectively linear or non-linear Froude-Krylov forces [137]. The goal of the research is to improve the accuracy of the linear spectral approach with knowledge of the origin of the differences between the linear spectral and non-linear temporal approach. The recommendation is to combine the research efforts from [137] with the novel NLDAM to benefit from a more accurate stress range spectrum in combination with the improvements as posed by the NLDAM.

9

Implementation

This chapter aims to promote implementation of the research findings in the design requirements of *DMO*. This recommendation is written, based on the following assumptions:

- The vessel's scantlings are initially based on static analysis of global and local loads. Hence, the fatigue analysis assumes a design wave bending moment and (in most cases) an exponential distribution of bending moments.
- Due to military loads, ultimate strength and residual strength requirements, a frigate will probably fulfil the fatigue requirements in most parts of the ship. The experience of *DMO* indicates that the main risk of steel weight increase is at superstructure endings and around large openings.
- A limited number of locations (up to 20) will be analysed in the detailed design phase with precise FE models, leading to restrictions in applicable construction details (a minimum FAT class).
- *DMO* aims to achieve an improved reliability at these locations.
- When a structural detail does not meet the fatigue life requirements either the local or global geometry is modified. The latter, in general, increases the weight of the vessel.

For all cases it is recommended to validate the input spectra of the vessel by means of (Virtual) Hull Monitoring. This reduces the uncertainty with regards to source 1 (see figure 2.1). Besides that, two implementation strategies with regards to source 4 and 5 are proposed, respectively for the short (section 9.1) and long term (9.2).

9.1. Short term: continuing with the LDAM

This short term implementation of the research findings is focused on implementing the knowledge, without significantly altering the assessment procedures. In the mean time it is recommended to validate the *NLDAM* further, and to train the respective parties in using and understanding this method.

As was concluded in section 7.4.3, the use of the *ENSC* provides a first significant improvement. The proposed steps in the process are:

1. The structure is assessed by means of the, currently implemented, *NSC*- or *HSSSC*-based fatigue methods. To avoid conservatism in both methods, it is recommended to apply the Walker mean stress correction to resemble the r_{lr} level of the S-N curves. This value is typically $r_{lr} = 0.5$, which includes conservatism. When using the *HSSSC* the second recommendation is to apply the *FAT100* S-N curve, instead of the *FAT90* (i.e. DNV-GL D curve) as is proposed in [27]. This is supported by the findings in chapter 6.
2. Details that do not meet the fatigue life requirements in step 1 are subject to a *ENSC*-based fatigue method. Here the stress averaging approach is recommended in contrary to the artificial notch radius as the stress averaging approach is proven in literature [112] to have a better performance and it allows analytical (i.e. reduced computational costs) calculations.
3. The details that do not meet the fatigue requirements in step 2 will be locally modified to either:
 - (a) Separate *MSC* sources.

- (b) Increase the weld quality requirements.
 - (c) Use post-weld treatment on the critical locations.
 - (d) Place sacrificial elements in the structure that will fail before the actual detail fails.
4. The details that do not meet the fatigue requirements after step 3 will be subject to global modifications of the geometry. This can be changes in the size or shape of the geometry. A typical modification would be to increase the plate thickness to reduce the structural far field stress level.

In this version of the implementation procedure the **LDAM** is used, which enables the engineer to modify the value of the critical damage. In this proposal the critical damage will not be a fixed constant, but it will be expressed as:

$$D_{\text{crit}} = f_A \cdot f_{EOM} \cdot f_{\text{crit}} \cdot 1 \quad (9.1)$$

It should be noted that for the current approach of **DMO** with the **LDAM**, $D_{\text{crit}} = 0.75$, independent of the details of the considered structure or detail.

f_A	Accumulation factor. For the LDAM this should be between 0.5 and 1.5. This factor should be based on the comparison of random VA data to the fatigue life that is predicted with the LDAM . It should be noted that the use of this factor was proposed by Schütz and is the RLDAM .
f_{EOM}	Ease-of-mind factor. Due to uncertainties in the determination of the safety factors the author of the specifications can round down or add a manual factor as is deemed fit.
f_{crit}	Criticality factor. For parts of the ship that are deemed critical (i.e. hull plating) this factor should be lower than for less critical parts (i.e. door-corners, superstructure parts). This factor is ideally linked to the distribution of the accumulation factor f_A .

When the vessel encounters slamming, which poses higher loads on the structure, the damage rate is higher. Literature data should indicate the suitable factor for frigates. The slamming factor for the total lifetime is however highly dependent on the operational profile. In line with the whipping factor as a function of the steepness [29] this is ideally defined per sea state, heading and ship speed.

The current practise at **DMO** is to account for slamming by means of a correction factor, imposed on the critical damage in the **LDAM** damage sum. Slamming should however be accounted for in the load sequence, which can be expressed by means of a rainflow-counted histogram, or a time-trace. This is recommended because slamming only occurs for a specific set of sea-states, and the damage contribution of non-slamming sea states are affected if a generalised correction factor is applied. If this data is not available (which might be, as it requires accurate measurements on-board, of which the validity for extrapolation to new-built vessels is essential) a first modification would be to derive a generalised correction "surface" from research results. This "surface" poses a different (interpolated) slamming factor for each sea state, or even for each element in the rainflow-matrix.

9.2. Long term: implementing the **NLDAM**

The fatigue life calculation is typically performed in the basic and detail engineering phase. That means that the amount local information with regards to weld geometries and structural details might be limited. Preferably the vessel is assessed with as little information as possible. Therefore this implementation advice is also formulated in steps of increasing complexity. The steps are identical to the procedure in section 9.1, with the exception that the first step is to assess the total structure with the **HSSSC** in combination with the **NLDAM**, fitted to the **HSSSC CA** and **VA** fatigue databases.

The **SCF**'s are calculated per **CA** specimen in [111] and **VA** specimen in section 7.3. These **SCF**'s easily translate the **ENSC** databases to **HSSSC** databases. This is however not part of this thesis work. The **HSSSC VA** database is required to find the θ_{VA} parameters for the **HSSSC**. Ideally the Walker mean stress correction is incorporated in this assessment to address the scatter due to mean stress variations.

9.2.1. Assessing the fatigue life using the NLDAM

The fatigue life at a preset level of probability of survival (P) and confidence (C) is to be calculated by the following procedure [75].

The lower prediction bound is obtained for all Monte Carlo samples. That means that a distribution of the predicted fatigue life at the lower prediction bound is drawn up. Per Monte Carlo sample the mean and standard deviation of the fatigue life are known, and the lower prediction bound equals : $w_p = w - X\sigma$. To extract the results at a certain confidence level the result at the respective percentile is used. As an example for the 95% probability of survival and 75% confidence level:

1. The distribution of the fatigue life per Monte Carlo sample provides the μ and σ of the fatigue life. These are assumed to follow a normal distribution.
2. The 95% probability of survival level, per Monte Carlo sample is calculated:

$$\mathbf{w}_{(1-95\%)} = \mathbf{w} - 1.96\sigma \quad (9.2)$$

3. The 75% confidence level is the sample of $\mathbf{w}_{(1-95\%)}$ that is closest to the 25% percentile.

Bibliography

- [1] H. Agerskov. Fatigue in steel structures under random loading. *Journal of Constructional Steel Research*, 53(3):283–305, 2000. ISSN 0143974X. doi: 10.1016/S0143-974X(99)00042-5.
- [2] H. Agerskov and J. B. Ibsø. Fatigue Life of Plate Elements with Welded Transverse Attachments Subjected to Stochastic Loading. In A.F. Blom, editor, *Proceedings of the Nordic Conference on Fatigue*, West Midlands, UK, 1993. EMAS Publishers.
- [3] H. Agerskov, R.I. Petersen, L. Lopez Martinez, and V. Askegaard. Fatigue Life of High-Strength Steel Plate Elements under Stochastic Loading. (May 1995), 1995. URL <https://www.researchgate.net/publication/258919425>.
- [4] A. Aïd, A. Amrouche, B. Bachir Bouiadjra, M. Benguediab, and G. Mesmacque. Fatigue life prediction under variable loading based on a new damage model. *Materials and Design*, 32(1):183–191, 2011. ISSN 02641275. doi: 10.1016/j.matdes.2010.06.010. URL <http://dx.doi.org/10.1016/j.matdes.2010.06.010>.
- [5] M. Aslam, B. Z. Jarkowski, and S. Jeelani. Prediction of Cumulative Fatigue Damage. Technical report, Department of the Navy Naval Air System Command, Washington, D.C., 1978. URL <http://www.dtic.mil/dtic/tr/fulltext/u2/a116409.pdf>.
- [6] ASTM E1049. Standard practices for cycle counting in fatigue analysis. Technical Report Reapproved 2017, 2017.
- [7] M. Ben-Amoz. A cumulative damage theory for fatigue life prediction. *Engineering Fracture Mechanics*, 37(2):341–347, 1990. ISSN 00137944. doi: 10.1016/0013-7944(90)90045-1.
- [8] S. Benkabouche, H. Guechichi, A. Amrouche, and M. Benkhettab. A modified nonlinear fatigue damage accumulation model under multiaxial variable amplitude loading. *International Journal of Mechanical Sciences*, 100:180–194, 2015. ISSN 00207403. doi: 10.1016/j.ijmecsci.2015.06.016. URL <http://dx.doi.org/10.1016/j.ijmecsci.2015.06.016>.
- [9] F.P. Brennan, K. Branner, J.H. den Besten, A.M. Horn, B. Ki Choi, W. Mao, T. Nakamura, E. Oterkus, I. Paranhos Pasqualino, G. Parmentier, C. Rizzo, J. Romanoff, J. Rörup, A. Samanta, A. Theodoulidis, F. Wang, G. Wang, and N. Chen. ISSC Committee III.2 Fatigue and fracture. In *19th International Ship and Offshore Structures Congress*, volume 1, pages 354–405, 2015. ISBN 9781439852347. doi: 10.1201/b15616.
- [10] J. L. Chaboche. Une loi differentielle d’endommagement de fatigue avec cumulation non-lineaire. *Revue Francaise de Mecanique*, (50-51):71–82, 1974. ISSN 03736601.
- [11] J. L. Chaboche and P. M. Lesne. A Non-Linear Continuous Fatigue Damage Model. *Fatigue and Fracture of Engineering Materials and Structures*, 11(1):1–17, 1988. ISSN 14602695. doi: 10.1111/j.1460-2695.1988.tb01216.x.
- [12] D. G. Chen. The method of determining the exponent d in the Corten-Dolan’s fatigue damage formula. *Journal of Mechanical Strength*, 18(1):21–24, 1996.
- [13] P.D. Chinh. *Shakedown*, pages 3069–3074. Springer US, Boston, MA, 2013. ISBN 978-0-387-92897-5. doi: 10.1007/978-0-387-92897-5_250. URL https://doi.org/10.1007/978-0-387-92897-5_{_}250.
- [14] M. Ciavarella, P. D’antuono, and A. Papangelo. On the connection between Palmgren-Miner rule and crack propagation laws. *Fatigue and Fracture of Engineering Materials and Structures*, 41(7):1469–1475, 2018. ISSN 14602695. doi: 10.1111/ffe.12789. URL <https://doi.org/10.1111/ffe.12789>.

- [15] H.T. Corten and T.J. Dolan. Cumulative fatigue damage. In *Proceedings of the international conference on fatigue of metals*, pages 235–242, London, 1954. Institution of Mechanical Engineering and American Society of Mechanical Engineers.
- [16] W. Cui. A state-of-the-art review on fatigue life prediction methods for metal structures. *Journal of Marine Science and Technology*, 7(1):43–56, 2002. ISSN 09484280. doi: 10.1007/s007730200012.
- [17] L. D’Angelo and A. Nussbaumer. Estimation of fatigue S-N curves of welded joints using advanced probabilistic approach. *International Journal of Fatigue*, 97:98–113, 2017. ISSN 01421123. doi: 10.1016/j.ijfatigue.2016.12.032. URL <http://dx.doi.org/10.1016/j.ijfatigue.2016.12.032>.
- [18] V. Dattoma, S. Giancane, R. Nobile, and F. W. Panella. Fatigue life prediction under variable loading based on a new non-linear continuum damage mechanics model. *International Journal of Fatigue*, 28(2):89–95, 2006. ISSN 01421123. doi: 10.1016/j.ijfatigue.2005.05.001.
- [19] H. den Besten. Fatigue damage criteria classification, modelling developments and trends for welded joints in marine structures. *Ships and Offshore Structures*, 13(8):787–808, 2018. ISSN 17445302. doi: 10.1080/17445302.2018.1463609.
- [20] H. den Besten. OE44085 05: Fatigue resistance (testing & damage criterion - lifetime relations), 2020. URL <http://library1.nida.ac.th/termpaper6/sd/2554/19755.pdf>.
- [21] H. den Besten. OE44085 07: Fatigue assessment concepts (hot spot structural stress concept), 2020.
- [22] H. den Besten. OE44085 10: Fatigue Influence Factors (Amplitude Variability), 2020.
- [23] J.H. den Besten. *Fatigue resistance of welded joints in aluminium high-speed craft: a total stress concept*. PhD Thesis, Delft University of Technology, 2015.
- [24] Det Norske Veritas Classification AS. Classification note 30.7: "Fatigue Assessment of Ship Structures". Technical report, Det Norske Veritas, 1322 Høvik, Norway, 2014. URL <https://rules.dnvgl.com/docs/pdf/DNV/cn/2014-04/CN30-7.pdf>.
- [25] DNV-GL. Part 3 Surface Ships Chapter 1 Hull structures and ship equipment. Technical Report December, 2015.
- [26] DNV-GL. DNVGL-RP-C203: Fatigue design of offshore steel structures. *DNV GL - Recommended Practice*, (April):176, 2016.
- [27] DNV-GL. Class Guideline: Fatigue assessment of ship structures. Technical report, 2018.
- [28] P. Dong. A structural stress definition and numerical implementation for fatigue analysis of welded joints. *International Journal of Fatigue*, 23(10):865–876, 2001. ISSN 01421123. doi: 10.1016/S0142-1123(01)00055-X.
- [29] I. Drummen, M. Schiere, R. Dallinga, and K. Stambaugh. Full and Model Scale testing of a New Class of US Coast Guard Cutter. *Ship Structure Symposium*, 2014.
- [30] I. Drummen, L. Rogers, A. Benhamou, R. Hageman, and K. Stambaugh. Hull Structure Monitoring of a New Class of US Coast Guard Cutters. 2019.
- [31] W. Elber. Fatigue Crack closure under Cyclic Tension. *Engineering Fracture Mechanics*, 2:37–45, 1970. doi: 10.1016/0013-7944(70)90028-7.
- [32] T. Endo, K. Mitsunaga, K. Takahashi, K. Kobayashi, and M. Matsuishi. Damage evaluation of metals for random or varying loading. In *Proceedings of the 1974 Symposium on Mechanical Behavior of Materials*, pages 371–380. Society of Materials Science, 1974.
- [33] Engineering Toolbox. Friction and Friction Coefficients. URL https://www.engineeringtoolbox.com/friction-coefficients-d_{_}778.html.
- [34] A Fatemi and L Yang. Cumulative fatigue damage and life prediction theories. *International Journal of Fatigue*, 20(1):9–34, 1998. ISSN 0142-1123. URL [http://dx.doi.org/10.1016/S0142-1123\(97\)00081-9](http://dx.doi.org/10.1016/S0142-1123(97)00081-9).

- [35] N. A. Fleck. Fatigue crack growth due to periodic underloads and overloads. *Acta Metallurgica*, 33(7): 1339–1354, 1985. ISSN 00016160. doi: 10.1016/0001-6160(85)90244-5.
- [36] R. Folsø, S. Otto, and G. Parmentier. Reliability-based calibration of fatigue design guidelines for ship structures. *Marine Structures*, 15(6):627–651, 2002. ISSN 09518339. doi: 10.1016/S0951-8339(01)00031-4.
- [37] A. M. Freudenthal and R. A. Heller. On Stress Interaction in Fatigue and a Cumulative Damage Rule. *Journal of the Aerospace Sciences*, 26(7):431–442, 1959. doi: 10.2514/8.8131.
- [38] W. Fricke, H. Petershagen, and H. Paetzold. Fatigue Strength of Ship Structures - Part I: Basic Principles. *GL Technology*, 1997.
- [39] W. Fricke, A. Babanin, S. Wang, A. Samanta, A.M. Horn, R. Sielski, K. Gotoh, Y. Garbatov, S. K. Ås, K. Braner, B.K. Choi, J. H. den Besten, P. Dong, I. Lillemäe, P. Lindstrom, M. Lourenço de Souza, G. Parmentier, Y. Quémener, C.M. Rizzo, J. Rörup, S. Vhanmane, R. Villavicencio, F. Wang, and J. Yue. ISSC Committee III.2 Fatigue and Fracture. In M.L. Kaminski and P. Rigo, editors, *20th International Ship and Offshore Structures Congress*, volume III, pages 87–106, 2018. ISBN 0803114982. doi: 10.3233/PMST200007.
- [40] N.E. Frost, K.J. Marsh, and L.P. Pook. *Metal Fatigue*. Clarendon Press, Oxford, 1974.
- [41] H. Gao, H-Z Huang, S.P. Zhu, Y-F Li, and R. Yuan. A modified model for non-linear fatigue damage accumulation with load interaction effects. *The Scientific World Journal*, 2014. doi: 10.1115/DETC201546953.
- [42] H. Gao, H.Z. Huang, Z. Lv, F.J. Zuo, and H.K. Wang. An improved Corten-Dolan's model based on damage and stress state effects. *Journal of Mechanical Science and Technology*, 29(8):3215–3223, 2015. ISSN 1738494X. doi: 10.1007/s12206-015-0721-x.
- [43] E. Gassner. Festigkeitsversuche mit wiederholter Beanspruchung im Flugzeugbau. *Luftwissen*, (6):61–64, 1939.
- [44] Eric Goodin, Alan Kallmeyer, and Peter Kurath. Evaluation of nonlinear cumulative damage models for assessing HCF/LCF interactions in multiaxial loadings. ... *engine high cycle fatigue (HCF) ...*, (February):1–14, 2004. URL <http://www.ndsu.nodak.edu/me/images/Kallmeyer/Papers/HCF2004Paper.pdf>.
- [45] T. Gurney. The influence of cycles of small stress range. *Cumulative Damage of Welded Joints*, pages 244–262, 2006. doi: 10.1533/9781845691035.244.
- [46] T. Gurney. The influence of narrow band, wide band and service loading. *Cumulative Damage of Welded Joints*, pages 193–243, 2006. doi: 10.1533/9781845691035.193.
- [47] T. Gurney. The influence of spectrum shape and block length. *Cumulative Damage of Welded Joints*, pages 147–192, 2006. doi: 10.1533/9781845691035.147.
- [48] E. Haibach. *Modifizierte lineare Schadensakkumulations-Hypothese zur Berücksichtigung des Dauerfestigkeitsabfalls mit fortschreitender Schädigung*. Laboratorium für Betriebsfestigkeit, LBF, Darmstadt, 50 edition, 1970.
- [49] E. Haibach and H. P. Lehrke. Das Verfahren der Amplituden-Transformation zur Lebensdauerberechnung bei Schwingsbeanspruchung. *Arch Eisenhuettenwes*, 1976.
- [50] Z. Hashin and A. Rotem. A cumulative damage theory of fatigue damage. Technical report, Tel-Aviv University, School of Engineering, Tel Aviv, 1977.
- [51] K. Hectors and W. de Waele. Modeling nonlinear fatigue damage accumulation in a welded runway girder. *Procedia Structural Integrity*, 28(2019):239–252, 2020. ISSN 24523216. doi: 10.1016/j.prostr.2020.10.030. URL <https://doi.org/10.1016/j.prostr.2020.10.030>.
- [52] M.A. Hirt and P.M. Kunz. Fatigue safety of existing steel bridges. [Ermüdungssicherheit bestehender Brücken aus Stah.]. *International Journal of Fatigue*, 65(11):399–406, 1998. ISSN 01421123. doi: 10.1016/S0142-1123(98)91011-8.

- [53] A. Hobbacher. Stress intensity factors of welded joints. 46(2):173–182, 1993.
- [54] A. F. Hobbacher. *Recommendations for Fatigue Design of Welded Joints and Components*. Springer International Publishing, 2 edition, 2019. ISBN 9781855733152. doi: 10.1007/978-3-319-23757-2_8.
- [55] (IACS) International Association of Classification Societies. Fatigue Assessment of Ship Structures. Technical Report 56, 1999.
- [56] J. B. Ibsø and H. Agerskov. An Analytical Model for Fatigue Life Prediction Based on Fracture Mechanics and Crack Closure. *Journal of Constructional Steel Research*, 37(3):229–261, 1996. ISSN 0143974X. doi: 10.1016/0143-974X(96)00006-5.
- [57] J. E. Inoma, D. G. Pavlou, and J. Zec. Implementation of linear, double-linear, and nonlinear fatigue damage accumulation rules for fatigue life prediction of offshore drilling top-drive tie-rods. *IOP Conference Series: Materials Science and Engineering*, 700(1), 2019. ISSN 1757899X. doi: 10.1088/1757-899X/700/1/012025.
- [58] J. Y. Jang and M. M. Khonsari. On the evaluation of fracture fatigue entropy. *Theoretical and Applied Fracture Mechanics*, 96(March):351–361, 2018. ISSN 01678442. doi: 10.1016/j.tafmec.2018.05.013. URL <https://doi.org/10.1016/j.tafmec.2018.05.013>.
- [59] M. Jimenez-Martinez. Fatigue of offshore structures: A review of statistical fatigue damage assessment for stochastic loadings. *International Journal of Fatigue*, 132(October 2019), 2020. ISSN 01421123. doi: 10.1016/j.ijfatigue.2019.105327.
- [60] L. M. Kachanov. On time to rupture in creep conditions (in Russian). *Izvestia Akademii Nauk SSSR, Otdelenie Tekhnicheskikh Nauk*, 8:26–31, 1958.
- [61] A. Kahl, W. Fricke, H. Paetzold, and H. Von Selle. Whipping investigations based on large-scale measurements and experimental fatigue testing. *International Journal of Offshore and Polar Engineering*, 25(4):247–254, 2015. ISSN 10535381. doi: 10.17736/ijope.2015.sh14.
- [62] N. D. Katopodes. Chapter 2 - Air-Water Interface. In *Free-Surface Flow: Shallow Water Dynamics*, pages 44–121. Butterworth Heinemann, 2019. ISBN 978-0-12-815487-8. doi: <https://doi.org/10.1016/B978-0-12-815487-8.00002-0>. URL <https://www.sciencedirect.com/science/article/pii/B9780128154878000020>.
- [63] K. H. Klippstein and C.G. Schilling. Pilot study on the constant and variable amplitude behavior of transverse stiffener welds. *Journal of Constructional Steel Research*, 12(3-4):229–252, 1989. ISSN 0143974X. doi: 10.1016/0143-974X(89)90057-6.
- [64] M. Köhler, S. Jenne, K. Pötter, and H. Zenner. *Load Assumption for Fatigue Design of Structures and Components*. 2017. ISBN 9783642552472. doi: 10.1007/978-3-642-55248-9.
- [65] S. Kwofie and H. D. Chandler. Fatigue life prediction under conditions where cyclic creep-fatigue interaction occurs. *International Journal of Fatigue*, 29(12):2117–2124, 2007. ISSN 01421123. doi: 10.1016/j.ijfatigue.2007.01.022.
- [66] S. Kwofie and N. Rahbar. An equivalent driving force model for crack growth prediction under different stress ratios. *International Journal of Fatigue*, 33(9):1199–1204, 2011. ISSN 01421123. doi: 10.1016/j.ijfatigue.2011.03.006. URL <http://dx.doi.org/10.1016/j.ijfatigue.2011.03.006>.
- [67] N. Lautrou, David Thevenet, and J. Y. Cognard. Fatigue crack initiation life estimation in a steel welded joint by the use of a two-scale damage model. *Fatigue and Fracture of Engineering Materials and Structures*, 32(5):403–417, 2009. ISSN 14602695. doi: 10.1111/j.1460-2695.2009.01344.x.
- [68] C.S. Lee, M.H. Kim, J. M. Lee, and M. Mahendran. Computational study on the fatigue behavior of welded structures. *International Journal of Damage Mechanics*, 20(3):423–463, 2011. ISSN 10567895. doi: 10.1177/1056789509359676.
- [69] Y-L. Lee and T. Tjhung. *Rainflow Cycle Counting Techniques*. Elsevier Inc., 2012. ISBN 9780123852045. doi: 10.1016/B978-0-12-385204-5.00003-3. URL <http://dx.doi.org/10.1016/B978-0-12-385204-5.00003-3>.

- [70] H. H. E. Leipholz. On the modified S-N curve for metal fatigue prediction and its experimental verification. *Engineering Fracture Mechanics*, 23(3):495–505, 1986. ISSN 00137944. doi: 10.1016/0013-7944(86)90158-X.
- [71] H.H.E. Leipholz. Lifetime Prediction for Metallic Specimens Subjected To Loading With Varying Intensity. *Advances and Trends in Structures and Dynamics*, 20(1):239–246, 1985. doi: 10.1016/b978-0-08-032789-1.50030-6.
- [72] J. Lemaitre and R. Desmorat. *Engineering damage mechanics : ductile, creep, fatigue and brittle failures*. Springer International Publishing, New York, 2005.
- [73] J. Lemaitre, J. P. Sermage, and R. Desmorat. A two scale damage concept applied to fatigue. *International Journal of Fracture*, 97(1-4):67–81, 1999. ISSN 03769429. doi: 10.1023/a:1018641414428.
- [74] D. Leonetti, J. Maljaars, and H.H. Snijder. Fitting fatigue test data with a novel S-N curve using frequentist and Bayesian inference. *International Journal of Fatigue*, 105(May 2019):128–143, 2017. ISSN 01421123. doi: 10.1016/j.ijfatigue.2017.08.024.
- [75] D. Leonetti, J. Maljaars, and H.H. Snijder. Probabilistic fatigue resistance model for steel welded details under variable amplitude loading – Inference and uncertainty estimation. *International Journal of Fatigue*, 135(January):105515, 2020. ISSN 01421123. doi: 10.1016/j.ijfatigue.2020.105515. URL <https://doi.org/10.1016/j.ijfatigue.2020.105515>.
- [76] M. Liakat and M. M. Khonsari. On the anelasticity and fatigue fracture entropy in high-cycle metal fatigue. *Materials and Design*, 82:18–27, 2015. ISSN 18734197. doi: 10.1016/j.matdes.2015.04.034. URL <http://dx.doi.org/10.1016/j.matdes.2015.04.034>.
- [77] Q. Liu, Y. Gao, Y. Li, and Q. Xue. Fatigue life prediction based on a novel improved version of the Corten-Dolan model considering load interaction effect. *Engineering Structures*, 221(July):111036, 2020. ISSN 18737323. doi: 10.1016/j.engstruct.2020.111036. URL <https://doi.org/10.1016/j.engstruct.2020.111036>.
- [78] M.A. Lont. Vermoeiings-restlevensduur van dekdelen uit "Hr.Ms. Tromp". Technical report, TNO Metaalinstituut, Delft, 1995.
- [79] I. Lotsberg. Assessment of design criteria for fatigue cracking from weld toes subjected to proportional loading. *Ships and Offshore Structures*, 4(2):175–187, 2009. ISSN 17445302. doi: 10.1080/17445300902733998.
- [80] I. Lotsberg. *Fatigue design of ship structures*. Cambridge University Press, New York, 2016. ISBN 9788578110796.
- [81] P. Lovegrove. DNV GL changes name to DNV as it gears up for decade of transformation, 2021. URL <https://www.dnv.com/news/dnv-gl-changes-name-to-dnv-as-it-gears-up-for-decade-of-transformation-194340#:~:text=0slo-%7C%2CNorway%7C%2C13January2021,marketsareundergoingfundamentalchange>.
- [82] X. Lu and S. Zheng. Strengthening of transmission gear under low-amplitude loads. *Materials Science and Engineering A*, 488(1-2):55–63, 2008. ISSN 09215093. doi: 10.1016/j.msea.2007.10.045.
- [83] X. Lu and S. Zheng. Strengthening and damaging under low-amplitude loads below the fatigue limit. *International Journal of Fatigue*, 31(2):341–345, 2009. ISSN 01421123. doi: 10.1016/j.ijfatigue.2008.08.004. URL <http://dx.doi.org/10.1016/j.ijfatigue.2008.08.004>.
- [84] X. Lu and S. Zheng. Changes in mechanical properties of vehicle components after strengthening under low-amplitude loads below the fatigue limit. *Fatigue and Fracture of Engineering Materials and Structures*, 32(10):847–855, 2009. ISSN 8756758X. doi: 10.1111/j.1460-2695.2009.01391.x.
- [85] Z. Lv, H. Z. Huang, S. P. Zhu, H. Gao, and F. Zuo. A modified nonlinear fatigue damage accumulation model. *International Journal of Damage Mechanics*, 24(2):168–181, 2014. ISSN 15307921. doi: 10.1177/1056789514524075.

- [86] S. Maddox. Assessing the Significance of Flaws in Welds Subject To Fatigue. *Welding Journal*, 52(9): 401–410, 1974. ISSN 0043-2296.
- [87] S. S. Manson and G. R. Halford. Practical implementation of the double linear damage rule and damage curve approach for treating cumulative fatigue damage. *International Journal of Fracture*, 17(2):169–192, 1981. ISSN 03769429. doi: 10.1007/BF00053519.
- [88] S. S. Manson and G. R. Halford. Re-examination of cumulative fatigue damage analysis—an engineering perspective. *Engineering Fracture Mechanics*, 25(5/6):539–571, 1986.
- [89] S.S. Manson. Interfaces between Fatigue, Creep and Fracture. *International Journal of Fracture Mechanics*, 2(1):328–363, 1966.
- [90] A. Mansour, P. Wirsching, M. Luckett, A Plumpton, and Et.al. *SSC-398 Assessment of Reliability of Ship Structures*. 1997.
- [91] S.M. Marco and W.L. Starkey. A concept of fatigue damage. In *Transactions of the ASME*, vol 76, pages 627–632, 1954.
- [92] M Matsuishi and T. Endo. Fatigue of metals subjected to varying stress. *presented to the Japan Society of Mechanical Engineers, Fukuoka, Japan*, 1968.
- [93] A. J. McEvily, S. Ishihara, and M. Endo. On the causes of deviation from the Palmgren-Miner rule. *ASTM Special Technical Publication*, (1439):369–380, 2003. ISSN 00660558. doi: 10.1520/stp11316s.
- [94] G. Mesmacque, S. Garcia, A. Amrouche, and C. Rubio-Gonzalez. Sequential law in multiaxial fatigue, a new damage indicator. *International Journal of Fatigue*, 27(4):461–467, 2005. ISSN 01421123. doi: 10.1016/j.ijfatigue.2004.08.005.
- [95] M.A. Miner. Cumulative damage in fatigue. *Journal of Applied Mechanics*, 12:159–164, 1945.
- [96] F. Mozafari, P. Thamburaja, A. R. Srinivasa, and N. Moslemi. A rate independent inelasticity model with smooth transition for unifying low-cycle to high-cycle fatigue life prediction. *International Journal of Mechanical Sciences*, 159(May):325–335, 2019. ISSN 00207403. doi: 10.1016/j.ijmecsci.2019.05.017. URL <https://doi.org/10.1016/j.ijmecsci.2019.05.017>.
- [97] F. Mozafari, P. Thamburaja, A. Srinivasa, and S. Abdullah. Fatigue life prediction under variable amplitude loading using a microplasticity-based constitutive model. *International Journal of Fatigue*, 134(October 2019):105477, 2020. ISSN 01421123. doi: 10.1016/j.ijfatigue.2020.105477. URL <https://doi.org/10.1016/j.ijfatigue.2020.105477>.
- [98] M. Naderi, M. Amiri, and M. M. Khonsari. On the thermodynamic entropy of fatigue fracture. *Proceedings of the Royal Society A: Mathematical, Physical and Engineering Sciences*, 466(2114):423–438, 2010. ISSN 14712946. doi: 10.1098/rspa.2009.0348.
- [99] NEN. NEN 2063 Arc welding. Fatigue loaded structures. Calculation of welded joints in unalloyed and low-alloyed steel up to and including Fe510 (Fe 52). Technical report, 1988.
- [100] NEN. Eurocode 3: Ontwerp en berekening van staalconstructies - Deel 1-9: Vermoeiing. Technical Report september 2012, 2012.
- [101] D. Oakley. Heavy steel plates for Economic Construction and Off-shore Structures, 2015. URL <https://www.oakleysteel.co.uk/heavy-steel-plates-economical-constructional-steelwork-offshore-structures>.
- [102] N. Osawa, N. Yamamoto, T. Nakamura, and J. Sawamura. Study on fatigue strength of Welded Joints Subject to High Frequency Superimposed Wave Loadings by Using Plate-Bending-Vibration Type Fatigue Testing Machines. 2015.
- [103] A. Ota, Y. Maeda, and N. Suzuki. Fatigue strength of transverse butt welded joints under random loading . *Welding International*, 11(12):958–965, 1997.
- [104] A. Palmgren. Die lebensdauer von kugellagern. *Zeitschrift des Vereins Deutscher Ingenieure*, 1924.

- [105] P. Paris and F. Erdogan. A critical analysis of crack propagation laws. *Journal of Basic Engineering*, pages 528–534, 1963.
- [106] F. G. Pascual and W. Q. Meeker. Estimating Fatigue Curves with the Random Fatigue-Limit Model. *Technometrics*, 41(4):277, 1999. ISSN 00401706. doi: 10.2307/1271342.
- [107] D. G. Pavlou. The theory of the S-N fatigue damage envelope: Generalization of linear, double-linear, and non-linear fatigue damage models. *International Journal of Fatigue*, 110(January):204–214, 2018. ISSN 01421123. doi: 10.1016/j.ijfatigue.2018.01.023. URL <https://doi.org/10.1016/j.ijfatigue.2018.01.023>.
- [108] H. Pereira, A. Jesus, A. Ribeiro, and A. Fernandes. Influence of loading sequence and stress ratio on Fatigue damage accumulation of a structural component. *Ciência & Tecnologia dos Materiais*, 20(1-2): 60–67, 2008. ISSN 0870-8312.
- [109] R.I. Petersen, H. Agerskov, and L. Lopez Martinez. Fatigue Life of High-Strength Steel Offshore Tubular Joints. Report No. R 1. Technical report, Department of Structural Engineering and Materials, Technical University of Denmark, Lyngby, 1996.
- [110] R.E. Peterson. Methods of correlating data from fatigue tests of stress concentration specimens. In *Stephen Timoshenko 60th anniversary volume*, page 179. The Macmillan Company, New York, 1938.
- [111] Y. Qin, H. den Besten, S. Palkar, and M. L. Kaminski. Fatigue design of welded double-sided T-joints and double-sided cruciform joints in steel marine structures: A total stress concept. *Fatigue and Fracture of Engineering Materials and Structures*, 42(12):2674–2693, 2019. ISSN 14602695. doi: 10.1111/ffe.13089.
- [112] Yanxin Qin, Henk den Besten, Saloni Palkar, and Miroslaw Lech Kaminski. Mid- and High-Cycle Fatigue of Welded Joints in Steel Marine Structures: Effective Notch Stress and Total Stress Concept Evaluations. *International Journal of Fatigue*, 142(July 2020), 2021. ISSN 01421123. doi: 10.1016/j.ijfatigue.2020.105822.
- [113] D. Radaj, C.M. Sonsino, and W. Fricke. *Fatigue assessment of welded joints by local approaches*. Woodhead Publishing Limited, Cambridge England, second edi edition, 2006.
- [114] W. Ramberg and W. R. Osgood. Description of stress-strain curves by three parameters. *National Advisory Committee For Aeronautics*, 1943.
- [115] K. Rege and D. G. Pavlou. A one-parameter nonlinear fatigue damage accumulation model. *International Journal of Fatigue*, 98:234–246, 2017. ISSN 01421123. doi: 10.1016/j.ijfatigue.2017.01.039. URL <http://dx.doi.org/10.1016/j.ijfatigue.2017.01.039>.
- [116] F.E. Richart and N.M. Newmark. An Hypothesis for the Determination of Cumulative Damage in Fatigue. In *Selected Papers By Nathan M. Newmark: Civil Engineering Classics*,, pages 279–312. ASCE, 1948.
- [117] K.O. Ronold and I. Lotsberg. On the estimation of characteristic S-N curves with confidence. *Marine Structures*, 27(1):29–44, 2012. ISSN 09518339. doi: 10.1016/j.marstruc.2012.03.002.
- [118] J. Rörup and H. Petershagen. The effect of compression mean stresses on the fatigue strength of welded structures. *Welding in the World*, 44(5):20–25, 2000. ISSN 00432288.
- [119] E. Santecchia, A. M.S. Hamouda, F. Musharavati, E. Zalnezhad, M. Cabibbo, M. El Mehtedi, and S. Spigarelli. A Review on Fatigue Life Prediction Methods for Metals. *Advances in Materials Science and Engineering*, 2016, 2016. ISSN 16878442. doi: 10.1155/2016/9573524.
- [120] J. Schijve. Fatigue of structures and materials in the 20th century and the state of the art. *International Journal of Fatigue*, 25(8):679–702, 2003. ISSN 01421123. doi: 10.1016/S0142-1123(03)00051-3.
- [121] Jaap Schijve. *Fatigue of structures and materials*. Springer, Delft, Netherlands, 2nd edition, 2009. ISBN 9781402068072. doi: 10.1007/978-1-4020-6808-9.

- [122] C. G. Schilling, K. H. Klippstein, J. M. Barsom, and G. T. Blake. *Fatigue of Welded Steel Bridge Members under Variable-amplitude Loadings - NCHRP Report 188*. Number November 2013. 1978. ISBN 0309027764.
- [123] W. Schütz. The prediction of fatigue life in the crack initiation and propagation stages—a state of the art survey. *Engineering Fracture Mechanics*, 11(2):405–421, 1979. ISSN 00137944. doi: 10.1016/0013-7944(79)90015-8.
- [124] D. G. Shang and W. X. Yao. A nonlinear damage cumulative model for uniaxial fatigue. *International Journal of Fatigue*, 21(2):187–194, 1999. ISSN 01421123. doi: 10.1016/S0142-1123(98)00069-3.
- [125] Ship Structure Committee. Mean Stress assessment in Fatigue Analysis and Design. *Ship Structure Committee*, 2013.
- [126] S. Silitonga, J. Maljaars, F. Soetens, and H. H. Snijder. Survey on damage mechanics models for fatigue life prediction. *Heron*, 58(1):25–60, 2013. ISSN 15744078.
- [127] C. M. Sonsino. Principles of variable amplitude fatigue design and testing. *ASTM Special Technical Publication*, 1(1439):3–23, 2003. ISSN 00660558. doi: 10.1520/stp11294s.
- [128] C. M. Sonsino. Fatigue testing under variable amplitude loading. *International Journal of Fatigue*, 29(6):1080–1089, 2007. ISSN 01421123. doi: 10.1016/j.ijfatigue.2006.10.011.
- [129] C. E. Strohmeyer. The determination of fatigue limits under alternating stress conditions. *Proceedings of the Royal Society of London, Series A*, 1914.
- [130] S. Subramanyan. A cumulative damage rule based on the knee point of the S-N Curve. *Journal of Engineering Materials and Technology, Transactions of the ASME*, 1976. ISSN 15288889. doi: 10.1115/1.3443383.
- [131] T. Svensson, P. Johannesson, and J. De Maré. Fatigue life prediction based on variable amplitude tests - Specific applications. *International Journal of Fatigue*, 27(8):966–973, 2005. ISSN 01421123. doi: 10.1016/j.ijfatigue.2004.11.010.
- [132] J. Tuitman. *Hydro-elastic response of ship structures to slamming induced whipping*. PhD thesis, Delft University of Technology, 2010.
- [133] van Bergen, J. Expert opinion, Specialist Naval Structures at Dutch Ministry of Defense, 2020.
- [134] K. Walker, S. Pendleberry, and R. McElwee. Effects of environment and complex load history on fatigue life. *ASTM STP*, 462(1), 1970.
- [135] P. H. Wirsching and M. Asce. Fatigue Reliability for Offshore Structures. 110(10):2340–2356, 1985.
- [136] Paul H. Wirsching and Y. N. Chen. Considerations of probability-based fatigue design for marine structures. *Marine Structures*, 1(1):23–45, 1988. ISSN 09518339. doi: 10.1016/0951-8339(88)90009-3.
- [137] M. Witvoet. *Mean Stress Effects in Temporal and Spectral Fatigue Analysis*. Unpublished master thesis, Delft University of Technology, 2021.
- [138] A. Wöhler. Über die Festigkeitsversuche mit Eisen und Stahl. *Zeitschrift für Bauwesen*, 20:73–106, 1870.
- [139] N. Xiaode, L. Guangxia, and L. Hao. Hardening law and fatigue damage of a cyclic hardening metal. *Engineering Fracture Mechanics*, 26(2):163–170, 1987. ISSN 00137944. doi: 10.1016/0013-7944(87)90194-9.
- [140] J. Xu, D. G. Shang, G. Q. Sun, H. Chen, and E. T. Liu. Fatigue life prediction for GH4169 superalloy under multiaxial variable amplitude loading. *Journal of Beijing University of Technology*, 38(10):1462–1466, 2012. ISSN 02540037.
- [141] Q. Xue, X. Du, and S. Wang. An Improved Fatigue Life Prediction Model Based on Loading Sequence. *Zhongguo Tiedao Kexue/China Railway Science*, 40(1):88–93, 2019.

- [142] X H Yang, W X Yao, and C M Duan. The review of ascertainable fatigue cumulative damage rule. *Engineering Science*, 5(4):82–87, 2003.
- [143] C-H. Yoo, K-S. Kim, Y-S. Suh, Y-L. Shim, Y-S. Ha, W-H. You, and H-J. Choi. An Experimental Study on Fatigue Life Evaluation of Welded Joints under Storm Loading. *Journal of the Society of Naval Architects of Korea*, 49(1):99–108, 2012. ISSN 1225-1143. doi: 10.3744/snak.2012.49.1.99.
- [144] R. Yuan, H. Li, H. Z. Huang, S. P. Zhu, and H. Gao. A nonlinear fatigue damage accumulation model considering strength degradation and its applications to fatigue reliability analysis. *International Journal of Damage Mechanics*, 24(5):646–662, 2015. ISSN 15307921. doi: 10.1177/1056789514544228.
- [145] J. Zhang. *Development of Frameworks for Numerical Modelling of Corrosion Fatigue in Offshore Structures Ontwikkeling van modellen voor numerieke simulatie van corrosie-vermoeiing in offshore constructies Jie Zhang*. PhD Thesis, Ghent University, 2019.
- [146] J. Zhang, X. Fu, J. Lin, Z. Liu, N. Liu, and B. Wu. Study on damage accumulation and life prediction with loads below fatigue limit based on a modified nonlinear model. *Materials*, 11(11), 2018. ISSN 19961944. doi: 10.3390/ma11112298.
- [147] Y. H. Zhang and S. J. Maddox. Investigation of fatigue damage to welded joints under variable amplitude loading spectra. *International Journal of Fatigue*, 31(1):138–152, 2009. ISSN 01421123. doi: 10.1016/j.ijfatigue.2008.04.006. URL <http://dx.doi.org/10.1016/j.ijfatigue.2008.04.006>.
- [148] Y. H. Zhang and S. J. Maddox. Fatigue testing of full scale girth welded pipes under variable amplitude loading. *Journal of Offshore Mechanics and Arctic Engineering*, 136(2), 2014. ISSN 1528896X. doi: 10.1115/1.4026025.
- [149] L. Zhao, S. Zheng, and J. Feng. Fatigue life prediction under service load considering strengthening effect of loads below fatigue limit. *Chinese Journal of Mechanical Engineering (English Edition)*, 27(6): 1178–1185, 2014. ISSN 10009345. doi: 10.3901/CJME.2014.0806.130.
- [150] S. P. Zhu, H. Z. Huang, and Z. L. Wang. Fatigue life estimation considering damaging and strengthening of low amplitude loads under different load sequences using fuzzy sets approach. *International Journal of Damage Mechanics*, 20(6):876–899, 2011. ISSN 10567895. doi: 10.1177/1056789510397077.
- [151] S. P. Zhu, H. Z. Huang, Y. Liu, L. P. He, and Q. Liao. A practical method for determining the Corten-Dolan exponent and its application to fatigue life prediction. *International Journal of Turbo and Jet Engines*, 29(2):79–87, 2012. ISSN 03340082. doi: 10.1515/tjj-2012-0013.
- [152] S. P. Zhu, Y. Z. Hao, J. A.F. de Oliveira Correia, G. Lesiuk, and A. M.P. de Jesus. Nonlinear fatigue damage accumulation and life prediction of metals: A comparative study. *Fatigue and Fracture of Engineering Materials and Structures*, 42(6):1271–1282, 2019. ISSN 14602695. doi: 10.1111/ffe.12937.
- [153] S. P. Zhu, D. Liao, Q. Liu, J.A.F.O. Correia, and A.M.P. De Jesus. Nonlinear fatigue damage accumulation: Isodamage curve-based model and life prediction aspects. *International Journal of Fatigue*, 128(January):105185, 2019. ISSN 01421123. doi: 10.1016/j.ijfatigue.2019.105185. URL <https://doi.org/10.1016/j.ijfatigue.2019.105185>.
- [154] S.P. Zhu, H.Z. Huang, and L.Y. Xie. Nonlinear fatigue damage cumulative model and the analysis of strength degradation based on the double parameter fatigue criterion. *China Mechanical Engineering*, 19(22):2753–2761, 2008.
- [155] F. J. Zuo, H. Z. Huang, S. P. Zhu, Z. Lv, and H. Gao. Fatigue life prediction under variable amplitude loading using a non-linear damage accumulation model. *International Journal of Damage Mechanics*, 24(5):767–784, 2015. ISSN 15307921. doi: 10.1177/1056789514553042.

A

Damage accumulation models

A.1. Continuum mechanics based models after 1950

The continuum mechanics (intact geometry) models are based on the estimation of the occurrence of fracture after a pristine specimen has accumulated damage, whilst being modelled as intact continuum. Working from the initial proposal by Palmgren and Miner, academics have proposed variations on this model to improve the validity under VA load. This section presents the models chronologically.

Theory:	<i>Load dependent damage</i>	
Theory by:	CORTEN-DOLAN	year: 1954
Type:	Phenomenological, non-linear, continuum, spectral	
Typical application:	Variety of fatigue sensitive details under a variety of load histories, amongst which (random) VA loads	

The model by Corten and Dolan defines the expression of "harm" for CA loading as (A.1) with m the number of damaged nuclei (as a function of the maximum stress level), r the coefficient of damage propagation rate proportional to the stress level and a the damage propagation exponent and H the resulting "harm" (not "damage" as this indicates a normalised instead of absolute value). It should be noted that m and r are not explicitly used in the calculation, but are merely listed to be used in the derivation to the damage formulation.

$$H = mrn^a \quad (\text{A.1})$$

For a VA load history the harm per stress block is accumulated to the total harm. Failure occurs when:

$$H_{\text{accumulated}} = \sum_{i=1}^k m_i r_i n_i^{a_i} = H_{\text{crit}} = m_1 r_1 N_1^{a_1} \quad (\text{A.2})$$

Defining $D = H_{\text{accumulated}}/H_{\text{crit}}$ and assuming $m_i = m_1$ (as crack nuclei do not disappear) and $a_i = a_1 = a$ (constant crack size exponent, is an assumption made by Corten and Dolan) yields:

$$D = \frac{\sum n_p}{N_f} = \sum_{i=1}^k \frac{n_i}{N_1} \left(\frac{r_i}{r_1} \right)^{1/a} \leq 1 \quad (\text{A.3})$$

Using $\left(\frac{r_i}{r_1} \right)^{1/a} = \left(\frac{\sigma_i}{\sigma_{\max}} \right)^d$ (posing that the coefficient of the damage propagation rate is proportional to the stress level: an assumption made by Corten and Dolan and cited by Gao et al. and Liu et al.):

$$D = \frac{\sum n_p}{N_f} = \sum_{i=1}^k \frac{n_i}{N_1} \left(\frac{\sigma_i}{\sigma_{\max}} \right)^d \leq 1 \quad (\text{A.4})$$

For VA loading the critical damage is typically expressed as a function of the i -th applied stress level (i.e. stress range of the respective spectral stress-block) σ_i and the maximum applied stress level σ_{\max} in the load history. The exponent d is an empirical material constant that is typically assumed to be constant at 4.8 for HSS and 5.8 for others [15]. This value is fixed for all load histories. More recent research has shown that this d

varies with load spectra [12, 142, 151] and proposals for modifications are presented [42, 77, 151]. The core of these modifications is the combination of the effects of damage and stress state in the exponent d .

The essence of the incorporation of the load interaction effect originates from the presence the term $\left(\frac{\sigma_i}{\sigma_{\max}}\right)^d$ in the damage formulation. The damage per cycle depends on the current stress, and the maximum of the load history. This approach has also been applied by Rege and Pavlou [115] and Lv et al. [85].

Summarising the benefits and downfalls of the Corten-Dolan model:

- + Accounts for observed nonlinear development (nonconstant damage increment).
- + Incorporates a loading ratio $\frac{\sigma_i}{\sigma_{\max}}$ per stress block to account (partially) for load interaction effects by relating the i -th stress level to the maximum stress level: this is the major benefit over the LDAM. The factor resembles a relative mean stress correction, and is therefor not strictly a load interaction representation (as decently analysed in [77]).
- The empirical constant d is a challenge to define: and even physically incorrect due to the independence of load level and cycle ratio. The value for d is in fact spectrum dependent.

Theory:	<i>Power-law isostress damage curves</i>	
Theory by:	MARCO-STARKEY	year: 1954
Type:	Phenomenological, non-linear, continuum, spectral	
Typical application:	(Metal) samples with little to no load uncertainty, variety of multi-level loading conditions.	

In an attempt to remedy the deficiencies of the LDAM [34], Marco and Starkey [91] developed a power-law modification of the Palmgren-Miner model to capture the non-linear load dependent damage accumulation. It is presented by (A.5) with $C_i(\sigma_i)$ a material parameter related to the respective load level. This is the first known "Damage curve approach", which is an accumulation model where the damage rate depends on load level and/or cycle ratio. A damage curve introduces non-linearity to the LDAM by formulating a load dependent damage curve.

$$D = \sum_{i=1}^k \left(\frac{n_i}{N_i}\right)^{C_i(\sigma_i)} \leq D_{\text{crit}} = 1 \quad (\text{A.5})$$

This theory assumes a damage increment (dD/D) proportional to the percentage of life consumed (dn/n) under constant stress amplitudes [115], and thus produces curved damage lines instead of the linear ones by Palmgren and Miner.

The usability of this theory is unfortunately limited, due to the requirement to calculate C_i for each different loading condition (both order and relative amplitude can differ) separately. Related to the non-linear nature of (A.5) and the requirement to experimentally determine C_i for each loading condition σ_i , the calculation will be computationally expensive [155]. Marco and Starkey consider C_i larger than unity, but closer to unity (and thus to Palmgren-Miner) for more severe load histories, as concluded by Aslam [5]. No articles with expressions for $C_i(\sigma)$ were found in literature.

Summarizing the benefits and downfalls of the Marco-Starkey model:

- + Accounts for observed nonlinear development (nonconstant damage increment).
- Parameter C_i , per load level i , is to be determined experimentally: it is a challenge to decide on representivity of the empirical C_i for other loading conditions. Like in the model by Corten and Dolan it is a spectrum dependent parameter, but here it is directly applied to the fatigue life instead of to the loading ratio.

Theory:	<i>Double Linear Damage Theory (DLDT)</i>	
Theory by:	MANSON	year: 1966
Type:	Phenomenological, bi-linear, continuum, spectral	
Typical application:	Steel base material under (random) VA loads.	

To avoid the computationally extensive procedure of the cycle-by-cycle Marco and Starkey model, it is proposed to approximate the non-linear function from (A.5) by a two-stage linear damage theory.

This theory separates the crack initiation and crack propagation stage under CA loading. This two-stage linear damage theory was the basis for the DLDT by Manson in 1966 [89] as presented in (A.6) and (A.7). The value for P is obtained by curve-fitting experimental data. The exponent 0.6 is the result of earlier work, where the derivation of the amount of cycles required to propagate a 0.013 inch (=0.33 mm) crack to failure finds $4N_f^{0.6}$. Manson and Halford argue that the formulation $4N_f^{0.6}$ is empirical, but can be extended to other databases than the one used for the derivation.

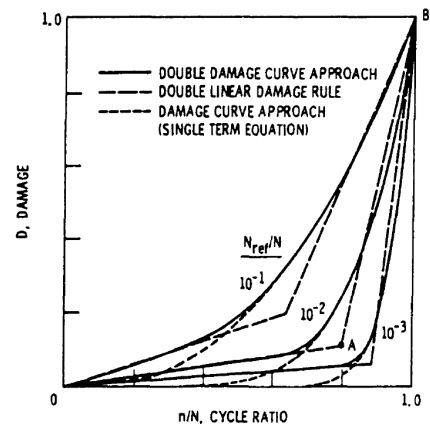


Figure A.1: Comparison of the DDCA with DLDT and DCA [88]

$$D_{init} = \sum_{i=1}^k \frac{n_i}{N_i - PN_f^{0.6}} \leq D_{crit,init} = 1 \tag{A.6}$$

$$D_{prop} = \sum_{i=1}^k \frac{n_i}{PN_f^{0.6}} \leq D_{crit,prop} = 1 \tag{A.7}$$

Manson and Halford developed this model further to the Damage Curve Approach (DCA) and Double Damage Curve Approach (DDCA) [87], as will be discussed in section A.2 as cracked geometry based models. For illustration figure A.1 shows the three theories and their difference.

The DLDT was successfully applied to offshore drilling top-drive tie-rods [57], where it proves to be consistently more conservative than the Palmgren-Miner model, because the Palmgren-Miner model overestimates the remaining life for components where the stress amplitude is decreasing. This finding is consistent with the results in [94].

Summarizing the benefits and downfalls of the Manson model:

- + By separating the crack initiation and propagation phase the nonlinear damage curve is bi-linear and does not require an empirical parameter: major benefit over the Marco-Starkey model.
- + Has been proven applicable and better than the LDAM for offshore drilling top-drive tie-rods (not a welded joint) by [57, 94].

Theory:	Modified Palmgren-Miner	
Theory by:	HAIBACH	year: 1970
Type:	Phenomenological, linear, continuum, spectral	
Typical application:	Wide variety of structures, including welded steel joints for maritime applications under (random) VA loads.	

As a modification to the Palmgren-Miner model that assumes no damage below the fatigue limit, Haibach proposed to extend the S-N curve below the fatigue limit with a line related to the slope of the Basquin relation of the original curve [48] by meas of $k_H = 2k - 1$. Adopting the Basquin relation yields the Haibach slope. This adds conservatism (but less than the Elementary Palmgren-Miner model from the previous section) to the Basic Palmgren-Miner model, as more damage is accumulated due to the removal of the infinite fatigue limit. However, it remains unknown how large this safety margin is, and whether the prediction will ultimately prove to be conservative or not [120].

See figure A.2 for a sketch of the relation between the linear intact geometry models with a close relation to the Palmgren-Miner model.

This Haibach-modification of the Palmgren-Miner model is incorporated in modern class codes and standards [27, 54, 55, 100].

Summarizing the benefits and downfalls of the Haibach model:

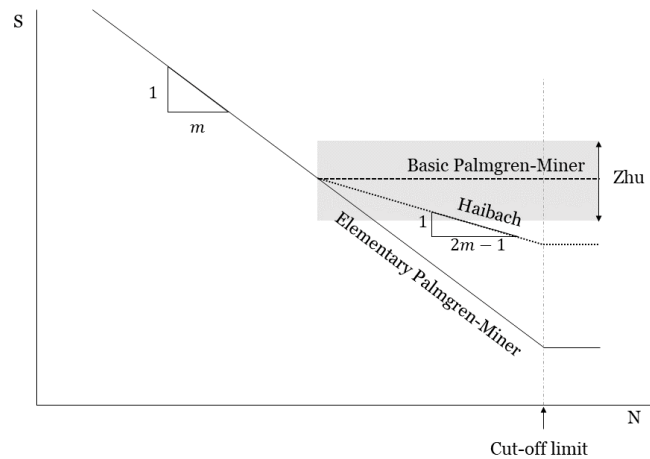


Figure A.2: Sketch of the S-N curves of the damage models closely related to the Palmgren-Miner model

- + Easy to implement.
- Does not solve the conceptual errors in Palmgren-Miner, it merely includes some of the low-stress amplitudes and their damaging nature.
- Does not model the observed non-linear nature of fatigue damage development.

Theory:	<i>Straight isodamage curves</i>	
Theory by:	SUBRAMANYAN	year: 1976
Type:	Phenomenological, non-linear, continuum, spectral	
Typical application:	Base materials subjected to (random) VA loads in the LCF and MCF region.	

The life curve modification model by Subramanyan [130] operates from the assumption, in line with Palmgren and Miner, that the S-N curve resembles a state of 100% fatigue damage [115]. Additionally there are combinations of stresses and amount of cycles below the endurance limit that resemble a state of 0% fatigue damage. Isodamage curves in between provide the gradual transition between both states.

The damage per load step i is given by (A.8), which poses the simplification of converging isodamage lines near the knee-point of the S-N curve. N_e is the endurance limit: the lifetime that corresponds with the transition of the sloped damage curves to the infinite lifetime. The damage is given as the ratio between the slope of an isodamage line through the point (n_i, σ_i) in the S-N diagram ($\tan\theta_i$), and the slope of the S-N curve ($\tan\theta_f$):

$$D_i = \left(\frac{\tan\theta_i}{\tan\theta_f} \right) = \left(\frac{\log N_e - \log n_i}{\log N_e - \log n_i} \right) \quad (\text{A.8})$$

The downfall of this isodamage curve is that it is contradicted [34, 130] by experimental data [50] that indicates that such isodamage lines converge near the knee point of the S-N curve. The work by [50] also showed the non-conservative nature of the approach by Subramanyan: the model predicts longer lifetimes than are observed from experiments. Also, Fatemi and Yang [34] point out that the method is not valid near the endurance limit due to the mathematical singularity at the knee-point. The use of a RFL would circumvent this.

Summarizing the benefits and downfalls of the Subramanyan model:

- Not valid near the endurance limit (HCF range), whereas HCF is typical for vessels. The use of a RFL would solve this issue.
- The isodamage curves that are not converging near the knee-point of the S-N curve are contradicted by experimental data.

Theory:	<i>Scaled Palmgren-Miner</i>	
Theory by:	SCHÜTZ	year: 1979
Type:	Empirical, linear, continuum, spectral	
Typical application:	Applications where the load spectrum is often similar (mechanical engineering applications, airplanes)	

The **RLDM** by **Schütz** [123], as presented in (A.9), incorporates the Palmgren-Miner model (4.6), but changes the critical damage D_{cr} based on experimental data of similar specific load histories. This allows a global incorporation of the **LI** and **LS** effects.

$$N_A = \frac{N_B \left(\sum \frac{n_i}{N_i} \right)_B}{\left(\sum \frac{n_i}{N_i} \right)_A} \quad (\text{A.9})$$

Here N_A and N_B are the predicted fatigue lives of respectively the unknown spectrum and the tested spectrum. $D_A = \left(\sum \frac{n_i}{N_i} \right)_A$ and $D_B = \left(\sum \frac{n_i}{N_i} \right)_B$ are the damage sums under the spectra of respectively the unknown and tested situations. Hereby the Schütz proposition is the **LDAM** with a safety factor [121].

A large downfall of this method is the challenge to prove the similarity of the measured dataset with the new sample. **Schütz** indicates this downfall as follows: "Considerable engineering judgement and a lot of experience will be necessary to avoid using this method in cases for which it is not suitable." [123]. Resulting, this method is not common in (the maritime) practise. It is however used in the work by **Leonetti et al.** in 2020 [75] to implicitly incorporate the **LI** and **LS** effects in the model.

Summarizing the benefits and downfalls of the Schütz model:

- + Incorporates the **LI** and **LS** effects implicitly.
- + Can be a beneficial combination with Hull Monitoring systems, as long as representivity of the load history can be assured.
- Requires representative measurements: the method is highly influenced by this experimental data.
- It models the fatigue damage increment as linear, which is physically incorrect.

Theory:	<i>Modified S-N curve</i>	
Theory by:	LEIPHOLZ	year: 1986
Type:	Physics-based, linear, continuum, spectral	
Typical application:	Metal base material under multi-level block-loading.	

Leipholz [70, 71] follows the trend initiated by **Freudenthal and Heller** [37] to replace the original S-N curve by a modified one. This modified S-N curve incorporates the life-reducing interaction effect. This modification resembles the approach by **Gassner**. The difference with the paper by **Freudenthal and Heller** is that damage increasing effect of high compressive loads is incorporated.

Initially, the **LDAM**-lifetime N is formulated as (A.10) with $\beta_i = n_i/N$ the life fraction per stress level. The subscript 0 is used in $N_{i,0}$ to express that the original S-N curve is used for the assessment.

$$\begin{aligned} N &= \left(\sum \frac{\beta_i}{N_{i,0}} \right)^{-1} \\ \frac{1}{N} &= \sum \frac{\frac{n_i}{N}}{N_{i,0}} \\ \frac{1}{N} &= \sum \frac{n_i}{NN_{i,0}} \\ D = 1 &= \sum \frac{n_i}{N_{i,0}} \end{aligned} \quad (\text{A.10})$$

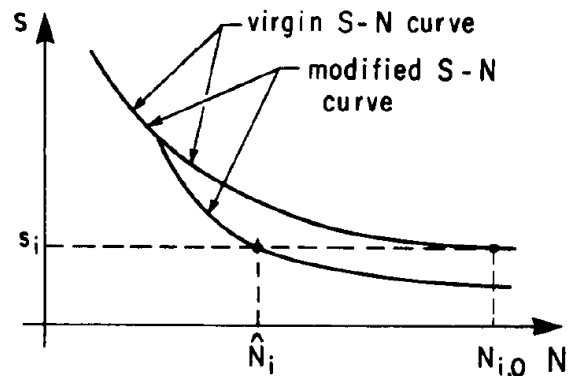


Figure A.3: Modified S-N curve by **Leipholz** [70]

The modification by Leipholz replaces this by (A.11). Figure A.3 shows the modified S-N curve that is captured in N'_i .

$$N = \left(\sum \frac{\beta_i}{N'_i} \right)^{-1} \quad (\text{A.11})$$

With β_i the frequency of cycles (n_i/N_{sum}) and N'_i the modified life at loading level σ_i .

N'_i is derived by solving (A.12) for measured datasets j . Per dataset the values for β_i are known, as well as the experimental life for this variable amplitude sequence $N^{(j)}$. That means that per stress block i in the sequence a variable amplitude test is required, in order to solve the system for \hat{N}_i . More datasets are to be used to verify the obtained predicted lifetime based on the previous datasets. It should be noted that all of these datasets have to be for the exact same block-load sequence.

$$N^{(j)} = \left(\sum_{i=1}^n \frac{\beta_i^{(j)}}{\hat{N}_i} \right)^{-1} \quad (\text{A.12})$$

The extension to stochastic loads is derived by Leipholz, of which the result is (A.13). Here p_i the probability distribution of damaging events with peak intensity s_i . For the derivation of this expected lifetime, see appendix B.3.

$$E(N) = \left(\sum_{i=1}^n \frac{p_i}{E\hat{N}_i} \right)^{-1} \quad (\text{A.13})$$

The paper by Zhang et al. [146] compares the Wöhler (Palmgren-Miner [95, 104]), Leipholz [70], and Chaboche [11] to the newly proposed model [146]. More on this model by Zhang et al. is included later. Their work properly illustrates the downfall of the Leipholz model by comparing measured data (on 41Cr4 steel under $R = -1$ with a set block-loading sequence for a compressor blade) to the results of the four models: the model accounts for the effects of low-amplitude loads, but neglects the effects of loading parameters. This effect describes the correlation between load parameters and damage accumulation by accounting for the non-linearity of the accumulation and the influence of the load variations (LS effect). Zhang et al. concludes that the relation between the loading conditions and the damage rate is of greater importance to address than the low-amplitude effect.

The results by Zhang et al. are for two steels for mechanical engineering applications: 40Cr and TL1114. The latter is a steel with max 0.14% carbon and a yield strength of 360 MPa [149]; these requirements that do not diverge significantly from those of EH36 (max 0.18% carbon and a yield strength of 355 MPa). 40Cr steel contains too much carbon to be properly welded in a shipyard, thus extrapolation of these results to EH36 welded joints is not recommended. For TL1114 this is concluded to be suitable.

Summarizing the benefits and downfalls of the Leipholz model:

- + The extension to stochastic loads allows a proper and cheap incorporation of the respective load spectra.
- Does not account for the non-linear nature of fatigue damage accumulation.

Theory:	<i>Bounded residual fatigue life estimation</i>	
Theory by:	BEN-AMOZ	year: 1999
Type:	Phenomenological, non-linear, continuum, spectral	
Typical application:	Two-stage loading, mild steel base material, extended to creep-fatigue interaction models	

The work by Ben-Amoz provides not an explicit model, but justifies the use of bounds on the fatigue life estimation. Initially the work presents the formulation by Subramanyan as lower and the LDAM by [95, 104] as upper bound. This is justified by two assumptions:

- Damage curves constitute a family of curves of which the base S-N curve is a member.
- Damage curves form a non-intersecting family of curves.

Working from the assumption that damage curve converge to the endurance limit (i.e. fatigue limit), which is captured in the formula from [130]:

$$\frac{n_2}{N_2} = 1 - \left(\frac{n_1}{N_1}\right)^\alpha \tag{A.14}$$

With:

$$\alpha = \log\left(\frac{N_2}{N_e}\right) / \log\left(\frac{N_1}{N_e}\right) \tag{A.15}$$

It should be noted that (A.14) can be rewritten to the damage equation (only valid for a two-stage block load):

$$D = \left(\frac{n_1}{N_1}\right)^\alpha + \frac{n_2}{N_2} = 1 \tag{A.16}$$

The second step in the work is the separation of the crack initiation and crack propagation phase, as was proposed by Manson.

Figure A.4 shows the research results of Ben-Amoz. The first two figures present for a low-high and high-low sequence respectively the datapoints: proving that the mean value per dataset falls within the bounds (indicated by solid lines). The paper also discusses the bounds on the scattered data, which are derived based on the standard deviation of the dataset. Figure A.4c shows in dashed lines the bounds for the total data scatter, and in solid lines the bounds for the mean values.

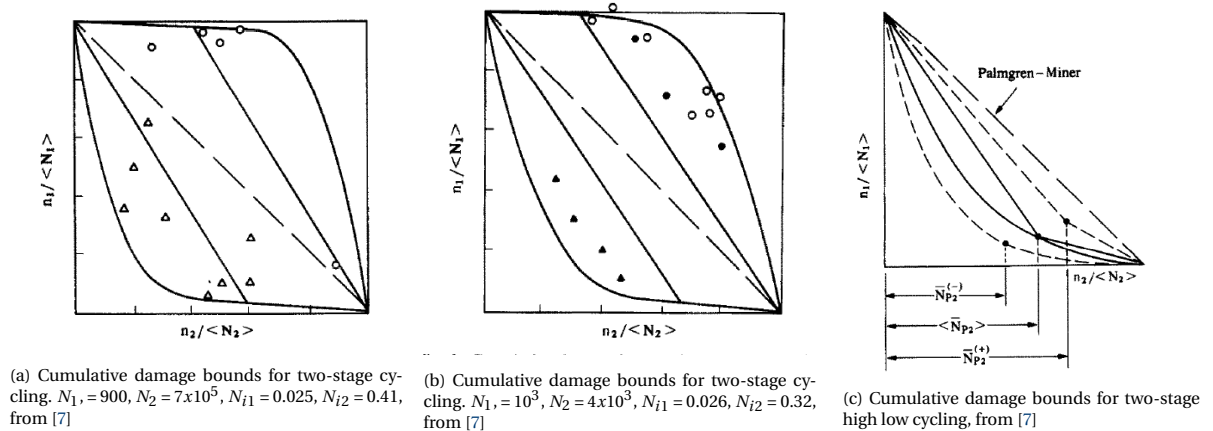


Figure A.4: Research results from Ben-Amoz

An interesting find of this research is that it substantiates the common assumption that the scatter in cumulative damage tests is mainly due to the scatter in the crack-initiation cycles: which is observed from the larger scatter on the left side of the diagram in figure A.4c.

Unfortunately the applicability under (random) VA loads has not (yet) been validated.

Summarizing the benefits and downfalls of the Schütz model:

- + Is suitable for the extension to reliability analyses by presenting bounds on the fatigue life.
- Has only been proved valid for two-stage block loading.
- The scatter in the fatigue life (uncertainty) is large, for the method binds the fatigue life by two models.

Theory:	<i>Sequential law</i>	
Theory by:	MESMACQUE	year: 2005
Type:	Phenomenological, non-linear, continuum, temporal	
Typical application:	(random) variable amplitude loads, multi-axial fatigue of welded joints	

The model as proposed by Mesmacque et al. [94], uses the Wöhler curve as the basis. Working from the hypothesis that for an equal physical state of damage the fatigue life is only dependent on the loading conditions, the model "walks" over the Wöhler curve to calculate per cycle the damage. This makes it a time-domain based model. The sequential law needs the full Wöhler curve, whereas this is in practise based on measurements that only reflect a part of the curve. The curve is approximated by the Basquin relation ($\sigma = aN^b$) over the whole domain. This model incorporates the loading history by means of the calculation of the actual damage per cycle, instead of per stress range.

An outstanding aspect of this model is that the damage is expressed in terms of the stress rather than the lifetime. However, as both are linked by means of the Wöhler curve, the method is still deemed to be of the continuum type.

The method is expressed by (A.17) for the initial load and by (A.18) for all successive loads. Here σ_{edi} is the damage stress (the corresponding admissible stress level at the $N_i - n_i$ life), σ_i is the actually applied stress and σ_u is the ultimate stress. σ_{equiv} is the damage equivalent stress level at level $i + 1$.

$$D_i = \frac{\sigma_{edi} - \sigma_i}{\sigma_u - \sigma_i} \quad (\text{A.17})$$

$$D_i = \frac{\sigma_{edi} - \sigma_i}{\sigma_u - \sigma_i} = \frac{\sigma_{equiv} - \sigma_{i+1}}{\sigma_u - \sigma_{i+1}} \quad (\text{A.18})$$

Due to the time-domain calculation of the damage the method is considered to be computationally expensive. Secondly, the time record of the stresses should be present, in practise this is usually in the form of a spectrum.

A great benefit is that the method uses the Von-Mises stress, making it relatively easy to expand the model to a multi-axial analysis. The latter is outside of the scope of this thesis.

Continuing on the work by Aïd et al. [4], Benkabouche et al. [8] proposed a method to account for random loading conditions, based on the S-N curve [119]. The work by Benkabouche incorporates the damage per load level according to the formula by [94]. The main contribution that adds value compared to [94] is the development of a numerical tool to perform the calculations and the analysis of multi-axial loads.

A large downfall of this method is the temporal (and thus expensive) nature of the calculation procedure.

Summarizing the benefits and downfalls of the Mesmacques model:

- + Allows the relatively cheap expansion to multiaxial fatigue: addressing further uncertainty sources in fatigue life-assessment.
- Requires a temporal (and thus expensive) calculation procedure.

Theory:	<i>Thermodynamic entropy-based model</i>	
Theory by:	NADERI	year: 2010
Type:	Physics-based and Empirical, non-linear, continuum, temporal	
Typical application:	(random) VA loading histories	

The hypothesis by Naderi et al. [98] is that the entropy generation is directly associated with the evolution of fatigue damage. The cumulative entropy is a measure of the fatigue damage. Failure occurs when the cumulative entropy reaches the **Fatigue Fracture Entropy (FFE)**. This is expressed as (A.19). The first term resembles entropy generation due to plastic deformation, the second entails the entropy generation due to

heat conduction. For HCF and MCF typically the sum of both terms is to be used, for LCF only the plastic deformation term suffices as it dominates the summation for LCF.

$$\gamma = \int_0^{N_f} \left(\frac{\Delta W_p}{T(N)} \right) dN + \int_0^{N_f} \left(\frac{k}{T(N)^2} \cdot \text{grad } T(N) \right) dN \quad (\text{A.19})$$

At fracture this yields $\gamma = \gamma_f$. The temperature is a function of the amount of cycles, as is experimentally determined per material. ΔW_p is the total plastic energy difference, T is the temperature, N the number of cycles, k the thermal conductivity. The total plastic energy is calculated as $W_p = \sigma : \dot{\epsilon}_p$ ¹.

The essence of the method is in the statement that the FFE is independent of the amplitude and the frequency of load, the geometry of the specimen, and the type of fatigue load. This is supported by experimental results [76, 97].

Fruitful implementations (and minor modifications) by others are in [58, 76, 96]. Jang and Khonsari [58] provide an analytical approach to determine the FFE, with the modification to properly consider the contribution of internal friction. Liakat and Khonsari [76] prove the validity of the FFE by comparing experimental and analytical results. Lastly Mozafari et al. [97] provide an integrated calculation method in the FE software Abaqus, as well as the confirmation of the validity of the method for uniaxial random loading. The criterion that Mozafari et al. uses is the FFE formulation from (A.19) for LCF.

It should be noted that this criterion, with "fracture" listed in the formulation, is considered as a continuum domain model. This is because the fracture is not modelled as a crack, but it is used to express the fatigue damage. Secondly, it is not a (continuum) damage domain criterion as the damage does not affect future damage development: the material is modelled as an intact continuum until fracture.

Summarizing the benefits and downfalls of the Naderi et al. model:

- + Has been proven valid for random loading.
- + The criterion is independent of the characteristics of the load spectrum.
- + Only requires experimentally determined material constants: allowing relatively few experiments.
- The criterion is conceptually quite different from the currently applied models at the shipyard's practise.

Theory:	<i>Fuzzy logic modification of the LDAM</i>	
Theory by:	ZHU	year: 2011
Type:	Phenomenologic, linear, continuum, spectral	
Typical application:	Steel base material	

Zhu et al. proposed to improve the Miner model by considering the LS effects in addition to the damage and strengthening mechanisms of low amplitude loads [150]. The proposed model adds the strengthening and damaging of the material at low amplitude loads to the Palmgren-Miner summation as is shown in (A.20). Here m' is the strengthening coefficient as is related to the material properties (to be obtained from experimental data), σ_i is the stress level that, on the Wöhler curve, matches with the amount of cycles n_i . $\mu_{\tilde{D}}(\sigma_i)$ is the membership function of the fuzzy set \tilde{D} and has a different formulation for stresses above and below the fatigue limit.

$$D = \sum_{i=1}^k \frac{n_i}{N_i} + \sum_{i=k+1}^r \frac{\frac{\exp(m'\sigma_i)}{m'\sigma_i} [1 - \exp(-m'\sigma_i n_i)] \mu_{\tilde{D}}(\sigma_i)}{N_0} = 1 \quad (\text{A.20})$$

The fuzzy logic modification of the LDAM was tested for normalised 45 steel with two-step block and multi-level (uniaxial) loading.

Figure A.2 shows the sketch of the intact geometry based models with a close relation to the Palmgren-Miner model, to relate the method by Zhu et al. to the elementary and basic Palmgren-Miner models as well as the Haibach modification.

¹The mathematical operator $x : y$ equals the derivative of the dependent variable $x(y)$ to y .

Summarizing the benefits and downfalls of the Zhu 2011 model:

- + Has been proven valid for multilevel loads.
- Does not account for the non-linear nature of fatigue damage evolution.

Theory:	Modified Corten-Dolan	
Theory by:	CORTEN-DOLAN modified by GAO	year: 2015
Type:	Empirical and Phenomenological, non-linear, continuum, spectral	
Typical application:	Steel base material	

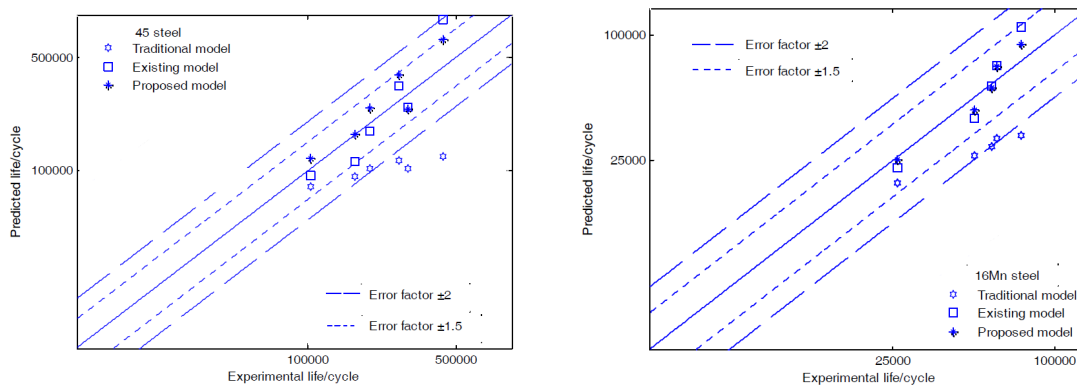
The study by Gao et al. [42] concludes that the original Corten-Dolan model provides less accuracy than the Palmgren-Miner model, whereas the modification as proposed by Gao et al. provides an equal or higher accuracy compared to the Palmgren-Miner model. The modification (originating from a paper with the same co-author Huang [154]) is presented in (A.22), where γ is the material constant that can be derived from experimental data and the criterion of fatigue failure. It therefore resembles the nature of the original d from (A.21). In blue the addition compared to the original model is indicated. The proposed model operates from the assumption that fatigue failure is influenced by both the degree of damage and the stress conditions, in a sense that d increases if the load increases, as a function of the cycle ratio. It should be noted that this work is only verified for two-step block loading, and recommendations for test on multi-level and random loading are reported.

$$D = \frac{\sum n_p}{N_f} = \sum_{i=1}^k \frac{n_i}{N_1} \left(\frac{\sigma_i}{\sigma_{\max}} \right)^d \leq 1 \quad (\text{A.21})$$

$$d = \exp \left(\left(\frac{n_i}{N_i} \right)^{\sigma_i / \sigma_{\max}} \right) + \gamma \quad (\text{A.22})$$

The use of γ in (A.22) is to express the dependency of the damage exponent of the material. Gao et al. thus assumes that the material poses a shift of the exponent.

Figure A.5 shows the research results from Gao et al. with the data from [124]. From this it is concluded that the improved model [42] can predict fatigue life more accurately than the traditional Corten-Dolan's model for normalized 45 steel, normalized 16 Mn steel, and hot-rolled 16 Mn steel. In [124] the comparison is also made with the Palmgren-Miner model. The research by Gao et al. indicates that the improved model is more accurate than the Palmgren-Miner model: for the Corten-Dolan model and considered modifications the errors are, in contrary to the Palmgren-Miner model, all within 50% [42].



(a) Comparisons of experimental and fatigue lives for normalized 45 steel as assessed using the three different models, from [42]

(b) Comparisons of experimental and fatigue lives for normalized 16 Mn steel as assessed using the three different models, from [42]

Figure A.5: Research results from Gao et al., comparing the traditional Corten-Dolan model [15], the existing model by Zhu et al. [151] and the proposed model by Gao et al. for two steel types.

Summarizing the benefits and downfalls of the modified Corten-Dolan model:

- + Incorporates a loading ratio $\frac{\sigma_i}{\sigma_{\max}}$ per stress block.
- + Accounts for load interaction effects: major benefit over LDAM.
- + Empirical d is now phenomenological ...
- ... but still requires empirically fitted parameters.

Theory:	<i>Natural logarithm cycle-by-cycle damage curve</i>	
Theory by:	ZUO	year: 2015
Type:	Phenomenological, non-linear, continuum, spectral	
Typical application:	Two-step block loads on (metal) base material	

The basis of the work by [Zuo et al.](#) is the determination of the equivalent number of cycles, yielding the same fatigue driving stress as the actual load history [155], hereby addressing the problems with the load history.

The work is captured in (A.23) with $\beta_i = n_i / N_i$, which is the expended life fraction at the respective loading stress. Combining this with the LDAM modification from [91], it provides a less computationally expensive model than other non-linear models [119].

$$D = \sum_{i=1}^n \beta_i \frac{\ln N_i}{\ln N_1} = 1 \quad (\text{A.23})$$

The verification of the model is however not very extensive. The main recommendation from [Zuo et al.](#) is to conduct further research on the load interaction and load sequence effects on fatigue life under random load spectra. A second recommendation is to also test for more complex loading histories than two-step block loads.

Summarizing the benefits and downfalls of the Zuo model:

- + Allows spectral, relatively cheap, approach.
- Has not (yet) been proven valid for multilevel and stochastic loads.

Theory:	<i>One-parameter damage curve</i>	
Theory by:	REGE-PAVLOU	year: 2017
Type:	Phenomenological, non-linear, continuum, spectral	
Typical application:	Two-block loading	

Operating from the assumption that the isodamage curves converge at the knee point of the Wöhler curve, [Rege and Pavlou](#) [115] proposed a one parameter model to capture the non-linear damage as accumulated in the material [115]. The researchers proceed here from the work by [Marco and Starkey](#) and [Subramanian](#) [91, 130], but add an exponent to the tangential formulation. The proposed damage formulation is:

$$D_i = \left(\frac{\tan \theta_i}{\tan \theta_f} \right)^{q(\sigma_i)} = \left(\frac{\log N_e - \log N_i}{\log N_e - \log n_i} \right)^{q(\sigma_i)} \quad (\text{A.24})$$

The $q(\sigma_i)$ exponent is to be derived from measurements. [Rege and Pavlou](#) propose for the four tested steel-types (SAE 4130, C-35, P355NL1 and 300 CVM maraging steel) to use (A.25), but warn for ruthless extrapolation to other materials. Of the tested materials P355NL1 has the closest resemblance to EH36.

$$q(\sigma_i) = (a\sigma_i)^b = \left(\frac{2\sigma_i}{\sigma_s} \right)^{-0.75} \quad (\text{A.25})$$

This model is not in line with the statement by [Schijve](#) that a one-parameter description does not suffice [121]. However, the results by [Rege and Pavlou](#) show a satisfying (and even closer than [94, 95, 104, 124]) agreement with experimental data of four different steel types [115]. The agreement is comparable to the results with the DLDT by [89].

Figure A.6 shows the research results by [Rege and Pavlou](#), providing the decent fit of the proposed model to the data. It is compared to [Shang and Yao](#) [124], [Mesmacque](#) [94], [Subramanian](#) [130] and the DLDT [89]. The dataset is from [Pereira et al.](#) [108].

Summarizing the benefits and downfalls of the Rege-Pavlou model:

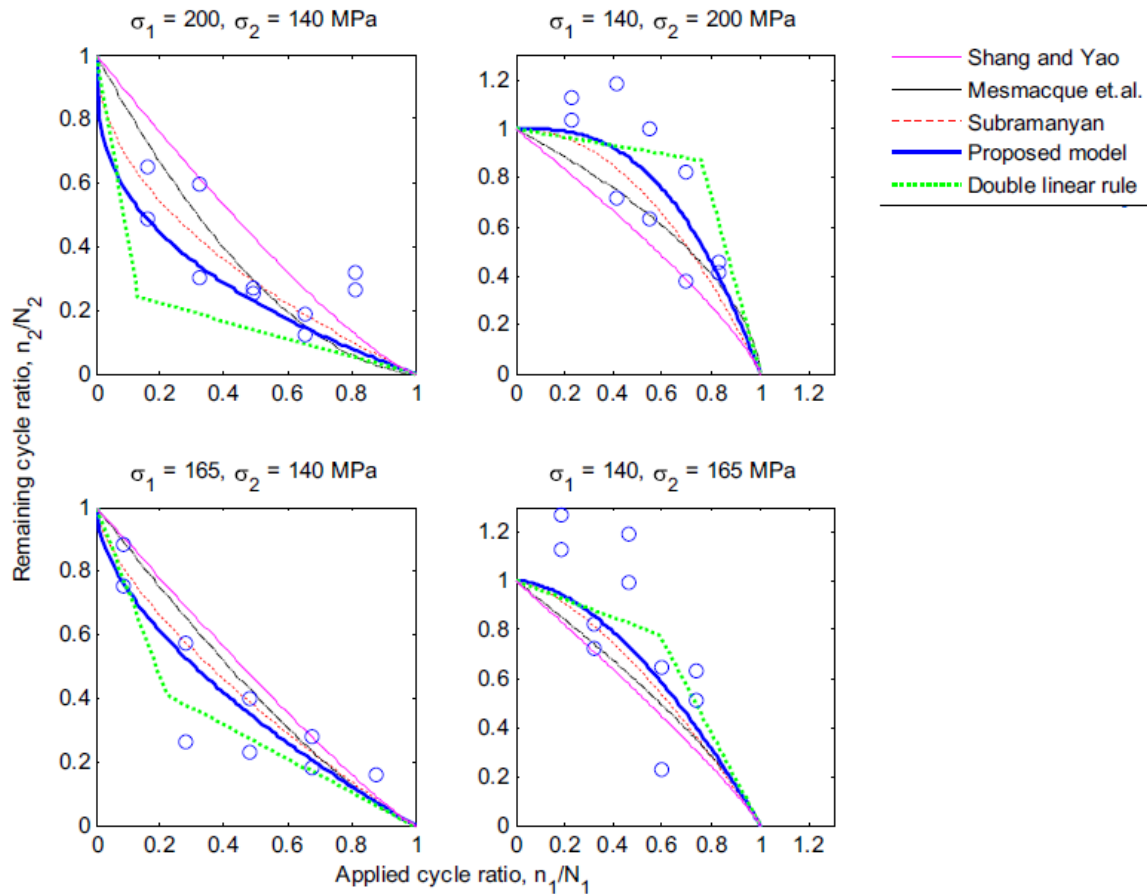


Figure A.6: Comparison of predicted fatigue life with experimental data for two-step cyclic loading of P355NL1 steel, from [115]

- Has not (yet) been proven valid for multilevel and stochastic loads.

Theory:	<i>S-N Fatigue damage envelope</i>	
Theory by:	PAVLOU	year: 2018
Type:	Phenomenological, non-linear, continuum, spectral	
Typical application:	Two-block loading of (metal) base materials	

Before the work of Pavlou [107] the non-linear damage models that base themselves on the S-N curves assume straight isodamage lines (with exception of the work by Rege and Pavlou [115]), of which Pavlou proves the straight nature to be incorrect by derivation in [107].

The proposal by Pavlou is to use curved isodamage lines in the S-N curve plot and to accumulate the damage done per stress block according to the to-rate damage curve. Figure A.7a shows an example of a four-stage stress history that adds to the damage done through the isodamage curve accumulation.

The isodamage curves from figure A.7a are derived using finite element analysis (see figure A.7b). Coloured damage zones and non-linear isodamage lines within the S-N fatigue damage envelope are obtained using the analogy of the isodamage lines with the temperature distribution through a material due to conduction heat transfer. The paper by Pavlou uses a designated ANSYS package to do so.

This S-N fatigue damage envelope approach proves to have an excellent agreement [107] with two-stage fatigue loaded specimens from literature [87]. Note that this data from [87] is for SAE4130 steel, which is a HSS.

Summarizing the benefits and downfalls of the Pavlou model:

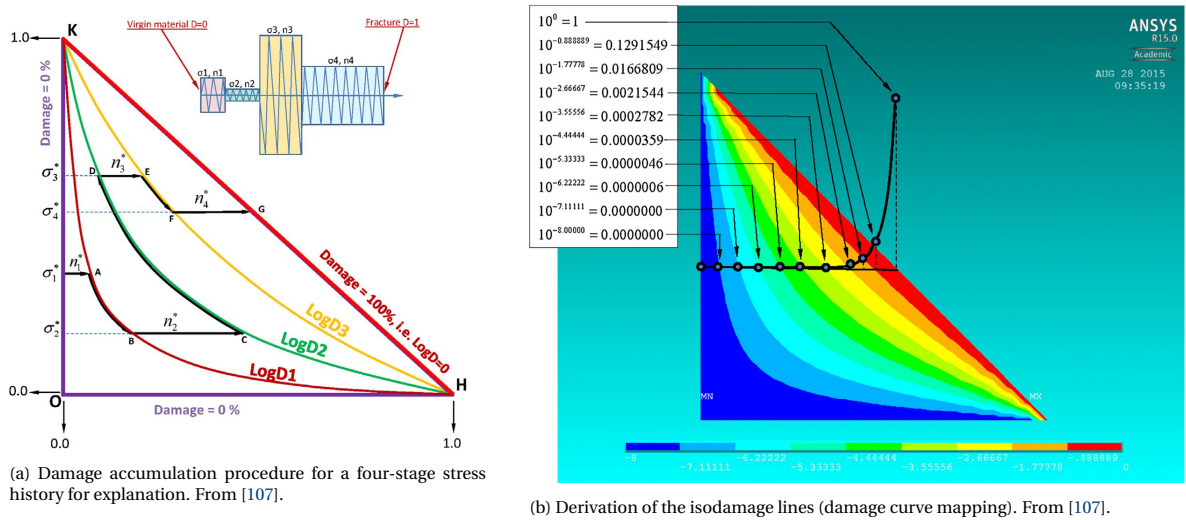


Figure A.7: S-N Fatigue damage envelope by Pavlou, illustration of the concept.

- Has not (yet) been proven valid for multilevel and stochastic loads.

Theory:	Modified Rege-Pavlou: Isodamage curves	
Theory by:	ZHU	year: 2019
Type:	Phenomenologic, non-linear, continuum, spectral	
Typical application:	(random) block and spectrum loading	

The paper by [Zhu et al. \[153\]](#) provides a modification of the damage model by [Rege and Pavlou](#) by explicitly incorporating the *LS* effect and the load weighted coefficient (R_{lr}) using an effect factor.

The model by [Zhu et al.](#) is presented in (A.26) with $\epsilon_{a,i}$ the strain amplitude at load-step i , l the load sequence weighted coefficient and s the load weighted coefficient. l and s characterise the respective contributions of these two aspects on the fatigue damage accumulation and can be determined by fitting the data of two-block loading fatigue tests. For P355NL1 steel this yields $l = 3.49$ and $s = 0.512$.

$$q(\sigma_i) = l \log(n_i) + s \log(\epsilon_{a,i}) \quad (A.26)$$

The damage is than expressed in the same manner as in the model by [Rege and Pavlou](#):

$$D_i = \left(\frac{\tan \theta_i}{\tan \theta_f} \right)^{q(\sigma_i)} = \left(\frac{\log N_e - \log N_i}{\log N_e - \log n_i} \right)^{q(\sigma_i)} \quad (A.27)$$

Figure A.8 provides the research results by [Zhu et al.](#) for the random loading condition on P355NL1 steel. It shows that for the newly developed model the predicted lifetimes all fall within a life factor of ± 2 to the experimental data.

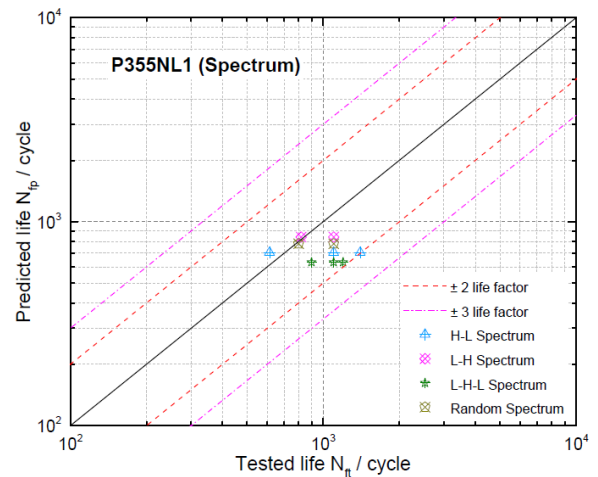


Figure A.8: Comparisons between tested lives and predicted lives of P355NL1 under spectrum loadings, from [152].

The model is cited in the review articles by [Jimenez-Martinez](#) and [Mozafari et al.](#).

Summarizing the benefits and downfalls of the [Zhu 2019](#) model:

- + Has been proven valid for (random) block and spectrum loads, although with a limited dataset.

- + Has a smaller error for the tested sequences than the models by Mesmacque et al., Subramanian, Manson and Halford and Rege and Pavlou.
- Does not have a physical foundation.

Theory:	Modified Corten-Dolan	
Theory by:	LIU	year: 2020
Type:	Phenomenological, non-linear, continuum, temporal	
Typical application:	Multi-level loads applied to steel and aluminium base materials.	

Continuing on the work by Gao et al., and following the train of thought from [141], Liu et al. [77] further updated the d formulation (Corten-Dolan exponent) per stress block, see (A.28).

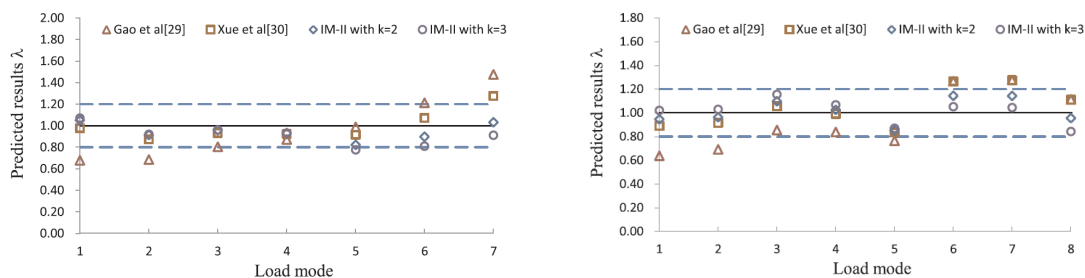
$$d_k = \left(\frac{\sigma_i}{\sigma_{i-1}} \right)^k \left\{ \exp \left(\frac{n_i}{N_i} \right) + \gamma \right\} \quad (\text{A.28})$$

This formulation is based on the following phenomena:

- The term $\exp \left(\frac{n_i}{N_i} \right)$ represents the effect of the damage state on the damage rate.
- The term $\left(\frac{\sigma_i}{\sigma_{i-1}} \right)^k$ represents the stress ratio between two consecutive load levels, to take the load interaction effect into account.

γ is, like in the theory by Gao et al., an empirical material-related constant. The exponent k is 0,1,2 or 3: the best fitting integer is selected for further use. For the considered materials the exponent $k = 2$ provides the best fit.

Figure A.9 presents the research results from Liu et al., showing the small scatterband of the novel model compared to the ones by Gao et al. and Xue et al..



(a) Comparison of predicted results for normalized 45 steel based on Scheme-I, from [77]

(b) Comparison of predicted results for hot rolled 16Mn steel based on Scheme-I, from [77]

Figure A.9: Research results from Liu et al., comparing three different models [42, 77, 141] for two steel types.

This novel method provides satisfactory results for five materials (Hot rolled 16Mn steel, Normalised 45 steel, Al2024-T42, Normalised 16Mn steel and Al6082-T6), but extrapolation to other materials is not recommended without further tests. The random load case was not part of the scope, whereas multilevel loads were. It should also be noted that this theory has only been tested for base material, not for welded joints.

Summarizing the benefits and downfalls of the Liu model:

- + Has been proven valid, and better than the model by Gao et al., for multilevel loads.
- Requires a temporal, computationally expensive, procedure to account of the load interaction effects.

A.2. Fracture mechanics based models

All operating from the assumption that the fatigue life is governed by the crack growth. For welded joints the assumption that the welding procedure yields a detail of which the crack initiation period is consumed, is typically adopted.

Theory:	<i>Paris relation: stable crack growth region</i>	
Theory by:	PARIS-ERDOGAN	year: 1963
Type:	Empirical, non-linear, fracture, temporal	
Typical application:	(residual) life time estimation of welded joints, where LEFM assumption is valid	

Paris and Erdogan [105] were the first to observe the approximately log-log linear relation between the crack tip stress intensity factor K_I and the crack growth rate da/dn in the stable crack growth region. The relation is presented in (A.29). This relation is a typical tool employed to estimate the residual fatigue life. It is only valid for weld toe notch defects, as the crack should be observed visually. The method assumes a stable crack growth (**LEFM**) until the through-thickness crack (or critical crack length) is obtained. In reality the last part of the crack development will be unstable crack growth due to the deteriorated geometry and the stress redistribution in the cracked material.

$$\frac{da}{dn} = C \cdot \Delta K_I^m \quad (\text{A.29})$$

$$N_g = \frac{1}{C \cdot \Delta \sigma_s^m} \cdot \int_{a_i}^{t_p} \left(\frac{1}{(Y_n(a) \cdot Y_f(a) \cdot \sqrt{\pi a})^m} \right) da \quad (\text{A.30})$$

To assess the (residual) life time under **VA** loading conditions, the term $\Delta \sigma_s$ has to be exchanged for the equivalent stress. To translate the temporal signal to a spectrum typically a rain-flow counting algorithm is employed. In Appendix C.1.1 the derivation of the equivalent stress for a spectrum that is separated into load-blocks, based on a summation of intercepts of the S-N curve is presented.

The work by Ciavarella et al. [14] provides a decent analysis of the relation between the Paris relation (and other crack propagation models) and the **LDAM**. The paper concludes that the reason of the deviation of fatigue life predictions using the **LDAM** might originate from its use in context involving the connection between crack initiation and crack propagation laws (which provides an unconservative damage estimate) and the sequence effects - in particular the **OL**'s - in long crack propagation (which provides a conservative damage estimate).

Summarizing the benefits and downfalls of the Paris relation:

- + Easy to integrate into an inspection regime, allowing to estimate the residual fatigue life.
- Sensitive to the initial crack length, typical application is residual life time estimation upon the inspection of a present crack.
- Does not account for **LI** and **LS** effects.
- Requires the, computationally expensive, temporal method.

Total life concept

The total life concept combines the life times spent in the crack initiation N_i and crack growth N_g domain:

$$N = N_i + N_g \quad (\text{A.31})$$

Here the crack initiation contribution is obtained from an intact-geometry (continuum) assessment.

Theory:	<i>Damage Curve Approach (DCA) and Double Damage Curve Approach (DDCA)</i>	
Theory by:	MANSON-HALFORD	year: 1981
Type:	Phenomenological, non-linear, fracture, temporal	
Typical application:	Multi-level block loads	

Richart and Newmark [116] were the first to introduce the concept of the damage curve, which means that the damage to cycle ratio relation depends on the applied stress per step. Proceeding on this concept Manson and Halford [87] proposed the DCA. Here the the damage is given as a function of the crack length a . The effects of load sequences under two-level loading are explained very well by this model [41]. However, it does not account of load interaction effects.

The damage is defined as (A.32) for a multi-level block load spectrum with i stress blocks, based on the crack growth derivation as is presented in [88]. It should be noted that this equation is based on inches instead of the metric system. The method is sensitive to the value of the initial crack length a_0 . In [51] the initial crack length a_0 is assumed to be zero.

$$D = \frac{1}{0.18} \left(a_0 + (0.18 - a_0) \beta_i^{\frac{2}{3} N_i^{0.4}} \right) \quad (\text{A.32})$$

$$\beta_i = \left[\left[\left(\frac{n_1}{N_{f1}} \right)^{\alpha_{1,2}} + \frac{n_2}{N_{f2}} \right]^{\alpha_{2,3}} + \frac{n_3}{N_{f3}} \right]^{\alpha_{3,4}} + \dots + \frac{n_{i-1}}{N_{f(i-1)}} \right]^{\alpha_{i-1,i}} + \frac{n_i}{N_{fi}} \quad (\text{A.33})$$

With:

$$\alpha_{i-1,i} = \left(\frac{N_{i-1}}{N_i} \right)^{0.4} \quad (\text{A.34})$$

Here the exponent $\alpha_{i-1,i}$ includes a hint of the block-equivalent of the load interaction effect: the exponent is a function of the amount of cycles of the previous stress block. It is called a "hint of" as the load interaction effect is not explicitly related to the amount of cycles. This is also the part of the equation that requires the temporal approach (analysis per stress block, instead of per spectrum block). The exponent 0.4 is attained by curve fitting of a three-level block loading in [87]. For other loading histories and spectra this value requires further testing.

For two-block loading this yields (A.35).

$$\left(\frac{n_1}{N_{f1}} \right)^{(N_{f1}/N_{f2})^{0.4}} + \frac{n_2}{N_{f2}} = 1 \quad (\text{A.35})$$

Double Damage Curve Approach (DDCA)

The DDCA models the damage curve as two linear and non-linear lines, as is shown in figure A.1, this is in contrary to the DCA which models one continuous non-linear relation between cycle ratio and damage. The difference with the DCA is the separation of the crack initiation (linear) and crack propagation phase (non-linear). For the initiation phase it closely resembles the DLDT, and in the propagation phase the DCA. When the life is related to a reference life (typically 1), the equation is given by:

$$D = \frac{n_i}{N_i} \left(q_1^\gamma + (1 - q_1^\gamma) \left(\frac{n_i}{N_i} \right)^{\gamma(q_2 - 1)} \right)^{\frac{1}{\gamma}} \quad (\text{A.36})$$

With

$$q_1 = \frac{0.35 \left(\frac{N_{ref}}{N_i} \right)^\alpha}{1 - 0.65 \left(\frac{N_{ref}}{N_i} \right)^\alpha} \quad (\text{A.37})$$

And

$$q_2 = \left(\frac{N_i}{N_{ref}} \right)^\beta \quad (\text{A.38})$$

The parameters and their typical values are:

γ Constant that represents two intersecting straight lines, typical value is 5.

α Material dependent parameter, to be determined experimentally. Typical value is 0.25.

β Material dependent parameter, to be determined experimentally. Typical value is 0.4.

Coefficients 0.35 and 0.65 should be experimentally validated for each material and loading history.

Summarizing the benefits and downfalls of the **DDCA** by Manson and Halford:

- + The method allows to create identical damage curves for different loads by employing the reference life N_{ref} [44].
- + The **DDCA** provides a better fit with the experimental data than the **DCA** as it better mimicks the different damage rates for crack initiation and propagation.
- For each loading history and material the coefficients 0.35 and 0.65 should be validated. This raises the challenge of defining equivalence in loading history.

Theory:	<i>Equivalent driving force (fatigue driving stress)</i>	
Theory by:	KWOFIE-RAHBAR	year: 2011
Type:	Phenomenological, piece-wise linear, fracture, temporal	
Typical application:	Metal base material subject to different loading conditions (varying R_{lr})	

With the origin in the work of **Kwofie and Chandler** [65], the paper by **Kwofie and Rahbar** [66] presents the derivation of the equivalent driving force for crack growth at different stress ratios R_{lr} . As **Zuo et al.** explains it: "The fatigue driving stress is a function of the applied cyclic stress, numbers of loading cycles, and the numbers of cycles to failure. It increases with loading cycles until the fatigue strength is reached when fracture occurs. By determining the equivalent number of cycles that yields the same fatigue driving stress as the previous loads, the remaining life can be predicted." This is presented in (A.39) with σ_{ar} the equivalent completely-reversed stress amplitude, σ_a the combined stress amplitude, α the mean-stress-sensitivity factor of the material, and R the stress ratio. The α indicates how sensitive the crack growth behaviour is to changes in the R ($= \sigma_{min} / \sigma_{max}$)

$$\sigma_{ar} = \sigma_a \exp\left(\alpha \left(\frac{1+R}{1-R}\right)\right) \quad (\text{A.39})$$

This equivalent stress assuming a constant growth rate.

$$\frac{da}{dN} = C_0 (\Delta K_0)^{m_0} = C_0 (\Delta K_R)^{m_0} \exp\left[am_0 \left(\frac{2R}{1-R}\right)\right] \quad (\text{A.40})$$

$$D = \sum \frac{n_i \ln(N_i)}{N_i \ln(N_1)} \quad (\text{A.41})$$

Load sequence effects are included by relating the damage of each stress (block) to the fatigue life of the first damaging block N_1 .

Summarizing the benefits and downfalls of the **Kwofie-Rahbar** model:

- + Accounts for **LS** effects.
- + Accounts for different R levels.
- Does not account for the non-linear nature of the accumulation.
- Requires an (computationally expensive) temporal calculation.

Hectors and de Waele [51] provide a decent comparison between the models by **Palmgren** and **Miner**, **Manson and Halford**, **Gao et al.**, **Kwofie and Rahbar** and **Mesmacque et al.**. The testcase of the paper is for a overhead crane runway girder: a different loadcase than frigate. The comparison is presented in table A.1, and it shows that the model by **Palmgren-Miner** performs the worst, based on the assessment of 12 H-L and 12 L-H two-stage block loadings at different load levels: it has the largest standard deviation and **Root Mean Square (RMS)** values. The best performing model is the **DCA** by **Manson and Halford**. Another observation is the fact that the average **Palmgren-Miner** critical damage is 1.10, with a standard deviation of 0.31. This indicates a normal distribution, in contrary to the log-normal distribution with $\mu = 1$ and $\sigma = 0.3$ from [27].

The paper by **Hectors and de Waele** also provides the insight that, for the considered multi-block sequences, the random load case damage is approximately the average of the H-L and L-H multi-block sequences. That

Table A.1: Research results from [Hectors and de Waele](#) for two-stage block loading for a combination of H-L and L-H sequences. Each value is given as an expression of $D_{\text{crit}} = N_{\text{predicted}}/N_{\text{experiment}}$.

Model	Average	Standard deviation	RMS
Miner	1.10	0.31	0.27
DCA[87]	1.05	0.22	0.21
[41]	1.06	0.23	0.21
[66]	1.09	0.27	0.24
[94]	1.06	0.24	0.22

means that the results from table A.1 can roughly be extrapolated to random block loads.

Theory:	<i>Modified DCA (Manson-Halford)</i>	
Theory by:	GAO	year: 2014
Type:	Phenomenological, non-linear, fracture, temporal	
Typical application:	Multi-level block loading histories for steel welded joints.	

The work by [Gao et al.](#)[41] is based on [87], but claims to be improved as it includes load interaction effects as well. Does not require extensive testing [115].

[Gao et al.](#) poses the implementation of the damage coefficient as proposed by [Xu et al.](#) [140], who suggested to modify the exponent parameter to include load interaction. Modification suggested is to have a different formulation for H-L than for L-H sequences:

$$\alpha_{i-1,i} = \left(\frac{N_{f(i-1)}}{N_{fi}} \right)^{0.4 \cdot \min\{\sigma_{i-1}/\sigma_i, \sigma_i/\sigma_{i-1}\}} \quad (\text{A.42})$$

This idea behind this modification is not new, the interaction factors with similar purpose have been proposed in [15, 37]. Secondly, it should be noted that the model by [Gao et al.](#) is not strictly a damage accumulation model (observation by [Hectors and de Waele](#)), as it does not accumulate damage from zero to one. [Gao et al.](#) sets failure at β_i (see (A.33)) equals 1, which does not have a physical background. [Manson and Halford](#) set failure at $D = 1$. As [Gao et al.](#) is the first to implement the model by [Xu et al.](#) to express the predicted fatigue life, this model is listed under the name of [Gao et al.](#) instead of [Xu et al.](#).

Finally, the method has been validated for two-level loading by [Gao et al.](#), and for multi-level block loading by [Hectors and de Waele](#). Both papers recommend further testing of (random) VA load histories.

Summarizing the benefits and downfalls of the Gao (2014) model:

- Requires an (expensive) temporal calculation.
- The expression of failure does not have a physical meaning.
- Has only been validated for multi-level block loads but not for random VA loads.

A.3. (Continuum) Damage mechanics based models

Continuum Damage Mechanics (CDM) describes the deteriorating material at continuum level, compared to the expensive procedure of modelling micro-mechanics. This deterioration is typically expressed as a reduced Young's modulus. The first work on CDM is the paper by [Kachanov](#) from 1958 [60], where it was applied to creep. The damage variable $0 < \phi < 1$ is used to describe the defect density where $\phi = 1$ equals no damage.

Damage mechanics based models are widely employed in the structural analysis of composites, as an effective Young's-modulus is used to express the capacity of the composite's elements.

Another typical application of CDM is for the assessment of corrosion fatigue as in the PhD thesis by [Zhang](#) [145]. Assuming a uniform degradation of the material due to corrosion, the analogy with the damage variable is made.

For the assessment of fatigue of welded joints under (random) VA loading is not common. The assessment of the fatigue life under VA loading is typically based on a local assessment in contrary to on a global basis. For the overview, this section contains the main models with regards to fatigue assessment based on CDM.

Theory:	<i>Cyclic hardening</i>	
Theory by:	XIAODE	year: 1987
Type:	Phenomenological, non-linear, damage, spectral	
Typical application:	Two-level block loads	

[Kachanov](#) [60] was the first author to introduce the effective stress as part of the constitutive equations in line with the hypothesis of equivalent strain. This can be used to analyse the effect of the previous damage on the novel stress field. The effective stress is typically expressed as:

$$\bar{\sigma} = \frac{\sigma}{1 - D} \quad (\text{A.43})$$

The damage variable D is expressed in a linear relation to the Young's modulus E :

$$D = 1 - \phi = 1 - \frac{\bar{E}}{E} \quad (\text{A.44})$$

Thereafter [Xiaode et al.](#) defines the three properties of continuum damage mechanics fatigue damage, and propose the damage evolution law (A.45):

1. A damage variable is introduced in cyclic stress-strain relation for the description of the fatigue process.
2. The value of the damage variable for a large load must not be smaller than that for a small load at the same number of cycles.
3. A cumulative damage law may be derived from the damage evolution equation.

$$D = \left(\frac{N}{N_f} \right)^{1/\beta + n'} \quad (\text{A.45})$$

(A.45) possesses properties 1 and 2. Property 3 is answered to by means of (A.46) for two-level block loading.

$$\frac{N_2}{N_{f2}} = 1 - \left(\frac{N_1}{N_{f1}} \right)^{(\beta_2 + n')(\beta_1 + n')} \quad (\text{A.46})$$

The cyclic hardening rate β from (A.47) is obtained by a least squares fit of experimental data to determine the constants a and b .

$$\beta = a \left(\frac{\Delta\sigma}{2} \frac{\Delta\epsilon_p}{2} \right)^b \quad (\text{A.47})$$

The model by [Xiaode et al.](#) was validated for two-level block loading and is listed in review articles [34, 119].

Summarizing the benefits and downfalls of the Xiaode model:

- + Upon fitting the parameters with experimental data, the model is easy to implement.
- The model has only been validated for two-level block loading.

Theory:	<i>Continuum damage accumulation</i>	
Theory by:	CHABOCHE-LESNE	year: 1988
Type:	Phenomenological, non-linear, damage, spectral	
Typical application:	(random) VA loading histories	

Addressing the linear life-stress relation in the Palmgren-Miner approach, [Chaboche and Lesne](#) [11] proposed a model based on continuum damage accumulation, the **Non-linear Continuous fatigue Damage (NLCD)** model. Whereas Palmgren-Miner is lacking a physical background, this one is derived from a physical basis.

The model has a close relation to the model by [Marco and Starkey](#) and the **DCA** by [Manson and Halford](#). Assuming that the fatigue behaviour is a continuum process and that damage accumulates continuously until failure, [Chaboche and Lesne](#) derived a differential equation to express the fatigue damage as a function of the amount of loading cycles [11]. It is based on the phenomenological model as was presented by [Chaboche](#) in 1974 [10] and is summarised with (A.48). Here D is the damage that is consistent with $1 - \phi$ from the **CDM**, β , a , M_0 and b_0 are coefficients from the model that are material dependent, σ_a is the maximum minus the mean tensile stress, and σ_m is the mean tensile stress.

$$dD = \left[1 - (1 - D)^{\beta+1} \right]^\alpha \left[\frac{\sigma_a}{M_0(1 - b_0\sigma_m)(1 - D)} \right]^\beta dN \quad (\text{A.48})$$

Here α equals:

$$\alpha = 1 - a \left\langle \frac{\sigma_{\max} - \sigma_f(\sigma_m)}{\sigma_u - \sigma_{\max}} \right\rangle \quad (\text{A.49})$$

With:

$$\sigma_f(\sigma_m) = \sigma_m + \sigma_f^\infty(1 - b_0\sigma_m) \quad (\text{A.50})$$

- $\langle x \rangle$ indicates the condition: if $x < 0$, $\langle x \rangle = 0$, else $\langle x \rangle = x$
- σ_f^∞ The fatigue limit at $R = -1$.
- σ_u Ultimate strength.
- $\sigma_f(\sigma_m)$ The fatigue limit for a non-zero mean stress.

Integration yields the formulation of the damage D :

$$D = 1 - \left(1 - \left(\frac{N}{N_f} \right)^{\frac{1}{1-\alpha}} \right)^{\frac{1}{\beta+1}} \quad (\text{A.51})$$

With:

$$N_f = \frac{1}{(\beta + 1)(1 - \alpha)} \left(\frac{\sigma_a}{M_0(1 - b_0\sigma_m)} \right)^{-\beta} \quad (\text{A.52})$$

Upon careful tuning of the parameters a , β , M_0 and b_0 for the respective material, [Chaboche and Lesne](#) state that the novel model is as simple to use as the **LDAM**.

The paper by [Zhang and Maddox](#) compares the model by [Chaboche and Lesne](#) to the modifications as they propose, experimental data, and [70]. The model by Chaboche outperforms the **LDAM** and the model by [Leipholtz](#) for the two considered loading histories. The analysis is performed for loads that are typical for shafts and axles in aerospace applications: extrapolation to maritime loadcases should be done with care.

The article by [Silitonga et al.](#) concludes that the model by [Chaboche and Lesne](#) as a simple engineering tool that does not offer a significant advantage compared to the **LDAM**, but provides a first and important step

towards more advanced CDM models.

Summarizing the benefits and downfalls of the Chaboche model:

- + The model is as easy to implement as the LDAM.
- Inadequate formulation for complex loading (OL's and UL's) [126].
- Limited improvement compared to the LDAM [126].
- The model will always be conservative as it counts every load cycle, regardless of the amplitude [146].

Theory:	Continuum damage accumulation	
Theory by:	LEMAITRE	year: 1999
Type:	Physics-based, non-linear, damage, temporal	
Typical application:	Multi-axial fatigue. fatigue of steel welded joints under VA block loading	

The proposal by Lemaitre [73] comprises a two-scale micro-meso continuum model. Here micro-plasticity and micro-damage are accounted for, which both are known to characterise HCF. As in HCF the damage and plasticity do not influence the elastic macro behaviour before the actual fracture stage [73]; hence this model captures the fatigue up to macro-crack initiation. Crack initiation is defined at $D = D_{crit}$. For HCF the model proves to decently capture the physics related to the high cycles like mean stress effect, non-linear damage accumulation, initial strain hardening and the non-proportional loading for bi-axial fatigue [73].

This model is a typical development for HCF in metals [126]. The work by Lautrou et al. [67] poses the fatigue crack initiation life estimation for steel welded joints by means of the model by Lemaitre et al.. For this the assumption of occurrence of elastic shakedown², related to the residual stress distribution in the material, is used to employ the two-scale model from [73]. This justifies elastic calculations for the Representative Volume Element (RVE) that is used to model the damaged continuum. The RVE is presented in figure A.10 where the superscript μ indicates microscopic properties. The work by Lautrou et al. does consider variable amplitude loading, but this is a composed succession of CA cycle-blocks.

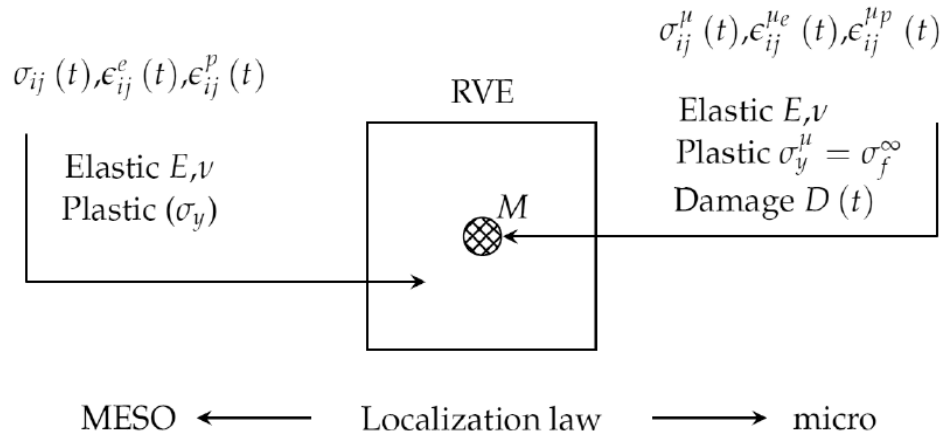


Figure A.10: Representation of the Representative Volume Element, figure from [72]

The fatigue damage rate (damage per cycle) is expressed as:

$$dD = \left[\frac{(\sigma_{eq} + k\sigma_f)^2 R_v^\mu}{2ES(1+k)^2(1-D)^2} \right]^s \frac{d\sigma_{eq}}{C(1+k)} \quad \text{if } \sigma_{eq} \geq \sigma_f \quad (\text{A.53})$$

With the triaxiality function on microscopic level:

$$R_v^\mu = \frac{2}{3}(1+\nu) + 3(1-2\nu) \left[\frac{\sigma_H(1+k)}{\sigma_{eq} + k\sigma_f} \right]^2 \quad (\text{A.54})$$

²"A structure made of elastic plastic material in a given loading scheme, after an initial stage of possible limited plastic deformation (of finite total plastic dissipation), may eventually shake down to some residual stress state, from which it subsequently responds elastically (and, hence, safely) to the external agencies." [13]

And σ_{eq} is the Von-Mises equivalent stress, k is a material parameter defined as $k = 3aE/2C$, a is the localisation coefficient, C the kinematic hardening parameter at microscale, E the Young's modulus and D the resulting damage. An important assumption in the model by [Lemaitre et al.](#) is that fatigue damage is only accumulated for stresses above the fatigue limit. σ_H is the hydrostatic³ stress at mesoscale (equal to the hydrostatic stress at microscale) and ν is the Poisson ratio of the respective material.

Summarizing the benefits and downfalls of the Lemaitre model:

- + Relatively easy extension to multi-axial fatigue.
- The model requires, the computationally expensive, temporal approach.
- Only crack initiation is modelled, whereas the welding procedure typically consumes this part of the fatigue life.
- No damage below the fatigue limit.
- Requires the, computationally expensive, temporal approach do properly consider load interaction effects.

Theory:	<i>Uniaxial cumulative model</i>	
Theory by:	SHANG-YAO	year: 1999
Type:	Physics-based and empirical, non-linear, damage, spectral	
Typical application:	Multi-level block loads of steel base material	

[Shang and Yao \[124\]](#) propose a cumulative damage model, based on the philosophy of [Chaboche and Lesne](#). The addition from [Shang and Yao](#) is to incorporate the energy dissipation in the model, to express the exponent of $(1 - D)$. See (A.55) for the equation of the damage rate dD . The exponent is given by (A.56) with H the Heaviside function, a and b are material constants to be obtained from curve-fitting of experimental data, K is a material constant under uniaxial CA loading. The strain hardening model is used ($\Delta\sigma/2 = K(\Delta\epsilon/2)^n$) is used to express the effects of multiple repetitive cycles on the hardening of the material.

$$dD = (1 - D)^{\alpha(\Delta\epsilon/2, \sigma_m)} \left[\frac{K(\Delta\epsilon/2)^n}{M_0(1 - b'\sigma_m)} \right]^\beta dN \quad (\text{A.55})$$

With:

$$\alpha(\Delta\epsilon/2, \sigma_m) = 1 - \frac{H(K(\Delta\epsilon/2)^n - \sigma_{-1}(1 - b\sigma_m))}{a \ln |K(\Delta\epsilon/2)^n - \sigma_{-1}(1 - b\sigma_m)|} \quad (\text{A.56})$$

Ultimately, the expression of the total fatigue life is give by (A.57).

$$N_f = aM_0^\beta \frac{\ln |K(\Delta\epsilon/2)^n - \sigma_{-1}(1 - b\sigma_m)|}{H(K(\Delta\epsilon/2)^n - \sigma_{-1}(1 - b\sigma_m))} \left[\frac{K(\Delta\epsilon/2)^n}{1 - b'\sigma_m} \right]^{-\beta} \quad (\text{A.57})$$

The model is validated for CA and two-level block loading, where it provides a better correspondence with experiments than the model by [11]. In [115] the model is discussed as a simple model that accounts for the mean stress. The work by [Zhu et al.](#) also compares the LDAM and a novel model to the model by [Shang and Yao](#): the fuzzy sets model from [150] outperforms the model by [Shang and Yao](#) for multi-level block loads.

Summarizing the benefits and downfalls of the Shang-Yao model:

- + Relatively easy to implement.
- + The model only requires experimentally determined material constants, no spectrum-constants.
- The model has only been validated for multi-level block-loading programs.
- The model was outperformed by [Zhu et al. \[150\]](#) for multi-level block-loads.

³In contrary to the convention in maritime technology to consider hydrostatic stress as a part of the loading conditions of a maritime structure, hydrostatic stress is also called the volumetric stress: a continuum mechanics concept that includes uniaxial stresses, but no shear stresses. The latter is indicated here.

Theory:	<i>CDM based model</i>	
Theory by:	DATOMMA	year: 2006
Type:	Physics-based and empirical, non-linear, damage, temporal	
Typical application:	Multi-level block loads applied to steel samples (but not to welded joints)	

A variation of the concept by [Chaboche and Lesne](#) is proposed by [Dattoma et al.](#) [18] where the expression for α as is given in (A.49) is modified to include an exponent in the stress term, see (A.58).

$$\alpha = 1 - a \left\langle \frac{\sigma_{a,i} - \sigma_f}{\sigma_u - \sigma_{a,i}} \right\rangle^d \quad (\text{A.58})$$

Here d is the exponent as proposed by [Dattoma et al.](#). This parameter is a material constant, to be determined experimentally. This novel model accounts for the material damage evolution at different load levels by not using the maximum minus the mean stress like the model by [Chaboche and Lesne](#), but by employing the actual stress level σ_a . Experimental fatigue data for hardened and tempered steel verified the model and show good agreement of the predicted and experimental fatigue life.

Summarizing the benefits and downfalls of the Datomma model:

- + Accounts for load interaction effects.
- Requires the, computationally expensive, temporal calculation.
- Has only been validated for multi-level block loads.

Theory:	<i>Strength degradation model based on Manson-Halford</i>	
Theory by:	YUAN	year: 2015
Type:	Phenomenological, non-linear, damage, temporal	
Typical application:	Fatigue reliability	

In the model by [Yuan et al.](#) [144] both the demand and capacity are expressed as a normal distribution with a given mean and standard deviation. The overlapping area of capacity and demand poses the expression of the probability of an unsafe structure. Strength degradation is expressed as a function of the amount of cycles. For this [Yuan et al.](#) proposes the residual strength δ_R evolution:

$$A_i = \frac{\delta_{R_i}(n_i)}{\delta_{R_{i-1}}(n_{i-1})} \quad (\text{A.59})$$

This function gives the expression of the residual strength degradation coefficient at stress σ_i , where $\delta_{R_i}(n_i)$ is the residual strength after n_i cycles at this stress level. This residual strength is expressed as:

$$\begin{aligned} \delta_{R_k}(n_k) &= A_0 \times A_1 \times A_2 \times \dots \times A_k \times \delta_{(0)} \\ &= \frac{\delta_{R_1}(n_1)}{\delta_{R_0}(n_0)} \times \frac{\delta_{R_2}(n_2)}{\delta_{R_1}(n_1)} \times \frac{\delta_{R_3}(n_3)}{\delta_{R_2}(n_2)} \times \dots \times \frac{\delta_{R_i}(n_i)}{\delta_{R_{i-1}}(n_{i-1})} \times \delta_{(0)} \\ &= \frac{\delta_{R_i}(n_i)}{\delta_{R_0}(n_0)} \times \delta_{(0)} \end{aligned} \quad (\text{A.60})$$

Expressing the residual strength evolution A for a certain stress level k , under the assumption that $A_{(k)} = A_0 \times A_1 \times A_2 \times \dots \times A_k$ and by using the recursion formulas, yields:

$$A_{(k)} = \left[1 - \frac{(1+b) \sum_{i=1}^k \sigma_i^c n_i}{\delta_{(0)}^{1+b}} \right]^{\frac{1}{1+b}} \quad (\text{A.61})$$

In the above function b and c are dimensionless parameters, related to the material and environmental conditions (e. g. temperature, wave loading spectrum, ...).

This yields per summation:

$$\delta_{R_k}(n_k) = \left[1 - \frac{(1+b) \sum_{i=1}^k \sigma_i^c n_i}{\delta_{(0)}^{1+b}} \right]^{\frac{1}{1+b}} \times \delta_{(0)} \quad (\text{A.62})$$

To now make the link to the fatigue life prediction the expression of the residual strength degradation coefficient A is introduced to express the residual strength degradation function ϕ_i (which Yuan et al. calls γ_i).

$$\phi_i = \exp \left[\alpha \cdot \left(\frac{1}{A_i} - 1 \right) \right] \quad (\text{A.63})$$

Proceeding from Manson-Halford, as modified by Xu et al. [140] and implemented by Gao et al. [41], the model by Yuan et al. multiplies the equation by Gao et al. with the residual strength degradation function ϕ_i :

$$D(n_i) = \phi_i \left(\frac{n_i}{N_{fi}} \right) \left(\frac{N_{f(i-1)}}{N_{fi}} \right)^{0.4 \min \left\{ \frac{\sigma_{(i-1)}}{\sigma_i}, \sigma_{(i-1)} \right\}} \quad (\text{A.64})$$

Summarizing the benefits and downfalls of the Yuan model:

- + Shows a good agreement with the multi-level block-loading that was tested.
- Requires the (computationally expensive) temporal calculation.

Theory:	<i>Chaboche and Lesne model with fuzzy logic</i>	
Theory by:	ZHANG	year: 2018
Type:	Phenomenological, non-linear, damage, temporal	
Typical application:	(random) VA loading histories, has only been validated for base materials.	

The research by Zhang et al. [146] proposes, as a modification to the Chaboche method, to incorporate fuzzy logic to describe the transition from stress ranges that do and do not contribute to the damage. The research shows that the Cauchy Membershipfunction (MF) provides the best fit in life prediction, whereas it still proves to be conservative for the applied testcase (a compressor blade). The improvement for this test-case is a relative error between the predicted life and measured data of respectively {35.18%, 16.09%, 8.38%} for the {Linear Palmgren-Miner model, Non-linear Chaboche model, Modified Chaboche model}. This results should be observed with care dependent on the case it is applied to, but show a promising picture for the modified Chaboche model.

Dependent on the relation of the respective load level σ_i to the lower limit of the strengthening stress σ_F and the fatigue limit σ_0 , the MF equals:

$$\mu_{\bar{D}}(\sigma_i) = \begin{cases} 0 & \sigma_i \in [0, \sigma_F) \\ \frac{1}{1 + \alpha'(\sigma_i - \sigma_F)^{-\beta'}} & \sigma_i \in [\sigma_F, \sigma_0) \\ 1 & \sigma_i \in [\sigma_0, +\infty) \end{cases} \quad (\text{A.65})$$

Even with the fuzzy logic modification the Chaboche model is slightly conservative, compared to measured samples: this is because it counts all load cycles in the damage accumulation, regardless of the amplitude. The fuzzy logic model is proven better than the original Chaboche model [146].

Summarizing the benefits and downfalls of the Zhang model:

- + Provides a predicted life time that is very close to the experimental life time.
- Requires the computationally expensive temporal approach.

B

Cited derivations

Note: all derivations as presented in this appendix are not by the hand of the author of this thesis, but citations (or elaborated versions of the citations) of the respective articles. They are presented here for clarity and completeness.

B.1. Miner's physical derivation of the LDAM

The derivation by Miner [95] of the LDAM is based on the principle of cyclic work. Cyclic work is the area between the path of stress and strain that is formed under cyclic loading and unloading. Miner employs this principle to derive the cumulative damage of a set of stress-blocks. Damage is defined as the fraction of work consumed, assuming a certain amount of work W_{failure} cumulatively consumed at failure, see (B.1).

$$D = \frac{W_n}{W_{\text{failure}}} \quad (\text{B.1})$$

Thermodynamic work for a set of n cycles at stress level σ is defined as:

$$W_n = W(\sigma, n) \quad (\text{B.2})$$

Assuming that the work of cycles with identical amplitudes is the same, this is expressed as:

$$W_n = nW(\sigma) \quad (\text{B.3})$$

It should be noted that this assumption neglects the LI and LS effects, underlining the main setback of the LDAM. Substitution in (B.1) yields:

$$D = \sum_{i=1}^k \frac{n_i W(\sigma_i)}{W_{\text{failure}}} \quad (\text{B.4})$$

Where, by denoting the number of cycles at stress level σ_i as N_i , the thermodynamic work for failure at this level is defined as:

$$W_{\text{failure}} = N_1 W(\sigma_1) = N_2 W(\sigma_2) = N_i W(\sigma_i) \quad (\text{B.5})$$

Substitution of (B.5) in (B.4) equals:

$$D = \sum_{i=1}^k \frac{n_i W(\sigma_i)}{N_i W(\sigma_i)} = \sum_{i=1}^k \frac{n_i}{N_i} \quad (\text{B.6})$$

B.2. Palmgren-Miner consistency with Fracture Mechanics

This derivation is first given in [86], and was cited by [45].

Using the Paris law (B.7). This limits the validity of the derivation to the Paris regime.

$$\frac{da}{dN} = C (\Delta K)^m \quad (\text{B.7})$$

With SIF K equal to the stress conditions adjacent to the crack tip. For an infinite plate subjected to an in-plane uniform stress, σ , perpendicular to a central through-thickness crack of length $2a$ this is:

$$K = Y \sigma \sqrt{\pi a} \quad (\text{B.8})$$

Here Y is a correction factor as a function of the crack geometry and the geometry of the considered sample. Substituting (B.8) into (B.7), yields (B.9).

$$\frac{da}{dN} = C (Y \Delta \sigma \sqrt{\pi a})^m \quad (\text{B.9})$$

Of which integration yields:

$$\int_{a_1}^{a_2} \frac{da}{(Y \sqrt{\pi a})^m} = C (\Delta \sigma)^m N \quad (\text{B.10})$$

Now, for an example of three stress blocks, this yields the following equations.

$$\left. \begin{aligned} \int_{a_i}^{a_1} \frac{da}{(Y \sqrt{\pi a})^m} &= CS_1^m n_1 \\ \int_{a_i}^{a_2} \frac{da}{(Y \sqrt{\pi a})^m} &= CS_2^m n_2 \\ \int_{a_2}^{a_f} \frac{da}{(Y \sqrt{\pi a})^m} &= CS_3^m n_3 \end{aligned} \right\} \quad (\text{B.11})$$

Assuming the final crack sizes of respectively each stress block and the total loading history, a_i and a_f , to be known this rewrites to (B.12) per stress block.

$$\int_{a_i}^{a_f} \frac{da}{(Y \sqrt{\pi a})^m} = CS_1^m N_1 = CS_2^m N_2 = CS_3^m N_3 \quad (\text{B.12})$$

As an example, for the first stress block, the division of the actual over the maximum load history yields:

$$\int_{a_i}^{a_1} \frac{da}{(Y \sqrt{\pi a})^m} / \int_{a_i}^{a_f} \frac{da}{(Y \sqrt{\pi a})^m} = \frac{CS_1^m n_1}{CS_1^m N_1} = \frac{n_1}{N_1} \quad (\text{B.13})$$

Summing the contributions of all stress blocks yields (B.14), proving the compatibility of the LDAM with an Linear Elastic Fracture Mechanics (LEFM) approach.

$$\frac{n_1}{N_1} + \frac{n_2}{N_2} + \frac{n_3}{N_3} = \frac{\left\{ \int_{a_i}^{a_1} \frac{da}{(Y \sqrt{\pi a})^m} + \int_{a_1}^{a_2} \frac{da}{(Y \sqrt{\pi a})^m} + \int_{a_2}^{a_f} \frac{da}{(Y \sqrt{\pi a})^m} \right\}}{\int_{a_i}^{a_f} \frac{da}{(Y \sqrt{\pi a})^m}} = 1.0 \quad (\text{B.14})$$

B.3. Leipholz derivation

This derivation is taken from the paper by Leipholz [70].

The derivation uses two axioms:

If f is a random variable and $E[f]$ is its expected value, than:

$$E[\sum_i a_i f_i] = \sum_i a_i E[f_i]$$

and

$$E[\prod_i f_i] = \prod_i E[f_i]$$

The damage per stress block i equals $D_i = n_i d_i$, with n_i the amount of cycles at this stress level, and d_i the damage per cycle at this stress level.

By definition $n_i = p_i N$, with p_i the probability of occurrence of a cycle with peak intensity s_i and N the total fatigue life.

By now applying the axioms:

$$E[D] = \sum_i E[D_i] = \sum_i E[n_i]E[d_i] = \sum_i E[p_i]E[N]E[d_i] = E[N] \sum_i E[p_i]E[d_i] \quad (\text{B.15})$$

Now stating the total damage as a physical constant: $D = \hat{N}_i d_i$ for any i . The expected value of this damage equals $E[D] = E[d_i]E[\hat{N}_i]$.

Substitution of the previous equations in (B.15) provides the final value of the expected damage:

$$E(N) = \left(\sum_{i=1}^n \frac{p_i}{E\hat{N}_i} \right)^{-1} \quad (\text{B.16})$$

B.4. Leonetti derivation

Leonetti et al. operates from the formulation of the SIF by as given:

$$\Delta K = M_w(a)Y(a)\Delta\sigma\sqrt{\pi a} \quad (\text{B.17})$$

To express the crack size a as a function of the amount of cycles the relation by Forman-Mettu is used:

$$\frac{da}{dn} = C\Delta K^m \left(1 - \frac{\Delta K_{th}}{\Delta K} \right)^p$$

(Which is non-trivial for $p > 0$, hence $p = 0$ is used)

$$\begin{aligned} &= C(M_w(a)Y(a)\Delta\sigma\sqrt{\pi a})^m \\ &= C(\Delta\sigma\sqrt{\pi})^m (M_w(a)Y(a)\sqrt{a})^m \end{aligned} \quad (\text{B.18})$$

$$\begin{aligned} \text{Adopting } Y(a) = Y \text{ makes } \frac{da}{dn} &= C(Y\Delta\sigma\sqrt{\pi})^m (M_w(a)\sqrt{a})^m \\ &= B(M_w(a)\sqrt{a})^m \end{aligned}$$

Here $M_w(a)$ is given by:

$$M_w(a) = \max\left(C_\alpha \left(\frac{a}{T}\right)^\alpha, 1\right) \quad (\text{B.19})$$

Assuming that the critical condition occurs for $M_w(a) > 1$, a is expressed as $\left(\frac{M_w(a)}{C_\alpha}\right)^{1/\alpha} T$.

Integration of both sides for the initiation to the current amount of cycles N_k , whilst assuming $Y(a) = Y = \text{constant}$, and m and C as material constants yields:

$$C_\alpha^{-m} T^{\alpha m} \int_{a_{ini}}^{a_k} a^{-m(\alpha+1/2)} da = C(Y\Delta\sigma\sqrt{\pi})^m \int_0^{N_k} dn = B \int_0^{N_k} dn = BN_k \quad (\text{B.20})$$

Of which the general solution reads:

$$a_k = \left(\frac{B}{C_\alpha^{-m} T^{\alpha m}} N_k [1 - m(\alpha + 1/2)] + a_{ini}^{1-m(\alpha+1/2)} \right)^{\frac{1}{1-m(\alpha+1/2)}} \quad (\text{B.21})$$

By performing the same integration, but now for the initiation to the total amount of cycles N (i.e. integrating over the total fatigue life), yields:

$$C_\alpha^{-m} T^{\alpha m} \int_{a_{ini}}^{\infty} a^{-m(\alpha+1/2)} da = C(Y\Delta\sigma\sqrt{\pi})^m \int_0^{N_k} dn = B \int_0^N dn = BN \quad (\text{B.22})$$

Stating that $-m(\alpha + 1/2) < -1$ ensures that the infinite integral over a gives a finite answer. The solution equals:

$$C_{\alpha}^{-m} T^{\alpha m} \frac{1}{1-m(\alpha+1/2)} [a^{1-m(\alpha+1/2)}]_{a_{ini}}^{\infty} = BN \quad (B.23)$$

$$\frac{B}{C_{\alpha}^{-m} T^{\alpha m}} = \frac{a_{ini}^{1-m(\alpha+1/2)}}{1-m(\alpha+1/2)} \frac{1}{N}$$

Substitution of (B.23) in (B.21) finally yields:

$$a = a_{ini} \left(1 - \frac{N_k}{N}\right)^{\frac{1}{1-m(\alpha+1/2)}} = a_{ini} (1-D)^{\frac{1}{1-m(\alpha+1/2)}} \quad (B.24)$$

Recalling:

$$\begin{aligned} \Delta\sigma_{th} &= \Delta\sigma_0 \frac{M_w(a_{ini}) Y(a_{ini}) \sqrt{a_{ini}}}{M_w(a) Y(a) \sqrt{a}} \\ &= \Delta\sigma_0 \frac{a_{ini}^{\alpha}}{a^{\alpha}} \sqrt{\frac{a_{ini}}{a}} \\ &= \Delta\sigma_0 \left(\frac{a_{ini}}{a}\right)^{\alpha+1/2} \\ &= \Delta\sigma_0 (1-D)^{\frac{\alpha+1/2}{1-m(\alpha+1/2)}} \end{aligned} \quad (B.25)$$

Now the **RLDM** is introduced to scale the critical damage parameter and expressing the final model as:

$$\Delta\sigma_{th,h} = \Delta\sigma_0 \left(1 - \frac{D_{h-1}}{D_{cr}}\right)^{\zeta} \quad (B.26)$$

With:

$$\zeta = f(\alpha, m) = \frac{\alpha + 1/2}{1 - m(\alpha + 1/2)} \quad (B.27)$$

C

Author's derivations

C.1. Equivalent stress formulations

The derivation of the equivalent stress is, for all combinations of the formulation of the S-N curve and a damage accumulation theorem, based on two assumptions:

- The accumulated S-N curve and equivalent description have the same damage mechanism (slope m).
- The accumulated S-N curve and equivalent description have the same fatigue strength (intercept $\log(C)$).

With regards to the notation: N always refers to the total amount of cycles from the rainflow counting procedure (i.e. the fatigue life).

C.1.1. Basquin relation with the LDAM

The first derivation is for the Basquin relation with the Palmgren-Miner (LDAM) damage summation. The result of the derivation is in accordance with the formulations in [54, 100, 128].

S-N relation: Basquin

The Basquin-type S-N curve, is given by:

$$\begin{aligned}\log(N) &= \log(C) - m \log(S) \\ &= \log(C) - \log(S^m) \\ N &= \frac{C}{S^m} = CS^{-m} \\ C &= NS^m\end{aligned}\quad (C.1)$$

Damage accumulation model: LDAM

Substituting the formulation of N from the Basquin relation (C.1):

$$\begin{aligned}D &= \sum_{i=1}^k \frac{n_i}{N_i} \\ 1 &= \sum_{i=1}^k \frac{n_i}{CS_i^{-m}} = \sum_{i=1}^k \frac{n_i S_i^m}{C} \\ C &= \sum_{i=1}^k n_i S_i^m\end{aligned}\quad (C.2)$$

Equivalent stress formulation

Stating that the equivalent stress relation is of the Basquin-type as well, and equating the exponent of the intercept $\log C$ from the Basquin relation and the LDAM yields:

$$\begin{aligned}NS_{eq}^m &= \sum_{i=1}^k n_i S_i^m \\ S_{eq} &= \sqrt[m]{\frac{\sum_{i=1}^k n_i S_i^m}{N}} \\ &= \sqrt[m]{\sum_{i=1}^k \frac{n_i S_i^m}{N}}\end{aligned}\quad (C.3)$$

C.1.2. ORFL with the LDAM

The second derivation is for the combination of the ORFL with the Palmgren-Miner model (LDAM).

S-N relation: ORFL

The ORFL-type S-N curve, is given by:

$$\begin{aligned}\log(N) &= \log(C) - m \log(S - S_{\infty}(\mu, \sigma)) \\ &= \log(C) - \log((S - S_{\infty}(\mu, \sigma))^m) \\ N &= \frac{C}{(S - S_{\infty}(\mu, \sigma))^m} \\ &= C(S - S_{\infty}(\mu, \sigma))^{-m} \\ C &= N(S - S_{\infty}(\mu, \sigma))^m\end{aligned}\quad (C.4)$$

Damage accumulation model: LDAM

Substituting the formulation of N from the ORFL-relation (C.4):

$$\begin{aligned}D &= \sum_{i=1}^k \frac{n_i}{N_i} \\ 1 &= \sum_{i=1}^k \frac{n_i}{C(S_i - S_{\infty}(\mu, \sigma))^{-m}} \\ C &= \sum_{i=1}^k n_i (S_i - S_{\infty}(\mu, \sigma))^m\end{aligned}\quad (C.5)$$

Equivalent stress formulation

Stating that the equivalent stress relation is of the ORFL-type as well, and equating the exponent of the intercept $\log C$ from the ORFL relation and the LDAM yields:

$$\begin{aligned}N(S_{eq} - S_{\infty}(\mu, \sigma))^m &= \sum_{i=1}^k n_i (S_i - S_{\infty}(\mu, \sigma))^m \\ S_{eq} &= \sqrt[m]{\sum_{i=1}^k \frac{n_i (S_i - S_{\infty}(\mu, \sigma))^m}{N}} + S_{\infty}(\mu, \sigma)\end{aligned}\quad (C.6)$$

C.1.3. GRFL and the LDAM

The third derivation is for the combination of the GRFL [74] with the Palmgren-Miner model (LDAM).

S-N relation: GRFL

The 6PRFLM (or GRFL)-type S-N curve, is given by:

$$\begin{aligned}\log(N) &= \log(C) - m \log(S) - \rho_{S_{\infty}} \log\left(1 - \frac{S_{\infty}(\mu, \sigma)}{S}\right) \\ \log(C) &= \log(N) + m \log(S) + \rho_{S_{\infty}} \log\left(1 - \frac{S_{\infty}(\mu, \sigma)}{S}\right) \\ &= \log\left(NS^m \left(1 - \frac{S_{\infty}(\mu, \sigma)}{S}\right)^{\rho_{S_{\infty}}}\right) \\ C &= NS^m \left(1 - \frac{S_{\infty}(\mu, \sigma)}{S}\right)^{\rho_{S_{\infty}}} \\ N &= CS^{-m} \left(1 - \frac{S_{\infty}(\mu, \sigma)}{S}\right)^{-\rho_{S_{\infty}}}\end{aligned}\quad (C.7)$$

Damage accumulation model: LDAM

Substituting the formulation of N from the GRFL-relation (C.7):

$$\begin{aligned}D &= \sum_{i=1}^k \frac{n_i}{N_i} \\ 1 &= \sum_{i=1}^k \frac{n_i}{CS_i^{-m} \left(1 - \frac{S_{\infty}(\mu, \sigma)}{S_i}\right)^{-\rho_{S_{\infty}}}} \\ C &= \sum_{i=1}^k n_i S_i^m \left(1 - \frac{S_{\infty}(\mu, \sigma)}{S_i}\right)^{\rho_{S_{\infty}}}\end{aligned}\quad (C.8)$$

Equivalent stress formulation

Equating the exponent of the intercept $\log C$ from the [GRFL](#)-relation and the [LDAM](#) yields:

$$\begin{aligned}
 NS_{eq}^m \left(1 - \frac{S_{\infty}(\mu, \sigma)}{S_{eq}}\right)^{\rho_{S_{\infty}}} &= \sum_{i=1}^k n_i S_i^m \left(1 - \frac{S_{\infty}(\mu, \sigma)}{S_i}\right)^{\rho_{S_{\infty}}} \\
 S_{eq}^m \left(1 - \frac{S_{\infty}(\mu, \sigma)}{S_{eq}}\right)^{\rho_{S_{\infty}}} - \sum_{i=1}^k \frac{n_i S_i^m \left(1 - \frac{S_{\infty}(\mu, \sigma)}{S_i}\right)^{\rho_{S_{\infty}}}}{N} &= 0
 \end{aligned} \tag{C.9}$$

Due to the nonlinear nature of the equation above, and the variable exponent $\rho_{S_{\infty}}$, there is no analytical solution present for S_{eq} . A numerical solution will be used (`fzero` in Matlab).

C.1.4. GRFL and the model by Hirt and Kunz

S-N relation: GRFL

See equation (C.7).

Damage accumulation model: Hirt and Kunz
--

Substituting the formulation of N from the [GRFL](#)-relation (C.7) in the damage accumulation rule by [Hirt and Kunz](#), a combination as implemented by [Leonetti et al. \[75\]](#):

$$\begin{aligned}
 E[\dot{D}] &= \sum_{i=1}^k \left[\frac{n_i}{N_i} \frac{n_i}{\sum_i n_i} \right] \\
 &= \sum_{i=1}^k \left[\frac{n_i}{CS_i^{-m} \left(1 - \frac{S_{\infty}(\mu, \sigma)}{S_i}\right)^{-\rho_{S_{\infty}}}} \frac{n_i}{\sum_i n_i} \right] \\
 N = \sum_{h=1}^{h_{tot}} E[\dot{D}]_j &= \sum_{h=1}^{h_{tot}} \left[\sum_{i=1}^k \left[\frac{n_i}{CS_i^{-m} \left(1 - \frac{S_{\infty, h}}{S_i}\right)^{-\rho_{S_{\infty}}}} \frac{n_i}{\sum_i n_i} \right] \right] \\
 C &= \sum_{h=1}^{h_{tot}} \left[\sum_{i=1}^k \left[\frac{1}{N} n_i S_i^m \left(1 - \frac{S_{\infty, h}}{S_i}\right)^{\rho_{S_{\infty}}} \frac{n_i}{\sum_i n_i} \right] \right]
 \end{aligned} \tag{C.10}$$

With:

$$S_{\infty, h} = S_0 \left(1 - \frac{D_{h-1}}{D_{cr}}\right)^{\zeta} \tag{C.11}$$

Equivalent stress formulation

Equating the exponent of the intercept $\log C$ from the [GRFL](#) relation and the [Hirt and Kunz](#) damage summation yields:

$$\begin{aligned}
 NS_{eq}^m \left(1 - \frac{S_{\infty}(\mu, \sigma)}{S_{eq}}\right)^{\rho_{S_{\infty}}} &= \sum_{h=1}^{h_{tot}} \left[\sum_{i=1}^k \left[\frac{1}{N} n_i S_i^m \left(1 - \frac{S_{\infty, h}}{S_i}\right)^{\rho_{S_{\infty}}} \frac{n_i}{\sum_i n_i} \right] \right] \\
 S_{eq}^m \left(1 - \frac{S_{\infty}(\mu, \sigma)}{S_{eq}}\right)^{\rho_{S_{\infty}}} &= \sum_{h=1}^{h_{tot}} \left[\sum_{i=1}^k \left[\frac{1}{N^2} n_i S_i^m \left(1 - \frac{S_{\infty, h}}{S_i}\right)^{\rho_{S_{\infty}}} \frac{n_i}{\sum_i n_i} \right] \right]
 \end{aligned} \tag{C.12}$$

Due to the nonlinear nature of the equation above, and the variable exponent $\rho_{S_{\infty}}$, there is no analytical solution present for S_{eq} . A numerical solution will be used (`fzero` in Matlab). The right-hand side of the equation can be solved, as all variables are known.

C.2. Ln or log₁₀

$$\begin{aligned}
 N &= 10^{\log_{10} C - m \log_{10} S - \rho_{S\infty} \log_{10} \left(1 - \frac{S_{\infty}}{S}\right)} \\
 &= 10^{\frac{\log C - m \log S - \rho_{S\infty} \log \left(1 - \frac{S_{\infty}}{S}\right)}{\log 10}} \\
 &= \left(10^{\log C - m \log S - \rho_{S\infty} \log \left(1 - \frac{S_{\infty}}{S}\right)}\right)^{\frac{1}{\log 10}}
 \end{aligned} \tag{C.13}$$

$$\begin{aligned}
 &= (10^A)^{\frac{1}{\log 10}} \\
 N &= e^{\log C - m \log S - \rho_{S\infty} \log \left(1 - \frac{S_{\infty}}{S}\right)} \\
 &= e^A
 \end{aligned} \tag{C.14}$$

Equating both:

$$\begin{aligned}
 (10^A)^{\frac{1}{\log 10}} &\stackrel{?}{=} e^A \\
 10^A &\stackrel{?}{=} (e^A)^{\log 10} \\
 &\stackrel{?}{=} e^{A \log 10} \\
 &\stackrel{?}{=} (e^{\log 10})^A \\
 &= 10^A
 \end{aligned} \tag{C.15}$$

Q. E. D.

D

DNV-GL HSSSC analysis

D.1. DMO CA sample

INPUT

Kp	0.9
c	1.12
pw	72 mm

Method A: Linear extrapolation
 Method B: 1.12 times stress at tp/2
 Mesh size: 1 mm

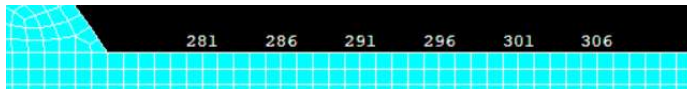
Boundary condition: Roller
Normal sample

FE Results

Main weld

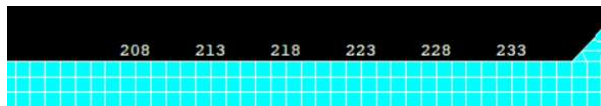
Select nodes > Nodal solution > X, Z and XZ component of stress

	Node	Sig x [N/mm]	Sig z [N/mm]	Sig xz [N/mm]	Sig 1 [N/mm]	Sig 2 [N/mm]	S eff [N/mm]
at tp/2	286	14697	3.8578	-4.83E+01	1.47E+04	3.70E+00	1.65E+04
at 3tp/2	306	13191	-5.54E-02	-3.69E+01	1.32E+04	-1.59E-01	1.48E+04



Counterweld

	Node	Sig x [N/mm]	Sig z [N/mm]	Sig xz [N/mm]	Sig 1 [N/mm]	Sig 2 [N/mm]	S eff [N/mm]
at tp/2	228	14156	-5.9337	-3.07E+01	1.42E+04	-6.00E+00	1.59E+04
at 3tp/2	208	13200	0.14567	3.67E+01	1.32E+04	4.34E-02	1.48E+04



Hot spot structural stress [MPa]

	Method A	Method B
Main weld	2.40E+02	2.56E+02
Counterweld	2.28E+02	2.47E+02

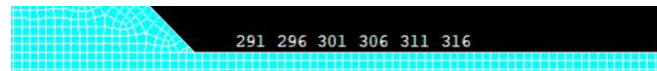
Double sample

FE Results

Main weld

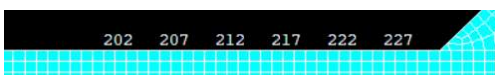
Select nodes > Nodal solution > X, Z and XZ component of stress

	Node	Sig x [N/mm]	Sig z [N/mm]	Sig xz [N/mm]	Sig 1 [N/mm]	Sig 2 [N/mm]	S eff [N/mm]
at tp/2	296	14201	4.9674	-5.07E+01	1.42E+04	4.79E+00	1.59E+04
at 3tp/2	316	12705	-8.54E-02	-3.76E+01	1.27E+04	-1.97E-01	1.42E+04



Counterweld

	Node	Sig x [N/mm]	Sig z [N/mm]	Sig xz [N/mm]	Sig 1 [N/mm]	Sig 2 [N/mm]	S eff [N/mm]
at tp/2	222	13623	-3.0204	8.54E-01	1.36E+04	-3.02E+00	1.53E+04
at 3tp/2	202	12444	7.61E-02	3.51E+01	1.24E+04	-2.28E-02	1.39E+04



Hot spot structural stress [MPa]

	Method A	Method B
Main weld	2.33E+02	2.47E+02
Counterweld	2.21E+02	2.37E+02

INPUT

Kp	0.9
c	1.12
pw	72 mm

Method A: Linear extrapolation
 Method B: 1.12 times stress at tp/2
 Mesh size: 1 mm

Boundary condition: Hinge
Normal sample

FE Results

Main weld

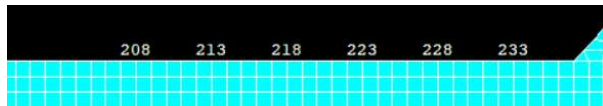
Select nodes > Nodal solution > X, Z and XZ component of stress

	Node	Sig x [N/mm]	Sig z [N/mm]	Sig xz [N/mm]	Sig 1 [N/mm]	Sig 2 [N/mm]	S eff [N/mm]
at tp/2	286	6949.6	1.5347	-4.21E+01	6.95E+03	1.28E+00	7.78E+03
at 3tp/2	306	5423.9	-1.70E-02	-3.67E+01	5.42E+03	-2.65E-01	6.07E+03



Counterweld

	Node	Sig x [N/mm]	Sig z [N/mm]	Sig xz [N/mm]	Sig 1 [N/mm]	Sig 2 [N/mm]	S eff [N/mm]
at tp/2	228	6911.6	-5.8794	-1.94E+01	6.91E+03	-5.93E+00	7.74E+03
at 3tp/2	208	5815.1	0.13072	3.70E+01	5.82E+03	-1.05E-01	6.51E+03



Hot spot structural stress [MPa]

	Method A	Method B
Main weld	1.20E+02	1.21E+02
Counterweld	1.16E+02	1.20E+02

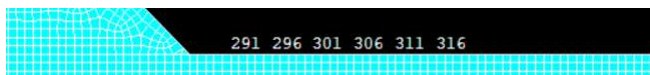
Double sample

FE Results

Main weld

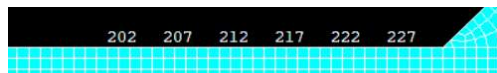
Select nodes > Nodal solution > X, Z and XZ component of stress

	Node	Sig x [N/mm]	Sig z [N/mm]	Sig xz [N/mm]	Sig 1 [N/mm]	Sig 2 [N/mm]	S eff [N/mm]
at tp/2	296	6580	2.5651	-4.44E+01	6.58E+03	2.27E+00	7.37E+03
at 3tp/2	316	5068.5	-4.16E-02	-3.71E+01	5.07E+03	-3.13E-01	5.68E+03



Counterweld

	Node	Sig x [N/mm]	Sig z [N/mm]	Sig xz [N/mm]	Sig 1 [N/mm]	Sig 2 [N/mm]	S eff [N/mm]
at tp/2	222	6741.9	2021.4	5.06E+00	6.74E+03	2.02E+03	7.55E+03
at 3tp/2	202	5454.2	1636.3	3.59E+01	5.45E+03	1.64E+03	6.11E+03



Hot spot structural stress [MPa]

	Method A	Method B
Main weld	1.14E+02	1.15E+02
Counterweld	1.15E+02	1.17E+02

INPUT

Kp	0.9
c	1.12
pw	72 mm

Method A: Linear extrapolation
 Method B: 1.12 times stress at tp/2
 Mesh size: 1 mm

Boundary condition: 5% of the load per side

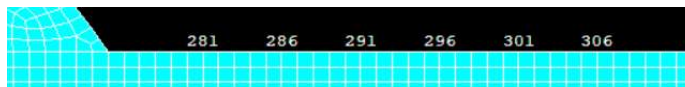
Normal sample

FE Results

Main weld

Select nodes > Nodal solution > X, Z and XZ component of stress

	Node	Sig x [N/mm]	Sig z [N/mm]	Sig xz [N/mm]	Sig 1 [N/mm]	Sig 2 [N/mm]	S eff [N/mm]
at tp/2	286	14799	3.8885	-4.84E+01	1.48E+04	3.73E+00	1.66E+04
at 3tp/2	306	13293	-5.62E-02	-3.69E+01	1.33E+04	-1.59E-01	1.49E+04



Counterweld

	Node	Sig x [N/mm]	Sig z [N/mm]	Sig xz [N/mm]	Sig 1 [N/mm]	Sig 2 [N/mm]	S eff [N/mm]
at tp/2	228	14252	-5.9344	-3.09E+01	1.43E+04	-6.00E+00	1.60E+04
at 3tp/2	208	13298	0.14587	3.67E+01	1.33E+04	4.44E-02	1.49E+04



Hot spot structural stress [MPa]

	Method A	Method B
Main weld	2.42E+02	2.58E+02
Counterweld	2.29E+02	2.48E+02

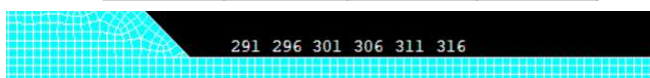
Double sample

FE Results

Main weld

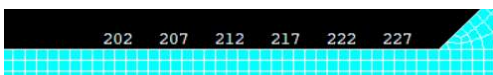
Select nodes > Nodal solution > X, Z and XZ component of stress

	Node	Sig x [N/mm]	Sig z [N/mm]	Sig xz [N/mm]	Sig 1 [N/mm]	Sig 2 [N/mm]	S eff [N/mm]
at tp/2	296	14305	5.0002	-5.08E+01	1.43E+04	4.82E+00	1.60E+04
at 3tp/2	316	12809	-8.40E-02	-3.76E+01	1.28E+04	-1.95E-01	1.43E+04



Counterweld

	Node	Sig x [N/mm]	Sig z [N/mm]	Sig xz [N/mm]	Sig 1 [N/mm]	Sig 2 [N/mm]	S eff [N/mm]
at tp/2	222	13717	-3.0096	7.96E-01	1.37E+04	-3.01E+00	1.54E+04
at 3tp/2	202	12540	7.60E-02	3.51E+01	1.25E+04	-2.21E-02	1.40E+04



Hot spot structural stress [MPa]

	Method A	Method B
Main weld	2.34E+02	2.49E+02
Counterweld	2.23E+02	2.39E+02

D.2. VA database samples

This appendix shows the DNV-GL method A FE results for each of the VA specimens. The markup provides a sketch of the readout points for the method A extrapolation. The arrow indicates the direction of the expected crack. The thick dots indicate the DNV-GL read-out points.

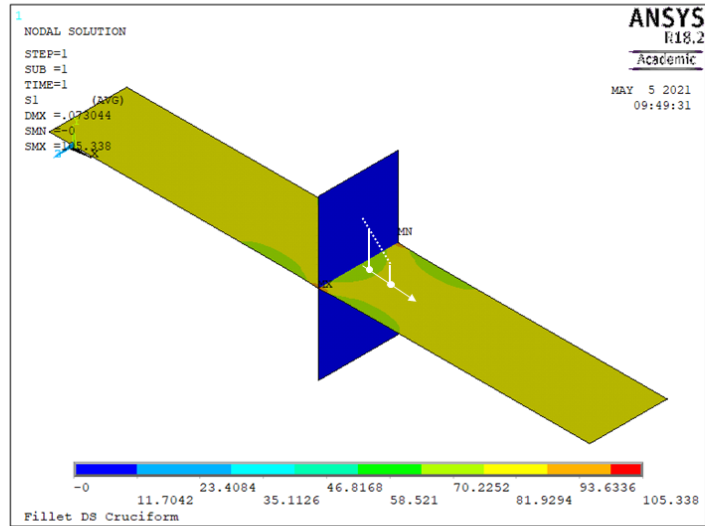


Figure D.1: DS Cruciform by Klippstein and Schilling

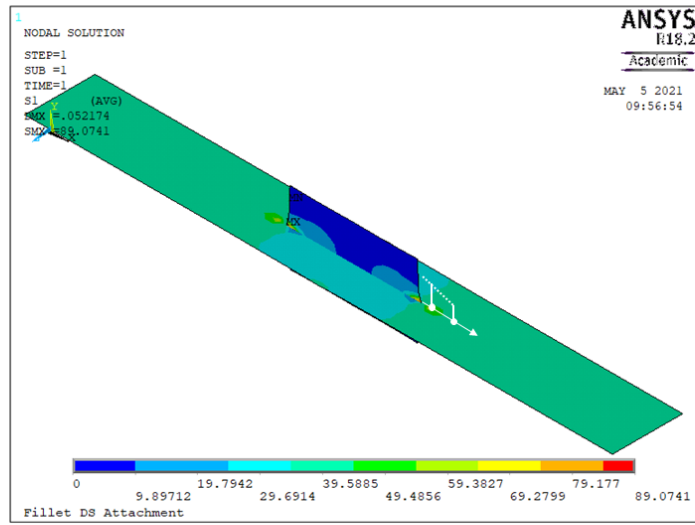


Figure D.2: DS Attachment by Agerskov et al.

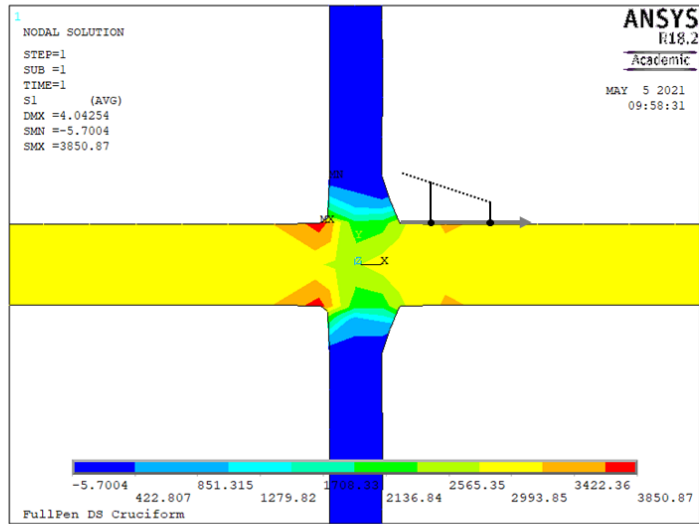


Figure D.3: DS Half-V cruciform by Agerskov et al.

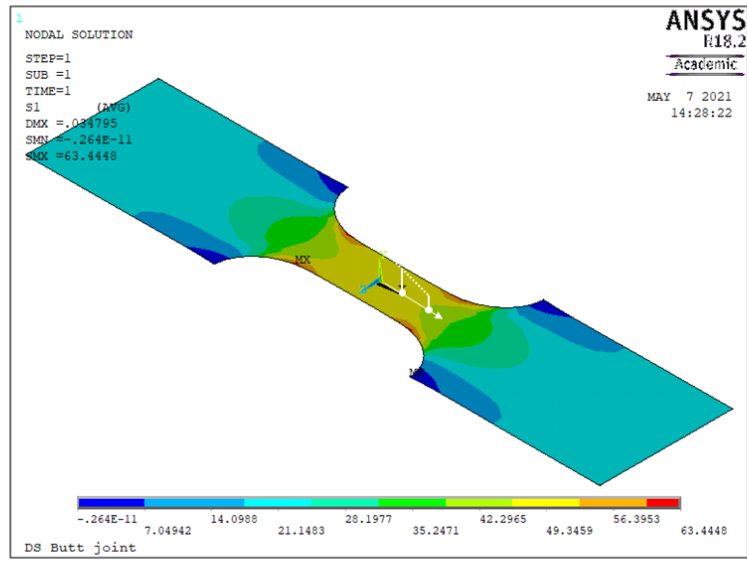


Figure D.4: DS Butt welds by Ota et al.

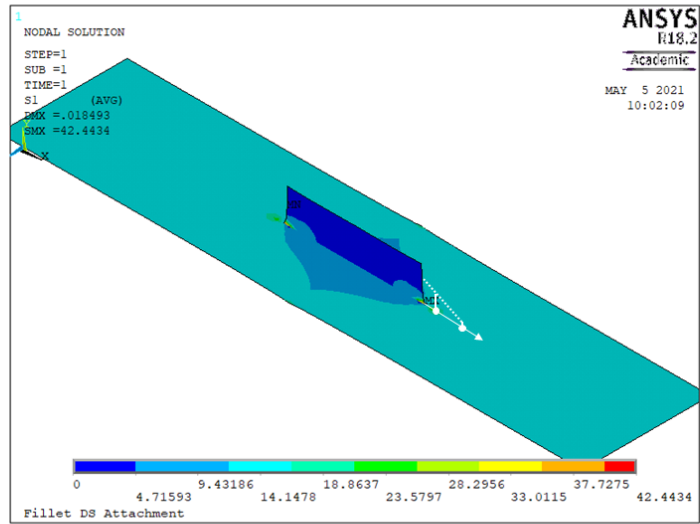


Figure D.5: DS Longitudinal attachment HS Type A by Zhang and Maddox

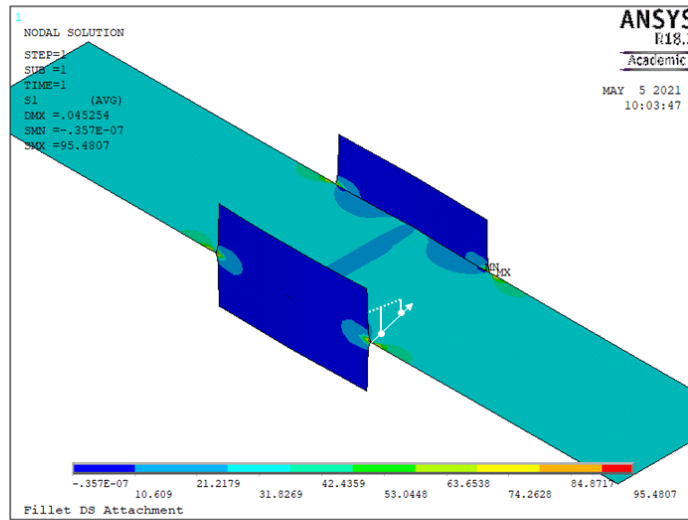


Figure D.6: DS Longitudinal attachment HS Type B by Zhang and Maddox

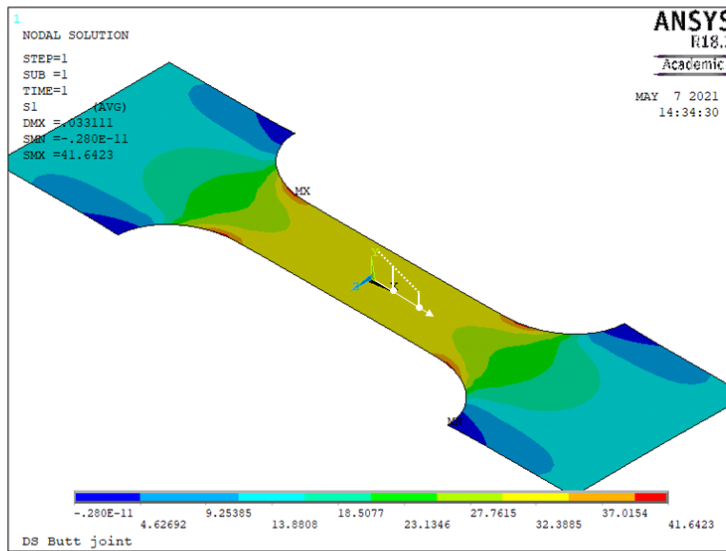


Figure D.7: SS Butt joint by Zhang and Maddox

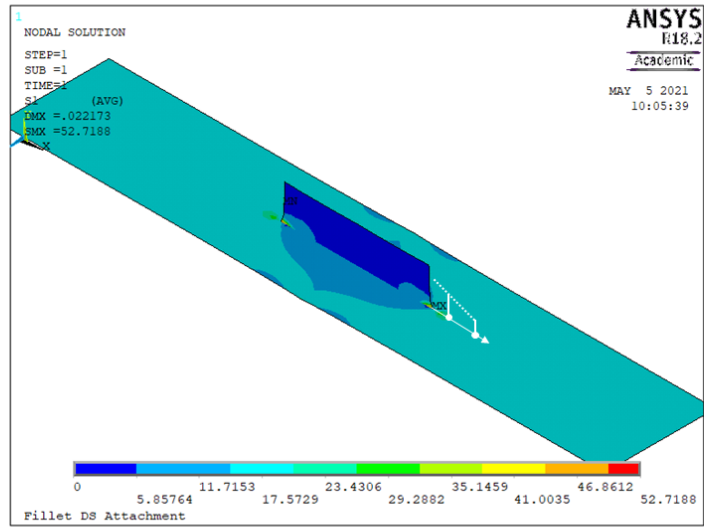


Figure D.8: DS Longitudinal attachment by Rörup and Petershagen

With the HSSSC calculated as prescribed by DNV-GL [27], see the files on the next pages.

Klippstein (1989)
Simple cruciform
 Mesh size: tp/2

FE Results

Main weld

Select nodes > Nodal solution > X, Z and XZ component of stress

	Node	Sig x [N/mm]	Sig z [N/mm]	Sig xz [N/mm]	Sig 1 [N/mm]	Sig 2 [N/mm]	S eff [N/mm]
at tp/2	673	73.693	16.956	9.34E-01	7.37E+01	1.69E+01	8.25E+01

Hot spot structural stress [MPa]

	Method A	Method B
	n.a.	9.24E+01
Corrected for simple cruciform joints	Ks	1.05
		9.71E+01

Method A: Linear extrapolation
 Method B: 1.12 times stress at tp/2

Agerskov (1995) HS A
Longitudinal attachment
 Mesh size: tp/2

FE Results

Main weld

Select nodes > Nodal solution > X, Z and XZ component of stress

	Node	Sig x [N/mm]	Sig z [N/mm]	Sig xz [N/mm]	Sig 1 [N/mm]	Sig 2 [N/mm]	S eff [N/mm]
at tp/2	1041	96.824	-5.0105	-2.82E-06	9.68E+01	-5.01E+00	1.08E+02
at 3tp/2	1263	59.952	-2.63E+00	-3.54E-07	6.00E+01	-2.63E+00	6.71E+01

Hot spot structural stress [MPa]

Method A	Method B
1.29E+02	1.21E+02

Agerskov (1995)
Half-V welded cruciform
 Mesh size: tp/2

FE Results

Main weld (half-V side)

Select nodes > Nodal solution > X, Z and XZ component of stress

	Node	Sig x [N/mm]	Sig z [N/mm]	Sig xz [N/mm]	Sig 1 [N/mm]	Sig 2 [N/mm]	S eff [N/mm]
at tp/2	128	3283.1	992.17	0.00E+00	3.28E+03	9.92E+02	3.68E+03
at 3tp/2	130	3122.8	9.37E+02	0.00E+00	3.12E+03	9.37E+02	3.50E+03

Counter-side

Select nodes > Nodal solution > X, Z and XZ component of stress

	Node	Sig x [N/mm]	Sig z [N/mm]	Sig xz [N/mm]	Sig 1 [N/mm]	Sig 2 [N/mm]	S eff [N/mm]
at tp/2	38	3213.1	959	0.00E+00	3.21E+03	9.59E+02	3.60E+03
at 3tp/2	36	3125.9	9.38E+02	0.00E+00	3.13E+03	9.38E+02	3.50E+03

Hot spot structural stress [MPa]

	Method A	Method B
Half-V side	3.77E+03	4.12E+03
Counter-side	3.65E+03	4.03E+03



Ota (1997)**Simple butt joint**

Mesh size: tp/2

FE Results**Main weld***Select nodes > Nodal solution > X, Z and XZ component of stress*

	Node	Sig x [N/mm]	Sig z [N/mm]	Sig xz [N/mm]	Sig 1 [N/mm]	Sig 2 [N/mm]	S eff [N/mm]
at tp/2	39	50.281	0.26413	-8.32E-04	5.03E+01	2.64E-01	5.63E+01

Hot spot structural stress [MPa]

	Method A	Method B
	n.a.	6.31E+01
Corrected for simple butt joints	Ks	1.13
		7.13E+01

Zhang (2009) HS A

Mesh size: tp/2

FE Results**Main weld***Select nodes > Nodal solution > X, Z and XZ component of stress*

	Node	Sig x [N/mm]	Sig z [N/mm]	Sig xz [N/mm]	Sig 1 [N/mm]	Sig 2 [N/mm]	S eff [N/mm]
at tp/2	1268	25.487	-1.0185	2.72E-04	2.55E+01	-1.02E+00	2.85E+01
at 3tp/2	1378	15.9595	-5.31E-01	1.34E-04	1.60E+01	-5.31E-01	1.79E+01

Hot spot structural stress [MPa]

Method A	Method B
3.39E+01	3.20E+01

Zhang (2009) HS B

Mesh size: 5mm

FE Results**Main weld**

	Node	Sig x [N/mm]	Sig z [N/mm]	Sig xz [N/mm]	Sig 1 [N/mm]	Sig 2 [N/mm]	S eff [N/mm]
at 5mm	163	29.327	0.59715	1.12E+01	3.32E+01	-3.23E+00	3.47E+01
at 15 mm	165	29.761	1.45E-01	6.79E-01	2.98E+01	1.30E-01	3.33E+01

Hot spot structural stress [MPa]

Method A	Method B
3.54E+01	3.89E+01

Zhang (2014)
Simple butt joint
 Mesh size: tp/2

FE Results

Main weld

Select nodes > Nodal solution > X, Z and XZ component of stress

	Node	Sig x [N/mm]	Sig z [N/mm]	Sig xz [N/mm]	Sig 1 [N/mm]	Sig 2 [N/mm]	S eff [N/mm]
at tp/2	47	31.301	-4.81E-02	3.44E-05	3.13E+01	-4.81E-02	3.51E+01

Hot spot structural stress [MPa]

	Method A	Method B
	n.a.	3.93E+01
Corrected for simple butt joints	Ks	1.13
		4.44E+01

Rorup (2002) HS A
 Mesh size: tp/2

FE Results

Main weld *ment of stress*

	Node	Sig x [N/mm]	Sig z [N/mm]	Sig xz [N/mm]	Sig 1 [N/mm]	Sig 2 [N/mm]	S eff [N/mm]
at tp/2	1426	31.937	-1.5457	-5.63E-06	3.19E+01	-1.55E+00	3.58E+01
at 3tp/2	1659	19.75	-8.10E-01	-4.22E-06	1.98E+01	-8.10E-01	2.21E+01

Hot spot structural stress [MPa]

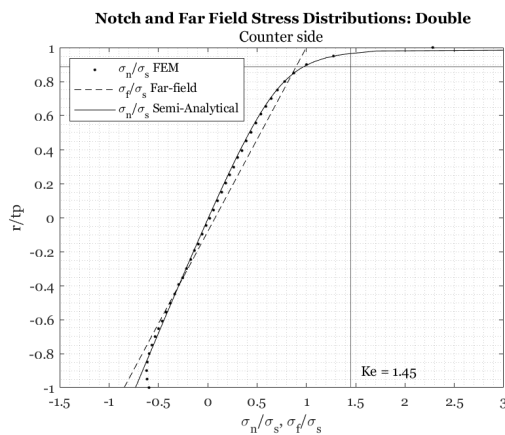
	Method A	Method B
	4.26E+01	4.01E+01

E

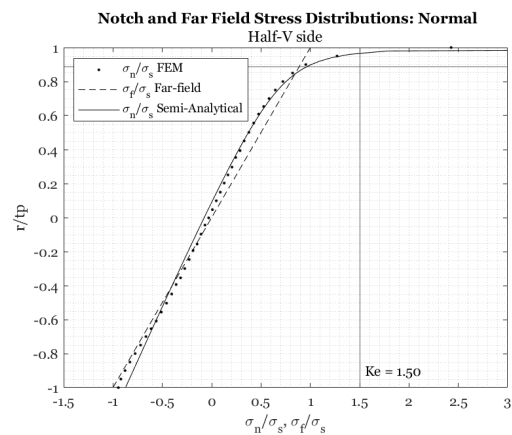
Through-thickness weld notch stress distributions

E.1. DMO CA sample

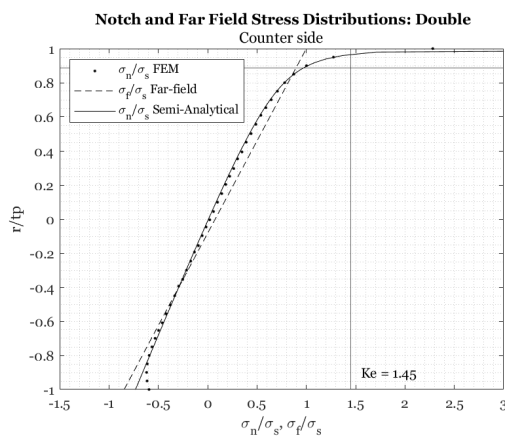
E.1.1. Modelled with a roller boundary condition



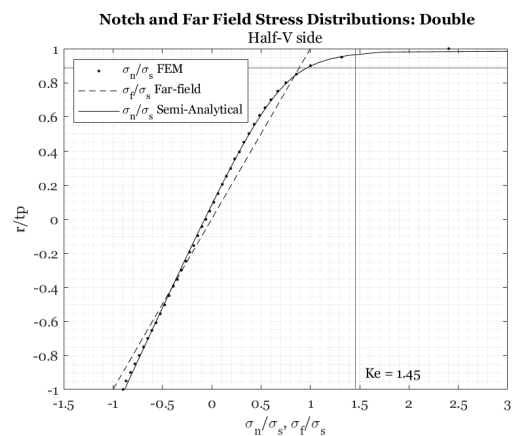
(a) Normal weld configuration



(b) Normal weld configuration



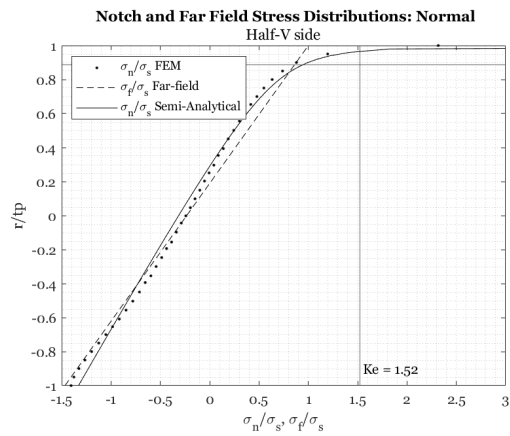
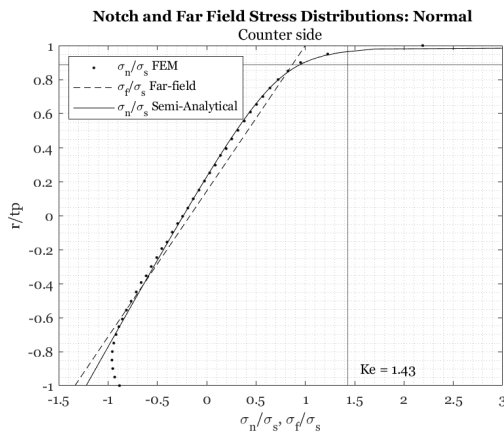
(c) Double weld configuration



(d) Double weld configuration

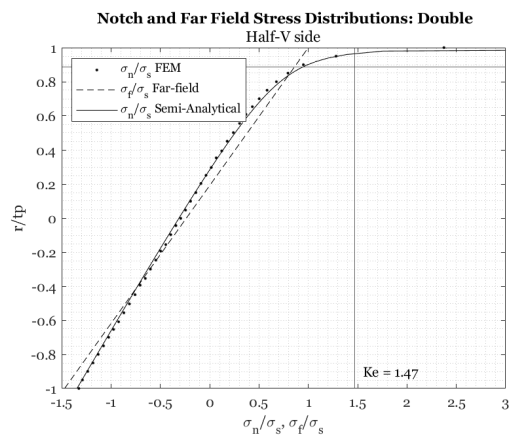
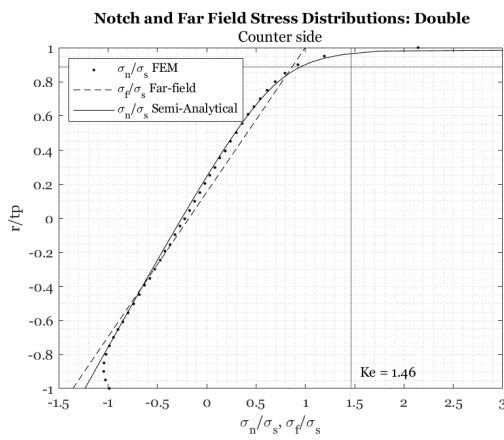
Figure E.1: Through-thickness weld notch stress distributions based on the structural stress over the base plate thickness at the notch location. Boundary condition: Roller.

E.1.2. Modelled with a hinged boundary condition



(a) Normal weld configuration

(b) Normal weld configuration

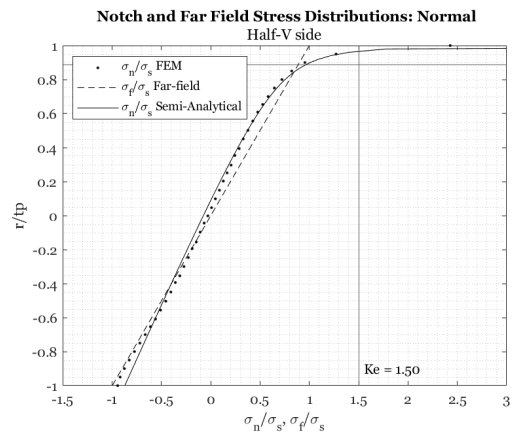
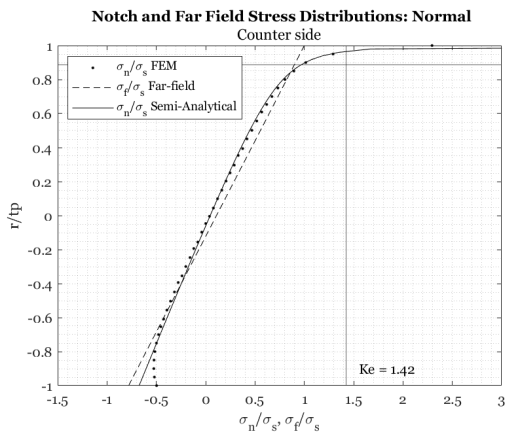


(c) Double weld configuration

(d) Double weld configuration

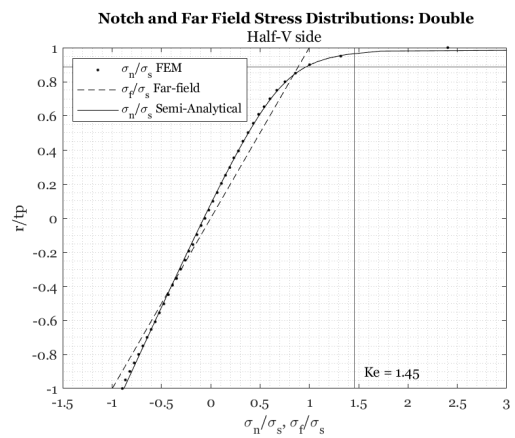
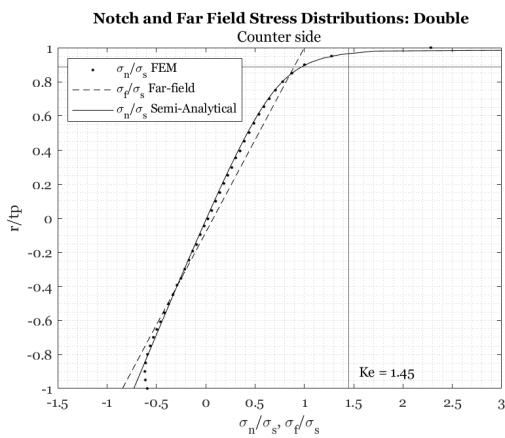
Figure E.2: Through-thickness weld notch stress distributions based on the structural stress over the base plate thickness at the notch location. Boundary condition: Hinge.

E.1.3. Modelled with 5% of the applied force at both boundary conditions



(a) Normal weld configuration

(b) Normal weld configuration

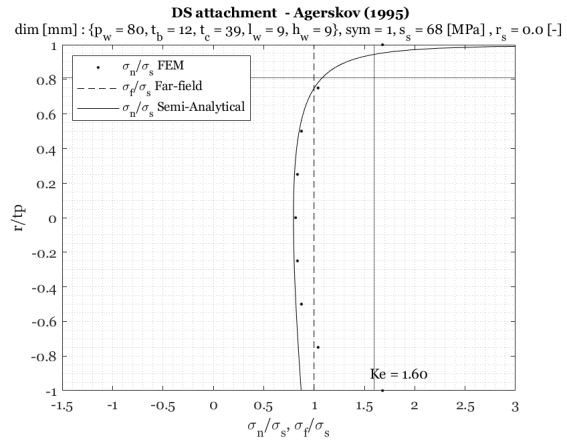
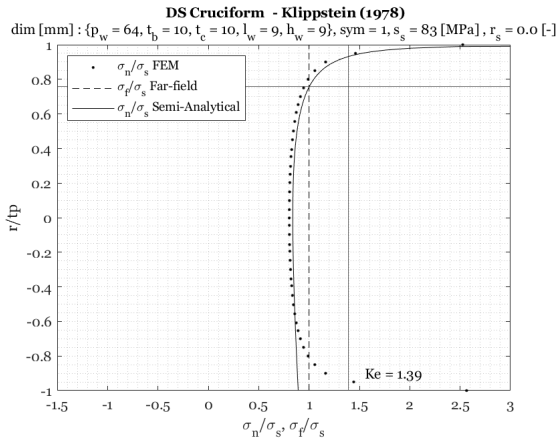


(c) Double weld configuration

(d) Double weld configuration

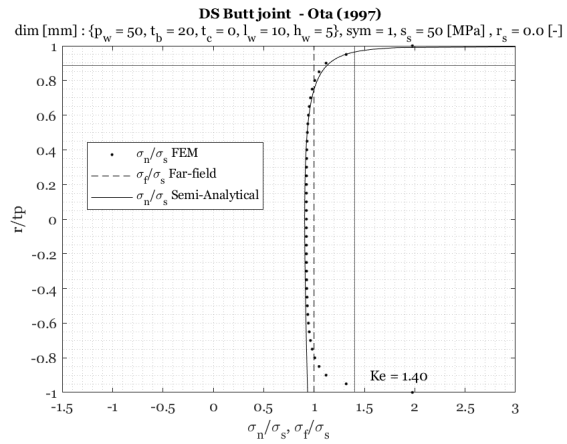
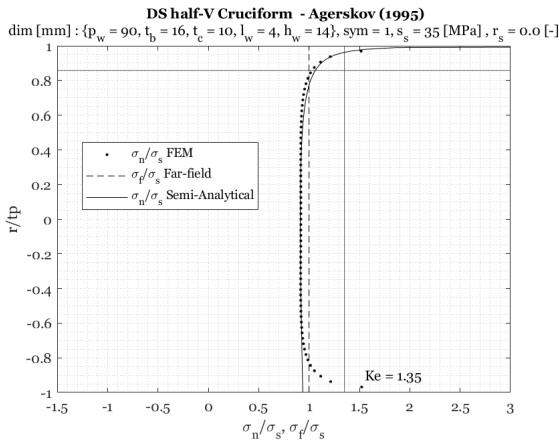
Figure E.3: Through-thickness weld notch stress distributions based on the structural stress over the base plate thickness at the notch location. Boundary condition: 5% of total force.

E.2. VA database samples



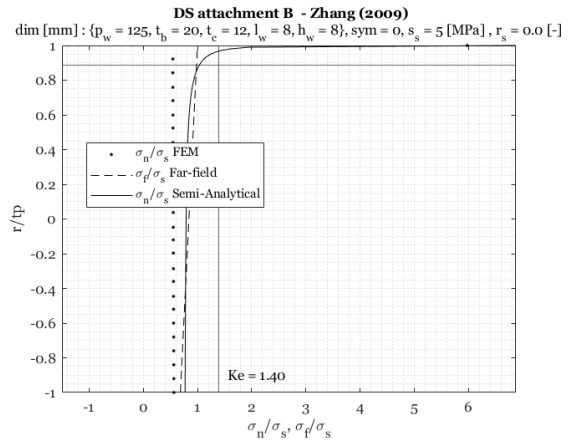
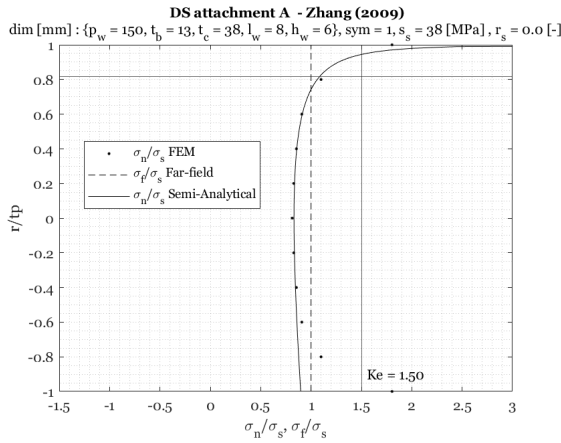
(a) DS Cruciform by Klippstein and Schilling

(b) DS Attachment by Agerskov et al.



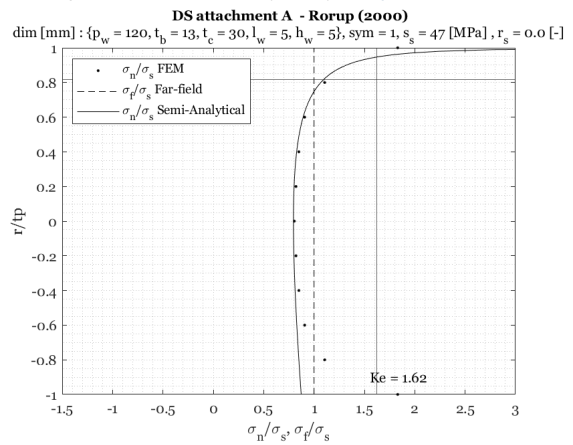
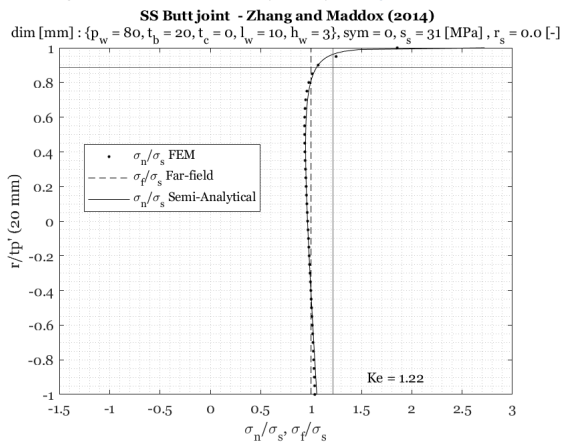
(c) DS Half-V cruciform by Agerskov et al.

(d) DS Butt welds by Ota et al.



(e) DS Longitudinal attachment HS Type A by Zhang and Maddox

(f) DS Longitudinal attachment HS Type B by Zhang and Maddox



(g) SS Butt joint by Zhang and Maddox

(h) DS Longitudinal attachment by Rörup and Petershagen

F

FE models for the ENSC

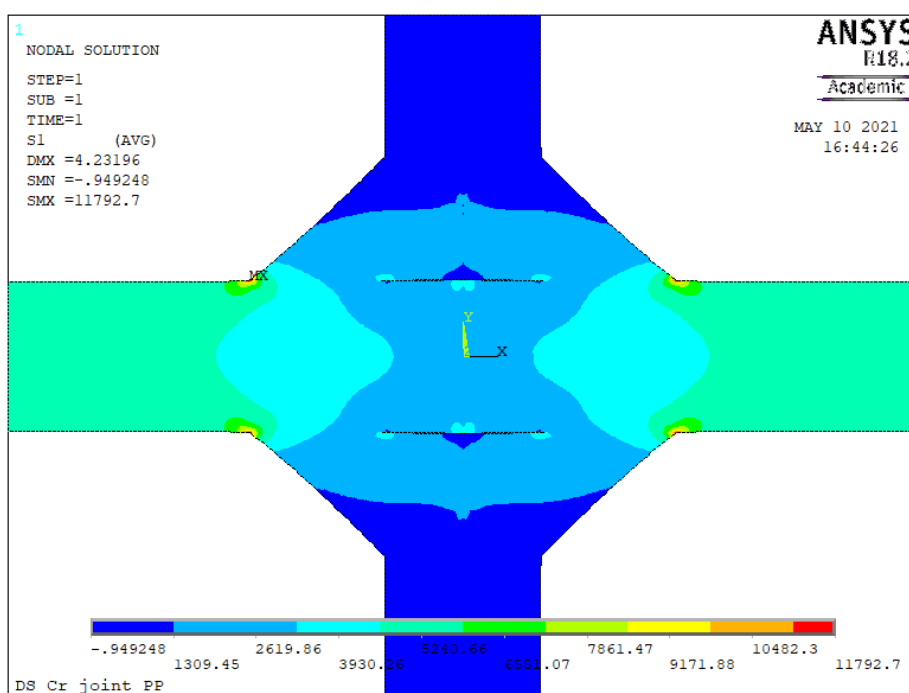


Figure F.1: DS Cruciform by Klippstein and Schilling

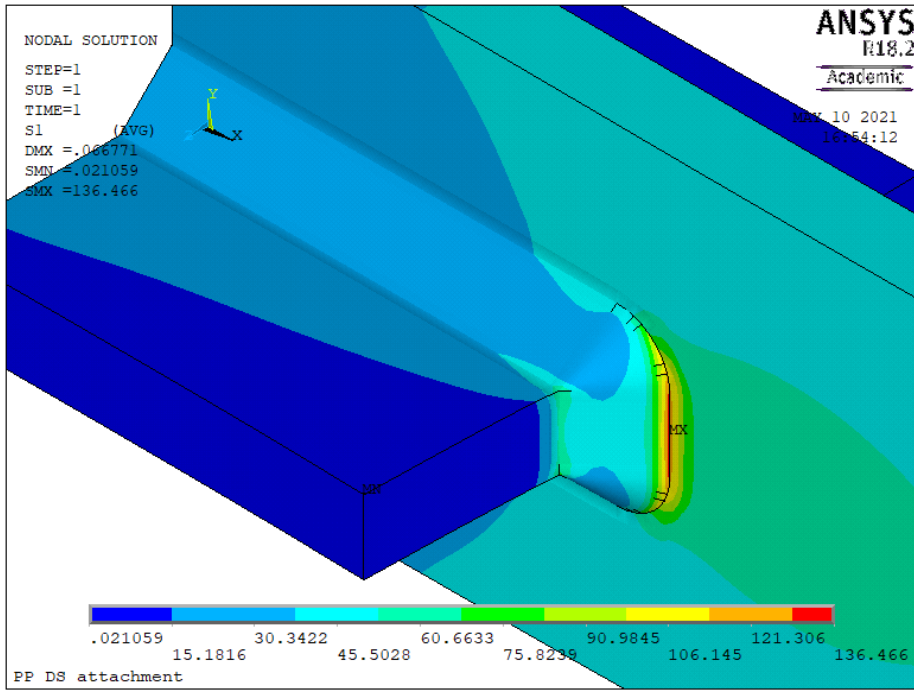


Figure E2: DS Attachment by Agerskov et al.

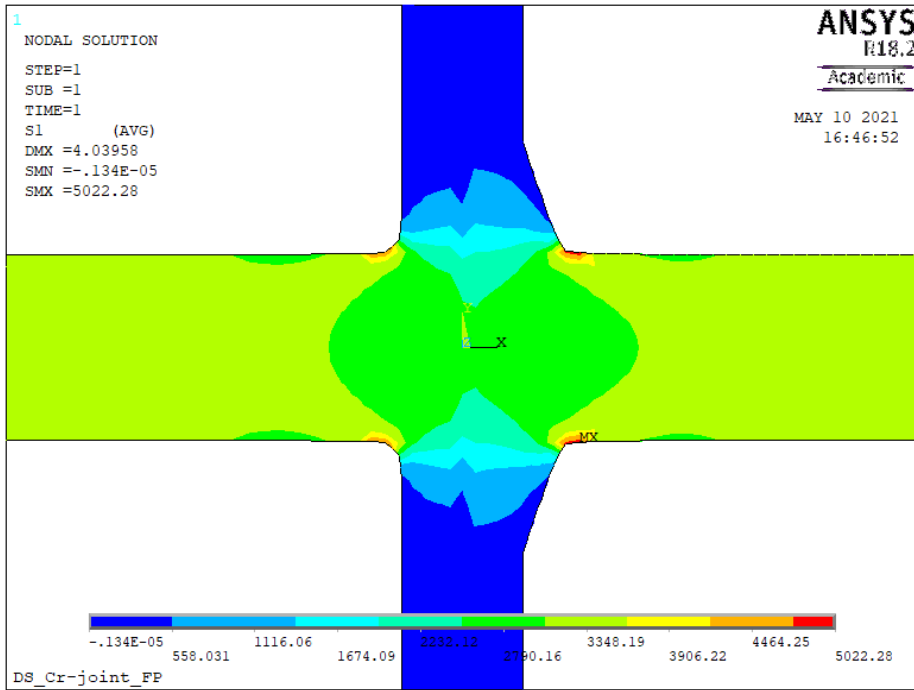


Figure E3: DS Half-V cruciform by Agerskov et al.

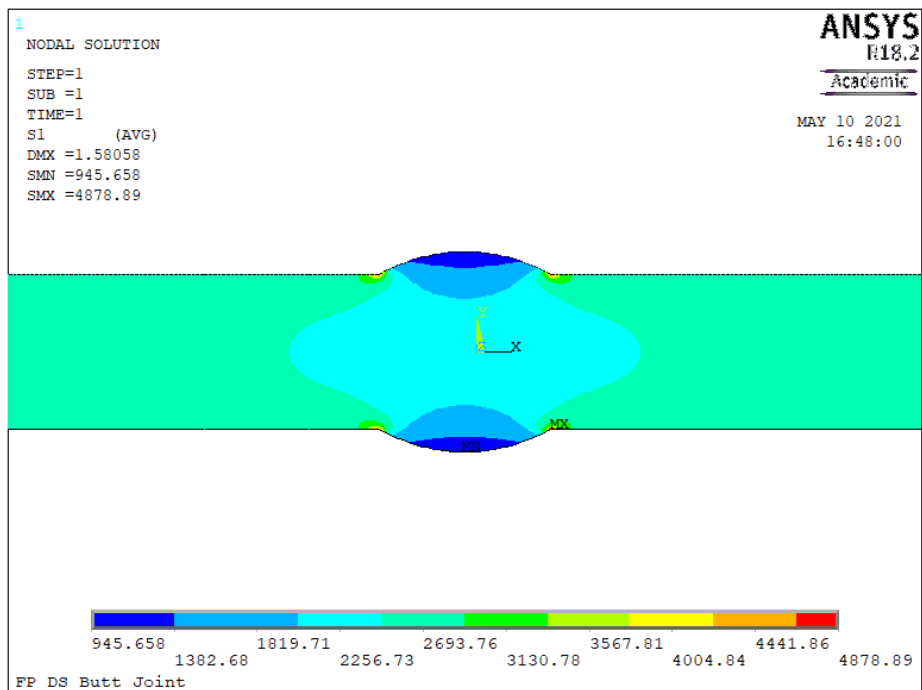


Figure F4: DS Butt welds by Ota et al.

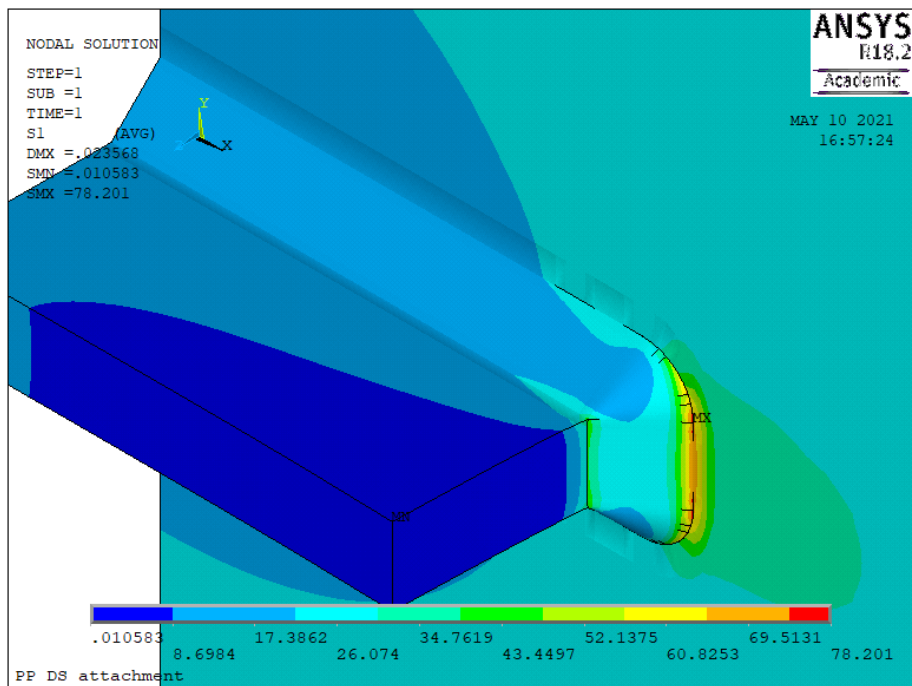


Figure E5: DS Longitudinal attachment HS Type A by Zhang and Maddox

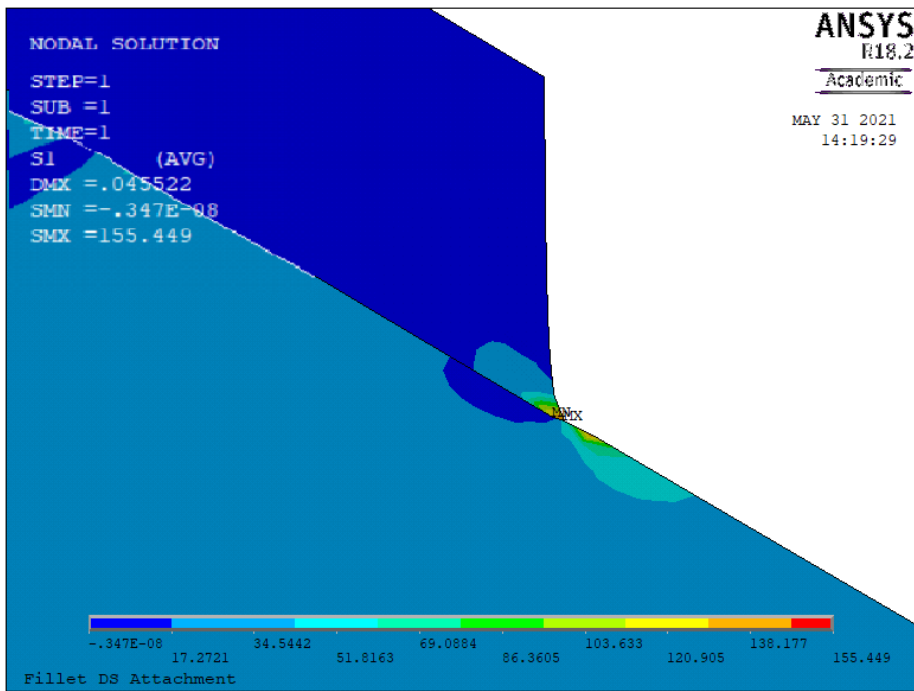


Figure F6: DS Longitudinal attachment HS Type B by Zhang and Maddox

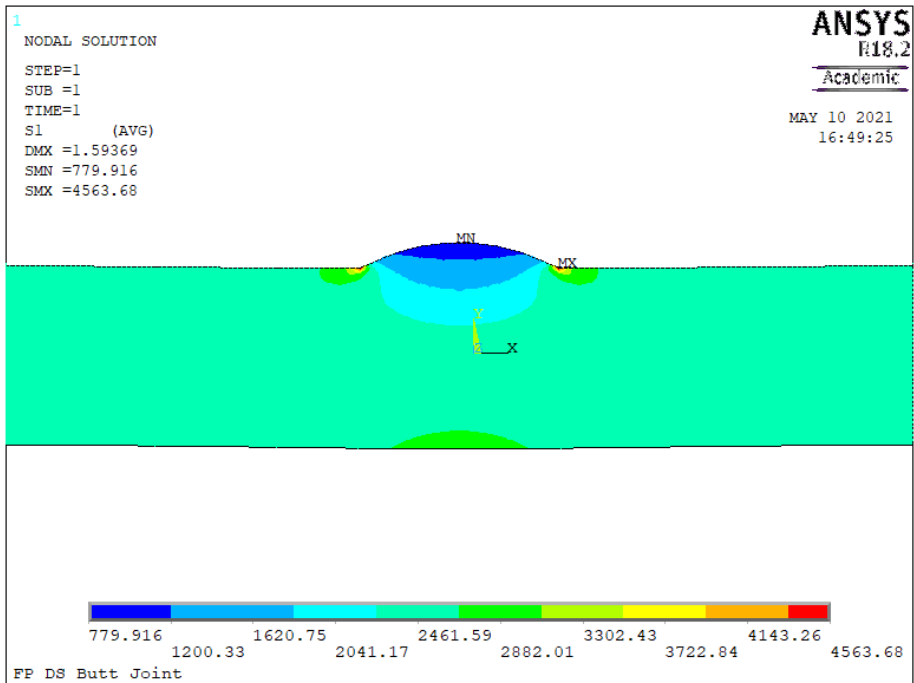


Figure F7: SS Butt joint by Zhang and Maddox

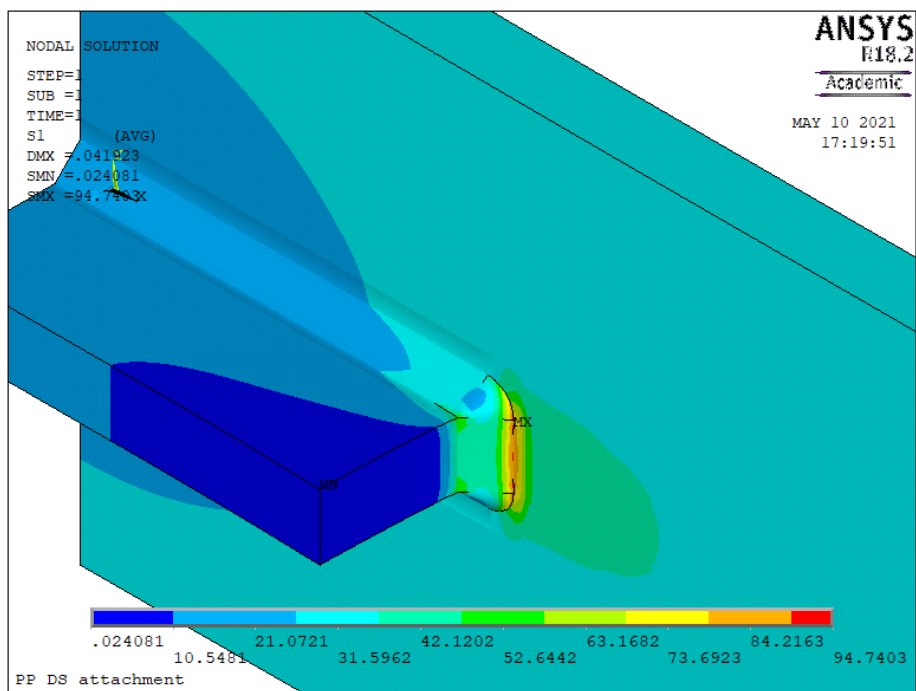


Figure E8: DS Longitudinal attachment by Rörup and Petershagen

G

Results of optimisation per dataset

G.1. Comparison of predicted and experimental N

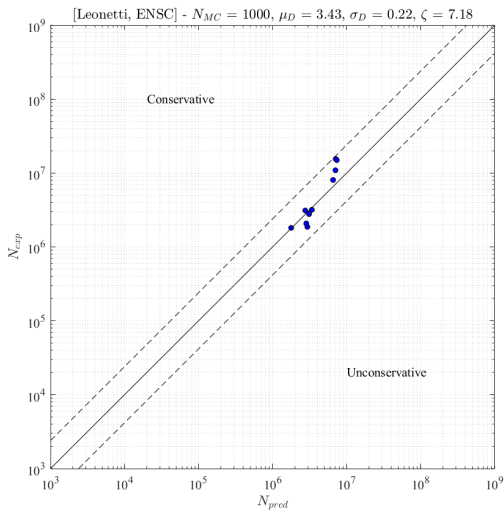


Figure G.1: PP DS Cruciform Rayleigh by Klippstein and Schilling

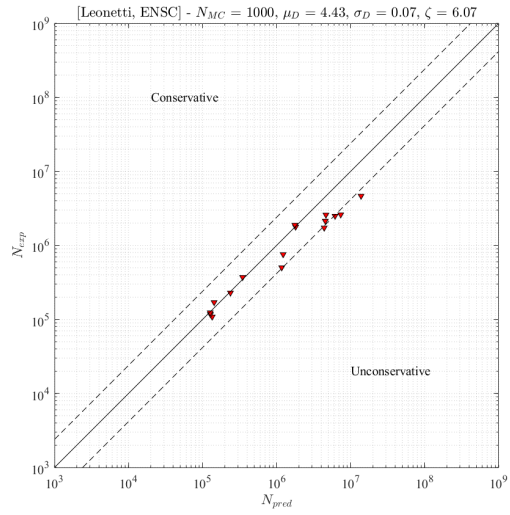


Figure G.2: PP DS Longitudinal attachment type A BROAD64 by Agerskov et al.

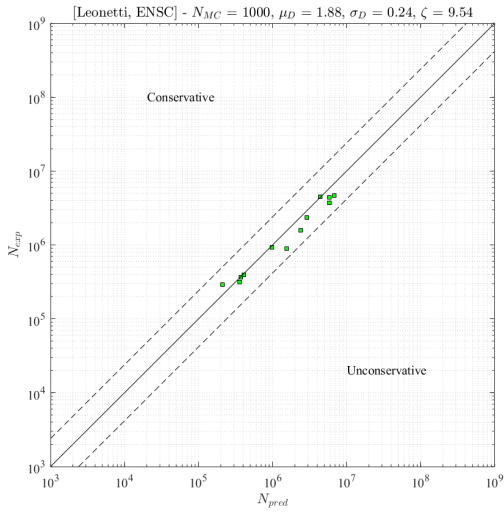


Figure G.3: PP DS Cruciform BROAD64 by Agerskov et al.

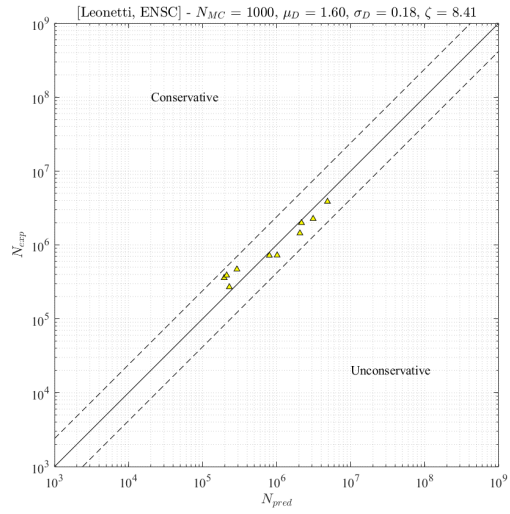


Figure G.4: PP DS Cruciform PMMOD64 by Agerskov et al.

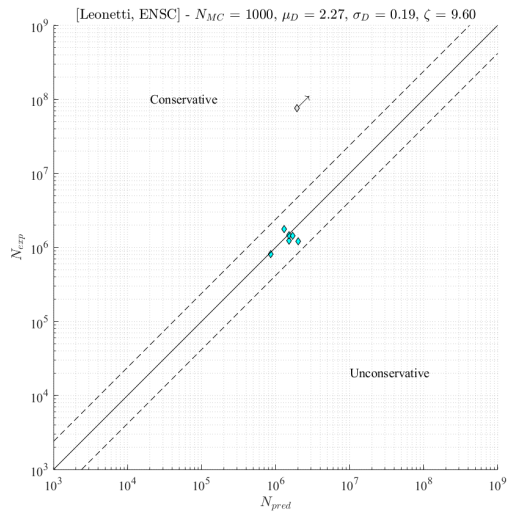


Figure G.5: FP DS Butt joint Rayleigh down by Ota et al.

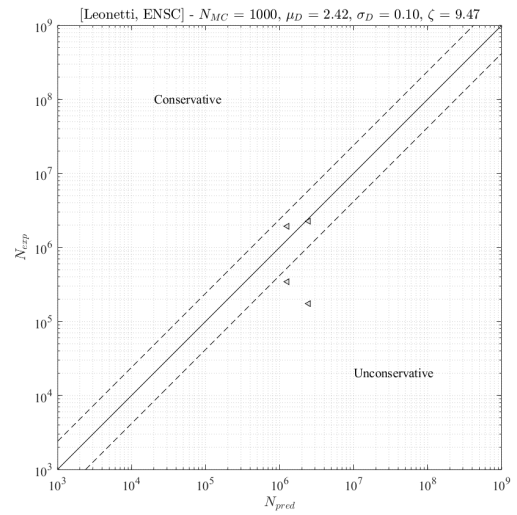


Figure G.6: FP DS Butt joint Rayleigh up by Ota et al.

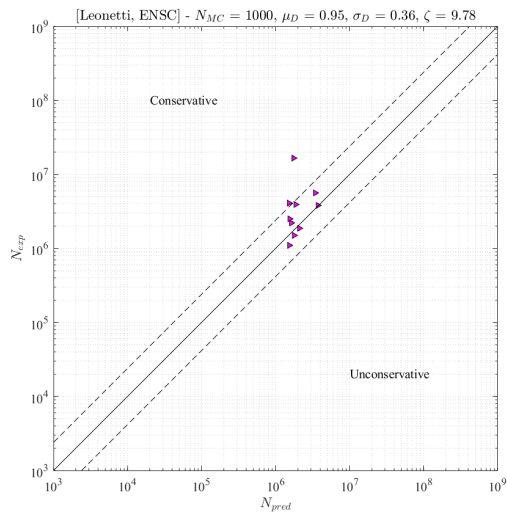


Figure G.7: PP DS Longitudinal attachment type A Linear by Zhang and Maddox

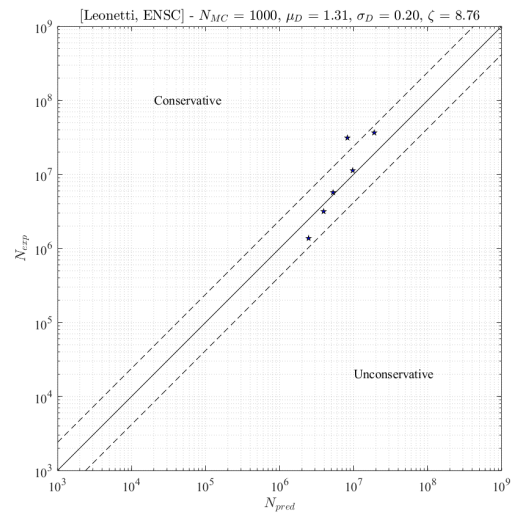


Figure G.8: PP DS Longitudinal attachment type B Linear by Zhang and Maddox

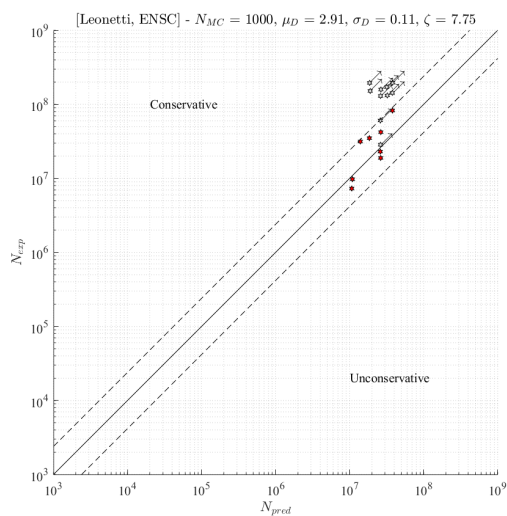


Figure G.9: FP SS Butt joint Log-Linear by Zhang and Maddox

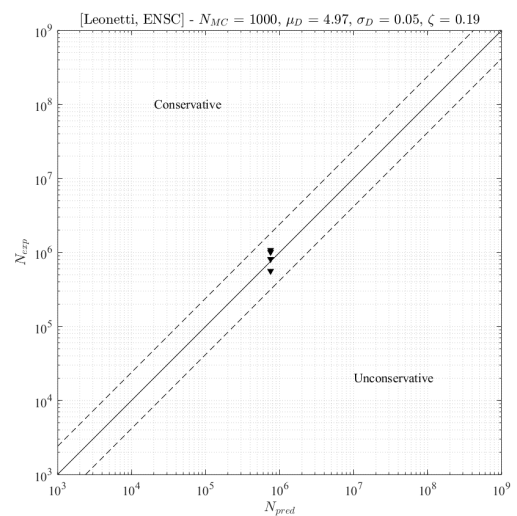


Figure G.10: FP DS Cruciform Rayleigh mod. by DMO

G.2. Comparison of CA and VA scatterbands

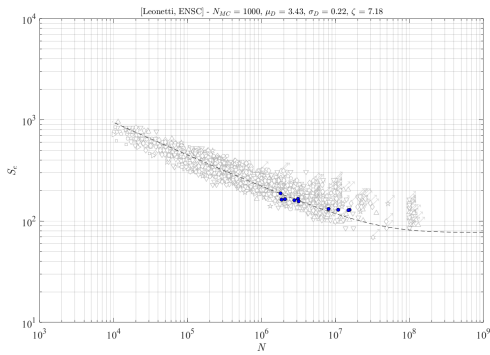


Figure G.11: PP DS Cruciform Rayleigh by Klippstein and Schilling

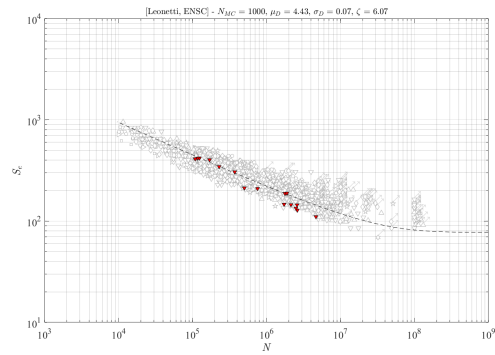


Figure G.12: PP DS Longitudinal attachment type A BROAD64 by Agerskov et al.

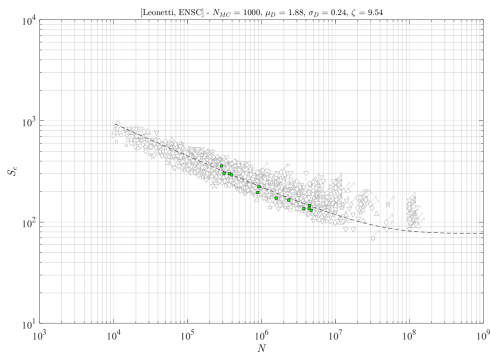


Figure G.13: PP DS Cruciform BROAD64 by Agerskov et al.

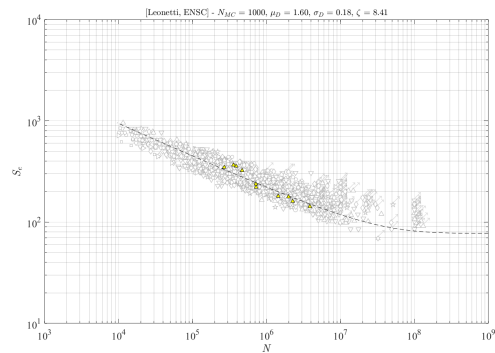


Figure G.14: PP DS Cruciform PMMOD64 by Agerskov et al.

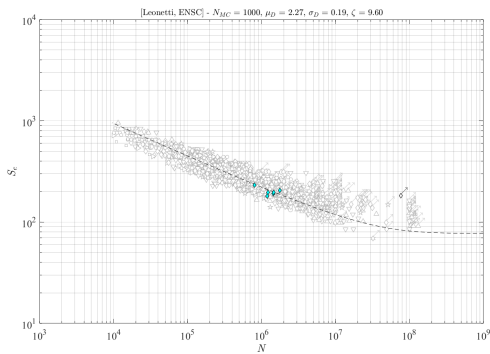


Figure G.15: FP DS Butt joint Rayleigh down by Ota et al.

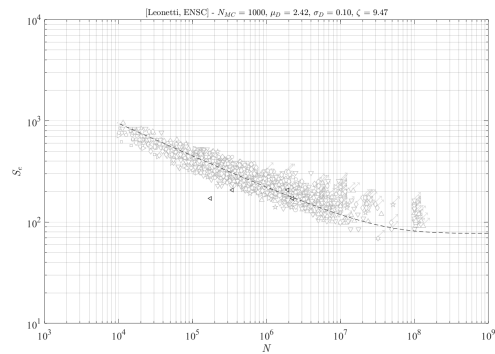


Figure G.16: FP DS Butt joint Rayleigh up by Ota et al.

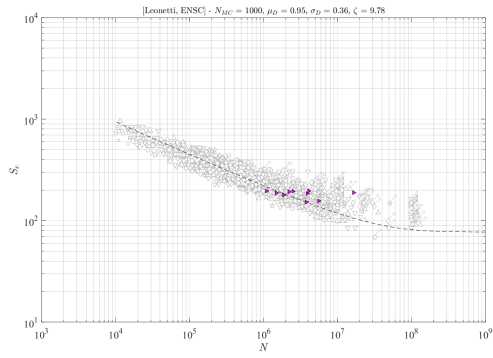


Figure G.17: PP DS Longitudinal attachment type A Linear by Zhang and Maddox

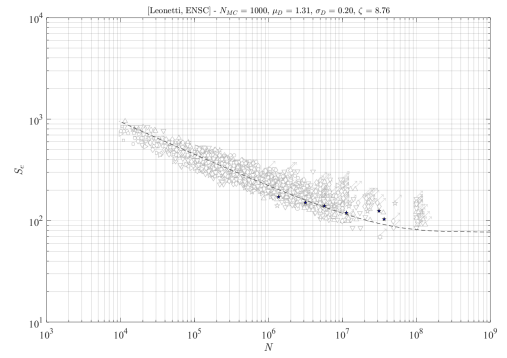


Figure G.18: PP DS Longitudinal attachment type B Linear by Zhang and Maddox

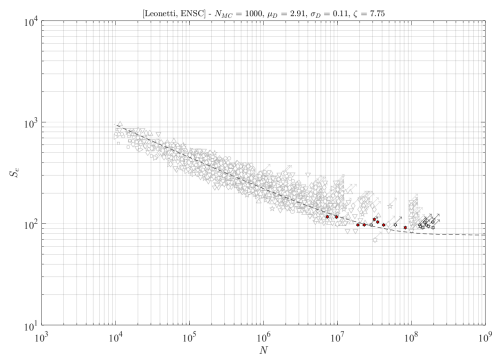


Figure G.19: FP SS Butt joint Log-Linear by Zhang and Maddox

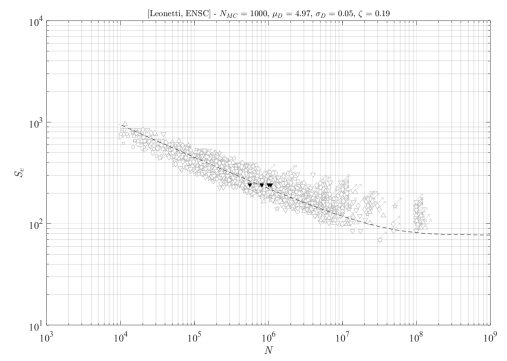


Figure G.20: FP DS Cruciform Rayleigh mod. by DMO

